University College London
Department of Electronic and Electrical Engineering

Variable focal length liquid crystal immersed microlenses

by

Lawrence Commander

July 20, 1998

A thesis submitted in conformity with the requirements
for the degree of PhD
Department of Electronic and Electrical Engineering
University College London

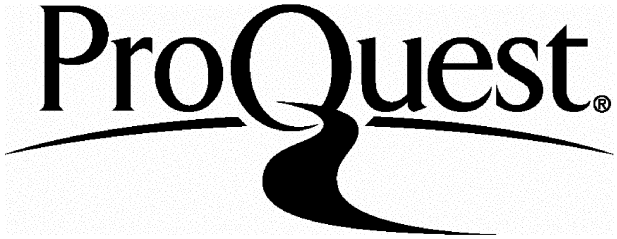

Acknowledgements

Many people have contributed directly or otherwise to my PhD experience and I want to thank them. I would like to thank my 2 supervisors Sally Day and David Selviah for the time they have taken to listen to what I have to say, patiently correct and train generally in the ways of academic science. Of course, they were not the only ones to help me, thanks also goes to Notis Stamos, Laki Panteli, Tim York, Mark Gardner and Robin Kilpatrick who have been a continuous help. In addition, I must thank Fabrizio Di Pasquale for the time time spent modelling my microlenses, David Prescott for his help in fabricating the photoresist microlenses, Lee, Scott and Tom for their help with the ever mysterious computer network and the members of the workshop for their skillful handiwork.

No PhD would be completed without those who reassure you there is more to life than lasers and lenses. I would like to thank my Mum and Dad, my two brothers, Eddy and Robin, Itziar my girlfriend and my friends, Richard and Mark for their support, interest and encouragement and the distractions that made the PhD experience a whole lot more fun.

Abstract

This thesis describes research to produce variable focal length microlenses by immersing refractive photoresist microlenses in a layer of nematic liquid crystal. The nematic liquid crystal has an electrically controllable refractive index in one polarisation, and therefore, the focal length of the lensing interface formed between the refractive microlenses and the liquid crystal can be voltage controlled.

Various designs of microlens cells have been fabricated, the first design had a focal length of $f = -910\mu m$ at 0V, ∞ at $\sim$1.5V and $560\mu m$ at 10V for a lens diameter of $100\mu m$ and $f = -1660\mu m$ at 0V, ∞ at $\sim$1.5V and $1100\mu m$ at 12V for a lens diameter of $150\mu m$. This original design microlens had a usuable tuning range limited to 4V and above (plus 0V) due to large aberrations caused by the liquid crystal structures.

The lenses' phase aberrations have been studied in a Mach-Zehnder interferometer. The first design ($150\mu m$ diameter) had aberrations ranging from an RMS value of 0.18λ to 0.55λ at 632.8nm, peaking at around 2V. The peak in aberration of the original design was partly due to voltage being dropped across the dielectric of the photoresist.

Microlenses, with an electrode on top of the photoresist, were fabricated to improve on the aberration performance of the original design. This "electrode on top" design of microlens had a focal length of $f = -1600\mu m$ at 0V, ∞ at $\sim$1.5V and $1450\mu m$ at 8V for a lens diameter of $150\mu m$. The electrode on top microlenses did not have the large aberrations of the original microlenses and, hence, their usable focal length range was not limited in the same way. The electrode on top design had an RMS aberration ranging from 0.071λ to 0.19λ without the peak of aberrations of the original design.

A 1-D Deuling model for the liquid crystal structure has been used to analyse the phase aberrations of the lenses. Deuling's analysis has been extended to deal with asymmetric pretilt at the surfaces and a computer program has been used to model columns of liquid crystal across the microlens. The resulting phase profiles are qualitatively the same as the aberrations measured for the two spherical lens designs.

The liquid crystal structure has been investigated by inspection in a polarising microscope, modelling of the liquid crystal and fabrication of simpler cylindrical microlenses. Using the microscope, it was seen that liquid crystal walls, disclinations and twist occur on the original design of microlenses. The walls' structure has been described as a combination of bend and twist of the liquid crystal directors. A structure for the liquid crystal after the walls have disappeared has been suggested with a twist of the liquid crystal being due to the fields inclined to the normal in the cell. The occurrence of wall structures has been reproduced in a 2-D finite element model of the liquid crystal which was also used to predict a design with reduced walls. This design, with a strip electrode opposite to the microlens, was fabricated as cylindrical microlenses and was found to agree with the model's predictions. However, additional walls occurred for conditions outside those which could be modelled. The final design of microlens with the electrode on top of the photoresist produced no walls in the liquid crystal and a reduced degree of twist, as well as the reduced aberrations.

Contents

List of Figures

Nomenclature

$\epsilon_\perp$ Dielectric constant perpendicular to the director

$\epsilon_{||}$ Dielectric constant parallel to the director

$\gamma = \frac{\epsilon_{||} - \epsilon_\perp}{\epsilon_\perp} = \frac{\Delta\epsilon}{\epsilon_\perp}$

$\kappa = \frac{k_{33} - k_{11}}{k_{11}}$

λ Wavelength

$\hat{n}$ Liquid crystal director

ϕ Director tilt (out of cell plane)

k_{11} Splay elastic constant

k_{22} Twist elastic constant

k_{33} Bend elastic constant

n_e Extraordinary refractive index (absolute)

n_o Ordinary refractive index

n_x Extraordinary refractive index (variable)

V Potential difference

$\mathbf{E}$ Electric field

$\mathbf{S}$ Order parameter

$\mathbf{s}$ Disclination strength

Chapter 1

Introduction

1.1 Aim and motivation

This thesis describes research to produce variable focal length microlenses. Microlenses are simply small lenses ($\lesssim 1mm$), there is nothing absolute which divides microlenses from more traditional lenses. One reasonably clear distinction is that microlenses are often formed and used in arrays. In this report, microlenses are combined with liquid crystal to give a focal length which can be electrically controlled.

500 million years ago some of the earliest microlens arrays known to man were being created. These lenses were part of the imaging system of animals we know as trilobites [Lan97b]. This same imaging system is quite possibly the most abundant technique used for imaging on Earth today as it is used in the eyes of insects. Despite this prevalence, it is not known what benefit these animals derive by using microlens arrays instead of single lenses [Lan97a].

People started producing microlenses at least 2 or 3 centuries ago. Robert Hooke melted the ends of thin strands of glass so that surface tension would form a lens (very similar to fibre microlenses 3 centuries later) and then he separated the lens and polished the other side flat [HDS91a]. In more recent years, the rise of optoelectronics has created a need to fabricate smaller optics in order to produce more compact systems and, thus, has given rise to a new field: micro-optics.

Recently, microlens fabrication has improved significantly in quality and reproducibility which makes them attractive for applications where previously they had not been successful [HDS91a]. Now they are used variously in photocopiers [BMBM85], lithography [Man96], laser beam formers and collimators [HDH97], CCD's [vMC93], SLM/TV's [CP96], optical wavefront measurement [SD95] and fibre couplers [BL93]. These are just the more successful applications known to the author, many others have been proposed.

New possibilities for applications open up if the focal length of the microlens can be varied. Some are improvements of current uses of microlenses, eg to simplify scanning in a confocal microscope. Others are entirely new uses, eg. DVD read optics. Since lenses and microlens are widely used, it is imagined that if variable focal length lenses could be developed and successfully applied then their availability would encourage adaptations for many other fields. Potentially, the technologies could be cheap (with mass production) by combining plastic molded optics and the technologies used for simple LCD displays (as in a digital watch). Alternatively, higher tolerance (but more

expensive) systems are also envisaged using glass and either a temperature controller or a feedback system to the voltage controller to provide a more stable device.

1.2 Design overview

The design of the microlenses described in this thesis is attractive because of its simplicity. The technology of fabricating photoresist microlenses has matured in the last decade. Many groups have reported diffraction limited lenses achieved with a few iterations of the photoresist processing to "iron out" problems and to optimise the thicknesses and other processing parameters. Once the processing technology has been mastered, it is very simple to add a liquid crystal layer and thus to be able to modulate the liquid crystal lens focal length. The basic concept is shown in figure 1.1.

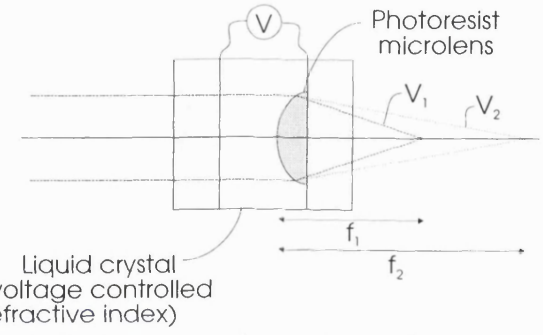

Figure 1.1: Basic concept of variable focal length microlens

Clearly, electrodes are required in order to apply voltages to the liquid crystal and these must be transparent. Fortunately, glass is readily available with transparent electrodes already in place for displays. Thus, the microlenses are formed on these substrates.

The big difficulty in fabricating high quality lenses is achieving uniformity in the liquid crystal. The liquid crystal refractive index is dependent on the molecular orientation so distortions of the structure significantly reduce the quality of the focus.

1.3 Layout of thesis

This thesis describes the basic design of the variable focal length microlenses, their optical quality and the liquid crystal structures which give rise to the optical properties seen. It starts by introducing relevant aspects of liquid crystal (chapter 2), in particular, optical phase modulation, Deulings 1-D model and liquid crystal alignment and then there is a review of research on microlenses and variable focal length lenses (chapter 3). Following on from those chapters is a chapter on the design of the microlenses and other possible variable focal length microlens designs (chapter 4) and then a description of the measurements done on the microlenses (chapter 5). Next there are the experimental results (chapter 6) including some of the many photographs taken on the polarising microscope of the liquid crystal structures, after which, there is a chapter on numerical modelling of the lens properties (chapter 7). Finally, there is a discussion chapter (chapter 8) followed by suggestions for further work (chapter 9).

Chapter 2

Liquid crystals

2.1 Introduction

Liquid crystals are central to the devices described in this thesis being the element which introduces the variability of optical phase. Since the body of work dedicated to them is far too great to review, this chapter will introduce and review aspects of liquid crystals relevant to the devices. There are many types and configurations of liquid crystals used in devices and in section 2.2, some of the more commonly used materials are considered from the point of view of optical phase modulation. In section 2.3, the technique used in the modelling of liquid crystal structures is considered. Finally, in section 2.4, the techniques available for liquid crystal alignment are discussed.

2.2 Optical phase modulation with liquid crystals

2.2.1 Nematic liquid crystals

Probably the most common type of liquid crystal currently used in devices is the nematic. Their prevalence is due to their application in digital watches and, more recently, laptop computers. The characteristics that make nematic liquid crystals used in displays attractive to the manufacturers of consumer goods is their low power consumption, cheapness and compactness [Pan80]. These same characteristics are attractive for many other applications.

The lower power consumption and small bulk are a result of the large electro-optic response of the materials. The large electro-optic response gives these same characteristics in optical phase modulation devices (which is what they are being used for in this research) as for displays. A nematic liquid crystal can produce a refractive index change of up to δn = 0.3 with with 8V applied (the liquid crystal gives a voltage dependent result not electric field dependent-see section 2.3) which gives an optical path difference of 3μm for a 10μm layer. To compare with a solid crystal, KD^*P - a material used in Pockels cells - has an electro-optic coefficient, r_{63}, of $\sim 23.3 \times 10^{-12} m/V$ thus, for a crystal in a field of 5kV/mm, the length required for an optical path difference of $2\mu m$ is 1cm [Hec87]. The solid crystals have the advantage of much faster response times than nematic liquid crystals, for a typical display configuration (Twisted Nematic) liquid crystals have a response time of 10's of milliseconds whereas solid crystals can respond in the order of nanoseconds. However, the solid crystals are generally much

more expensive; the price for a $3 \times 3 \times 40mm$ bar of Cadmium Selenide (anti-reflection coated) is ~$1,000→$1,500[Cle97] whereas 5g of liquid crystal E7 (standard mixture), enough to fill 100 cells ($25mm \times 25mm \times 27\mu m$), costs ~£70-£80 [Mer97].

The large difference in electro-optic effect is due to the different mechanisms by which the effect is achieved. The Kerr and Pockels effects are caused by deformation of the electronic structure of the materials [YY84]. The Kerr effect is also observed in liquids where the change in refractive index is attributed to a partial alignment of anisotropic molecules by the E-field. In liquid crystals, however, the molecules are already mutually aligned and what takes place is a change in the orientation of alignment, rotating towards (or, in some cases, away from) the applied field. It is the combination of molecular alignment and ability to reorientate which give liquid crystals their large electro-optic response.

Molecular structures

The molecules of nematic liquid crystals used in this thesis have the general form [KW93] shown in figure 2.1. The molecules are elongated and are often described as rod shaped (N.B.: in this thesis, the liquid crystal directors (see below) will be drawn as rods not the molecules - see figure 2.2).

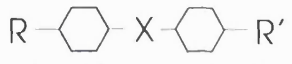

Figure 2.1: The basic structure of a class of nematic liquid crystal molecules. R and R′ are side chain groups and X is a linking group, the three are linked by 2 aromatic rings.

As the name implies, liquid crystals are liquids with some of the properties of crystals. In particular, they retain some of the ordering of crystals. Nematic liquid crystals have the lowest degree of order of the various known liquid crystal types; their molecules are not randomly orientated but, on average, are aligned in a particular direction. The average direction of the molecules is called the *director* and is denoted by $\hat{n}$. A schematic of the molecular arrangements is shown in figure 2.2, with the directors drawn as a rod (as will be used for the rest of this thesis).

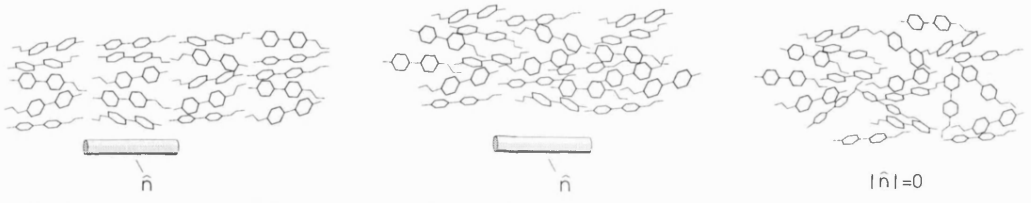

(a) Molecular crystal, orientational and lattice ordering

(b) Nematic, orientational ordering

(c) Isotropic, no ordering

Figure 2.2: Change in order in a nematic liquid crystal in the crystal, nematic and isotropic phases. The orientation and size of the directors, $\hat{n}$, are shown underneath.

Going from the crystal to the nematic state, the positional order (lattice structure) is lost and the orientational order is reduced. Then from the nematic to isotropic state the remaining orientational order is lost.

The degree of order varies not just between states but also within the nematic state

itself, depending on the temperature. The degree of order is measured by the order parameter, S, and is given by the equation:

$$S = \left\langle \frac{(3\cos^2\alpha - 1)}{2} \right\rangle \tag{2.1}$$

where α is the angle between the molecules at a given instant and the director orientation $\hat{n}$ [Col90]. S will be 0 for a randomly aligned material (isotropic) and 1 if all the molecules are parallel to the director. Typical values for the order parameter start at 0.9 above the solid-nematic transition temperature down to 0.3 when the temperature has risen to just below the nematic-isotropic transition.

The ordering of the liquid crystal is local; it does not prohibit fluctuations of the director over distances much larger than the molecular dimensions. Changes of director orientation occur, typically over distances of a few microns [De Jeu80]. The distortions of the director can be described using a continuum theory with elastic coefficients determining the forces acting between neighbouring regions of liquid crystal (see section 2.3).

In figure 2.2, the director orientation is denoted by a vector but where the $\hat{n}$ and $-\hat{n}$ states are indistinguishable. If the molecules have a permanent dipole, then there are equal numbers in the two orientations and their effect cancels out. If such polar molecules are splayed then a net dipole can result (which is known as the flexoelectric effect) [dP93].

The reorientation of the director in an electric field does not come from a response by the material's permanent dipole since it has none. Instead, it occurs because of the anisotropic polarizability of the liquid crystal which results in a dielectric anisotropy, $\Delta\epsilon$. In the case of materials with a positive dielectric anisotropy, $\Delta\epsilon(= \epsilon_{||} - \epsilon_{\perp}) > 0$, the dielectric constant parallel to the director ($\epsilon_{||}$) is larger than the dielectric constant perpendicular to the director ($\epsilon_{\perp}$). The liquid crystal is then in a lower energy state when aligned to an electric field, and thus they can be aligned by one.

To wield complete control over the director orientation, it is also necessary to be able to rotate the directors away from the direction of the applied field. Fortunately, the ability to do this is easily supplied by the interaction of nematic liquid crystals and a substrate or substrates. Surfaces can be treated so that liquid crystal in contact with them will align with a defined orientation with respect to them (see section 2.4). This area of liquid crystal will then align surrounding areas thereby reducing elastic distortion.

With 2 surfaces close together and a thin layer of nematic liquid crystal between them, the aligning effect of the surfaces is sufficient to align all the liquid crystal directors parallel to the surfaces. If an electric field of sufficient strength is applied in a different direction then it can distort the director orientations but, when the field is released, the directors relax back to be parallel to the surfaces. These two effects provide a mechanism (suitable for devices) for controlling the liquid crystal orientation, but the next question is - how does this produce optical phase modulation?

Optical properties

Liquid crystals, as used in this thesis, do not, strictly, have a controllable refractive index, rather, the refractive index they present to incident light is controllable. The refractive

index change is possible is possible because the liquid crystals are birefringent. The majority of known thermotropic nematic liquid crystals, including the liquid crystals described in this thesis, are uniaxially birefringent. For a birefringent material, the effective refractive index depends on the angle of the incident light in relation to the material orientation. A more detailed description is given below starting with the optical properties of uniaxially birefringent materials and then moving on to properties specific to liquid crystals.

A uniaxially birefringent material has two refractive indices which is manifestly demonstrated by the formation of a double image of an object when observed through a birefringent material [Hec87] (although this effect would be difficult to see in the case of a liquid crystal, due to the small effect of thin layers). In fact, *birefringence* simply means doubly refracting. The refractive index that light encounters in a birefringent material is dependent on its polarisation, thus, the two images seen are in orthogonal polarisations. These two refractive indices are called the *ordinary* and *extraordinary* refractive indices.

The polarisation directions of the images are defined by the optic axis of the material (fixed relative to the director in a liquid crystal). For a positively birefringent material, the larger, extraordinary refractive index, n_e, is encountered by the polarisation which is parallel to the optic axis. If a light wave is incident on the liquid crystal travelling along the optic axis then there will be no component of polarisation parallel to the axis and only the lower, ordinary refractive index, n_o, will be encountered. These two possibilities are illustrated in figure 2.3.

Of course, the possibilities shown in figure 2.3 are 2 special cases. In general, the light can come from any angle in which case the refractive index, n_x, encountered by the polarisation which is co-planar with the optic axis is a projection of the extraordinary refractive index into the polarisation direction. This is shown in figure 2.4.

It is clear from the above discussion that the refractive index, and hence optical phase, is only being varied in one polarisation. To calculate the value of the refractive index for a particular angle of incidence, a construction can be used called the *index ellipsoid.* The index ellipsoid is a surface given by the equation [KW93]:

$$\frac{\eta^2}{n_o^2} + \frac{\xi^2}{n_o^2} + \frac{\zeta^2}{n_e^2} = 1 \tag{2.2}$$

where ζ is an axis coaxial with the director and η and ξ are axes orthogonal to ζ as illustrated in figure 2.5.

The direction of the incident light beam defines a plane which cuts through the ellipsoid forming an ellipse at their intersection. The two principal axes of this new ellipse are n_x and n_o, as is shown in figure 2.6.

The value of n_x is dependent on the angle, ϕ, between the incident ray and the director and is given by the formula [KW93]:

$$\frac{1}{n_x^2} = \frac{\sin^2\phi}{n_o^2} + \frac{\cos^2\phi}{n_e^2} \tag{2.3}$$

Liquid crystals differ from solid birefringent materials in that the orientation of liquid crystal can easily and non-mechanically be changed. It is the dependence on orientation of n_x coupled with the ability to control the liquid crystal director orientation

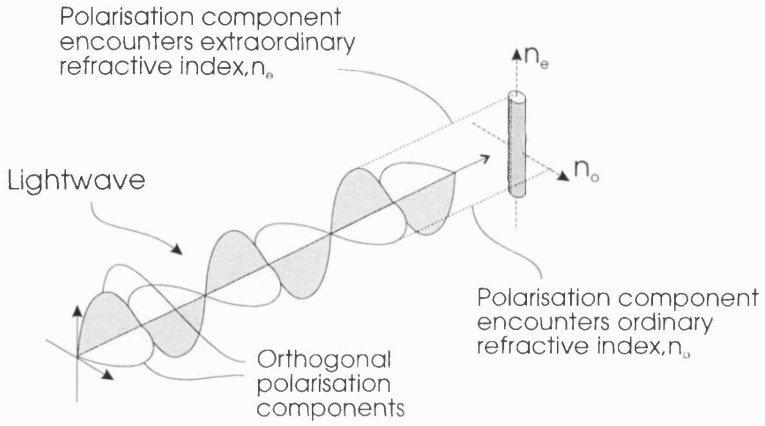

(a) Lightwave polarisations encountering extraordinary and ordinary refractive indices

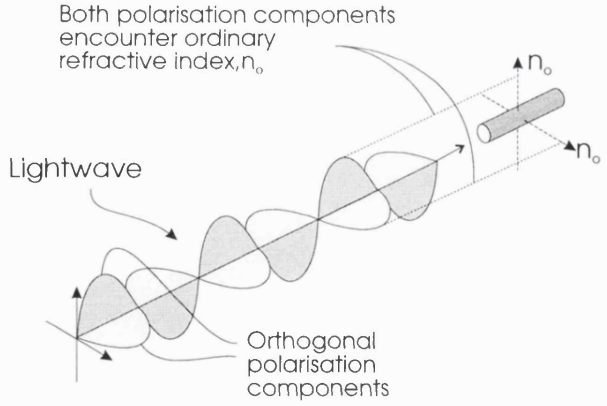

(b) Lightwave polarisations encountering ordinary refractive index only

Figure 2.3: Two possible refractive indices encountered by a lightwave depending on its angle of incidence relative to the optic axis/director

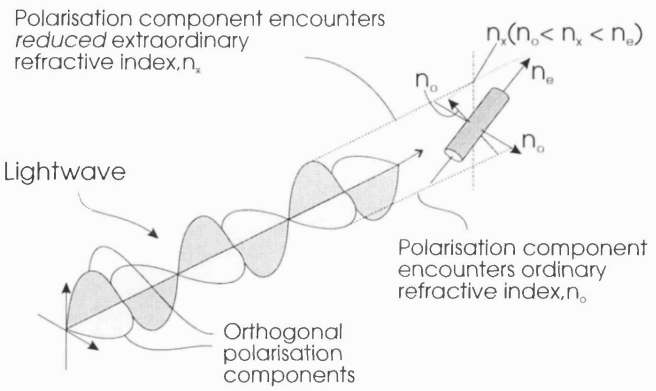

Figure 2.4: Lightwave incident from arbitrary angle encounters refractive index n_x which is between n_e and n_o.

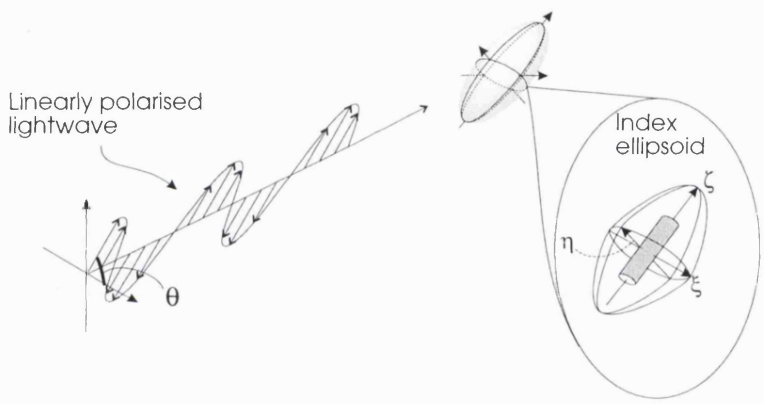

Figure 2.5: Lightwave incident from arbitrary angle upon the index ellipsoid.

which means that liquid crystal materials can be used as a controllable refractive index medium.

As mentioned previously, the liquid crystal refractive index can only be varied for one polarisation of light, the one parallel to the long axis of the ellipse, n_x. It is, therefore, up to the designer of a device for optical phase modulation to make sure the light is appropriately polarised. However, in some of the cases investigated later in this thesis, it is not practically possible to have the light polarised parallel to the n_x axis. Also, it can sometimes be instructive to arrange the polarisation otherwise to see birefringence effects. Thus, further consideration follows of the more general case.

Birefringence fringes

The incident lightwave polarisation will not in general be parallel to the n_x axis but will be at some angle θ (a linear incident polarisation is shown but the same analysis is valid for any polarisation). To calculate the effect of a uniaxial birefringent material, the lightwave is split into 2 components, one, E_x, parallel to the n_x axis and the other, E_o, parallel to the ordinary axis, n_o . These two components are then treated separately and then recombined as they leave the material. The only change between the two components is their phase difference. The phase difference between the two beams is

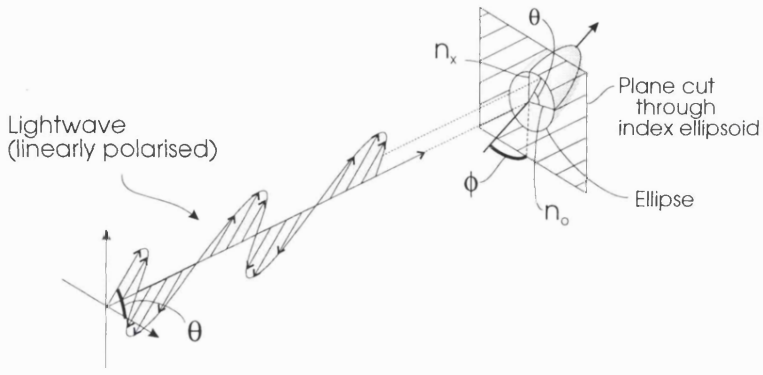

Figure 2.6: Lightwave direction defines a plane which then cuts through the index ellipsoid. There is an ellipse at the intersection of the two surfaces with principal axes n_x and n_o.

given by

$$\text{phase difference} = \frac{2\pi(n_x - n_o)d}{\lambda} \tag{2.4}$$

where d is the thickness of the material and λ is the wavelength of the light. The resultant lightwave then includes a term for this phase difference:

$$E_{Resultant} = E_o e^{i(kz-\omega t)} + E_x e^{i(kz-\omega t+\frac{2\pi(n_x-n_o)d}{\lambda})} \tag{2.5}$$

This equation represents a new polarisation which is not necessarily linear, and is, in fact, in general elliptical. There are a couple of special cases worth mention. If the phase difference is π (i.e. a half wavelength) then the resultant polarisation will be linear (assuming linear incident polarisation) but at a new angle rotated from the original polarisation by twice the angle between the incident polarisation and either of the ellipse axes. Birefringent materials are often fabricated to meet this specification and are called *half waveplates*. The second special case worthy of note is the when the phase difference is $\frac{\pi}{2}$ which produces circularly polarised light (if $\theta = 45°$). Such a configuration is often called a *quarter waveplate*.

To convert the change to an intensity modulation (in order for an observer to see the effect), a polariser (often called the analyser to distinguish it from the input polariser) has to be introduced after the liquid crystal layer, as is shown in figure 2.7.

With a polariser in place, the intensity of the light, I, will then vary according to *theta*, the angle of the ordinary axis to the input polarisation orientation, and χ, the angle between the polariser and the input polarisation orientation [BW80]:

$$I = I_o\left(\cos^2\chi - \sin 2\theta \sin 2(\theta-\chi)\sin^2\left[\frac{\pi(n_x-n_o)d}{\lambda}\right]\right) \tag{2.6}$$

where I_o is the intensity of the original input beam, polarised at θ.

Due to the dependence of the intensity on the material thickness, d, and refractive index, n_x, interference fringes will be observed if either of these quantities vary across

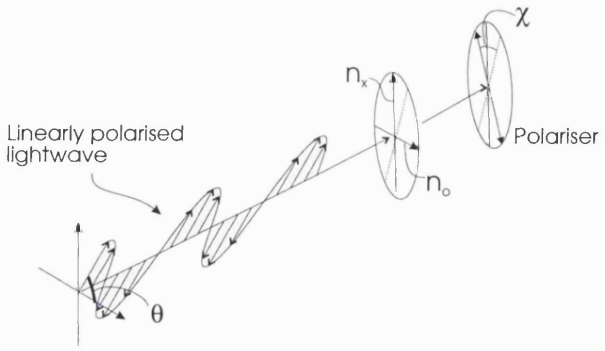

Figure 2.7: Introducing a polariser after the liquid crystal in order to see the effect of the polarisation change.

the sample, provided that the input polarisation is not parallel to either n_o or n_x ($\theta \neq \frac{m\pi}{2}$where $m = 0, 1, 2...$). These fringes are called *birefringence fringes.*

In the above calculations, the optic axis orientation was assumed to be uniform through the thickness of the sample (or rather along the path of the light). For liquid crystals, however, it is common for the director orientation (and hence the optic axis) to vary through the sample. Often a liquid crystal cell will be produced so as to induce a twist of the liquid crystal. This situation is considered below.

Twisted nematics

If there is a distortion of the director whereby it rotates towards or away from the light propagation direction (*i.e.* in figure 2.6, ϕ varies through the cell) then the effect is simply a reduction or increase of birefringence. If, however, director twists around the propagation direction, then the calculation is significantly more complex. The resulting affect on the transmitted light depends on the rate at which the director twists. The rate of twist is defined by the *pitch*, p, which is distance required for one complete revolution (360°) of the director. If the pitch is equal to the wavelength then one circular polarisation will be reflected and the other transmitted. The liquid crystals which do this called *cholesterics* and will not be further discussed here. The regime relevant to this work is the *Mauguin limit.* The Mauguin limit is defined the region where the wavelength is much less than the pitch-birefringence product, i.e. [dP93]:

$$\lambda \ll p(n_x - n_o) \tag{2.7}$$

In this regime, the polarisation components are guided by the liquid crystal following the twist. The two components still emerge with a phase difference as in equation 2.4 thus, in general, the emerging polarisation will be elliptical. However, if linearly polarised light is incident parallel to either n_x or n_o then it will emerge still linearly polarised but rotated by the same angle as the twist.

2.2.2 Ferroelectric liquid crystals

Ferroelectric liquid crystals have been used for optical phase modulation for a number of years since they are commonly used in spatial light modulators (SLM's). These

ferroelectric liquid crystals have a permanent dipole (unlike the nematics described previously). They became popular after the invention of a configuration called the *surface stabilised ferroelectric liquid crystal* or *bookshelf geometry* [KW93] which enabled displays to be fabricated using ferroelectrics. The interest is in part caused by faster switching times of this configuration as compared to twisted nematics. A liquid crystal display (LCD) using a ferroelectric can have switching times between 1-1000 times faster than a nematic LCD [Col90].

The speed of the ferroelectrics is much more attractive for phase modulation devices where it is not simply the human eye which determines the desired speed. The drawback of ferroelectrics, both for LCDs and for phase modulation is that they are binary.

The ferroelectrics used in the surface stabilised configuration are in the *smectic C** phase, different from the nematic phase described in the previous section. The smectic C phase is one of a group of phases known as *smectics*.

Smectics are distinguished from nematics in that they are more ordered. Whereas nematic liquid crystals have only orientational ordering, smectics are orientationally ordered and positionally ordered as well. The smectic C phase is ordered in layers with the orientation inclined to the layers (see figure 2.8).

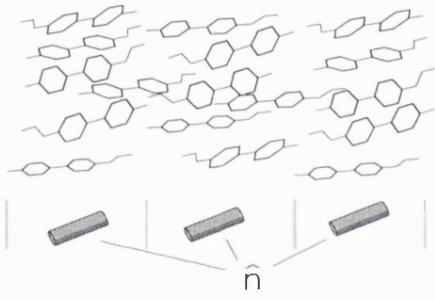

Figure 2.8: Three layers of the smectic phase with their directors, $\hat{n}$, shown underneath

The phase used in the devices is the smectic C* phase, a modification of the smectic C phase. The '*' is there to indicate that a chiral dopant has been added to the material. The chiral dopant has the effect of causing the director to rotate around the normal to the layers such that the directors follow a helix as shown in figure 2.9.

Figure 2.9: Smectic C* phase, its directors rotating around following a helix

To produce the surface stabilised configuration, the smectic C* liquid crystal is placed between two narrowly separated glass substrates. As with the nematic, the smectic liquid crystal is aligned by the surfaces such that it lies parallel to them, however, this is clearly not compatible with the helical rotation of the director. The result is that the liquid crystal can lie in two positions, the two orientations which are parallel to the surfaces, and still lie on the cone of orientations which follow the helix (see figure 2.10).

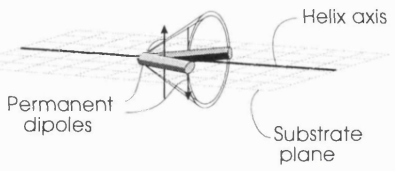

Figure 2.10: Director's cone of orientation restricted to 2 orientations

As can be seen from the figure, the permanent dipoles are orientated perpendicular to the director and, in the surface stabilised configuration, perpendicular to the substrates. This provides a mechanism for switching between the two states, since the dipole will orientate towards an applied field. Thus, a DC field will switch the directors.

The explanation above shows that the structures are bistable and hence the display is binary. It only remains to describe how the switching produces an optical phase change.

Modulation of light

The devices are optimised for amplitude modulation, i.e. as used in displays, and this use will be described first. The devices depend on the rotation of polarisation due to the liquid crystal birefringence. As with the nematic devices described previously, the ferroelectric liquid crystal is uniaxially birefringent. The device is set-up (through the choice of cell thickness and material birefringence) such that normally incident light with its polarisation vector at 45° to the director, will result in an output polarisation rotated by 90° to the input. The director is at an angle (called the *cone angle*, figure 2.10) of ideally 22.5° (the angle depends on temperature) to the helix axis such that by switching the liquid crystal, the director rotates through 45°. Thus, if the director started at 45° to the incident polarisation then, after switching, it will be at 0° or 90°. In both cases, the liquid crystal will have no affect on the light polarisation direction.

For phase modulation, the polarisers are in a different configuration. To achieve phase modulation, the configuration uses the fact that one rotation of a linear polarisation through 180° is equivalent to a phase change of 180° (or π). The polarisers are crossed, with the input polariser parallel to the helix axis. In this configuration, either of the director orientations will alter the resultant polarisation of the output. Both polarisations will be elliptical but with the major ellipse axes tilted in opposite directions away from the original input. The 2nd polariser then cuts out the component parallel to the input but leaves the two possible orthogonal components, which are π out of phase with each other. The device reduces the intensity of the two components by an equal factor depending on the cone angle and the optical retardation [BNPY92]. The device is inherently binary which renders it unsuitable for continuously variable optics.

Deformed helix ferroelectrics

An adaptation of the surface stabilised configuration, which can produce multi-level phase is called the *deformed helix ferroelectric*. This is basically the same configuration but with weaker surface alignment and a much smaller pitch. The result of these changes is that, with no voltage applied, the helix is unaffected by the surfaces [FS89]. As the voltage is applied, however, the helix unwinds so that, at a critical voltage, it has the same structure as the surface stabilised configuration.

Optically, the difference between the wound and unwound helix is a difference of birefringence. The helix is wound tight enough that it is not resolved by the light and, thus, encounters the average birefringence. This average birefringence varies with the unwinding of the helix. Using this configuration, beam-steerers and tunable wavelength filters have been demonstrated [WVO+92, CDC96].

It is difficult to get good quality alignment in deformed helix ferroelectrics and this has stopped the widespread application of this configuration in devices [KW93].

2.2.3 Polymer dispersed liquid crystal

Another liquid crystal arrangement which is used in displays is *polymer dispersed liquid crystal* (PDLC). This also can be modified for use as part of an adaptive optical phase element [TNS+95]. PDLC has the advantages of being faster than nematics and insensitive to the light polarisation.

PDLC is not a new phase like smectic or nematic, simply a different way of packaging the liquid crystal. The liquid crystal part of the devices described below are, in fact, nematics.

Conventionally, PDLC devices are made as electrically controllable scatterers [Mer92a]. The scattering is due to the refractive index difference between a liquid crystal and the surrounding matrix of polymer as illustrated in figure 2.11. The liquid crystal droplets are randomly orientated (though within each droplet there may be an ordered structure) without any electric field. When a field is applied, the liquid crystal directors rotate towards it such that they present a uniform refractive index to the incident light. If this refractive index is the same as the surrounding polymer then the medium is optically homogeneous and transmits light.

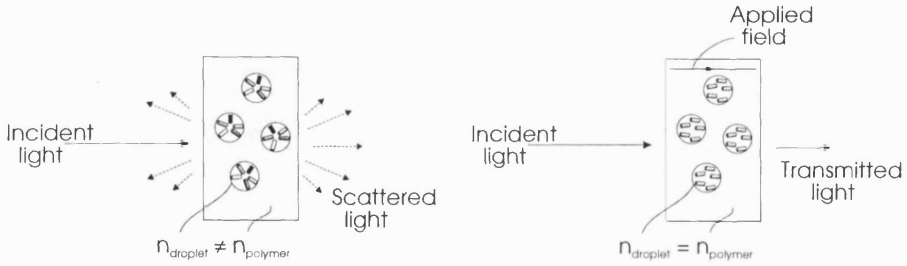

(a) The liquid crystal crystal refractive index, with its randomly ordered directors between droplets, is different from the surrounding polymer, thus the droplets scatter light

(b) With a field applied the liquid crystal droplets are uniformly aligned and so for the normally incident light there is no refractive index difference between droplet and polymer

Figure 2.11: PDLC arranged as an electrically controllable scatterer

PDLC's thus have applications in displays and as light shutters for privacy or daylight control [MLES91]. However, they can also be used to give phase modulation, for example to create a switchable selective reflector using a Bragg grating [KKTS97]. This is achieved by using smaller droplets ($0.1\mu m$ instead of $2 - 4\mu m$).

In either display or phase modulation devices, the droplets can be produced optically. The basic mechanism of formation is as follows: UV curable monomer and liquid crystal are mixed together in the desired ratio, then the monomer is UV cured so that it forms a polymer. The liquid crystal is not soluble in the polymer, unlike the monomer, and so

as the polymer is created, the liquid crystal comes out, forming droplets. The droplet size is determined by the rate of polymerisation, the relative concentrations of materials and the materials used [DGW+88]. A faster cure gives smaller droplets. In the case of the Bragg grating mentioned above, an Ar^+ laser was used for curing which was split into two and interferred in the monomer to create the grating structure.

Sutherland *et al* have fabricated holograms and diffractive optical elements with PDLC [TNS+95]. These they fabricated using a pre-polymer suitable for a high resolution optical recording [SNTB93], however, since the material was optimised for high spatial frequencies (due to the diffusion/polymerisation process) they needed to add a high spatial frequency where there were only lower low frequencies present (eg. a diffractive lens) [DCG+96].

2.3 Modelling of nematic liquid crystal

2.3.1 Deuling's analysis

Models of liquid crystal devices have been developed based on the continuum theory of liquid crystals (for example see references [Ber83], [Deu72] and [DFDD96]). These models deal with varying degrees of complexity from 1-D untwisted structures to 3-D time resolved structures. The continuum theory does not deal with individual molecules but instead treats the liquid crystal as an elastic continuous medium. Because the liquid crystal is anisotropic, the elastic coefficients are as well. Distortions are commonly dealt with in terms of three elastic coefficients for splay, twist and bend (see figure 2.12).

(a) Splay, k_{11} (b) Twist, k_{22} (c) Bend, k_{33}

Figure 2.12: The three director deformations with their corresponding elastic coefficients

However, the work reported here is designed to use untwisted nematic structures and thus fortunately the model is simpler. A model of the deformation of the nematic liquid crystal due to an electric field (in 1 dimension) has been developed by Deuling [Deu72] and is presented here.

The liquid crystal is described by its director, $\hat{n}$, as a function of position, $\underline{r}$. The liquid crystal is assumed to be contained in a cell of two parallel substrates separated by a distance d; the axis normal to the substrates is defined as the z axis with liquid crystal/substrate interfaces being located at $z = 0$ and $z = d$. The liquid crystal is aligned homogeneously, *i.e.* the molecules lie in the plane of the cell with no field applied, and the tilt, ϕ, of the liquid crystals refers to the angle of the director with respect to this plane.

The equilibrium liquid crystal tilt profile will occur when the free energy is minimised. The expression for the additional free energy (due to the distortion of the crystal structure) at any point $\underline{r}$ is:

$$\Delta F = \frac{1}{2}\Big\{k_{11}[\nabla.\hat{n}(\underline{r})]^2 + k_{22}[\hat{n}(\underline{r}).\nabla \wedge \hat{n}(\underline{r})]^2 + k_{33}[\hat{n}(\underline{r}) \wedge \nabla \wedge \hat{n}(\underline{r})]^2 - \underline{D}.\underline{E} - \underline{H}.\underline{B}\Big\} \tag{2.8}$$

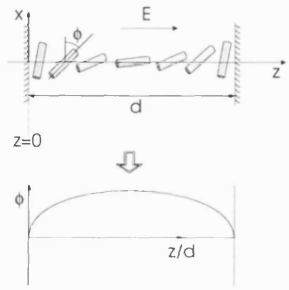

Figure 2.13: Parameters used to describe liquid cell in the model

where k_{11}, k_{22}, k_{33} are the splay, twist and bend elastic coefficients respectively and $\hat{n}$ is the liquid crystal director.

In this case the molecules all lie in the x, z plane (z being the direction through the cell and x being one of the axes in the cell (the rubbing direction). There is no twist so the k_{22} term is zero.

$$[\hat{n}(\underline{r}).\nabla \wedge \hat{n}(\underline{r})]^2 = 0 \tag{2.9}$$

Also $\frac{\partial}{\partial x}, \frac{\partial}{\partial y} = 0$ (defining ϕ to be the tilt angle of the molecules out of the x, y plane)

$$\hat{n} = L_x\underline{x} + L_z\underline{z}, \text{ where } L_x = \cos\phi, \; L_z = \sin\phi \tag{2.10}$$

so that

$$[\nabla.\hat{n}(\underline{r})]^2 = \cos^2\phi\Big(\frac{d\phi}{dz}\Big)^2 \tag{2.11}$$

and

$$[\hat{n}(\underline{r}) \wedge \nabla \wedge \hat{n}(\underline{r})]^2 = \sin^2\phi\Big(\frac{d\phi}{dz}\Big)^2 \tag{2.12}$$

There is no magnetic field applied so the $\underline{H}.\underline{B}$ term is zero. The $\underline{D}.\underline{E}$ term is equal to $E_z D_z$ but since the liquid crystal is dielectrically anisotropic E_z depends on the tilt of the liquid crystal molecules. With the electrodes on the substrate surfaces

$$\underline{D} = D_z\underline{z} \tag{2.13}$$

and

$$D_z = \epsilon_o E_z(\epsilon_{\|}\sin^2\phi + \epsilon_{\perp}\cos^2\phi) \tag{2.14}$$

$$= \epsilon_o\epsilon_{\perp}E_z(1 + \gamma\sin^2\phi) \tag{2.15}$$

where $\gamma = \frac{\epsilon_{\|}-\epsilon_{\perp}}{\epsilon_{\perp}} = \frac{\Delta\epsilon}{\epsilon_{\perp}}$

Substituting these equations into the free energy equation and integrating over the whole cell, we get:

$$\Delta F = \int_V \Delta F dV \tag{2.16}$$

$$= \frac{A}{2}\int_o^d \left(k_{11}\cos^2\phi\left(\frac{d\phi}{dz}\right)^2 + k_{33}\sin^2\phi\left(\frac{d\phi}{dz}\right)^2 - \epsilon_o\epsilon_\perp E_z^2(1+\gamma\sin^2\phi\right)dz \tag{2.17}$$

The Euler-Lagrange theorem states that for an integral I of a function G:

$$I = \int_a^b G(y(x), \frac{dy(x)}{dx}, x)dx \tag{2.18}$$

the integral will be minimised when

$$\frac{\partial G}{\partial y} - \frac{d}{dx}\left(\frac{\partial G}{\partial(\frac{dy}{dx})}\right) = 0 \tag{2.19}$$

This equation can be very useful when the integral, I, gives the total energy of a system, as then the 'minimum' of the integral is also the equilibrium condition. Thus, the equation for the minimisation of free energy is:

$$\frac{\partial(\Delta F)}{\partial\phi} - \frac{d}{dz}\left(\frac{\partial(\Delta F)}{\partial(\frac{d\phi}{dz})}\right) = 0 \tag{2.20}$$

where ΔF is:

$$k_{11}\cos^2\phi\left(\frac{d\phi}{dz}\right)^2 + k_{33}\sin^2\phi\left(\frac{d\phi}{dz}\right)^2 - \epsilon_o\epsilon_\perp E_z^2(1+\gamma\sin^2\phi) \tag{2.21}$$

Substituting in this expression, the equation becomes

$$2(k_{33}\sin^2\phi + k_{11}\cos^2\phi)\frac{d^2\phi}{dz^2} + 2(k_{33}-k_{11})\sin\phi\cos\phi\left(\frac{d\phi}{dz}\right)^2 = -2\gamma\epsilon_o\epsilon_\perp E_z^2\sin\phi\cos\phi \tag{2.22}$$

multiplying by a $\frac{d\phi}{dz}$ integrating factor and rearranging:

$$\frac{d}{dz}(k_{11}(1+\kappa\sin^2\phi)\left(\frac{d\phi}{dz}\right)^2) = \frac{d}{dz}(\frac{\gamma D_z^2}{\epsilon_o\epsilon_\perp(1+\gamma\sin^2\phi)^2}) \tag{2.23}$$

where $\kappa = \frac{k_{33}-k_{11}}{k_{11}}$.

Thus, integrating gives

$$k_{11}(1+\kappa\sin^2\phi)\Big(\frac{d\phi}{dz}\Big)^2 = \frac{D_z^2}{\epsilon_o\epsilon_\perp(1+\gamma\sin^2\phi)^2} + C \tag{2.24}$$

where C is the constant of integration and from the boundary condition $\phi = \phi_{max}$, $\frac{d\phi}{dz} = 0$ (ϕ_{max} being the maximum tilt angle)

$$C = \frac{-D_z^2}{k_{11}\epsilon_o\epsilon_\perp(1+\gamma\sin^2\phi)^2} \tag{2.25}$$

Equation 2.24 can then be rearranged to give an expression describing the gradient of the tilt through the cell:

$$\frac{d\phi}{dz} = \pm D_z\sqrt{\frac{\gamma}{\epsilon_o\epsilon_\perp k_{11}}}\sqrt{\frac{sin^2\phi_{max} - \sin^2\phi}{(1+\kappa\sin^2\phi)(1+\gamma\sin^2\phi)(1+\gamma\sin^2\phi_{max})}} \tag{2.26}$$

Rearranging and integrating (taking the positive case)

$$z = \int_0^z dz \tag{2.27}$$

$$= \frac{1}{D_z}\sqrt{\frac{\epsilon_o\epsilon_\perp k_{11}}{\gamma}}\sqrt{(1+\gamma\sin^2\phi_{max})}\int_{\phi_o}^{\phi}\sqrt{\frac{(1+\kappa\sin^2\phi)(1+\gamma\sin^2\phi)}{\sin^2\phi_{max} - \sin^2\phi}}d\phi \tag{2.28}$$

where ϕ_o is the pretilt on one of the substrates.

In the case where cell is symmetric, *i.e.* the pretilts on both substrates are equal, then the maximum tilt angle will occur at the centre of the cell: $\phi = \phi_{max}$ at $z = \frac{d}{2}$ so for this case the solution can be normalised:

$$\frac{z}{\left(\frac{d}{2}\right)} = \frac{\int_{\phi_o}^{\phi}\sqrt{\frac{(1+\kappa\sin^2\phi)(1+\gamma\sin^2\phi)}{\sin^2\phi_{max}-\sin^2\phi}}d\phi}{\int_{\phi_o}^{\phi_{max}}\sqrt{\frac{(1+\kappa\sin^2\phi)(1+\gamma\sin^2\phi)}{\sin^2\phi_{max}-\sin^2\phi}}d\phi} \tag{2.29}$$

This is a more convenient solution than equation 2.28 since the integrals must be calculated numerically many times to give a tilt profile ($\phi(z)$ is desired, not $z(\phi)$), this requires less computing time.

This is where Deuling finished his calculation of the tilt profile, but this still leaves his calculation of $\phi_{max}(V)$. The voltage is calculated from:

$$V = \int_l \underline{E}.\underline{dl} = \int_0^d E_z dz \tag{2.30}$$

From equation 2.15 we can substitute:

$$dz = \pm\frac{1}{D_z}\sqrt{\frac{\epsilon_o\epsilon_\perp k_{11}}{\gamma}}\sqrt{\frac{(1+\kappa\sin^2\phi)(1+\gamma\sin^2\phi)(1+\gamma\sin^2\phi_{max})}{\sin^2\phi_{max}-\sin^2\phi}}d\phi \tag{2.31}$$

and from equation 2.28

$$E_z = \frac{D_z}{\epsilon_o\epsilon_\perp}\frac{1}{(1+\gamma\sin^2\phi)} \tag{2.32}$$

we get

$$V = 2\int_{\phi_o}^{\phi_{max}}\frac{1}{\epsilon_o\epsilon_\perp(1+\gamma\sin^2\phi)}\sqrt{\frac{\epsilon_o\epsilon_\perp k_{11}}{\gamma}}\sqrt{\frac{(1+\kappa\sin^2\phi)(1+\gamma\sin^2\phi)(1+\sin^2\phi_{max})}{\sin^2\phi_{max}-\sin^2\phi}}d\phi \tag{2.33}$$

From this result we have the, perhaps, surprising conclusion that the maximum tilt angle and hence the tilt profile is independent of the cell thickness, d. The physical reason for the liquid crystal's voltage response being independent of cell thickness can be understood by considering a region of liquid crystal somewhere in the middle of the cell. If the cell thickness is increased, then there are two effects: the electric field is reduced (assuming a constant voltage) and the elastic restoring force from the cell walls (transmitted through the intervening liquid crystal) is also reduced. Thus, the physical meaning of the above equations is that the two effects are balanced and the liquid crystal response is independent of the cell thickness. This means, that for defined pretilts and incident light angle, we can draw a graph of refractive index vs voltage (eg. see figure 4.6).

Finite Elements

Another modelling technique has been developed for liquid crystal devices using Finite Element methods, by Fabrizio Di Pasquale. The theory and results from F. Di Pasquale's work will be outlined in the chapter 7.

2.4 Alignment layers

2.4.1 Alignment types

In most liquid crystal devices, it is necessary to align the liquid crystal uniformly and in a defined direction without the application of an electric or magnetic field. An aligning force defines the off-state of a device and returns the liquid crystal to that state after an applied field is removed.

There are two basic types of liquid crystal alignment: *homeotropic* and *homogeneous.* Homeotropic alignment is where the molecules are normal to the cell wall, as shown figure 2.14a. Homogeneous alignment is where the molecules lie in the plane of the cell, as in figure 2.14b.

It is the properties at the surface which are set and this induces the desired structure in the bulk. A twisted structure is achieved by orientating two homogeneously aligning substrates such that the directors on the two surfaces will be at an angle to each other.

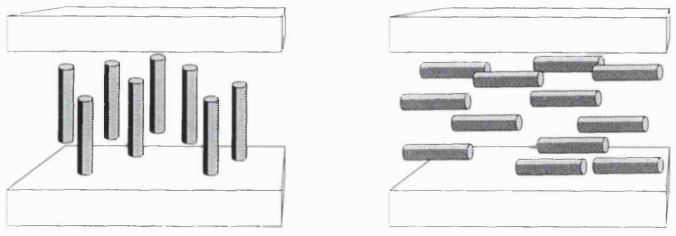

(a) Homeotropic (b) Homogeneous

Figure 2.14: Two alignment types; homeotropic, normal to the cell, and homogeneous, in the plane of the cell

For most, if not all, devices requiring a homogeneous alignment, it is not sufficient that the director be in the plane of the cell, since this allows for any orientation in the plane. Devices generally require that the alignment is in a defined direction in the plane, with the directionality being uniform across the device.

2.4.2 Pre-tilt

Pre-tilt is the angle of the director on the surfaces to the plane of the cell in the absence of any electric or magnetic field. For many applications, a pre-tilt is required due to the way the liquid crystal interacts with an applied electric (or magnetic) field. The (nematic) liquid crystals used are non-polar, the dielectric anisotropy causes the liquid crystal to reorientate, thus there is no preferred orientation with respect to the electric field. This means that if a liquid crystal cell were aligned perfectly parallel to the substrates (and normal to the electric field) the liquid crystal could turn one of two ways towards the electric field. Over a cell it is likely that different regions would turn different ways creating *walls* (rapid variations in the crystal structure, see figure 2.15 and section 2.4.4).

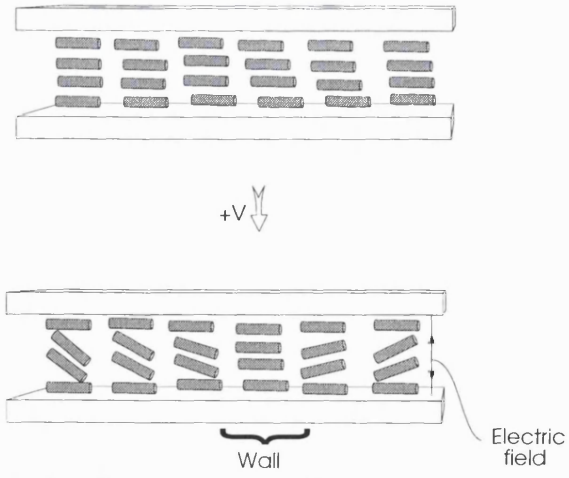

Figure 2.15: Liquid crystal wall structure caused between 2 regions which have rotated in the opposite direction when electric field was applied

To avoid the formation of walls it is desirable that the liquid crystal already be inclined slightly to the electric field (*i.e.* it has a pre-tilt). This will occur if, at the

surfaces, the liquid crystal is at an angle before the electric field is actually applied. The direction which the molecules stick up from the surface needs to be defined so that the molecules at both surfaces are parallel (see figure 2.16).

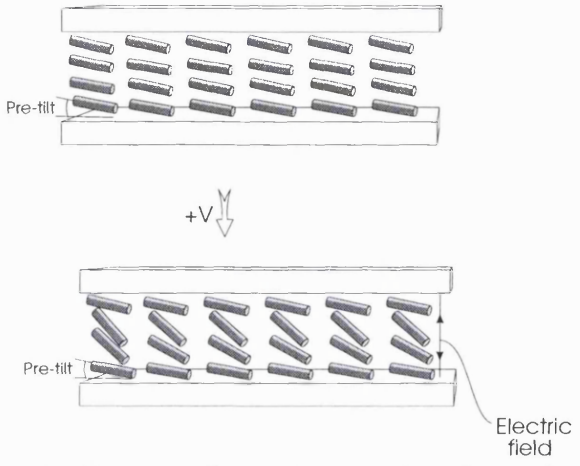

Figure 2.16: Uniform pre-tilt avoids walls when electric field applied

Pre-tilt can also be important in twisted structures used in twisted nematic (TN) displays. In a 90° twisted structure there can be a degeneracy, a left handed or right handed twist will both meet the boundary conditions. However, if both surfaces have an equal pre-tilt, then it can be arranged that one handedness will result in zero splay whilst the other will not, thus favouring the unsplayed handedness. In a display, this approach would be used in conjunction with a chiral dopant.

2.4.3 Methods of alignment

All the types of alignment discussed here (bar one) are induced by treatment of the surfaces of the substrates. The surfaces align the liquid crystal in contact with the surface which is sufficient in a thin liquid crystal layer ($\lesssim 200\mu m$ [De Jeu80]) to align the whole layer.

Surface relief

It has been shown that uni-directional microgrooves on a surface will induce liquid crystal alignment. This was predicted by showing that alignment minimises the elastic energy of the liquid crystal. The approach was suggested and demonstrated by Berreman [Ber73] using polishing cloths (or leather laps) with polishing materials such as diamond paste, cerium oxide and jeweler's rouge. In fact, the polishing powders are not always necessary - the rubbing can be achieved with paper or tissues but the powders are required if the substrate material is hard (eg Silica or fluoride). A photoresist layer can be used if a softer substrate is desired [WGK73] and this also suggests the option of creating the microgrooves photolithographically by exposing a grating. However, if the topography of the surface is to dominate the aligning process, the period of the grating must be of submicron pitch [CB79]. Alignment still occurs in larger pitch grooves but it is dominated by flow alignment. In fact, flow is a possible method of alignment [PBJ66], however the reproducibility is not good. An additional consideration in using a grating

is that a grating will diffract light, needless to say, a potential problem in an optical device.

Berreman also reported that the geometrical alignment due to the grooves competes with molecular aligning techniques (which will be described in the following sections). For a surface profile $z = A \sin qx$ (period of surface $\lambda = \frac{2\pi}{q}$) the interaction energy, U, is given by [Cog82]

$$U = \frac{K}{4} A^2 q^3 \tag{2.34}$$

where K is the elastic constant of the liquid crystal (*i.e.* approximating the splay, twist and bend elastic constants to all be equal). For example, for an alignment energy of $1 \times 10^{-5} J/m^2$ with a pitch, λ, of $0.1\mu m$ and an elastic constant of $10^{-11} N$ a depth of $4 \times 10^{-3} \mu m$ is required. If the pitch of the grating is lengthened to $1\mu m$ the required grating depth is $0.13\mu m$. For comparison, alignment energies for various techniques are given in table 2.1. These energies are all for the alignment in the plane, *i.e.* the energy required to rotate the director around on the substrate rather than to pull it away.

Technique	**Liquid Crystal**	**Energy** (J/m^2)	**Reference**
Rubbed Polyimide	GR41	$7 \times 10^{-6} \rightarrow 1 \times 10^{-4}$	[LVMU93]
Rubbed PVA	GR41	$1 \times 10^{-6} \rightarrow 1 \times 10^{-5}$	[SSU92]
Rubbed Polyimide	5CB	$0.5 \times 10^{-4} \rightarrow 1 \times 10^{-4}$	[SKS+90]
Rubbed Polyimide	5CB	$1 \times 10^{-5} \rightarrow 1 \times 10^{-4}$	[RXM+95]
Rubbed Glass	MBBA	7×10^{-6}	[KW73]
SiO_x evap. 60°	5CB (at 30°C)	2×10^{-5}	[IKK95]
Fluorinated polyvinyl-cinnamate	5CB	2×10^{-6}	[AKR+98]
Stacked Polyimide Langmuir-Blogett film	5CB	$2 \times 10^{-6} \rightarrow 1 \times 10^{-5}$	[IAA+95]

Table 2.1: In-plane (torsion) anchoring energies associated with various alignment techniques

A different and also widely used aligning technique is the oblique deposition of Silicon Oxide (SiO_x)[Jan72]. Again, it is the topology of the surface which is important. The oblique deposition results in a sawtooth structure in the silicon. This produces good alignment with reliability and so is used in some small displays (eg. digital watches). However, it is not so good over larger displays and requires a flat and uniform substrate[Cog82].

Another recently reported process which generate aligning surface structures is the stripped film method [KM97]. The method involves creating a sandwich of polyimide and PVA on the glass substrate and then peeling off the PVA layer, leaving behind a thin layer of polyimide. Although pre-tilt was reported control over the angle was limited. The alignment quality is described as 'fairly good'.

Alignment by rubbing

Rubbing is one of the most successful alignment techniques even though it has some inherent problems [Sch93]. Rubbed alignment is used in laptop computer displays despite the fact that the rubbing process can damage the display by generating dust particles and electrostatic charge. The advantage of the rubbing technique is that it can generate uniform alignment and pre-tilt over a large area.

A polymer layer which has been rubbed can produce excellent alignment and has been used since its discovery in 1911 [Mau91]. Since these layers are soft, only cloth is required to rub them. The polymers layers should ideally be thin to improve uniformity and often they are spun onto the substrate to achieve reproducible results. Polyvinyl Alcohol and Polyimide are two polymers which have been recommended [Cog82] as aligning agents due to their widespread successful use.

The mechanisms involved in the rubbing method of liquid crystal alignment are not well understood. It has recently been shown that the surface polymers are aligned by the rubbing process (at least for polyimide) [TRL+95] and it is reasonable to conjecture that this polymer alignment will cause alignment in the liquid crystal. It is difficult to separate this mechanism from the one proposed by Berreman since the rubbing procedure is likely to cause microgrooves [Kah82], however, other papers [LSU93, KLY95] suggest that the aligned polymers are the more dominant effect. Also poorly understood are the mechanisms affecting pre-tilt and surface anchoring strength. It is known that the rubbing strength and polymer concentrations used can significantly affect the anchoring strength and pre-tilt angle [KFM+88, SKN92, SK92] with stronger rubbing producing stronger anchoring but also an exponential increase in fibres left on the rubbed polymer [WHO+97]. An expression for the rubbing strength has been proposed by Seo *et al* [SKN92]:

$$RS = NM\left(\frac{2\pi rn}{v} - 1\right) \tag{2.35}$$

where N is the number of repeated times for the rubbing, M is the depth of the deformed fibres of the cloth due to the pressed contact, n is the rotation rate of the drum, v is the translating speed of the substrate and r is the radius of the drum. Seo *et al* found that rubbing would start to have an effect for a rubbing strength of 60mm whilst a strong rubbing strength was about 500mm.

Photoalignment

It has been shown that it is possible to have a 'programmable' alignment layer using a silicone polyimide copolymer doped with a dichroic dye. The dye orientates depending on the polarisation direction of incident light which reorientates the surrounding alignment layer [GSSS94]. This raises the possibility of a display which can be written and read optically and may be rewritten. The same effect has also been demonstrated with dye doped PVA [IiKK+93].

These photosensitive aligning agents have been demonstrated as the basis for liquid crystal gratings [GS94] and re-writeable holograms [CB93]. Also, it is possible to use the same techniques with liquid crystal monomers which can then be polymerised preserving

the alignment directions [SGS94] and thus any holograms recorded will be unaffected by further exposure.

Another similar technique, linear photopolymerization, was first demonstrated in 1992 by Schadt *et al* [SSKC92]. Instead of using a guest-host aligning layer, this method relies on linear polymerization of the alignment layer (polyvinylmethylcinnamate-PVMC) and, thus, is not reversible (unlike the guest-host system). Again, polarised light is used, this time it is polarised UV which defines the final alignment direction, perpendicular to the light polarisation. The technique has a few drawbacks in that it has low thermal stability (alignment lost after prolonged exposures at temperatures approaching $100°C$ [WWLK95]) and does not produce pre-tilt. A modified technique using 2 exposures has been demonstrated [HSK+95], however, only pretilts of 0.30° were generated. The out-of-plane anchoring energies for the polyvinylcinnamate are 2 orders of magnitude less than those for rubbed polymer samples [BBS96] and it seems reasonable to conjecture that the in-plane energies will be similarly smaller. More recently, a fluorinated polyvinylcinnamate photoalignment layer has been demonstrated [AKR+98] which, when polymerised in a magnetic field, gave a pre-tilted alignment. However, the in-plane anchoring energy was weak ($2 \times 10^{-6} J/m^2$) and only pre-tilts of $(15-25)°$ were demonstrated.

Originally, the linear photopolymerization technique was demonstrated using monomer (PVMC) spun onto the substrate but it has subsequently been shown that the same effect can be achieved with the monomer in a mixture with the liquid crystal used in the device[JK94]. This has the property that the alignment is not surface induced but it is bulk induced alignment.

As with the guest host method, it has since been demonstrated that liquid crystalline polymers can be fabricated [SSSK95a] which have the property of being (optically patternable) retarders. This technology can be integrated with a liquid crystal layer to make displays [SSSK95b], in particular a super twisted nematic (STN) configuration which is compensated for the interference colours which otherwise occur off-axis (*i.e.* replacing the optical compensation layers which would be used in an STN device).

Alternate photoalignment materials that have been investigated are Langmuir-Blodgett films [SSK+93] which demonstrated alignment but of poor quality [AMIY95] and polyimide [CJB+96, WWLK95] which is a strong aligning layer but requires long exposure times and there are no reports of pre-tilt. A promising photoalignment material is polysiloxane which can generate stable pre-tilted alignment [YPP+97]. The required baking of $\sim 200°$ may cause problems for other material (eg photoresist) and it is not clear how much control of the pre-tilt angle is possible.

Homeotropic alignment

The homeotropic alignment of liquid crystals has found far fewer applications to date than homogenous alignment. The earliest way discovered to achieve homeotropic alignment on glass is to clean it in acid, more recently, however, it is achieved using surfactants [Cog82]. One of the most commonly used agents is lecithin which is comprised of a polar group which attaches to the glass surface and a long aliphatic chain to which the liquid crystal molecules couple.

If the substrate can be processed to be smooth or coated with a smooth polymer or oxide layer this will result in homogeneous alignment but, in general, the alignment is

not uniform [Cog82].

Jain and Kitzerow have demonstrated that it is possible to achieve homeotropic alignment with photopolymerisation if the photopolymer is mixed with the liquid crystal and is just above the nematic to isotropic transition temperature [JK94] when polymerised.

2.4.4 Walls and defects

Definitions

A wall defect is simply a distortion of the director field which forms between regions of different orientations. The wall appears when an external force (eg. a magnetic or electric field) acts on two regions, accentuating an orientation difference between them and compressing the distortion, as is shown in figure 2.15.A wall is not a crystallographic defect in the liquid crystal since the director is continuous. Because the effective refractive index of the liquid crystal depends on the orientation of the director, the wall is generally clearly visible in a polarising microscope.

When a wall is compressed sufficiently (*i.e.* the applied field is high enough) the wall breaks into 2 *disclination* lines. A disclination is a crystallographic defect, it is a point or a line where the director is undefined. There are several types of disclination which can be characterised by their *strength*, s. In general, only disclinations of strengths $s = +\frac{1}{2}, -\frac{1}{2}, +1$ and -1 are observed [Cha92]. These strengths are a measure of how much the director is rotated if one follows the director orientation whilst circumnavigating a disclination. A strength of $s = \frac{1}{2}$ represents a half rotation of the director for one journey around the disclination (remembering that $\hat{n}$ and $-\hat{n}$ are equivalent) and a strength of $s = 1$ represents a complete rotation of the director. An $s = \frac{1}{2}$ disclination is always a point defect whereas an $s = 1$ can be a line disclination.

Walls and disclinations are important in liquid crystal devices from the point of view of the optical properties as they can scatter or locally focus the light (for example, see figure 6.27 (on page 119)). In a device with uniform, parallel alignment (such as are the subject of this thesis), walls should not occur in the off-state. Walls can occur when an electric field has been applied if there is a variation of pre-tilt. This case has been studied by Stieb *et al* [SBM75] and some of their findings are described below.

Disclination lines are thinner than the walls since a wall is a smeared out distortion [dP93]. Another difference is that a wall extends through the thickness of the layer whereas the disclinations are more localised (usually near one of the surfaces). The result of these differences is that disclinations can be much harder to see in a polarising microscope if there is any other structure in the cell (especially if a defect follows the shape of the structure).

Structures of walls

The evolution (with increasing voltage) of walls in the liquid crystal, due to domains of opposite pre-tilt, is a process which occurs in stages. At first, the when the liquid crystal is only switched slightly there is no wall. Then, as the voltage gets higher, a wall gradually forms, necessitating an extra deformation (to that imposed by the electric field) which is a combination of bend and twist. At higher voltages still, the deformation associated with the wall becomes twist only (see figure 2.17). The wall structures which form under the influence of an electric field have been studied by Stieb *et al.* Their work

was an extension of the study of walls formed under a magnetic field which have been described by Léger [Lég73].

Stieb *et al* [SBM75] classified wall loops which form under the application of an electric field into 3 types: 'S', 'C' and 'T' walls. The letters correspond to the type of director deformation induced by the electric field on either side of the wall. All three configurations are for parallel aligned cells. An S deformation describes the director between parallel pre-tilts (eg see figure 2.16). A C deformation occurs between surfaces with opposite pre-tilts, one positive, one negative (this structure is only stable when the director is completely switched at the centre of the cell). A T wall occurs between a twisted (360°) and untwisted region. The S walls have been studied in the most detail [SBM74] and is described further below.

If we imagine a domain with one pre-tilt surrounded by a domain of an opposite pre-tilt then there is a wall between them in the form of a loop. A slice through an S wall loop is shown in figure 2.17 for 2 voltages. It can be seen (figure 2.17a) that if we go from one domain to the other, crossing the wall in between, going perpendicular to the director, then to go from one to the other requires twist. However, if we do the same but going in the same direction as the director, no twist is required, only bend. In some parts of the loop there will be twist walls, in others, bend walls, and in most parts a combination of the two. Since a twist wall may require a different energy than a bend wall (the twist elastic coefficient, $k_{22} \neq k_{33}$, the bend elastic coefficient), the loop is not circular but elliptical with the ellipticity ratio defined by $\sqrt{k_{33}/k_{22}}$.

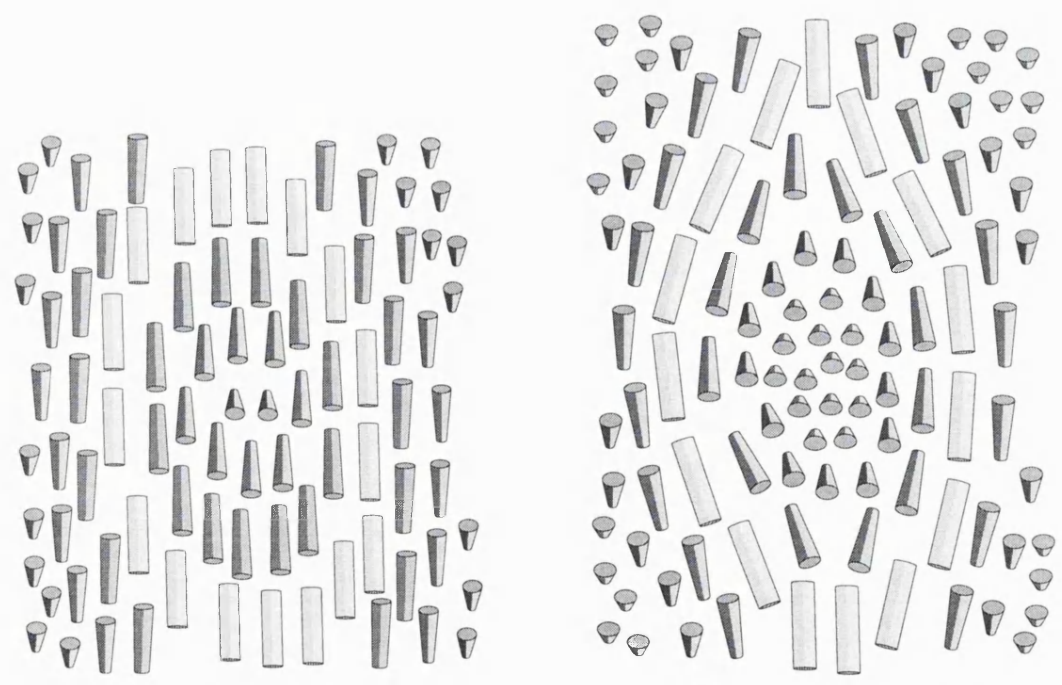

(a) Bend/Twist (low voltage)

(b) Mostly twist (higher voltage)

Figure 2.17: A slice through a wall loop structure (perpendicular to the wall) at two voltages

A. Steib *et al* added a modification to this model (which proposed by Léger), since they observed that the ellipticity could be changed with voltage. They concluded that since the bend wall requires more energy than the twist wall ($k_{33} > k_{22}$), the bend wall

transforms into a twist wall as the applied voltage increases. This is the third stage of the wall forming process.

As shown in figure 2.17a, at lower voltages the wall consists of a bend and twist deformation. In the rubbing direction (vertical in the figure), the director bends. Perpendicular to the rubbing direction, the director twists. However, as shown in figure 2.17b, as the voltage is increased the nature of the wall changes. More of the wall becomes twisted, the directors at the centre of the wall turn to facilitate the change and the bend deformation is restricted to a smaller section of the wall. Since the two sides of the loop (left and right) have the opposite sense of screw they cannot combine. The remaining bend section appears as a distinct kink as shown occurring wherever the wall changes direction, going against or with the rubbing direction. Both C and T walls lack these kinks [SBM75] making them an easy identification mark of the S walls.

Steib *et al* also noted a couple of other effects whilst studying the S walls. One was that at high fields the walls ceased to be completely vertical in the cell due to the effect of hydrodynamic flow. The walls then appeared as two lines at the bottom and top surfaces connected by a grey interface region. Secondly, they noted that the walls could split into 2 disclination lines associated with the top and bottom of the cell (strength, $s = \frac{1}{2}$ and $-\frac{1}{2}$).

Chapter 3

Review of microlenses and variable focal length lenses

3.1 Introduction

This chapter consists of two reviews bundled together. The two subjects are not unrelated, both concerning lenses, and there is some overlap between the two. The first is a review of microlenses (section 3.2) concentrating on refractive microlenses. The second part of the chapter (section 3.3) deals with lenses and microlenses with a focal length which can be varied.

3.2 Microlenses

There is no fundamental difference between microlenses and 'ordinary' lenses (macrolenses), the distinction being one of scale. Microlenses are usually taken to have a diameter no greater than a few millimetres and can have diameters down to a few microns. The difference is perhaps better indicated by the manner of fabrication and usage.

Macrolenses are commonly formed by cutting and polishing (in the case of glass) or by injection molding (for plastics). The smaller size of microlenses makes it practical to use the techniques of chemical etching, thermal reflow and diffusion doping. Microlenses are generally (though not exclusively) formed on (or within) a substrate which facilitates handling and is convenient for the purposes of this research (i.e. with a view to creating a liquid crystal cell).

The clearest distinction between ordinary lenses and microlenses is that microlenses are often fabricated and used in arrays. Although there is no fundamental reason why macrolenses are not similarly used in arrays, it is rare. Microlenses, however, are formed just as easily in arrays as singly. Since each microlens often fills only a small part of a substrate, it makes sense to fill up the rest of the substrate with more microlenses. As many of the processes of microlens fabrication make use of masks (lithographic or otherwise), it is a simple task to repeat the pattern across the mask such that the microlenses are formed in arrays (or any other desired pattern).

The primary interest for this thesis is surface relief refractive lenses since these lenses can be integrated effectively with liquid crystal to give a variable focal length. GRIN

lenses and diffractive lenses can also be combined with liquid crystal but the combination with a GRIN lens produces several disadvantages as described in chapter 4 and diffractive lens cannot be made continuously variable without be able to change the position of the steps in the structure.

3.2.1 Melt and reflow technique

Microlens arrays have been applied in optical systems by humans since at least the beginning of the 20th Century [Lip08] but, for a long time, development of such systems was held back by the cost and low quality of the microlens arrays available [HDS91a]. Since the 1980's, various techniques have been invented to overcome this obstacle causing a renewal of interest in the subject.

One of the most attractive techniques invented so far is the so called *melt and reflow* technique invented by Wada *et al* [WYA+81] and applied to the fabrication of microlens arrays by Popovic *et al* [PSC88]. It is attractive because of the simplicity and ease of fabrication in a research environment (provided cleanroom and photolithography facilities are available). It is commercially attractive since the surface relief structures can be transferred by embossing into plastics, with the resultant possible cost benefits of cheap materials and simple production processing.

The melt and reflow technique uses a binary mask and only a single step of lithography thereby avoiding the problems of mask alignment in a multistep process. First of all, a layer of photoresist must be spread uniformly across the desired substrate. The uniformity is important since it decides the uniformity of focal lengths of the final microlenses. This is achieved by the standard microchip lithography technique of coating the top surface of the substrate with photoresist and then spinning it so as to throw off most of the photoresist leaving only a thin, uniform layer. The layer thickness is dependent the surface tension of the resist and the acceleration due to the spin speed. The relation of layer thickness to spin speed is published by the resist manufacturer with the resist.

Then the photoresist is exposed to UV through a mask of the desired pattern (usually an array of circles-to give spherical microlenses). After development, there are islands of photoresist left on the substrate. These islands are then heated so that they melt. Once melted, the photoresist forms droplets, the surface tension giving them a spherical shape, i.e. a lens profile. The profile is preserved when the resist is cooled and becomes a solid again. The whole process is shown schematically in figure 3.1.

In fact, this method is not as versatile as it first appears since the surface tension will not support all curvatures [Hut90b]. The shape of the melted photoresist droplet is not determined solely by surface tension, the wetting angle is also crucial. The wetting angle is determined by the surface tension between the substrate, photoresist and surrounding vapour [EC96] as illustrated in figure 3.2.

The wetting angle, θ, is given by Young's equation:

$$\gamma_{sv} = \gamma_{sp} + \gamma_{pv} \cos\theta \tag{3.1}$$

where γ_{sv}, γ_{sp} and γ_{pv} are the surface tensions between the substrate-vapour, substrate-photoresist and photoresist-vapour combinations respectively.

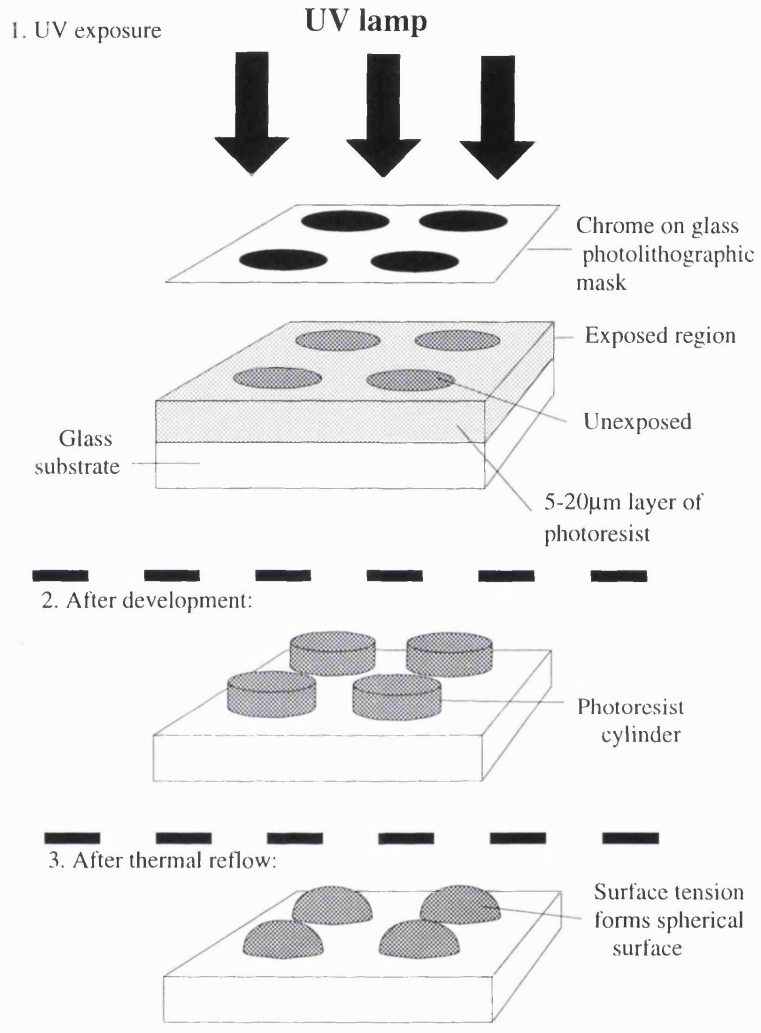

Figure 3.1: The process of forming photoresist microlenses by melt and reflow

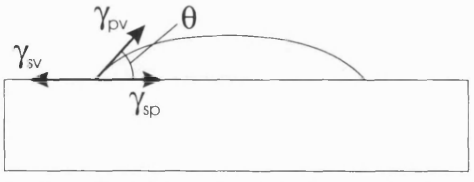

Figure 3.2: The angle at the interface between the photoresist/vapour, substrate/vapour and substrate/photoresist surfaces. The γ's are the surface tensions and θ is the wetting angle.

If the wetting angle is incompatible with the curvature resulting from the surface tension then the lens may be flat topped or even sag in the middle [HSD90]. The possible numerical apertures are given by the relation between the wetting angle and the surface tension. For a resist/glass interface the possible range is 0.25 to 0.6 [DSHD91] depending on the initial thickness of photoresist used. To calculate the thickness of photoresist required for a particular numerical aperture it is simply a case of calculating the volume of the desired lens and then deducing the height of the photoresist island necessary for the island to have the same volume. For a spherical lens, Daly *et al* [DSHD91] calculated the thickness, T_{sph}, to be

$$T_{sph} = \frac{h}{6}\left(3 + \frac{4h^2}{D^2}\right) \tag{3.2}$$

where h is the thickness at the centre of the desired lens, and D is the lens diameter.

The equivalent thickness, T_{cyl}, necessary for a cylindrical lens is

$$T_{cyl} = \frac{1}{2}\left(\frac{2R^2}{D}\sin^{-1}\frac{D}{2R} - R + h\right) \tag{3.3}$$

where R is the radius of curvature of the lens.

If lower numerical apertures are required, one way to increase the range of possible curvatures is to add a 'base' layer between the microlens and substrate to reduce the wetting angle. This was suggested by Haselbeck *et al* [HSSS93] who demonstrated the idea with a layer of hard baked photoresist, fabricating microlenses with N.A.'s between 0.1 and 0.3.

Alternatively, Daly *et al* [DSHD91] suggested immersing the microlenses in refractive index oil to achieve longer focal lengths (see figure 3.3). This idea has been put into practice by Poon *et al* [PRS+93] who achieved a range of N.A.'s of 0.14 to 0.025.

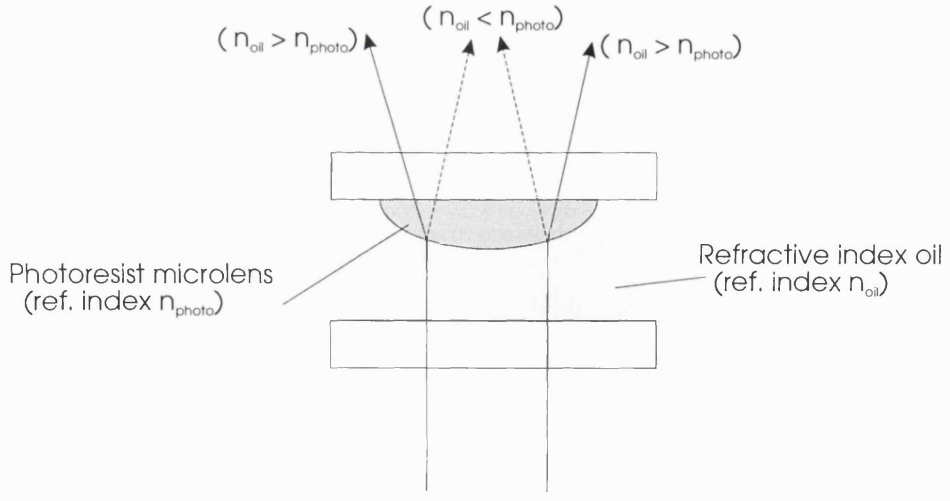

Figure 3.3: Long focal length microlenses by immersion of photoresist microlens in refractive index oil

A similar immersion approach has been used at Hughes Danbury Optical Systems to convert an array of negative concave lenses into positive lenses [CP96].

3.2.2 Half-tone masks and maskless lens formation

Long focal length lenses can be achieved by modifying the melt and reflow technique. The microlenses can be pre-formed using multiple exposures to produce a stepped structure which is then annealed into the desired lens shape (see figure 3.4) [BH91]. An analogous approach has been used to fabricate microlenses in gallium phosphide and indium phosphide using mass transport [LDWM89]. The gallium phosphide was heated to $1000°C$ for 81 hours in a flow of PH_3 (1.5%) and H_2 to produce smooth lenses starting from a six level structure.

Figure 3.4: Long focal length microlenses by annealing a preformed structure

Of course, the preformed approach looses some of the inherent simplicity of the melt and reflow technique since it requires multiple exposures and, thus, alignment between exposures. Liau have produced a single step method where the width of rings is varied, so that they are thinnest at the eventual lens edge (see figure 3.5).

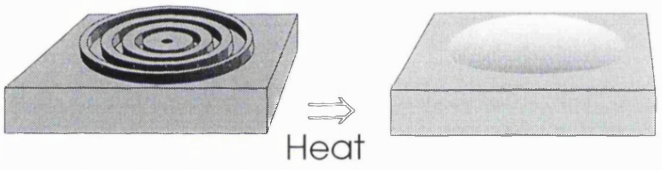

Figure 3.5: Long focal length microlenses by mass transport of ringed structure

A larger focal length range is possible if there is no restriction that the mask must be binary. An example, which retains the attraction of remaining almost standard IC processing is *photosculpting*. Photosculpting is a technique where the depth of the removed photoresist is dependent on the exposure. A desired relief profile can be produced in one exposure by the use of halftone masks. Halftone is the technique developed for book and newspaper printing (and is used is this thesis), where a greyscale picture is represented by a variation of the size or density of printed dots, thus allowing apparent greyscale from an inherently binary structure. Using this approach, with variable dot size, Purdy [Pur93] produced refractive and diffractive microlenses. The disadvantage with the halftone technique is the more complex mask development. To produce the mask the resist needs to be calibrated by measuring the dot sizes that produce a certain depth of photoresist removal. Using this data the mask can be designed for the desired structure. The second problem is that very small feature sizes are required. The features must be significantly smaller than the wavelength of light such that the individual dots are not reproduced.

A separate approach by Hutley dispenses with the need for a chrome on glass mask, instead using a photoreduced print-out from a dot-matrix printer. The desired shape is projected onto the photoresist, through a lens array if the shape is required to be arrayed (see figure 3.6). In the case of a circularly symmetric pattern, the mask can be rotated in order to give better uniformity across the image. Extending this idea

further, the original mask doesn't have to be circularly symmetric at all, but just has to give the correct exposure when rotated, thus microlenses can be fabricated using a cam shape [Hut95].

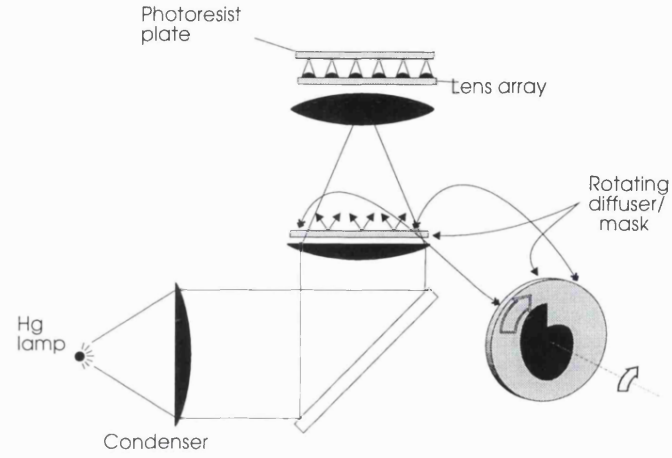

Figure 3.6: Microlenses fabricated from a rotating spiral mask

It is even possible to fabricate microlenses lithographically with no mask at all. This can be done by laser writing the desired pattern into the resist, altering the exposure appropriately to the desired shape. This has been demonstrated by Hessler *et al* [HGRK95]. Alternatively, a fringe pattern can be set up to create a microlens array. Hutley [Hut90a] produced a hexagonal array of lenses by using a 3 beam interference pattern. However, this technique actually produces 2 sets of microlenses the 2nd ones being much smaller and formed at the interstitial sites of the large lenses. This is a result of the 'chicken wire' arrangement of the intensity pattern resulting from the 3 interfering beams.

3.2.3 Etching

Microlenses made in photoresist can be made more durable by transferring the shape of the microlenses into the substrate [Sav94]. Also, the transfer can improve the microlens transmission characteristics as photoresist absorbs as evidenced by their red or yellow appearance in the photographs in the results chapter. The shape can be transferred by simultaneously etching the resist and the substrate, as shown in figure 3.7.

Microlenses have been transferred into a variety of substrates using two different methods of etching: *reactive ion etching* (RIE) and *ion beam milling* (IBM). Some of these substrate materials are shown in Table 3.1.

In RIE, a gas (or a mixture of gases) is excited by a high frequency electric field, ionising the gas so that it forms a plasma. The gas is then accelerated towards the sample electrode where it forms volatile compounds with the sample which are removed by pumping out the chamber. The acceleration of the ions gives the etching a directionality, which for microlenses would usually be carried out perpendicular to the substrate since a symmetric structure is desired. The gas used depends on the material to be etched; 0_2 being used for photoresist and for a SiO_2 substrate, CHF_3 is used.

IBM works by erosion of the sample by energetic ions. It is less material dependent

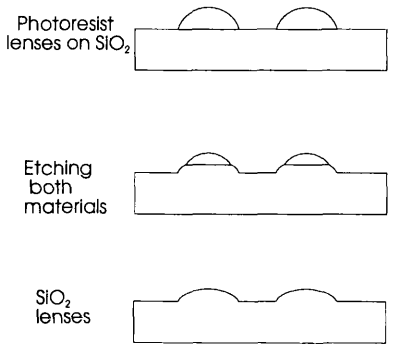

Figure 3.7: Transferral of the photoresist profile into a SiO_2 substrate by etching lens substrate

Substrate material	Etching method	Reference
SiO_2	RIE	[Sav94], [EHSS93], [MNFT92], [TRM+95]
Si	RIE	[Sav94]
Si	IBM	[GHA+93]
CdTe	IBM	[GHA+93]
InP	IBM	[WYA+81]
YAG:Nd, Glass:Er,Yb	IBM	[TRM+95]

Table 3.1: Substrate materials and methods used for etching photoresist microlens profiles into a substrate

since it does not require particular gases appropriate to the sample composition.

The dependence of the RIE process on etching gases can be advantageous or problematic. It is a major problem when the appropriate gas for a particular substrate is unknown or unavailable. On the other hand, the fact that the etching of the photoresist and substrate depend on different gases allows the profile to be modified as part of the etching process. The rate at which the materials are etched depend on the flow rate of their respective etch gases, therefore, the ratio of the two etch rates can be controlled. The ratio of the etch rates (substrate to resist) is called the *selectivity.* Tarazona *et al* have achieved a selectivity between SiO_2 and positive photoresist of 0.3 to 3 [TRM+95]. The gas flows can be adapted during etching which will have the effect of changing the curvature transferred between the top and bottom of the microlens. This can be used to correct spherical aberration.

The IBM process also shows a selectivity between the substrate and resist but the selectivity is a lot less adaptable. For YAG:Nd and resist Tarazona *et al* found a selectivity of 0.12 and for glass:er,yb/resist they measured 0.6 (using a mixture of Ar and O_2) in both cases.

3.2.4 Other microlens forming techniques

Shaping photoresist is by no means the only method of producing microlenses. Borrelli at Corning has developed a photolytic method for producing microlenses [BMBM85]. Borrelli used photosensitive glass, which when exposed to UV and heated, becomes

opaque and more dense, shrinking in the process. Thus, by exposing the glass through a mask of circles, leaving a cylinder of unexposed glass, and then heating, the region surrounding the cylinder presses in on the unexposed region, forcing it out at the surfaces (see figure 3.8). Where the glass is forced out the glass forms a hemisphere which minimises its surfaces tension, thus the result is lens (a cylinder with two convex ends surrounded by opaque material).

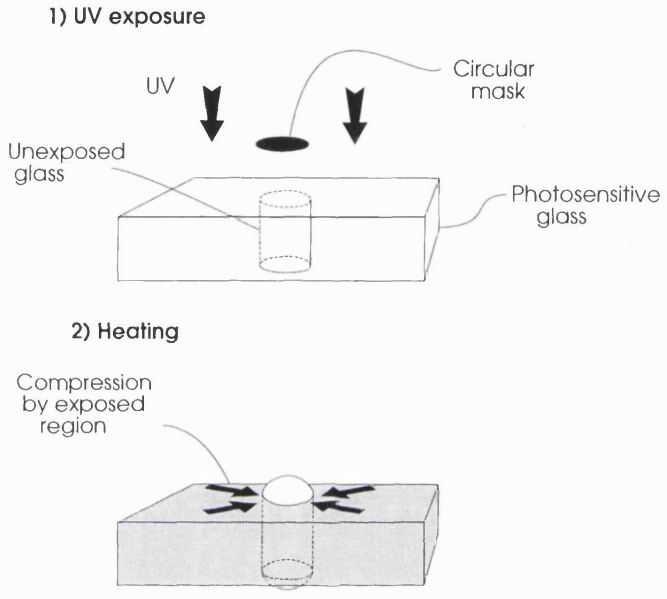

Figure 3.8: Microlenses fabricated by the Corning photolytic technique

Another process, much more similar to the melt and reflow technique, uses the LIGA (German acronym for the main process steps lithography, electroforming, replication) process. Göttert *et al* have applied the technique to the fabrication of microlenses in Polymethyl methacrylat (PMMA) [GFM95]. The process differs from the melt and reflow technique in that, before melting the islands of photoresist, the PMMA polymer is partly cracked by a 2nd exposure (to x-rays not UV as in the melt and reflow technique). The 2nd exposure reduces the glass transition temperature and since the exposure affects the top of the PMMA more than the bottom, there is a difference in melting point between the bottom and top of the lenses. Thus, it is possible to partly melt the islands creating a lens profile at the top of the PMMA with vertical walls at the sides (see figure 3.9).

Using this process, it is possible to make lenses which can be separated from their substrate (or copied by hot embossing and subsequently separated) [OGI+97]. The lenses have the advantage that their flat sides means that they are more easily handled (than melt and reflow lenses) when not attached to a substrate.

Another method of microlens manufacture which relies on the surface tension of a droplet has been presented by Keyworth *et al.* Their method relies on the accurate dispensation of optical adhesive on a substrate. They then cure the adhesive to form a solid lens [KCMM97]. This method does not require a lithographic mask but does need accurate (computer controlled) dispensing equipment.

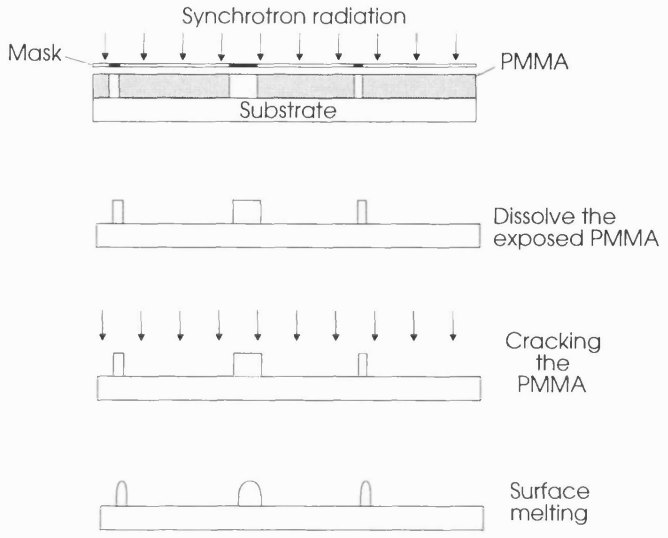

Figure 3.9: Microlenses fabricated by the LIGA process

3.3 Variable focal length lenses and microlenses

The form potential to form switchable lenses utilising the controllable birefringence of liquid crystals has been recognised since the end of the 1970's. Manufactured optical systems often include a focal length variation which is created by a translation of some of the lenses within the system. If a non-mechanical solution was available, such as that offered by liquid crystals, it may prove better for some applications (eg where an absence of moving parts is desired).

The lenses described here are generally refractive lenses rather than diffractive since the focal length of a diffractive lens is dependent on the radii of the zones [Hec87], and thus to change the focal length of a diffractive system requires that the position of the zones change. In general, changing the position of the modulation is harder than changing the modulation itself.

This section is divided into 4 subsections; the first deals with lenses that derive their focusing power from their shape (subsection 3.3.1), the second with lenses rely on patterned electrodes for their focusing (subsection 3.3.2), the third is concerned with lenses which use patterned alignment to focus (subsection 3.3.3) and finally there is a brief comparison of all the lenses reviewed (subsection 3.3.4).

3.3.1 Shape lenses

One of the most common non-mechanical optical systems with a variation of focal length is the human eye. Here the 'crystalline' lens changes shape, adapting the focal length of the eye [Hec87]. I am not currently aware of a suitable and available material which is transparent, elastic, adaptable and of optical quality which could be used to fabricate an analogous system.

A lens system has been fabricated where the shape of the lens is varied but the material used to form the lens is a liquid. Gorman *et al* used used liquid droplets of hexadecanethiol (HDT) on a gold surface where the profile of the droplet can be volt-

age controlled to give a variable focal length lens [GBW95]. The device exploits the large changes in wettability between the two substances when a voltage is applied. The sensitivity to voltage is due to a self-assembled monolayer which forms between the two materials. The change of wetting angle causes the drop to expand or retract thus changing the profile and focal length. The droplet was immersed in an aqueous electrolyte in order that a voltage could be applied. Clearly, this device has the disadvantage that it will not be robust.

Originally, the idea of using nematic liquid crystal to form a liquid crystal lens was proposed and patented by Berreman [Ber80] (patent filed 1977). The idea was investigated by Sato [Sat79] with applications such as spectacle lenses [Oka86] and camera auto-focusing devices [Nis86] proposed as applications.

Sato's work showed that the problem with these devices was the thickness of liquid crystal used. The liquid crystal response time increases with the square of the cell thickness and with thicker cells it is hard to maintain the structure. The centre thickness of the lenses produced by Sato was $490\mu m$ which gave a very slow response time ($\sim$300 sec.) and a significant loss due to scattering/absorption. These difficulties prohibited serious development.

To reduce the cell thickness, Sato *et al* fabricated a Fresnel structure [SSS85]. This lens had maximum thickness of $50\mu m$, i.e. a factor of 10 reduction from the previous design. However, it is likely that this design, which is a mixture of diffractive and refractive, will have significant intensity fluctuations for different focal lengths.

A thinner Fresnel lens ($12\mu m$) was fabricated by Ferstl and Frisch [FF96] which thus had a much faster response time. On and off-axis lenses were demonstrated with response times of 40ms. The lens structure used was a Fresnel zone plate which means, of course, the lensing is not refractive and only switchable lensing was demonstrated.

3.3.2 Electrode lenses

To achieve an acceptable switching speed a liquid crystal cell must be kept thin. For a cell which derives its optical power from its shape, this restriction means having very shallow curvatures and, therefore, very low numerical apertures and very little change in focusing power when a voltage is applied to the liquid crystal.

Nose, Masuda and Sato made smaller lenses (microlenses) [NMS91] thus avoiding the problems of a thicker cell. They did this by using hole-patterned electrodes to create a non-uniform electric field distribution thus causing the liquid crystal to form a graded index lens (see figure 3.10). This has the advantage of using flat substrates (which makes the liquid crystal alignment easier) but the refractive index profile will only be circular (*i.e.* lens-like) for a part of the usable range of focal lengths and cannot make a lens which can be either positive or negative depending on the applied voltage.

Kowel *et al* also have used a patterned electrode with liquid crystal to form a lens [KCK84] but instead of using edge effects to create their non-uniform electric field, they patterned the electrodes in strips so they create the desired voltage profile. This only achieved very low numerical apertures (N.A. 0.001) and requires a system to control the voltages to all the electrodes. Riza *et al* made a similar device but used a resistive chain patterned onto the substrate to generate the voltage gradient in the electrodes [RD93]. Again, the numerical the aperture achieved was small (0.004).

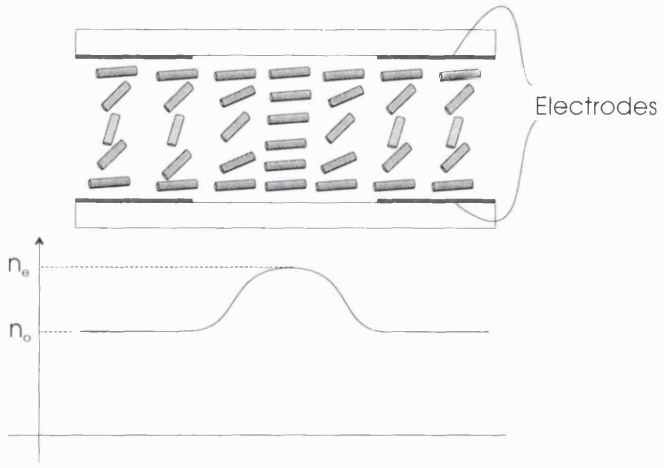

Figure 3.10: GRIN microlens formed due to electric field in between an electrode gap

A way to increase the possible numerical aperture whilst still using the same optical modulation range is to use a diffractive structure. Williams *et al* has produced Fresnel lens [WPPC89] and McOwan *et al* a Gabor lens [MGH93], both using patterned electrodes. However, being diffractive and lacking any way to change the electrode configuration, both are switchable lenses but without continuous variation of focal length. If a diffractive lens is formed on a spatial light modulator (SLM) then this flexibility is possible but only long focal lengths are achievable due to the finite pixel size. Tam [Tam92] gave an equation for the shortest achievable focal length for given diameter of lens, D, assuming a quadratic phase profile and that all light from the outermost pixel arrives in phase:

$$f = \frac{\Delta x D}{\lambda} \tag{3.4}$$

where Δx is the pixel size. Tam used an SLM with $30\mu m$ pixels giving an NA of 0.009. In order to increase the the variability of the system NA combined two SLM's with two lenses in order to shorten the focal length of the system, giving a final NA of 0.037.

An alternative approach fabricating a lens with an electric field has been demonstrated by Naumov *et al* [NLGV98]. They have avoided the need for patterned electrodes by using a resistive electrode and using the impedance of the liquid crystal to create the desired electric field profile. By changing the voltage and frequency of the applied signal they can change the focal length. The lenses reported have very large aberrations for the shorter focal lengths (0.8λ at 0.5m).

A deformed helix ferroelectric liquid crystal has also been used to make a liquid crystal (cylindrical) lens which has the advantage of a faster response time ($20\mu s$) than is possible with nematic liquid crystals (min response time ~10ms for $3.4\mu m$ cell gap) [EDMM96]. However, the focal line has several significant side lobes (~1/3 of the peak intensity).

3.3.3 Alignment lenses

It is also possible to fabricate a lens by patterning the alignment structure in a liquid crystal cell. This has been demonstrated by Patel and Rastani [PR91] who made a Fresnel zone plate with alternating orthogonal liquid crystal alignment directions from one zone to the next. This is an elegant approach in that the lens is thereby acting in both polarisations at once. The liquid crystal modulates the phase in all zones but in alternating polarisations. However, it is again a diffractive structure and has a switchable focal length rather than a continuous variation of focal length.

3.3.4 Lens comparison

There is a limit to how much the focal length of any lens using liquid crystal can be varied. This limit will be dependent on the optical modulation available and how quickly it is possible to vary the refractive index/optical path difference across the lens (i.e. the maximum possible gradient of refractive index). The limits encountered by the lenses described above are shown in Table 3.2.

Lens type	**Diameter**	**Max N.A.**	**Focal length range**	**Diffraction limited**	**Reference**
Hole patterned electrodes	0.29mm	0.09	1.7→5.3mm, ∞	No	[NMS91]
Patterned electrodes (Cyl.)	20mm	0.001	10,000mm $\rightarrow \infty$	Yes	[KCK84]
Resistor chain + patterned electrodes (Cyl.)	1mm	0.004	120mm $\rightarrow \infty$	Yes	[RD93]
Lens shaped cell	20mm	0.06	160→220mm	No	[Sat79]
Gabor lens patterned electrode	9.8mm	0.01	490mm, ∞	n.a.	[MGH93]
Immersed surface relief Fresnel zone plate	0.5mm	0.03	8.5mm, ∞	n.a.	[FF96]
Fresnel zone plate patterned electrode	20mm	0.01	1,000mm, ∞	n.a.	[WPPC89]
Fresnel zone plate patterned alignment	2.9mm	0.005	310mm, ∞	n.a.	[PR91]
2 phase SLM's + 2 lenses	7.3mm	0.037	98→148mm	Yes	[Tam92]
Distributed reactive electrical impedance	6.5mm	0.01	500mm $\rightarrow \infty$	No	[NLGV98]
Deformed helix ferroelectric LC (Cyl.)	3mm	0.003	500mm $\rightarrow \infty$	No	[EDMM96]

Table 3.2: Comparison of various switchable and variable lenses reviewed

The maximum NA can be calculated for a liquid crystal lens which derives its focusing

power from the electrode structure. If we consider the edge of an electrode and make the assumption that the effect of the electrode extends into the neighbouring liquid crystal by a distance equal to the cell thickness then we have the maximum possible gradient of refractive index vs position across the device. Consider figure 3.11.

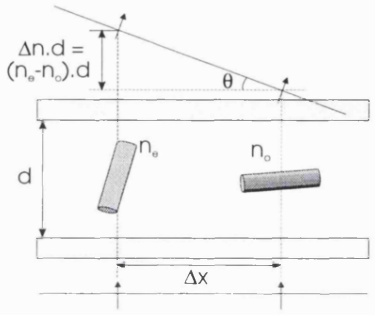

Figure 3.11: Construction for calculating the maximum deflection θ_{max}.

The maximum possible angle of deflection is given by optical path (which is Δnd, for a cell thickness, d) and distance between the two values which we took to be d. Thus, the tangent of the maximum deflection angle, θ_{max}, is

$$\begin{aligned} \tan\theta_{max} &= \frac{\Delta nd}{d} \\ &= n \end{aligned} \tag{3.5}$$

If the liquid crystal layer is part of a lens structure, then maximum N.A. will be defined by the maximum possible deflection angle:

$$\begin{aligned} N.A._{max} &= \sin\theta_{max} \\ &= \sin(\tan^{-1}\Delta n) \end{aligned} \tag{3.6}$$

Liquid crystal birefringences go up to 0.3 thus the $(N.A._{max})_{max} \simeq 0.29$.

Dispersion

Yamaguchi and Sato have also done an analysis of the optical properties of liquid crystals in terms of the values usually quoted for glasses, *i.e.* Abbé numbers and Cauchy coefficients. Since their results apply to all the lenses using liquid crystal, they are described in this final section. Results for the Abbé numbers for various liquid crystal are reproduced in figure 3.12.

The dispersion is inversely proportional to the Abbé number, v_d, and thus increases to the right in the graph. As can be seen, the liquid crystal dispersion is generally higher than that of the glasses. Abbé numbers are calculated from the formula given in equation 3.7.

$$v_d = \frac{n_d - 1}{n_f - n_c} \tag{3.7}$$

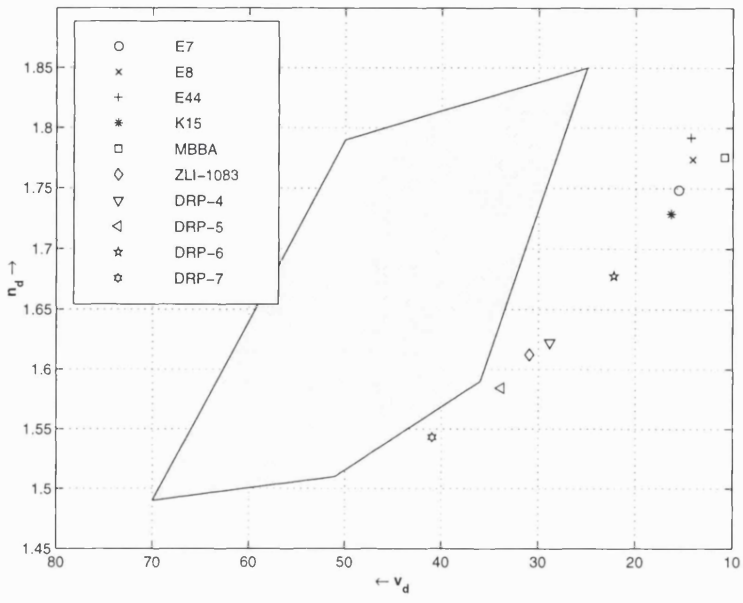

Figure 3.12: Refractive index vs Abbé number (at the sodium 'D' line, 587.6nm). Produced from data in ref [YS89]. The shaded area ( ) corresponds to the area where most commonly used glass types are to be found [Hec87]. Liquid crystal data is for the extraordinary refractive index n_e at $20°C$.

where n is the refractive index at the wavelengths referred to by the subscripts d, f and c, the spectroscopic lines at wavelengths 486.1nm(f), 587.1nm(d) and 636.3nm(c). For example, liquid crystal E7 has a refractive index, n_d of 1.7486 and a variation $(n_f - n_c) = 0.048$ $(v_d = 15.57)$. This compares with $(n_f - n_c) = 0.032$ for the high dispersion glass, SF6 ($v_d = 25.5$, $n_d = 1.805$), or $(n_f - n_c) = 0.008$ for the low dispersion glass, BK7 ($v_d = 64.0$, $n_d = 1.51$). Clearly, if a liquid crystal lens is to replace a glass lens then chromatic aberrations are likely to be worse.

The temperature dependence of liquid crystals is much greater than that of glass. Liquid crystal E7 has a temperature dependence, dn/dT, for n_e of $\sim 1.4 \times 10^{-3}/°K$ at $20°C$. For SF6 glass the figure for dn/dT is $8 \times 10^{-6}/°K$ and for BK7 the figure is $2 \times 10^{-6}/°K$ [Sch98], a factor of 1000 less.

Chapter 4

Design and theory of liquid crystal over microlens

4.1 Introduction

In all the variable focal lengths lenses reviewed in the previous chapter, the material used to form the lens was liquid crystal. A slightly different approach is taken for the lenses investigated in this thesis, in that, we start with an existing lens and then liquid crystal modulates the optical power of that lens.

This chapter contains a consideration of the lens design, starting with various possibilities for the design (section 4.2) within the approach mentioned above, then the chosen design and its variations (section 4.3) and, finally, the practicalities of constructing the lens cell (section 4.4).

4.2 Possible designs

There are many ways to construct a device which uses liquid crystal to modulate the optical power of a lens. A few of the alternatives are considered here.

Before considering individual designs, there is one question which is common to all the designs, and that is the trade-off between the liquid crystal layer thickness and the response time of the devices. The rise and decay time constants for a parallel nematic are given by the equations [KW93]:

$$\tau_{rise} = \frac{\tau_o}{\left(\frac{V}{V_{Th}}\right)^2 - 1} \tag{4.1}$$

$$\tau_o = \tau_{decay} = \frac{\gamma_1 d^2}{k_{11}\pi^2} \tag{4.2}$$

where V and V_{Th} are the applied and threshold (for switching to start) voltages respectively, γ_1 is the rotational viscosity, d is the layer thickness and k_{11} is the splay elastic constant.

The time constants calculated by equations 4.1 and 4.2 apply to the rate of change of orientation of the liquid crystal. Both equations show that the liquid crystal response

time increases with the square of the liquid crystal layer thickness. This means a compromise thickness is necessary between a layer thickness big enough to incorporate the desired surface relief structure and a layer thin enough to give an acceptable response time. The thinner mass-produced liquid crystal cells (*i.e.* displays) are fabricated with a $5-10\mu m$ cell gap. Since the response time for a $5-10\mu m$ layer is of the order of 10's of milliseconds [KW93], the response time of a $200\mu m$ layer will be $\sim$10 seconds.

4.2.1 Non-surface relief

The idea of a uniformly aligned liquid crystal layer on a surface relief structure immediately suggests a problem since relief structures can affect the liquid crystal alignment. In fact, surface structures can even be used to generate alignment (see section 2.4). This raises the immediate question, is it necessary to place the liquid crystal on the non-flat surface?

An alternative design to the liquid crystal on top of the surface relief is liquid crystal on the flat side of a plano-convex or plano-concave lens. Or, if a microoptic design is desired, a convenient alternative is a GRIN (*GR*aded *IN*dex) lens, with liquid crystal on the end as is shown in figure 4.1.

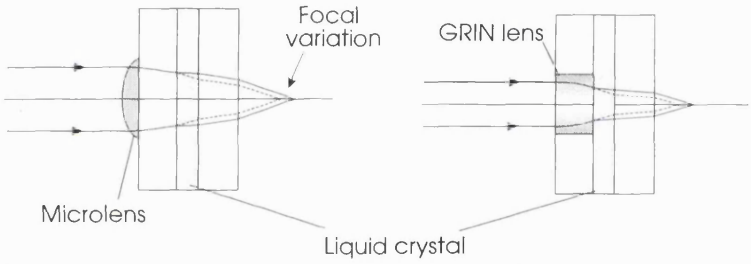

Figure 4.1: Change of focal position of a microlens or GRIN lens using a liquid crystal layer

These arrangements mean that the liquid crystal is between two flat substrates and, thus, it is relatively simple to create a uniform director angle across the cell (or the area of the cell corresponding to the end of the lens).

There are 2 disadvantages with this arrangement. The first is that only the position of the focus is being altered in this device, not the optical power of the lens. Whether or not this is a disadvantage depends on the system where the device is being used. If the system requires a change of beam divergence or spot size then the above arrangement is not any use. For this design, the possible change in focal position is a function of the product of the liquid crystal birefringence and the layer thickness. The layer thickness of liquid crystal is limited to about $5-200\mu m$ if uniformly aligned samples are required [De Jeu80]. Since liquid crystals have a birefringence of < 0.3, the maximum shift of focal position is $60\mu m$. This limitation does not apply to the surface relief microlens immersed in liquid crystal.

The second disadvantage of this design is that it is dependent on the light converging (or diverging) through the liquid crystal layer. Light rays travelling through the layer will be spread over a range of angles. This spread creates a twofold problem. Firstly, since the effective refractive index of the liquid crystal is dependent on the orientation of the light incident upon it, the refractive index will vary for different light rays across

the beam (see figure 4.2a). Secondly, the polarisation direction of the light will no longer be parallel to the liquid crystal extraordinary axis (see figure 4.2b) and some of the light beams will change polarisation due to the birefringence of the liquid crystal layer (cf. conoscopy). Both of these considerations are aside from the fact that focusing through a plane piece of glass (the cell walls) will introduce spherical aberration.

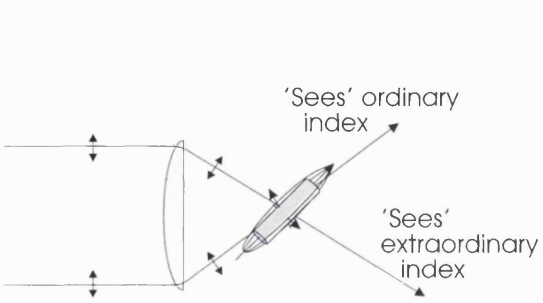

(a) Due to their variation of direction, rays encounter refractive indices in the liquid crystal

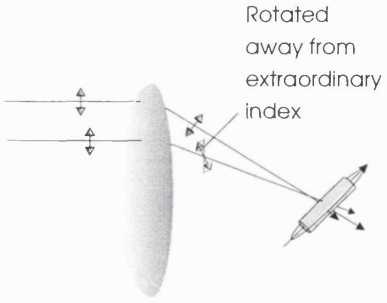

(b) Rays out of the plane containing the optic axis and the liquid crystal alignment direction have their polarisation vector deflected away from the extraordinary liquid crystal axis such that the light will be affected by the birefringence of the liquid crystal

Figure 4.2: Considerations concerning rays focusing into a liquid crystal layer

To estimate the effect of the liquid crystal layer consider again figure 4.2. The ray diagram shown in figure 4.2a is one of the simpler possible cases since the refractive index encountered is always increasing from rays at the bottom of the lens to rays at the top, thus the overall effect will be a tilt. However, in the more general case, the ray which encounters the maximum refractive index need not originate at the bottom or the top of the lens, thus the overall effect will be an astigmatism (shorter focal length in the plane of the liquid crystal alignment) and some tilt.

4.2.2 Fresnel lens

Liquid crystal layers generally have more desirable characteristics in thinner layers. The response time is faster and there is less scattered light (intensity reduction due to scattering in nematic liquid crystals is around 18dB/cm [Bli83], *i.e.* 0.36dB in $200\mu m$ which corresponds to an 8% scattering loss). This means there is a restriction on the thickness of any optical components which are to be immersed in liquid crystal (assuming the layer to be at least as thick as the component).

One way to reduce the thickness of a lens is to replace it with a Fresnel lens (NB this is not a diffractive based zone plate-see below). However, if a Fresnel lens is to be immersed in liquid crystal then the variation of focal length might not necessarily be achievable. Consider the lens shown in figure 4.3.

If one considers the device from the point of view of refraction then there is no problem with the design. Each ray will be refracted at the liquid crystal/Fresnel lens interface according to the surface angle and refractive index difference. Thus, as the liquid crystal refractive index changes so will the position of the focus.

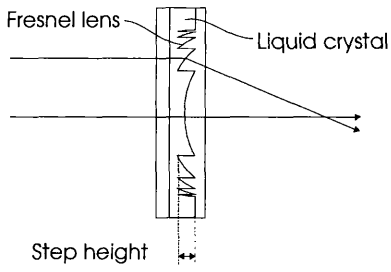

Figure 4.3: Liquid crystal immersed Fresnel lens, with a constant step height for the Fresnel lens

However, in reality, the effects of diffraction cannot be ignored and so the step height becomes important. If, instead of the smooth curve drawn, the Fresnel lens was instead made of just two steps (*i.e.* a purely diffractive element) then clearly the focal position could not be varied. The effect of altering the liquid crystal refractive index would be to change the optical path difference between the steps and, thereby, alter the efficiency of the diffraction rather than the angle of the diffracted beams. However, in the design drawn in figure 4.3, the Fresnel lens profile is not binary and thus it less clear what the overall result would be.

The conclusion from these two conflicting observations is that the Fresnel lens will be variable when refraction is a reasonable approximation to the performance of the device. We can ignore the effects of diffraction if the step height and refractive index difference are sufficiently large that optical path difference between steps is larger than the coherence length of the light. If the liquid crystal layer thickness is set, say, at $5 - 10\mu m$ and the refractive index difference is 0.1 then the coherence length needs to be less than $0.5 - 1\mu m$. The coherence length, L_c of a broadband source is given by [BW80]:

$$L_c = \frac{\overline{\lambda}^2}{\lambda_1 - \lambda_2} \tag{4.3}$$

where λ_1 and λ_2 are the wavelengths at edges of the bands and $\overline{\lambda}$ is their mean. Thus, the coherence length of a white light source (400-700nm) is $1\mu m$, *i.e.* the step height needs to be $\gtrsim 10\mu m$.

There are two practical difficulties envisaged in the construction of the device. The first is simply the difficulty of constructing the Fresnel lens structure. One of the potential advantages of a Fresnel lens over a more traditional lens in the liquid crystal cell is that the maximum aperture size is larger for the Fresnel lens than for the traditional lens (assuming a desired focal length and layer thickness). However, another look at figure 4.3 shows that the outer zones of the lens have very high aspect ratios which will be hard to fabricate [HRP+97]. The second potential fabrication problem concerns the alignment of the liquid crystals. Firstly, any spun-on polymer alignment layer would tend to collect in the corners formed at the step between zones and, if rubbing were employed as an alignment technique, the surface profile would be likely to deflect the cloth fibres and, thus, the overall rubbing direction would be non-uniform. Secondly, whichever alignment technique is used, it is likely to be affected by the surface profile, since the grooved structure itself promotes alignment [Ber73] along the grooves.

4.2.3 PDLC

All the devices using a nematic liquid crystal layer described in this thesis have the limitation that they are variable for only one polarisation. Of course, two devices could be used in series, however, this approach is likely to give rise to problems since the separation of the two focii (which cannot be less than the substrate thickness) will be large relative to the short focal lengths of the devices.

Another restriction inherent with the use of a layer of nematic liquid crystal is the relatively slow switching time (see beginning of section 4.2). One way around these problems is to use polymer dispersed liquid crystal (PDLC) instead (see section 2.2.3). PDLC works for both polarisations and the response time of PDLC can be much faster than a layer of nematic alone since, in effect, the liquid crystal is divided into many smaller cells. However, these smaller cells also mean higher threshold voltages since the droplet size is not matched by the electrode separation.

To use PDLC in a lensing device, the droplet size needs to be reduced such that it is much less than the wavelength of light (see chapter 2). In this way, the light will not be scattered but, instead, the PDLC can be treated as medium with a refractive somewhere between the droplet and polymer refractive index. Assuming the refractive index of the polymer/liquid crystal combination will be proportional to the relative concentrations and refractive indices of each:

$$n_{PDLC} = \frac{\rho_{lc} n_{lc} + \rho_p n_p}{\rho_{lc} + \rho_p} \tag{4.4}$$

where ρ_{lc} and ρ_p are the concentrations (by volume) of the liquid crystal and polymer respectively and n_{lc} and n_p are their refractive indices.

The refractive index of the droplets can be controlled in the same way as a bulk nematic liquid crystal, thus the layer can act as a variable phase retarder. The range of tuning of phase retardation increases with the liquid crystal birefringence, layer thickness and the concentration of liquid crystal in the layer. The voltage required to switch the liquid crystal also increases with the layer thickness (assuming electrodes on either side of the layer) but decreases with liquid crystal concentration. Therefore it makes sense to maximise the proportion of liquid crystal. The maximum concentration of liquid crystal is given by the solubility in the polymer before curing, for example, the solubility of E7 in Norland 65 Optical Adhesive (NOA-65) is 66.4% at room temperature [KW93].

The effective refractive index of the liquid crystal, n_{lc}, will vary with applied voltage. When there is a field applied well above threshold, the directors will align with the field and the refractive index will be approximately n_o. Making the approximation that with randomly aligned droplets (*i.e.* no field applied), we can take the average refractive index $(n_e + 2n_o)/3$ then the effective liquid crystal refractive index will vary between the two values. For example, for E7 the liquid crystal refractive can vary between 1.52 and $(1.74 + 2 \times 1.52)/3 = 1.59$ and, if immersed in NOA 65 (refractive index 1.52) to 66% concentration, the resulting layer will have refractive index between 1.52 and 1.57. To get a 2π phase shift at $\lambda = 632.8nm$ would thus require $60\mu m$ of PDLC.

Droplet sizes can be varied between 0.01 and 20μm [DGW+88], the size of droplets being controlled by various parameters including curing temperature, UV curing intensity, relative concentrations of materials, viscosity and materials used. A faster

polymerisation of the polymer results in smaller droplets. The droplet size is very important for the scattering properties, the scattering cross section, σ, for small droplets ($2kR|n_{lc}/np - 1| \ll 1$ where R is the droplet radius and $k = \frac{2\pi}{\lambda}$) is

$$\sigma \sim k^4 \langle R^6 \rangle \tag{4.5}$$

The transmitted light intensity can then be calculated from the expression

$$I = I_o e^{-\alpha z} \tag{4.6}$$

where the attenuation coefficient, α, is given by $\alpha = \rho_{lc}/\rho_p(\sigma/v_d)$ and ρ_{lc} and ρ_p are the concentrations (by volume) of the liquid crystal and polymer respectively and v_d is the averaged volume of the liquid crystal droplets ($= \frac{4\pi}{3}\langle R^3 \rangle$). Matsumoto *et al* have fabricated a fine droplet system (diameters $< 100\mu m$) and observed scattering losses of 1-5dB/cm [MHHK96] at $1.3\mu m$. Given the above dependence on wavelength (λ^{-4}) the value at 632nm would be 18-90dB/cm.

4.3 Chosen design(s)

The design which was investigated was not any of the 3 mentioned above. The implemented design was a compromise between ease of fabrication and expected performance. The non-surface relief design was simpler but can be rejected due to the problems associated with focusing light into the liquid crystal. The other two (Fresnel lens and PDLC) have potential advantages over the chosen design but also more potential difficulties. Thus, these 2 designs can be seen as options for further work.

4.3.1 Initial design

The design which is the subject of the majority of this thesis is a development of the work of a previous PhD student, Peter Poon. The basic design, started not as a way to vary the focal the length of a microlens but simply as a way to get long focal length microlenses. Microlenses made by the technique of melting and reflow of photoresist are attractive because of their relative simplicity/ease of fabrication [POO95]. However, the lenses produced this way have a restricted range of NA's achievable, longer focal lengths not being achievable. To get around this restriction, Poon *et al* immersed the lenses in refractive index oil [PRS+93] as illustrated in figure 3.3.

As well as making lenses of longer focal lengths, Poon's design also provides an easy way that focal length can be changed, should the system requirements alter, by replacing the refractive index oil. However, it was also realised that if the oil were replaced with nematic liquid crystal then, for one polarisation, the focal length of the lenses could be electrically controlled (see figure 4.4).

As mentioned at the beginning of section 4.2, it is better to have a thinner liquid crystal layer since this means the liquid crystal will respond faster. However, the thin layer imposes a restriction on the photoresist centre thickness. Thus, for microlens apertures greater than the liquid crystal layer thickness, the possible numerical aperture of the microlens is restricted.

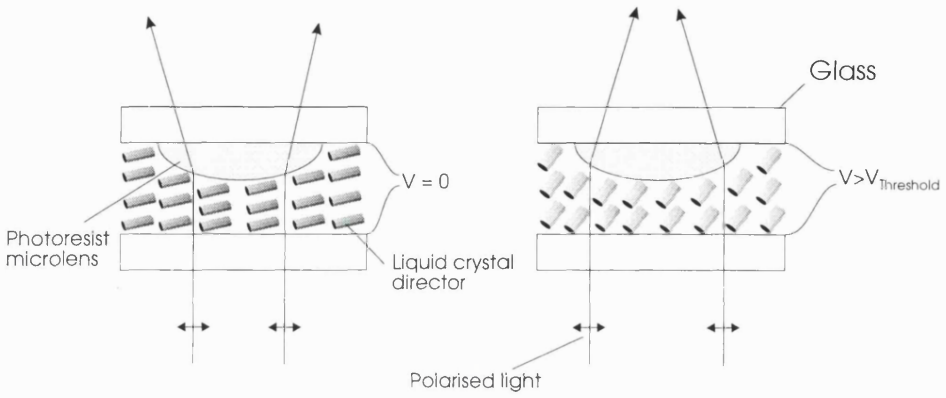

Figure 4.4: The variation of focal length by the voltage control of the liquid crystal director orientation

Commercially available liquid crystals have refractive indices which vary from $1.47 \lesssim n \lesssim 1.81$ [Mer92a, Mer92b]. The photoresist has a refractive index of around 1.64 [POO95], thus the maximum possible refractive index difference between the photoresist and the liquid crystal is only 0.2. Therefore, assuming a microlens in air with an N.A. of 0.4, the immersed microlens will have a maximum numerical aperture of 0.11. Thus, if a reasonable size of numerical aperture is required then the original N.A. of the microlens in air must be large.

The first microlenses made (by C.H. Chia) were fabricated using a mask containing an array of circles as shown in figure 4.5. Of the lenses fabricated using this mask, the $100\mu m$ lenses had the most spherical profile as measured by the Alpha step machine [CHI94] and were chosen as the principal lenses to be investigated.

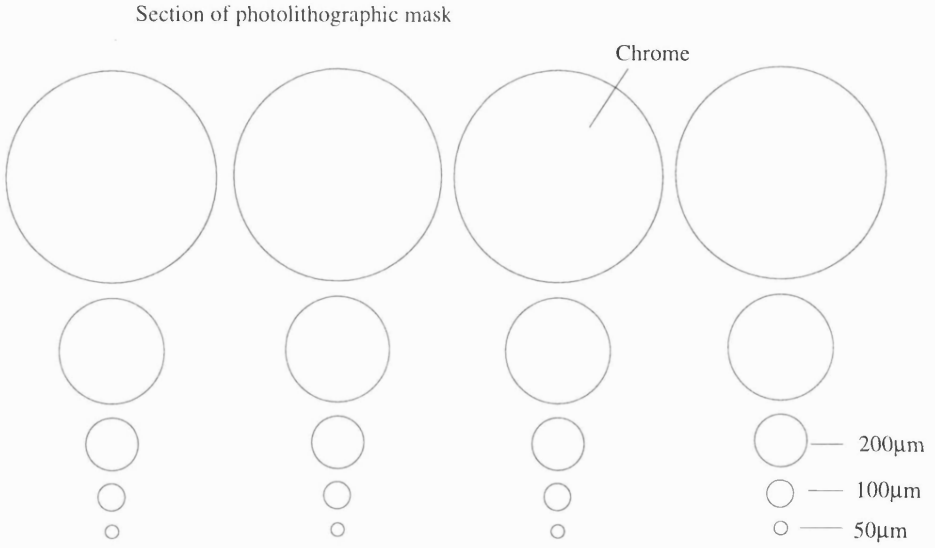

Figure 4.5: Part of the mask used for the fabrication of the first microlenses

At a later time, arrays of microlenses were constructed using a mask designed by Peter Poon [POO95]. This mask produced lenses of various sizes depending on the mask area used. Lenses of $250\mu m$ and $125\mu m$ and $150\mu m$ diameter were produced.

The design/theoretical focal length of the lenses has been calculated. For this, the average refractive index vs voltage profile has been calculated for a liquid crystal cell. The cell was assumed to have a pre-tilt of 2° on each surface and to be filled with liquid crystal E7. The calculation is based on a numerical simulation (see chapter 7). In figure 4.6 a plot of the averaged refractive index (average through the cell) vs voltage is shown.

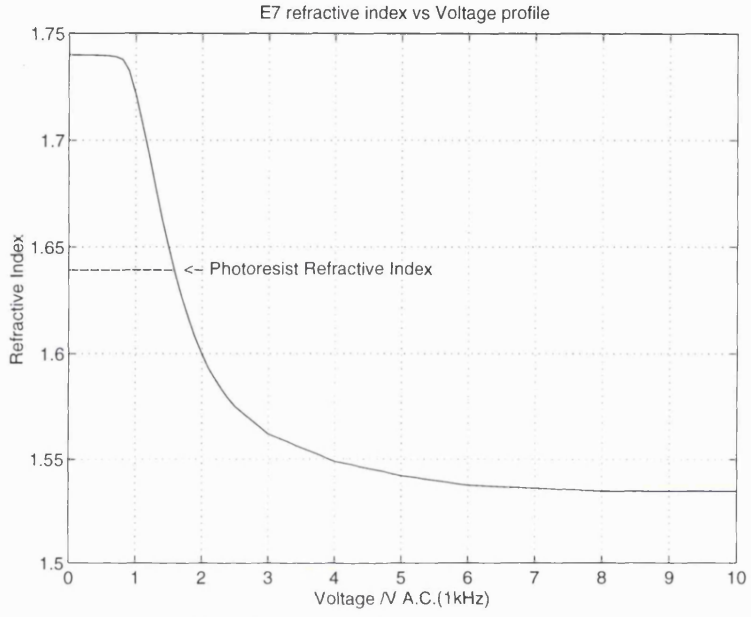

Figure 4.6: Calculated average liquid crystal refractive index vs voltage. The director profile of the liquid crystal has been calculated through the cell and then the average calculated.

From the data in figure 4.6, it is a simple task to plot the focal length vs voltage graph assuming that the relation expressed in figure 4.6 holds true for the liquid crystal on the microlens as well. As can be seen from figure 4.6, the photoresist refractive index is roughly half way between the extraordinary and ordinary values for E7, thus around 1.6V the focal length of the lens should be infinite.

The curvature of the original (D = $100\mu m$) unimmersed microlenses has been calculated from their original focal lengths [CHI94] and the photoresist refractive index. This gives a radius of curvature, R = $72.5\mu m$. Then from the curvature and refractive indices the theoretical focal length vs voltage has been calculated (see figure 4.7).

4.3.2 Cylindrical lens design

The original lens design has been modelled using finite elements methods by Fabrizio Di Pasquale. The model can give 2-D plots of liquid crystal structures. Because the approach is 2-D, it can predict wall and disclination structures in the liquid crystal. Using this model, F. Di Pasquale successfully predicted the walls seen in the original design (see chapter 7). He then used his model to predict a new structure which eliminated the wall at the side of the lens [DFDD96].

It was decided to build a lens corresponding to these predictions in order to test them and the model. Since the model is a 2-D model, this meant fabricating cylindrical

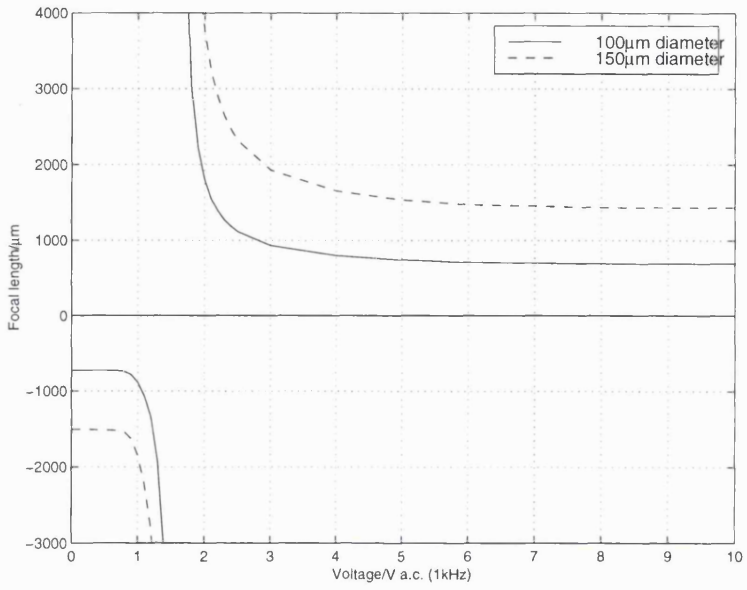

Figure 4.7: Calculated liquid crystal immersed microlenses (diameters $100\mu m$ and $150\mu m$) focal length vs voltage.

lenses. Cylindrical lenses are also convenient since the 2-D liquid crystal structure is simpler than the 3-D one and, therefore, the liquid crystal structures should be easier to understand.

The first cylindrical lens design is a cylindrical version of the original design. A slice in the rubbing direction through the cylindrical lens and the centre of the spherical lens should appear the same. The two are shown schematically in figure 4.8.

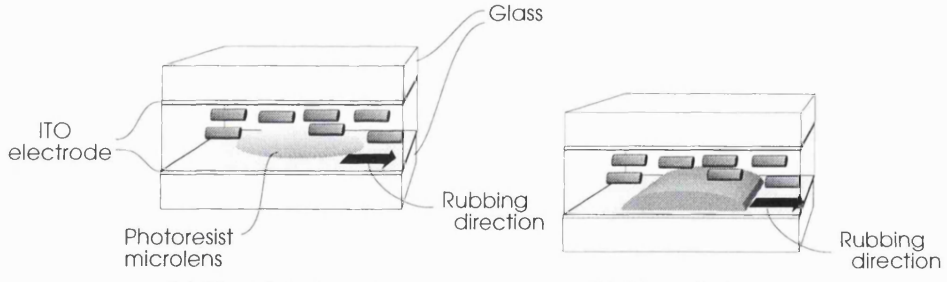

(a) The original design

(b) The cylindrical version of the original design

Figure 4.8: The original lens design and its cylindrical version

As mentioned above, Fabrizio Di Pasquale had predicted from his model a new design which eliminated a liquid crystal wall from the original design. The new design consisted of a different electrode pattern on the surface opposite to the microlens, replacing the planar electrode of the original design. The new electrode was a strip electrode wider than the original lens as illustrated in figure 4.9. The mask for the cylindrical lenses and the corresponding electrode is shown in figure 4.10 (NB the design contains an error-one of the masks should be a mirror image since they opposite substrates, so only one of the arrays could be used in practice).

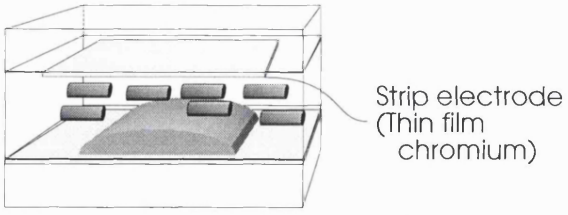

Figure 4.9: The cylindrical lens with a strip electrode opposite

4.3.3 Final design

The measurements of the lens aberrations (see chapter 6) suggested that the original design was flawed in one respect. In the original design, it was assumed that the average refractive index vs voltage relation is independent of the cell thickness, thus it did not matter that the liquid crystal layer thickness varied due to the presence of the microlens. In fact, the assumption isn't true for all cases, but only when the layer thickness and electrode separation are proportional to each other by a constant factor. Therefore, it was decided to make a microlens with the electrode on top of the photoresist. Both cylindrical and spherical lenses of this type have been produced as are shown in figure 4.11.

4.3.4 Optical system design

The microlenses discussed above have a limited maximum possible aperture. However, the *system* in which the lenses are incorporated can have a larger effective aperture. Some of the factors involved in the system design are discussed below.

Taking the example of a DVD disc read-head, the principle requirement is that there is a variation of the focal position of $600\mu m$, in order to read the 2 layers of the disc. This variation can easily be achieved with the microlenses (see chapter 6). However, the specifications for the numerical aperture (N.A.) are 0.6 and 0.45 [Bra96]. The lower N.A. is required for reading CD format discs, the higher N.A. for the DVD disc format. These figures compare with 0.048 and 0.052 for the final design of lens.

The numerical aperture of a lens system is not limited by individual lenses in the system, thus the system needs to be designed to increase the numerical aperture above that of the microlenses. Increasing the N.A. comes at the expense of reducing the longitudinal magnification. Assuming the first and second focal lengths (f and f') of the lens are equal, the two magnifications are related through the equation [BW80]:

$$M_L = \frac{\Delta l'}{\Delta l} \tag{4.7}$$

$$= -M_T^2 \tag{4.8}$$

$$= \left(\frac{\tan u}{\tan u'}\right)^2 \tag{4.9}$$

where M_L and M_T is the longitudinal and transverse magnification respectively, l and l' are the axial object and image distances and u and u' are the ray angles in the object and image space.

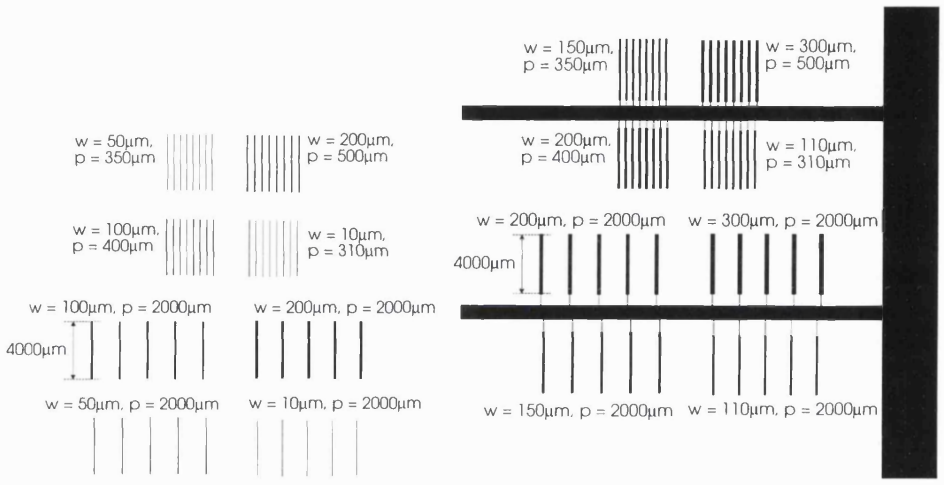

(a) The cylindrical microlens mask

(b) The cylindrical electrode mask

Figure 4.10: The masks patterns used for creating the cylindrical lenses and there electrodes ('w' is the widths of the rectangles, 'p' is the pitch of each group)

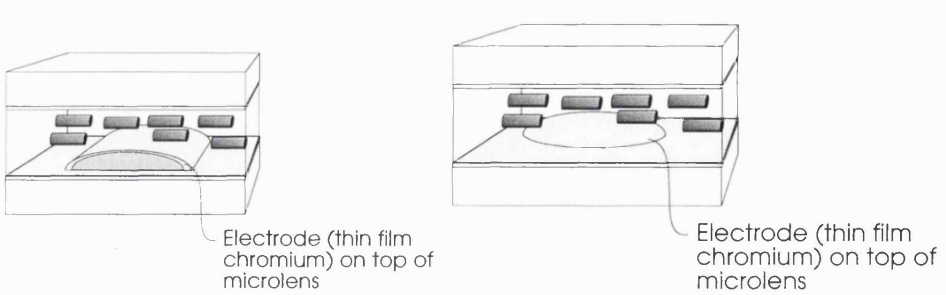

(a) The cylindrical microlens with the electrode on top of the photoresist

(b) The spherical microlens with the electrode on top of the photoresist

Figure 4.11: The two designs with the electrode on top of the microlens

Recalling that $N.A.' = n' \sin u'$ and assuming air for the object and image space ($n = n' = 1$) and $\tan u \approx \sin u$ then

$$M_L = \left(\frac{N.A.}{N.A.'} \right)^2 \tag{4.10}$$

For the DVD read head the NA needs to be increased by a factor of 10 which reduces the focal length shift by a factor of 100.

4.4 Cell construction

4.4.1 Photoresist microlens manufacture

All of the microlenses have been formed using the melt and reflow of photoresist as is described in section 3.2.1. This is a single step lithography process which is, in principle, very simple.

First of all, the substrates are cleaned consecutively with trichloroethane, acetone, methanol and, finally, isopropyl alcohol. The substrate is baked to remove any remaining solvent. Then the substrate is spin coated with a thick photoresist (Shipley STR 1110) to a thickness of $14\mu m$. The solvent in the photoresist is removed with a 30 minute pre-bake (85°C). The sample is exposed to an mercury lamp through the appropriate mask on a mask aligner (Zeiss). There are, in fact, two exposures, the first is to remove the 'edge bead' of photoresist which builds up at the sides of the sample in the spinning process, the second is through the designed mask (see section 4.3). The photoresist is then developed in 351 developer which leaves islands of photoresist where there was chrome on the mask.

The final stage is to bake the photoresist so that it melts and is shaped by surface tension. Thus, with circular islands the photoresist forms a section of a sphere and the rectangular patterns form part of a cylinder. The process is shown schematically in figure 3.1 and the process sheet is given in table 4.1.

At this point, it is possible to etch the microlens shape into the substrate (although etching has not been carried out for this work). However, etching is not possible with ITO coated glass, but microlenses could be formed on uncoated quartz (at least for use with visible wavelengths) if they were to be etched.

4.4.2 Cell assembly

Once the photoresist microlenses are ready then the cell can be assembled. Now the microlens slide, together with another plain ITO coated piece of glass, become the substrates for the liquid crystal. The cell assembly consists of two stages: treating the substrates so they will align the liquid crystal and putting the cell components together.

The liquid crystal alignment was produced by a layer of PVA on the two inner surfaces of the cell (see section 2.4). For the first cells made, this layer was deposited by dip coating the substrate in a PVA/water solution. Later cells were fabricated using spin coating which was more effective for creating a uniform alignment (see section 6.4.1).

The solution used for spin coating was 3% by weight of PVA (molecular weight 125,000) desolved in deionised water deposited onto the substrate through a syringe with

Substrate cleaning		
Ultrasonic bath in Tricholoroethane	10 mins	
(Rinse in:) Acetone		
Methanol		
Iso-Propyl Alcohol		
Dry with N_2		
Hot Plate	90° C	
Resist spinning	Shipley STR1110	
Spin speed	1200rpm	
Spin time	40 secs	
Soft bake	oven (85° C)	30 min
Expose and develop		
Expose on mask aligner	120 secs	
(Karl Suss MJB3)		
to remove edge bead		
Develop in 351 : H_2O (ratio 1:3)	5-10 mins	
Rinse in deionised water		
Dry with N_2		
Expose on mask aligner	150 secs	
(through microlens mask)		
Develop in 351 : H_2O (ratio 1:3)	5-10 mins	
Rinse in deionised water		
Dry with N_2		
Lens shaping		
Melt resist in oven	140°C	30 mins

Table 4.1: Process sheet for microlens manufacture

0.45μm filter. The substrates were cleaned in IPA and a cleanroom wipe (the photoresist being too sensitive for any more aggressive solvents, eg acetone). The substrate was spun at 4,000 rpm for 30 seconds and then placed in oven at 80°C for 30 minutes to drive off the water.

The rubbing of the alignment layers also altered from the first lenses to the last (see section 6.4.1). The very first lenses were produced by using a cleanroom wipe on a mechanical slide. The final lenses were fabricated using a velvet type rubbing cloth on a motor driven rubbing machine (see figure 4.12).

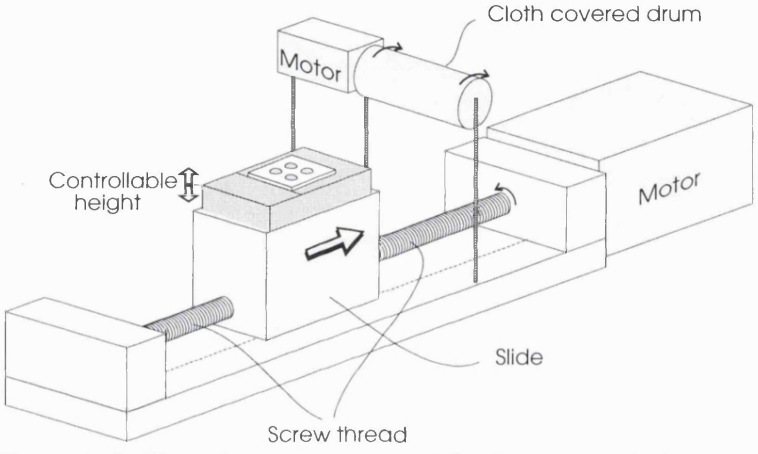

Figure 4.12: The rubbing machine used for liquid crystal alignment

The rubbing machine works by passing the liquid crystal substrate under a rotating, cloth covered drum (radius $30 \pm 0.5mm$). With this arrangement, the strength of the rubbing can be altered, in principle, in 3 ways - the speed of slide can be changed, as can the rotation rate of the drum, or the height of the substrate can be varied. However, the motor driving the slide was not designed to be variable so slide speed was left unaltered ($1.02 \pm 0.01mm/s$). The motor driving the drum was a DC motor whose speed could be changed by varying the applied voltage. However, the motor driving the rubbing cloth drum was specified to work at 12V and due to problems within the gearbox would not work at a constant speed at lower voltages, becoming jerky instead. At 12V, the motor drove the drum at $210 \pm 10rpm$). Thus, only the height of the rubbing sample was varied for optimising the rubbing procedure (see section 6.4.1). A fibre deformation of 1 ± 0.25mm was used as the optimum rubbing height (defining *fibre deformation* to be the distance the slide was moved upwards from its initial contact with the ends of the fibres). Each substrate was only rubbed once thus the rubbing strength, RS (see section 2.4.3, was $650 \pm 150mm$.

Finally, the parts of the cell are ready to be assembled. The two rubbed PVA coated surfaces (one with microlenses) are placed facing each other with their rubbing directions anti-parallel as shown in figure 4.13. Strips of Mylar, 27μm thick, are placed down the sides of the cell to define the cell gap, the strips being parallel to the rubbing direction. Both substrates are left with part of the surface exposed (i.e. the substrates are not matched exactly) to enable the attachment of wires to the electrodes. UV curable glue is placed around the rim of the cell forming almost a complete loop with only a small gap left in one side (a side without a spacer) to permit filling with liquid crystal. The

cell is then clamped together to force the two substrates together upto the thickness of the spacers and the glue is cured with a UV lamp.

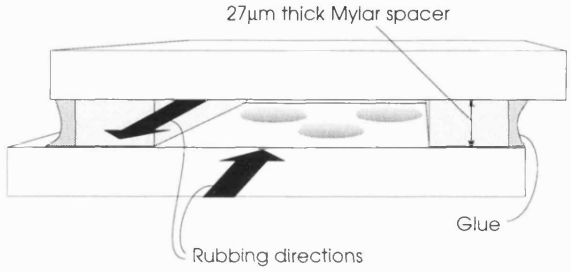

Figure 4.13: The two cell walls of the liquid crystal assembled separated by Mylar spacers

To fill the cell a vacuum chamber is used. A small bath of liquid crystal is placed in the bottom of a chamber with the cell to be filled held with a movable rod above it. The chamber is then evacuated, the cell is then dipped into the liquid crystal bath with the hole left in the glue seal entering the bath first. Finally, air is allowed to re-enter the chamber forcing the liquid crystal into the evacuated cell. The filling direction is the same as the rubbing direction (hence the spacers have to be parallel to the rubbing direction) as the act of flowing also aligns the liquid crystal in the flow direction.

The liquid crystal used in this work was the liquid crystal E7. The material was chosen because it is both a widely used material with documented properties, and also a stable material and with a high birefringence. The properties of E7 are given in table 4.2.

Parameter	Value	Reference
Splay constant, k_{11} (20°C)	11.10pN	[Mer92a]
Twist constant, k_{22} (20°C)	8.8pN	[RTD79]
Bend constant, k_{33} (20°C)	17.10pN	[Mer92a]
Perpendicular dielectric, $\epsilon_{\perp}$ (20°C, 1kHz)	5.2	[Mer92b]
Parallel dielectric, $\epsilon_{\|\|}$ (20°C, 1kHz)	19.0	[Mer92b]
Ordinary refractive index n_o (20°C, 632.8nm)	1.519	[YS89]
Extraordinary refractive index n_e (20°C, 632.8nm)	1.738	[YS89]
Rotational viscosity, γ_1 (20°C)	0.20 Pa s	[KW93]

Table 4.2: Material parameters for liquid crystal E7

The cell is now almost complete, it just needs to be sealed. To this end, the cell is clamped again (despite the spacers and glue the substrates can still bow) and the remaining gap is filled with UV curable glue which is cured whilst the cell is still clamped. The liquid crystal should be protected from the UV light as it can be damaged by exposure to UV (as was unfortunately discovered by experience during this work).

For one of the designs there was an additional step which was missed out in the above description. The strip electrode design (see section 4.3.2) requires alignment of the strip electrode with its corresponding photoresist lens. This was not possible in

the mask aligner since the risk of putting glue into such an expensive instrument was too great. Instead, optomechanical mounts were used to position the substrates (one x-y combination and one rotation mount) meanwhile the alignment was observed in an ordinary microscope. The drawback of this arrangement was that it was not possible to clamp the cell together as effectively with optical mounts (see section 6.5).

Chapter 5

Measurement of cell performance

5.1 Introduction

In this chapter, the methods used to characterise and analyse the the microlenses are described. The cell performance was tested in a number of ways. Firstly, the variation of focal length with voltage was measured. Secondly, having established a voltage dependent focal length, the quality of the lensing was measured including the effect on the polarisation of the light. From these results, it appeared that the observed aberrations were due to the liquid crystal structure and the last part of the investigation centred on the nature of the liquid crystal structure. Finally, the temporal response of the lenses was measured since it will be a major consideration in many applications.

There have been 4 principal techniques used in the investigation of the liquid crystal immersed lenses. The measurement of focal length (section 5.2) was carried out with a microscope. The aberrations of the lenses (section 5.3) were measured by interferometry. Again using the microscope, the polarisation of the light transmitted by the cell has been investigated (section 5.4), particularly with regard to deviations from the input polarisation. Walls and disclinations, which form in some of the devices when a voltage is applied, have also been studied with the microscope(section 5.5). Birefringence profiles of the lenses (section 5.6) were generated using interferometry, but using a different form of interferometry than was used for the aberration testing. Finally, the response times of the lenses have been measured for different voltages (section 5.7).

5.2 Focal length

The focal length is relatively easily measured on a microscope (see figure 5.7) if there is micrometer control of the focus of the microscope. To measure the focal length, firstly the image of the focal spot is located and the micrometer position recorded and then the image of microlens aperture is found and its position is noted. The focal length is taken to be the difference of the two positions. This illustrated in figure 5.1. The microlens was positioned as is shown in the figure, *i.e.* the light passed first through the liquid crystal and then the photoresist lens. This arrangement is chosen for two reasons; it is the configuration for a plano-convex lens which minimises spherical aberration (when imaging infinity[Hec87]) and it minimises the range of angles of the light rays passing through the liquid crystal (since the liquid crystal refractive index is orientation

dependent, the fewer the angles, the more uniform is the effective refractive index).

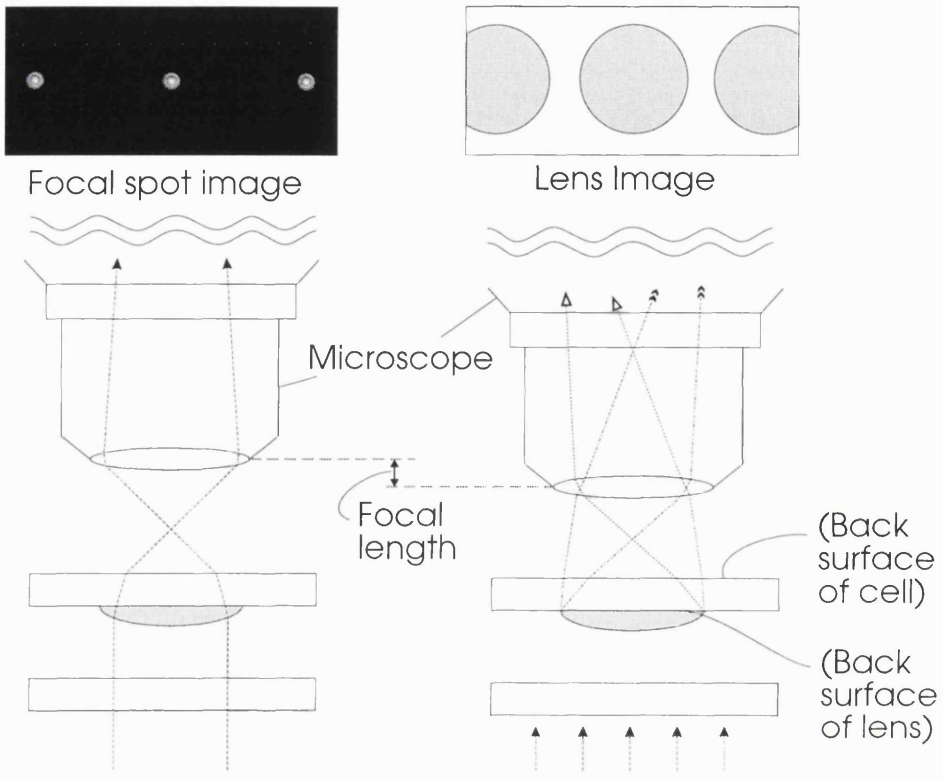

Figure 5.1: Arrangement for measuring the microlens focal length

The focal length measured in this way is the back focal length since the focal length is defined as the distance between the principal and focal planes. For a plano-convex lens the principal planes are near the apex of the convex side [Hec87] as shown in figure 5.2. This distance is not, however, the back focal length of the lens cell since the back focal length is the distance between the last surface and the focus. In this case, the last surface is the non-microlens side of the microlens substrate (see figure 5.1).

Finally, it might be thought that the focal length *measured* would be shortened due to light passing through the glass substrate after the lens, as is shown in figure 5.3(a). However, in fact, the measured focal length will be unaffected since a corresponding shift of position happens to the image of the lens and, thus, the two effects cancel each other out.

If the actual position of the focus relative to the back of the substrate needs to be known then this shift still has to be calculated. For this purpose, a ray diagram is shown in figure 5.3(b). Considering the triangle formed by Δf, x and the ray we can say

$$\begin{aligned} \tan\theta_{air} &= \frac{x}{\Delta f} \\ &= \frac{d\tan\theta_{air} - d\tan\theta_{glass}}{\Delta f} \end{aligned} \tag{5.1}$$

Rearranging....

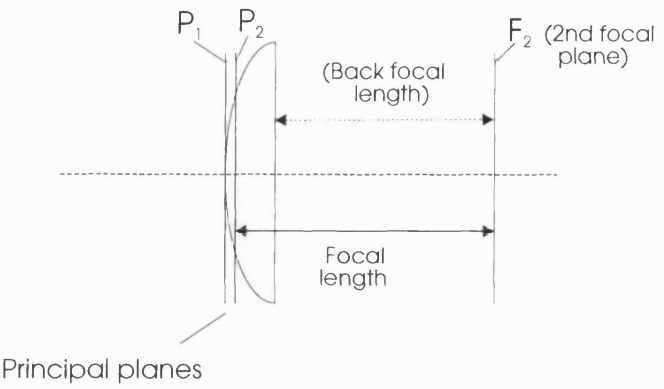

Figure 5.2: Location of the principal planes relative to a plano-convex lens

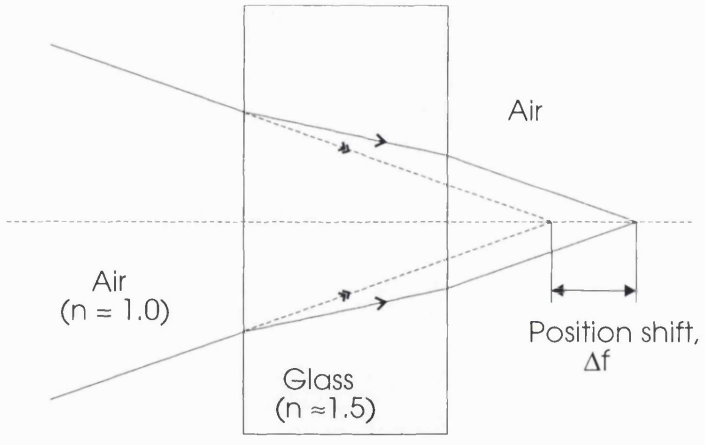

(a) Effect of a plane piece of glass on a converging bundle of rays (equally true for rays in the opposite direction, i.e. diverging).

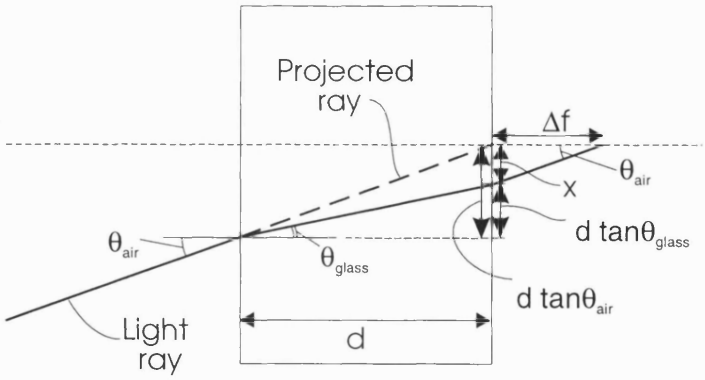

(b) Ray diagram construction to calculate Δf, the shift. Δf is calculated along a line parallel to the optic axis rather than the optic axis itself, as this simplifies the calculation.

Figure 5.3: Bundle rays converging through a plane piece of glass (eg. microlens substrate)

$$\Delta f = d\left(\frac{\tan\theta_{air} - \tan\theta_{glass}}{\tan\theta_{air}}\right) \tag{5.2}$$

From Snell's law we can say

$$n_{air}\sin\theta_{air} = n_{glass}\sin\theta_{glass} \tag{5.3}$$

For small angles $\sin\theta \simeq \tan\theta$, thus

$$\begin{aligned}\Delta f &= d\left(\frac{\sin\theta_{air} - \left(\frac{n_{air}\sin\theta_{air}}{n_{glass}}\right)}{\sin\theta_{air}}\right) \\ &= d\left(1 - \frac{n_{air}}{n_{glass}}\right)\end{aligned} \tag{5.4}$$

For glass of refractive index $n_{glass} = 1.5$, $\Delta f = d/3$, thus for the 1.1mm thick microlens substrates the shift will be 367μm.

The fact that the approximation $\sin\theta = \tan\theta$ is made, is indicative of the fact that as the rays become more inclined to the normal they arrive at different locations along the optical axis. This is because spherical aberration is added to a converging beam when it passes through a plane parallel plate. Thus, in this measurement we are ignoring the effect of spherical aberration. Fortunately, the higher NA microscope objectives have a correction ring to allow for the spherical aberration introduced by a microscope slide so the approximation is justified.

5.3 Lens aberrations

A lens is a device for changing the curvature of a wavefront, as is illustrated in figure 5.4. The ideal final wavefront is a section of a sphere, centred on the image point. For an imaging system, or indeed any system requiring many point to many point imaging it is not possible using spherical wavefronts to have perfect spherical wavefronts for all the image points and, thus, systems are designed as a compromise to give the best overall performance [Hec87]. The deviations from the perfect spherical wavefront are described as *wavefront aberrations.*

A standard way to measure the aberrations of a lens or lens system is to use interferometry. Since an ideal refractive lens system changes the wavefront shape by changing the phase across the wavefront, the measurement of the lens quality should be a measurement of the phase profile of the lens for the object to image distance at which it will be used. However, the phase information of light is too rapidly varying to be measured directly, instead it can be inferred by interferometry [Hec87].

Interferometry is based on measuring the fringes due to 2 or more beams interfering, the intensity of the combination being dependent on the phase difference of the beams. If the beams are mutually coherent then the phase difference can be constant (and hence measurable) although the phases are not. One basic interferometer type, a *Mach-Zehnder* interferometer, consists of a light source, 2 beam splitters and 2 mirrors as shown in figure 5.5.

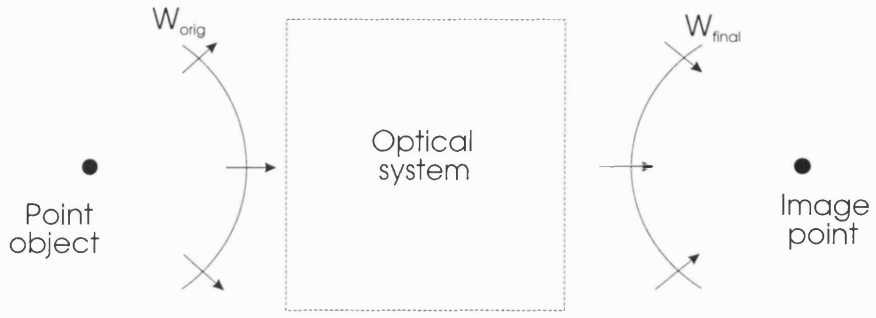

Figure 5.4: Basic function of an ideal lens or lens system

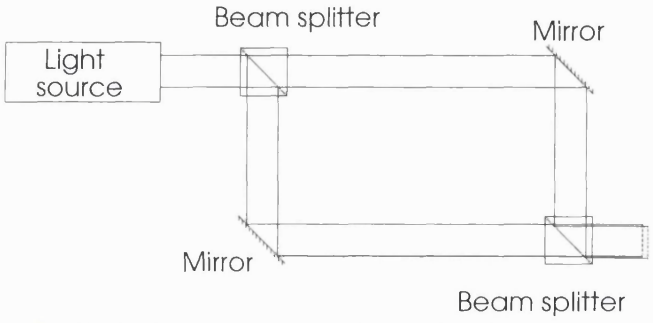

Figure 5.5: The basic configuration of a Mach-Zehnder interferometer

Since the intensity across the combined beam is dependent on the relative phase of the two beams at that point, any differences introduced into part of one beam is easily identified. For instance, if the original beams were planar but then whilst split apart one beam goes through a lens, the fringes will be circular.

Interferometry is a sensitive technique since 2 fringes represent an optical path difference of only $\sim 0.5\mu m$ (using visible light). Thus, if the difference between wavefronts is significant there will be large numbers of fringes across the field of view, too many in fact for a CCD camera with a limited pixel number to be able to image. Therefore, it is not convenient simply to place the lens under test in one arm of the interferometer. There are 2 ways to reduce the difference between the test and reference arms. One is to introduce a high quality lens in the reference beam or the other is to recollimate the test beam with a second lens. For the testing of the microlenses there is an additional problem that the microlenses are very small and the CCD camera does not have sufficient magnification for the lens to fill the field of view, so additional magnification must be provided.

The aberrations of the microlenses have been tested on a standard Mach-Zehnder interferometer appropriate for microlens testing [HDS91b]. The interferometer consists of a polarised He-Ne laser being divided into test and reference beams by a beam splitter which are then reflected off mirrors into the test and reference optics and finally recombined in a 2nd beam splitter (see figure 5.6).

The test optics consists of the microlens under test plus a microscope objective. The objective serves 2 purposes, one is to reduce the divergence of the beam exiting the microlens and the 2nd is to image and magnify the microlens aperture. The reference optics is simply a plano-convex lens orientated to minimise spherical aberration. The

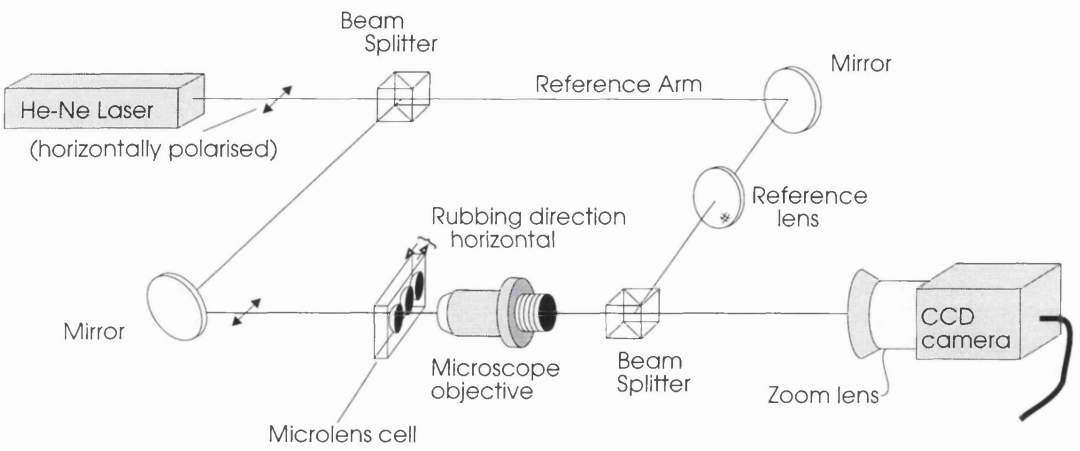

Figure 5.6: Mach-Zehnder used for microlens aberration testing

resulting fringe pattern is captured by a CCD camera with a zoom lens.

The microscope objective must capture all the light exiting the microlens which means it must have a numerical aperture (N.A.) larger than the microlens. The objective used had an N.A. of 0.55 compared to 0.45 for the highest N.A. microlenses (without liquid crystal).

Microscope objectives are designed to a standard where they form their image 160mm behind the shoulder of the objective screw thread. The standard was developed so that objectives are interchangeable on a single microscope and between different microscopes. In order to minimise any aberration introduced by the objective, it is best to use it at its designed object to image distance. Therefore, the objective was positioned so as to form an image of the microlens 160mm behind the objective shoulder. The zoom lens was then focused on that image.

The laser beam was not expanded as it was already much larger than the microlenses ($\sim$1.5mm beam diameter compared to $< 200\mu$m lens diameter) and expanding the beam would simply reduce the intensity passing through the microlens. The polarisation of the laser was parallel to the rubbing direction.

The reference lens was positioned such that the fringes observed were relatively broad ($\sim$10 fringes across the lens image) and as straight as possible. This occurs when the images of the centre of curvature (*i.e.* looking through the beam splitter) of the reference and test beams are equidistant from the viewer and are almost coincident.

The analysis of the fringes was done on a PC. The *Frin II* fringe analysis software was purchased from Oxford Frame Store Applications (OFSA) which enabled on-line analysis of the data. This package consists of a frame grabber with 4 frames of memory and some software to identify fringes and calculate the resultant phase profile (having first removed the tilt component). The fringe analysis works by fringe tracking, viz. the software works on one image only, first identifying minima and maxima working across the image data (the fringes are assumed to be vertical and can be rotated if they are horizontal); the minima and maxima are collected into fringes and, finally, the fringes are ordered.

The identification of the fringes is not always a straightforward process, the software can give incorrect fitting due to gaps in the fringes. These gaps are generated by dust

in the optics, polarisation changes due to twisted liquid crystal structures, scattering structures in the liquid crystal (disclinations, dust) or low transmission due to absorption of the photoresist. To overcome these problems, there are two stages of data editing during processing. The captured image can be altered by a smoothing routine or by the user 'painting' on it, overwriting problematic features. Obviously, care needs to be taken in editing the image. For example, it should be ensured that the fringes thus joined by 'painting', really belong together by shifting the fringes to see if they join when moved. Once the fringes have been identified (assuming the data was good enough not to cause the fringe identification routine problems) then the generated *fringe* data can be edited. The fringe order can be changed, fringes can be deleted or joined together but fringes cannot be added to the data.

5.4 Polarisation

The effect of the lens cell on the polarisation of the transmitted light is useful as a measure of the quality of the alignment. More importantly, a polarisation change could adversely affect the application of the device into a system.

If one considers a layer of uniformly aligned liquid crystal with polarised light incident upon it, since the liquid crystal is a birefringent material, the light passing through the layer will, in general, be changed in polarisation (see section 2.2.1). The only exceptions to this are the special cases either where the birefringence and thickness give a full-wave layer or where the incident light polarisation is parallel to the extraordinary axis or the ordinary plane of the liquid crystal. In addition, if the liquid crystal is twisted through the layer, the polarisation will change (see section 2.2.1).

In all the devices studied in this thesis, the intention is always to have the incident light polarisation parallel to the extraordinary refractive index, viz. the tunable refractive index. This is one of the particular cases where the polarisation does not change. For this to be possible, the liquid crystal director must lie uniformly in the same plane. This plane should be defined by the rubbing direction and the normal to the cell. There are two ways the structure could deviate from this design; either there can be variations on the macroscopic scale of the alignment (*i.e.* the alignment is poorly or non-uniformly defined) or there can be a twist through the depth of the cell.

The observations of the polarisation properties of the lenses have been made using a polarising microscope, shown in figure 5.7. It is a relatively simple task to see whether the alignment is uniformly in the required plane. The cell is observed between crossed polarisers with the rubbing direction aligned with either of the two polarisers. If the liquid crystal director lies in the rubbing direction across the whole cell then no light will be transmitted through the second polariser. However, wherever there is a deviation of the director, the light polarisation will be modified by the liquid crystal and light will be seen at that point. This is illustrated in figure 5.8.

An example of an unaligned cell as seen between crossed polarisers is shown in figure 5.9. There are two distinct features to what is seen, dark lines which come together at various points and horizontal bands of red and blue. The coloured bands are birefringence colours caused by the wavelength dependence (see equation 2.6) of the polarisation rotation in combination with a variation of cell thickness across the photograph. The dark lines are where the liquid crystal director coincides with one of

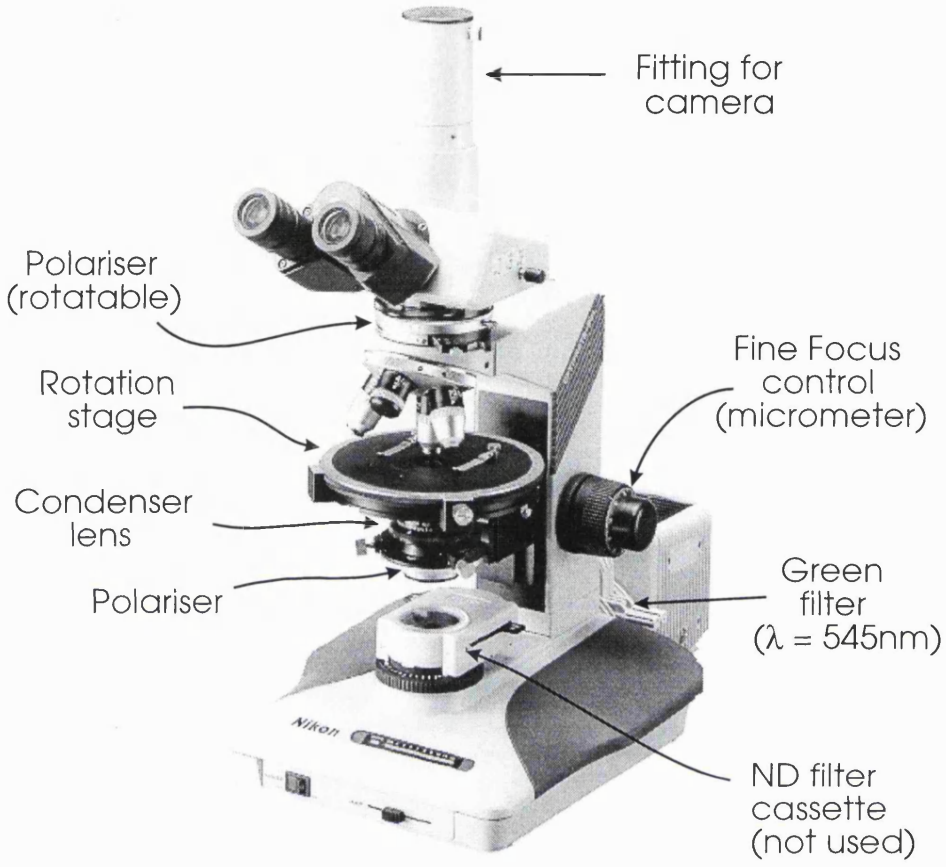

Figure 5.7: Polarising microscope used for lens cell investigation.

the two polariser orientations. The places where the dark lines come together in pairs or groups of four are where there are singularities or disclinations in the liquid crystal director orientation. Where the lines emanate from such a point, the lines are described as *brushes*. The singularities can be points (with 4 brushes) or lines (2 brushes) [dP93], the lines being seen end-on.

In aligned cells, such as the lens cells, brushes are rarely seen and it is only the deviations from the alignment direction that need to be noted. The observation of the liquid crystal between crossed polarisers provides a measure of quality of the alignment. In fact, the arrangement shown in figure 5.8 is very convenient since there is good contrast between the mis-aligned and aligned areas. The more the alignment layer is uniform, the better will be the extinction of the light by the 2nd polariser. Thus, the alignment process can be optimised by comparing the light transmitted between samples (see section 6.4.1).

When trying to determine the twist structure of the liquid crystal from the light polarisation properties, the Mauguin limit (see section 2.2.1) becomes an important consideration. If we are sufficiently above the Mauguin limit then the degree of rotation of a polarisation corresponds to the twist of the liquid crystal. Otherwise, inferring the structure is more difficult. At its thinnest, the liquid crystal layer should be 7μm thick. Assuming a 180° twist, this gives a twist pitch of 14μm. If the liquid crystal

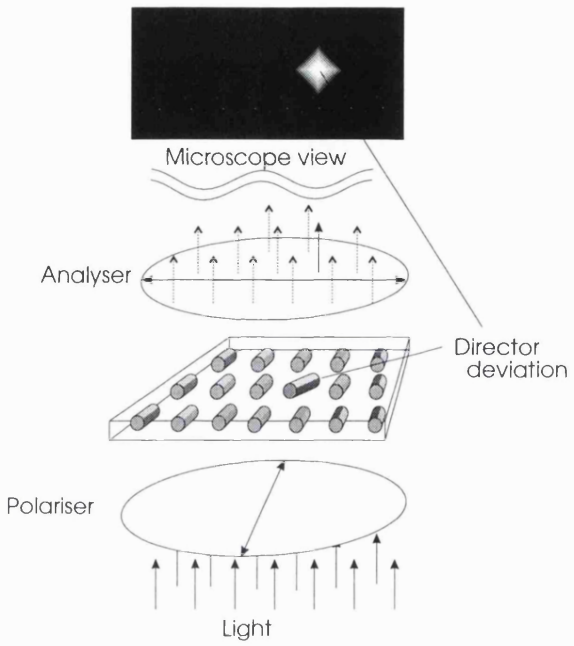

Figure 5.8: A deviation of the liquid crystal as seen down the microscope between crossed polarisers with the rubbing direction aligned with one of the polarisers.

is unswitched, the birefringence $(n_x - n_o)$ of E7, the material used, is 0.22. Therefore, the birefringence-pitch product is 3μm compared to the wavelength of roughly 0.5μm. This indicates that if the twist is uniformly spread through the layer thickness, the Mauguin limit seems a reasonable approximation. If, however, the twist is concentrated in one part of the cell thickness and/or the liquid crystal is partially switched, the approximation becomes more questionable.

5.5 Wall and disclination observation

Wall structures in liquid crystal are readily identified in a polarising microscope. A wall is a rapid distortion of a director field which is kept from smearing out by an electric or magnetic field (see section 2.4.4). Since the liquid crystal refractive index is dependent on the director orientation, a wall creates a rapid change of refractive index. Thus, the wall focuses the light making it easily identifiable. A disclination is much smaller than a wall and thus is much harder to see. In particular where there is an edge (*i.e.* the side of the lens) the disclination can be hidden, especially as the disclination can be pinned to that edge.

Further information on the walls and disclinations can be gathered by applying a low frequency (~10 Hz) electric field which causes hydrodynamic flow. The flow distorts the liquid crystal walls causing them to tilt making them more visible from above (*i.e.* when looking down the microscope - see section 6.4.3).

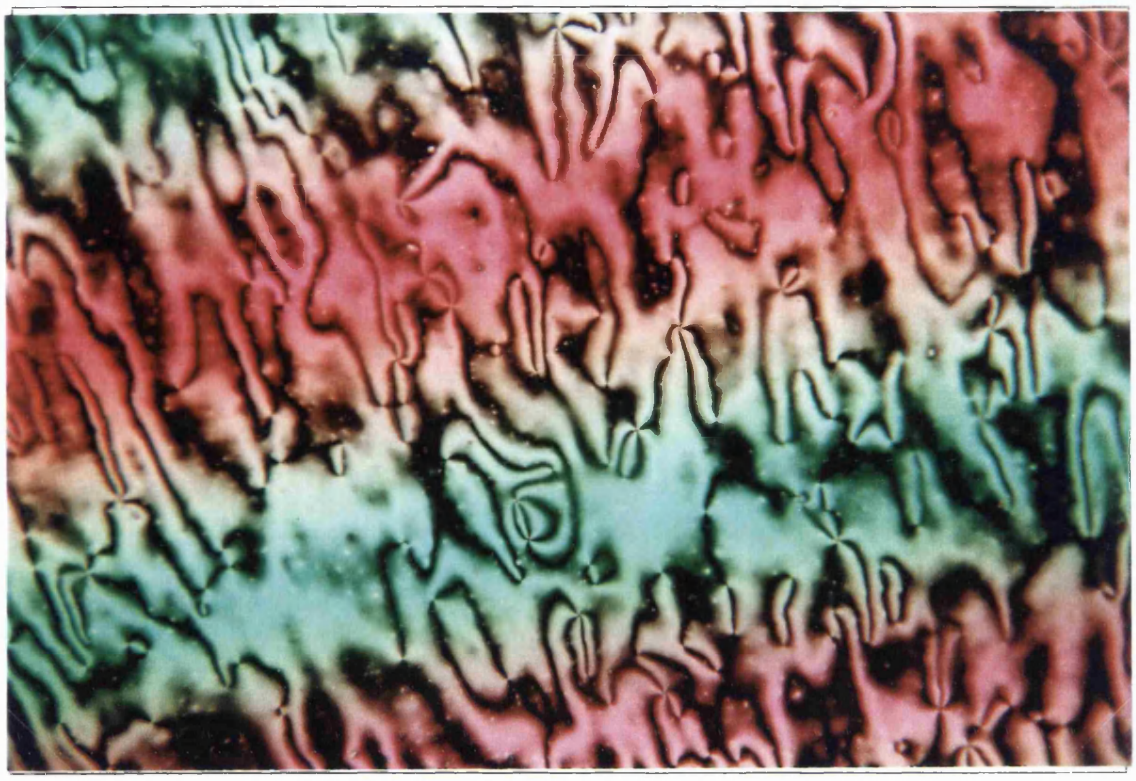

Figure 5.9: *Schlieren texture* of unaligned liquid crystal as seen between crossed polarisers.

5.6 Birefringence

The Mach-Zehnder interferometer proved a useful tool in examining the structures of the liquid crystal (see sections 5.3 and 6.3), however, it was not used with all the devices. The cylindrical lenses proved difficult to measure in the Mach-Zehnder. This is because, for cylindrical lenses, the microlens objective (see figure 5.6) must be replaced with a cylindrical lens. The problem created is that the cylindrical lens does not produce a true image, it can only recombine light which has diverged in one plane. In principle, this would not be a problem if the lenses under examination were sufficiently homogeneous in the orthogonal direction. However, it was not the case. By examining, the birefringence fringes of the lens cell it was possible to extract information about the liquid crystal structure without these problems.

A second motivation for investigating the birefringence properties is that it isolates the liquid crystal properties from the optical properties of other elements. When considering the optical properties of the lenses, it is useful to be able to separate out the non-uniformities of the liquid crystal from any other imperfections. This is possible by examining the birefringence properties since the liquid crystal should be the only part of the devices which is birefringent.

When illuminating a birefringent layer through crossed polarisers (see figure 5.10), the intensity of transmitted light is dependent on several factors. The equation for the transmitted light through crossed polarisers is (see equation 2.6):

$$I_T = I_o \sin^2 2\theta \sin^2 \left(\frac{\pi(n_e - n_o)d}{\lambda} \right) \tag{5.5}$$

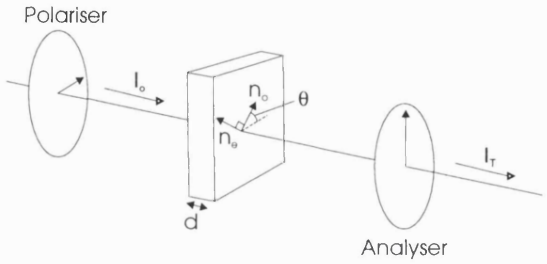

Figure 5.10: A birefringent layer (liquid crystal) between crossed polarisers

Since, in the microlens cell, the liquid crystal layer thickness, d, is varying, birefringence fringes can be seen across the lens (assuming θ is not 0° or 90°) when viewed between crossed polarisers with no voltage applied. As a voltage is applied and the liquid crystal rotates towards the cell normal, the liquid crystal layer presents less and less birefringence to the incident light and the fringes reduce in number and become broader. By measuring the location of the fringes, information on the birefringence/cell thickness product (Δnd) can be obtained.

Measuring the birefringence fringes has the advantage that the measurement relates purely to the liquid crystal structure (assuming the liquid crystal to be the only birefringent material in the optical path), whereas optical phase measurements are affected by all the optical components.

Ideally, the same fringe analysis software would be used on the birefringence fringes as the phase fringes (see section 5.3), however, the birefringence fringes have characteristics which make them difficult to process in the same way as the phase fringes. Unlike the phase fringes, the birefringence fringes are non-uniform in width since the layer thickness variation is non-uniform. Since the birefringence fringe non-uniformity cannot be changed without altering what is being measured, it is difficult to use the fringe analysis package which works best with a uniform spatial frequency. Also, the fringes on the spherical lenses are inevitably circular which the fringe analysis software cannot deal with.

Thus, for the above two reasons only the cylindrical lenses had their birefringence fringes measured. The lens and fringe image was captured by the frame grabber and the image was displayed on the computer monitor. Then the fringe positions were measured relative to the side of the the lens using a ruler. The set-up for measuring the birefringence, a modified version of the interferometer for aberration testing, is shown in figure 5.11.

An extra liquid crystal layer was included in the optical path with its rubbing direction parallel to the liquid crystal on the microlens. This extra liquid crystal layer means that birefringence can be added to the optical path and thus the fringe order can be deduced.

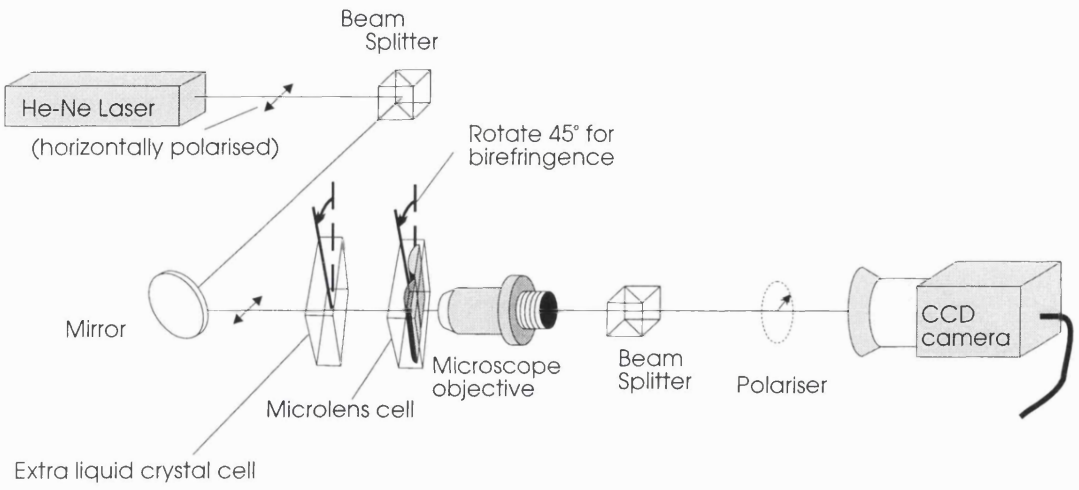

Figure 5.11: Setup used for liquid crystal birefringence measurements

5.7 Timing measurements

The microlenses have been designed with a thin liquid crystal layer expressly because otherwise the thicker liquid crystal layer would slow down the response. Beyond this consideration, however, no attempt has been made to optimise the response time of the microlenses during this investigation. Although no attempt has been made specifically to make the lenses change state faster, the speed of the response has been measured.

A simple measure of the speed of the lenses is the time required is the time required for the focal spot intensity to complete 90% of its eventual change. This is likely to be an appropriate measure for application purposes. To measure this, the experiment shown in figure 5.12 was set-up.

Again, this experimental set-up is a modified version of the interferometer experiment. A signal generator (Philips PM5150) was used to synchronise the application of a voltage with the recording of data. Initially, a calibrated optical power meter (Newport Model 835) was used for taking the light intensity readings, however, it was found that the meter wasn't fast enough for the quickest responses of the lenses (the optical power meter is capable of taking results every ~300ms judging by the fact that LabView could not get a response any faster than this). A higher power laser than the one used for the interferometry was required (15mW vs. 0.95mW) to ensure sufficient light for the power meter for all focal lengths of the microlenses.

Thus, measurements were also taken with a photodiode in place of the power meter and aperture (the aperture not being required due to the photodiode being already small enough). Since LabView needs devices on an IEEE bus in order to talk to them, it could not talk to the photodiode. Instead, a storage oscilloscope (Tektronix 2430A) was used to record the data (simultaneously with the signal generator output) which was then plotted to deduce the response time.

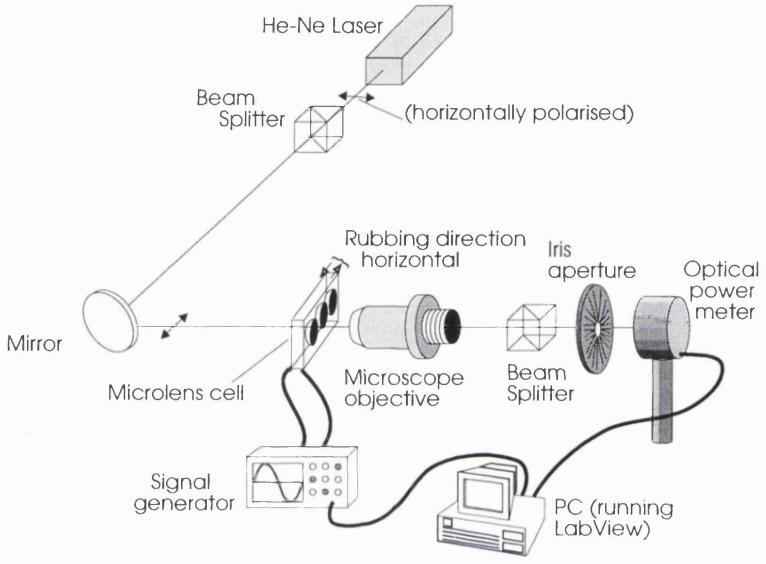

(a) Set-up using optical power meter

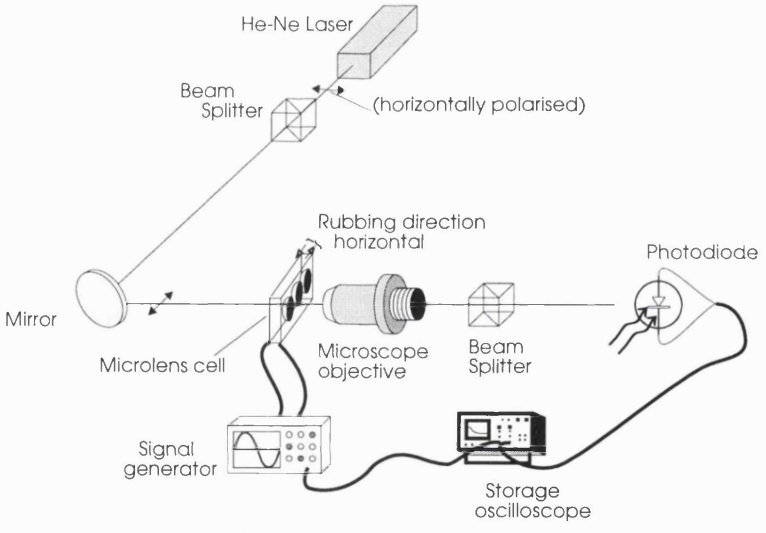

(b) Set-up using a photodiode

Figure 5.12: Experimental set-up for measure the response time of the lenses

Chapter 6

Experimental Results

6.1 Introduction

The first part of the measurements concerned the performance of the lenses, but it became apparent that the liquid crystal structure on switching had a significant rôle in the lensing properties. Thus, the results of the measurements fall broadly into 2 categories: the lensing properties of the devices and the nature of the liquid crystal structure.

The lensing properties are characterised by the focal length and its variation with voltage (section 6.2) whilst the quality of the lensing is measured by the lens aberrations (section 6.3). The structure of the liquid crystal has been studied using a polarising microscope (section 6.4) so much of the results are in the form of photographs (contained in a separate section at the end of the chapter). The profile of the liquid crystal birefringence (section 6.5) provides both details of the lensing properties and gives some insight into the liquid crystal structure. Finally, there is section on the time response of the switching (section 6.6). The chapter begins by examining the results concerning the focal properties of the lenses.

6.2 Focal length

The most important quantity that characterises the lenses is their focal lengths and how they vary with voltage. The focal lengths were measured on a microscope, imaging the microlens aperture and then the focal spot and recording the difference in position from the microscope micrometer postioner, as is described in the measurements chapter (section 5.2). The focal length vs voltage plot for the first microlenses fabricated is presented in figure 6.1. The focal length for the polarisation corresponding to the ordinary refractive index of the liquid crystal does not vary with voltage and is the same as the value for the extraordinary refractive index when 10V or more are applied, namely 560μm.

It was initially surprising that above 3V the focal length rises as the voltage increases. This rise was not expected in the original design (see section 4.3.1). The cause of this rise is an aberration similar to spherical aberration (S.A.) causing a shorter focal length around 3V than would otherwise be the case. This aberration reduces as the voltage increases thus causing the focal length to get longer (see section 6.3).

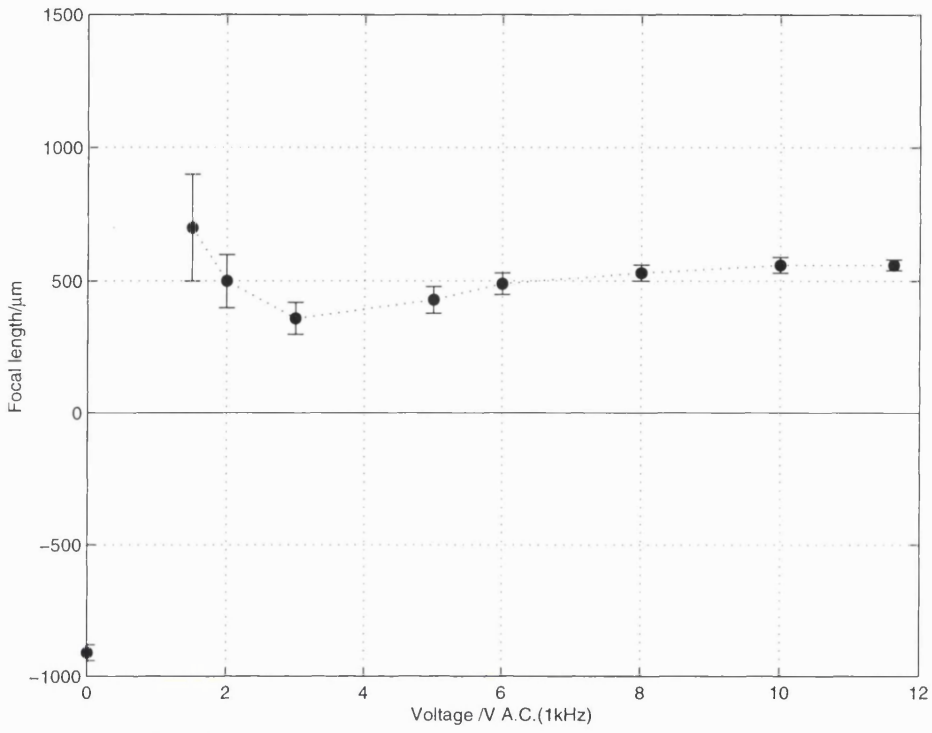

Figure 6.1: The focal length vs voltage results for the original D=100μm lenses

As can be seen from the error bars on the graph, the greatest uncertainty in the measurements is at around 1.5V. In fact, more results around this voltage range would have been desirable but identifying the focus was increasingly difficult as the range was approached. The cause of the imprecision is a combination of two factors; firstly, there is an asymptote in focal length around this range (see figure 4.7) and, secondly, the aberrations of the lenses are largest in this range (see section 6.3). It is unfortunate that the aberrations of the lenses are large in the 1-3V range since this voltage range is where the simple theory (*i.e.* ignoring the effect of the microlenses on the liquid crystal structure-see section 4.3.1) predicts the refractive index should be changing fastest with voltage (see figure 4.6).

The design with the electrode on top of the microlens does not suffer from large aberrations in the 1-3V range (see section 6.3). The focal length vs. voltage relation for these lenses is shown in figure 6.2 together with results for the original design again (but with a larger diameter than the ones described above). The shortening of the focal length of the original design around 1-1.5V is probably the effect of the large aberrations. The rise in focal length seen above 3V with the original lenses does not occur in the electrode on top design since the S.A.-like aberration has been eliminated by the change of electrode position.

The lenses whose results are presented in figure 6.2 are longer focal length lenses than the first lenses since the later lenses were fabricated with larger diameters (which have longer focal lengths for the same deposited thickness of photoresist-see section 3.2.1). The new lens design was fabricated using an array mask (circles of 150μm diameter) in

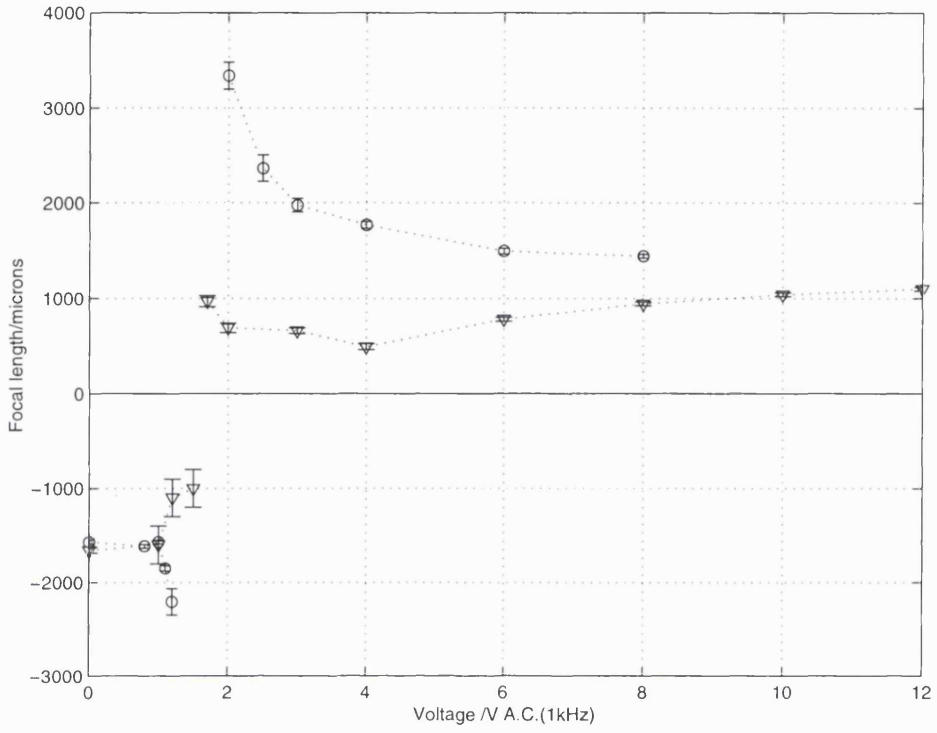

Figure 6.2: The focal length vs voltage results for the microlenses (D=150μm) with the electrode on top (o) and the original design (∇)

order to investigate the issues that arise in an array device (see section 6.4.3). The fact that the original lens design has a focal length which is shorter than the design with the electrode on top is due to the spherical aberration as mentioned above (alternatively, the shorter focal length can be viewed as a result of distortion of the electric field due to the photoresist acting as an patterned-electrode lens, cf. Ref. [NMS91]).

6.3 Interferograms

The testing of lenses by interferometry is long established and is usually a straightforward process. With the advent of interferogram software, the analysis is often almost automated (see section 5.3). However, in the case of liquid crystal immersed microlenses the results are harder to process because of the effect of the liquid crystal on the light polarisation.

As seen in section 6.4.1, the light coming out of the lens can be changed in polarisation (relative to the input) and the change depends on the part of the lens through which the light passed. Since the reference beam is linearly polarised (parallel to the initial polarisation of the test beam) the result of any change of polarisation is a loss of contrast in the interferogram. An example is shown in figure 6.49 (on page 143). Unfortunately, the fringe analysis software package used does not have a way of including what is, in effect, a partial aperture obscuration (see section 6.4.1) - effectively another aberration of the lens. Thus, only the phase aberrations were measured.

A 2nd unusual aspect of the interferogram analysis carried out for this thesis is illustrated in figure 6.3. In this picture of the fringes, 2 fringes combine apparently into a single fringe yet when the phase of the reference arm is changed these two fringes are shown not to be of the same order. This can happen because of twist in the liquid crystal and it means that care has to be taken when recording interferogram data, shifting the fringes (changing the phase in the reference arm) to identify the correct order of the fringes.

Figure 6.3: Interferogram of array of original microlens design (D=150μm). Note the 2 fringes combining into a single fringe (at the centre of the magnifying glass symbol).

The interferometric results from the original lens design are shown in figures 6.4 and 6.5. It can be seen from these results that the aberrations increase markedly when the voltage is sufficient to start the liquid crystal switching (roughly > 1V) and then as the voltage increases further, the aberrations reduce. The effect of wavefront aberrations on focusing quality is non-linear. Small phase aberrations do not result in significant change in image quality, indeed, 0.07λ is usually considered diffraction limited (Maréchal criterion [BW80]). However, as the aberration gets larger, light from some parts of the aperture will cancel out the light from other parts. When the aberrations become greater than 0.5λ then any additional aberration will make little difference since 0.5λ means part of the light exiting the aperture is already in anti-phase to other light beams. As the measurements indicate, the usable voltage range is above 4V (see also figure 6.2).

There are 2 characteristics of the aberrations that have been identified (above 0V). The first is a curvature difference between the centre of the phase map and the second is a symmetric aberration about a line in the rubbing direction through the lens centre.

The curvature difference in the phase map is the spherical-like aberration mentioned in the previous section. The difference is due to the liquid crystal not being as switched in the centre of the lens as at the edge. The liquid crystal response is determined by the applied voltage not the applied electric field (see chapter 2) and, in this design, some of the voltage is dropped across the dielectric of the photoresist, thus, there is, in effect, a lower applied voltage where the photoresist is thicker.

The initial saddle shape of the wavefront in the rubbing direction can be explained by the alignment. In theory, the liquid crystal aligns with the alignment layer (plus a couple of degrees for the pre-tilt) which means that the liquid crystal director on the surface of the microlens will follow the profile of the microlens. That is, as shown in

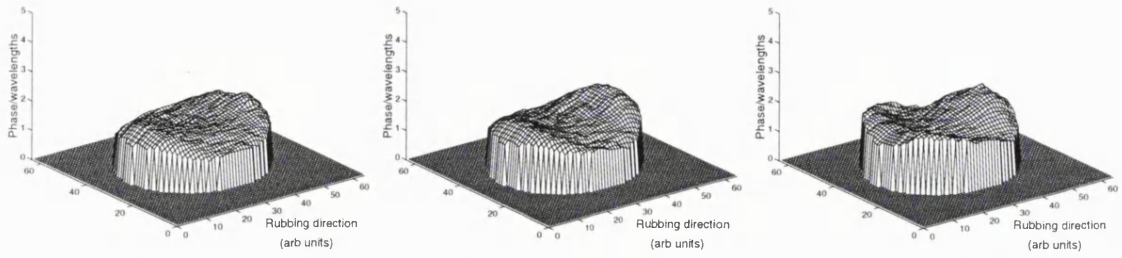

(a) 0V (RMS: 0.18λ) (b) 1V (RMS: 0.22λ) (c) 1.2V (RMS: 0.22λ)

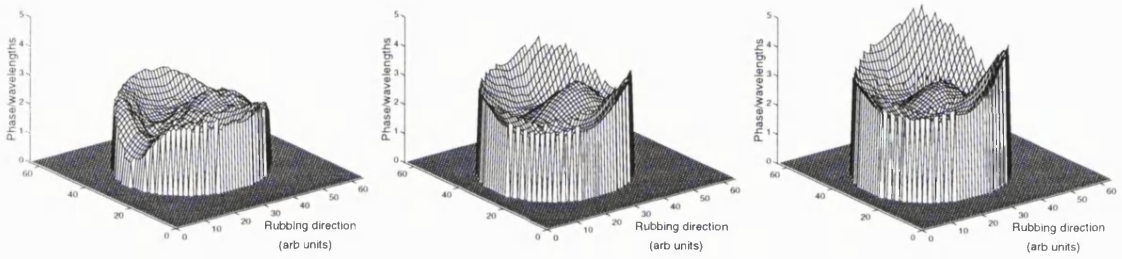

(d) 1.5V (RMS: 0.35λ) (e) 1.7V (RMS: 0.45λ) (f) 2V (RMS: 0.55λ)

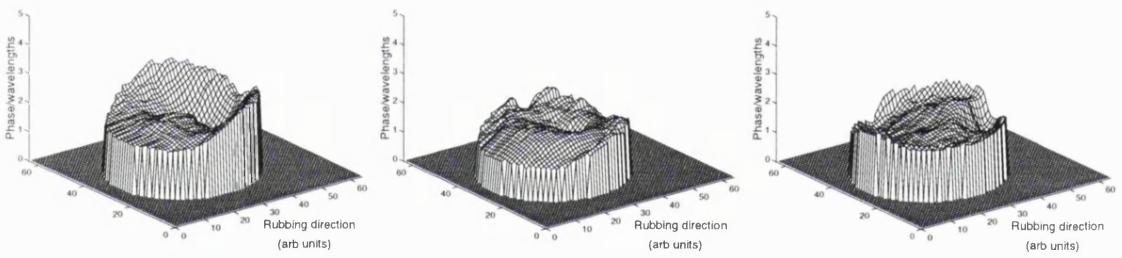

(g) 3V (RMS: 0.38λ) (h) 4V (RMS: 0.20λ) (i) 8V (RMS: 0.27λ)

Figure 6.4: Wavefront aberration plots of the original microlenses (D=150μm).

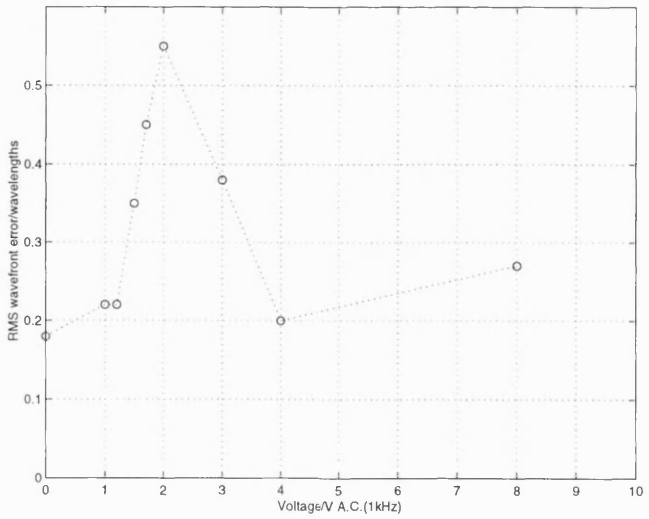

Figure 6.5: RMS wavefront error (λ) vs Voltage for 150μm diameter lenses. Original design.

figure 6.6, travelling in the rubbing direction, the director on the surface just before the lens is at 2° to the plane of the cell and then, once on the lens, the orientation starts at 42° and goes to −38° on the other side of the lens before reverting to the orientation on the glass surface, namely 2°. Since the pre-tilt affects the director profile and, thus, the effective refractive index, it reasonably explains the saddle shape. In fact, these boundary conditions were used in a model which produces results (see chapter 7) similar to the measured data.

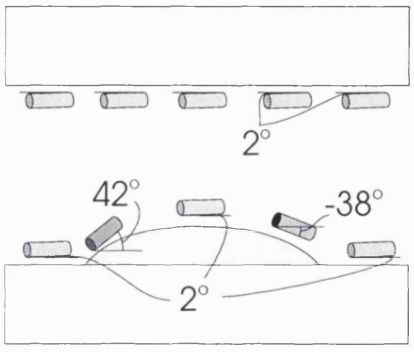

Figure 6.6: Pre-tilt variation as the pre-tilt follows the surface profile, plus 2°

The explanation above is convenient because the well-defined and rigid boundary conditions allow modelling of the device. However, there are 2 problems with the explanation. One, is simply the question of how credible are the assumed boundary conditions. The sharp transitions in director orientation at the lens edge seem unlikely in an elastic medium (unless a disclination is present in which case it is entirely reasonable). Secondly, the conclusion from the polarisation measurements (see section 6.4.1) that the liquid crystal is twisting is something which has not been included in the model. The assumption that the director on the microlens surface follows the profile of the lens produced reasonable agreement up to $\sim 2V$ when used in a computer model (see section 7.3). It seems reasonable to suggest that the twist becomes important above this voltage and that this is why the modelling matches the experiment less well at higher voltages.

The results of the interferometric testing of the lenses with the electrode on top of the microlens are shown in figure 6.8. The most notable feature of these aberration plots is the absence of any aberrations, as compared to the original lens design (NB: note the change in scale between figures 6.4 and 6.8). The most marked aberration is a saddle shape which is evident at 6V and above. This saddle type aberration is reasonable if the pretilt varies in the rubbing direction but not orthogonal to it and, indeed, it appears in the modelling predictions (see chapter 7) albeit in different proportions to those measured. If we examine the plot of the RMS error vs voltage (see figure 6.7), there is a large change for the better compared to the plots for the original design for 1-3V shown in figure 6.5. This improvement is especially beneficial since the refractive index of the liquid crystal should be changing fastest in this region (see figures 4.6 and 4.7), a fact which also renders the saddle aberration less important since the focal length is not changing much in its corresponding voltage range anyway.

One factor not recorded in the interferogram plots is the tilt of the wavefront coming out of the lenses. The interferogram analysis software requires that the reference

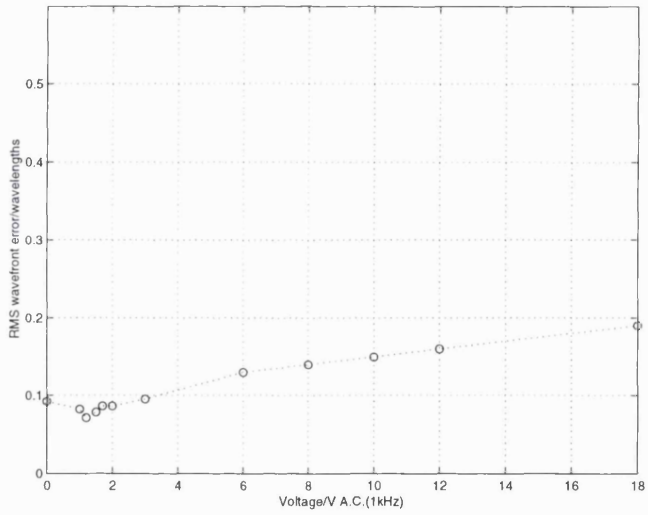

Figure 6.7: RMS wavefront error (λ) vs Voltage for 150μm diameter lenses. Electrode on top of the microlens design. (Vertical scale the same as figure 6.5)

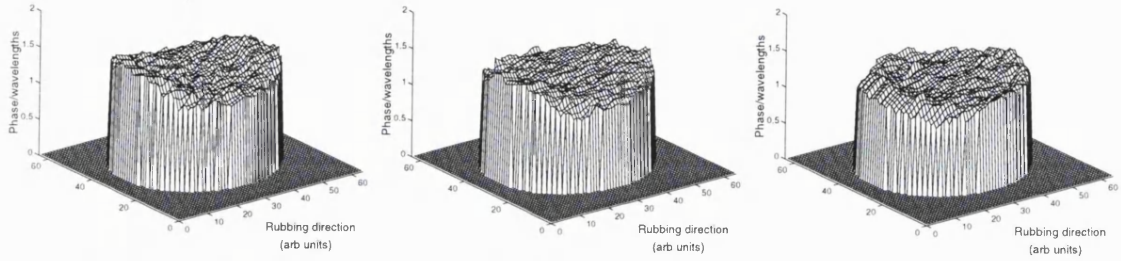

(a) 0V (RMS: 0.092λ) (b) 1V (RMS: 0.082λ) (c) 1.2V (RMS: 0.071λ)

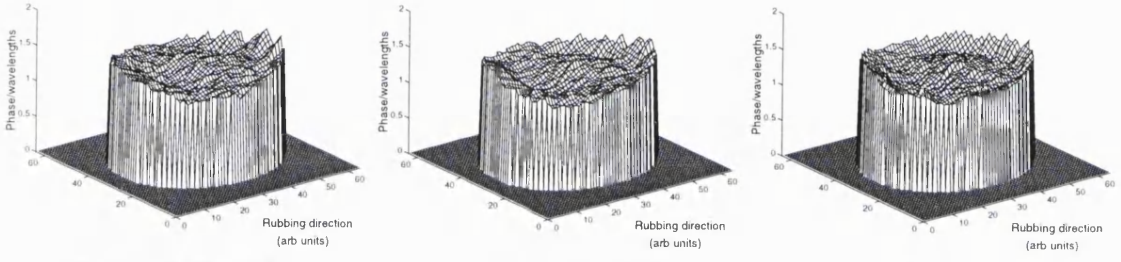

(d) 1.5V (RMS: 0.078λ) (e) 1.7V (RMS: 0.086λ) (f) 2V (RMS: 0.086λ)

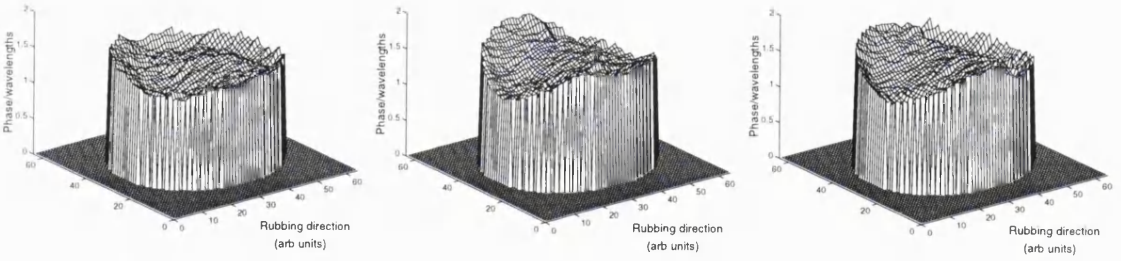

(g) 3V (RMS: 0.095λ) (h) 6V (RMS: 0.13λ) (i) 8V (RMS: 0.14λ)

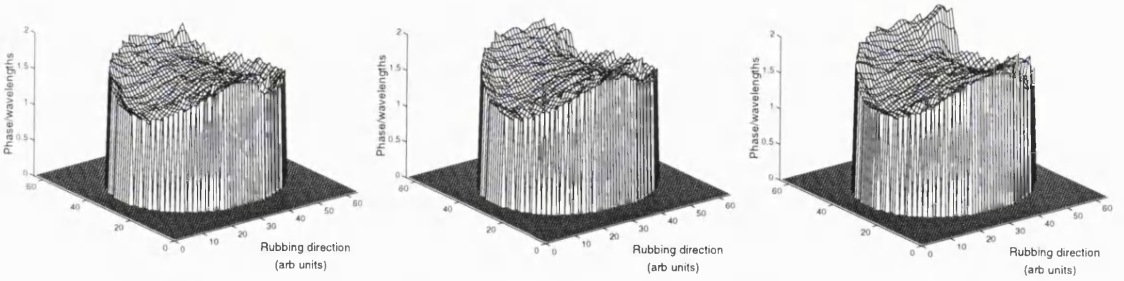

(j) 10V (RMS: 0.15λ) (k) 12V (RMS: 0.16λ) (l) 18V (RMS: 0.19λ)

Figure 6.8: Wavefront aberration plots of the electrode microlenses (D=150μm).

wavefronts be tilted w.r.t. the test arm and then automatically removes the tilt as part of its analysis. Unfortunately, the program does not record the amount of tilt removed. This is unfortunate since there is a variation of the tilt coming out of the microlens. It can be seen in the birefringence fringes so measurements of birefringence fringes were also taken (on the cylindrical microlenses only - see section 6.5).

As mentioned above whilst measuring the microlens aberrations it became evident that for some parts of the lens the polarisation of the light was being altered by the liquid crystal - an effect that could only occur if the liquid crystal in that region was no longer in the plane defined by the rubbing direction and the cell normal. The effect of this deformity can not easily be analysed by measuring the phase aberrations of the lenses. These affects are discussed in the next section.

6.4 Liquid crystal structure

There are 2 criteria for the desired liquid crystal structure. The first is that the liquid crystal director is always parallel to one plane, namely, the plane containing the rubbing direction and the vector normal to the cell. This condition ensures that the refractive index is being changed only for the intended polarisation. The second criteria is that the liquid crystal structure is uniform in the sense that, across the microlens, the liquid crystal introduces the same optical path per unit distance averaged over the liquid crystal thickness. This section is concerned primarily with the first criteria and only with gross deviations (in the form of liquid crystal defects) from the second.

A liquid crystal which is non-uniform or misaligned in one area will, in general, change the polarisation of the light transmitted in that area. The resultant variation of polarisation of the light exiting the device will reduce the quality of the focus since orthogonal polarisations cannot interfere (the two polarisations must be treated separately).

The quality of the lenses can also be reduced by liquid crystal defects. Walls and disclinations (liquid crystal defects) occur in some of the devices when a voltage is applied to them. Those defects can scatter light and promote polarisation changes. Also, they are often slow to disappear (assuming they disappear at all), relative to the time required for the switching of the liquid crystal, thus increasing the effective response time of the lens (see section 6.6).

The liquid crystal structure arises from the interaction of the liquid crystal alignment and the electric field distribution. It is generally simpler to modify the alignment technique than it is to alter the electric field distribution by designing a new mask and fabricating the structure. Hence, it was possible to be more speculative in trying different alignment techniques than was the case in trying new electrode/photoresist designs. The results of various alignment techniques are detailed below, in particular, with regard to their performance in terms of polarisation preservation and disclinations.

6.4.1 Polarisation changes with original design

A micrograph (*micro*scope photo*graph*) of the original lenses, made by C.H. Chia, can be seen in figure 6.20 (on page 112). A polarising microscope was used which contains 2 polarisers, one above and one below the sample (see chapter 5). In the micrograph, the two polarisers are crossed, thus with no liquid crystal the micrograph would have

appeared black. The cell was inserted with the PVA rubbing direction (liquid crystal alignment direction) parallel to the first polariser such that if the liquid crystal director was uniformly aligned the picture would still be uniformly dark. Wherever the liquid crystal director deviates from the rubbing direction, the polarised input light propagates along the two optical axes of the birefringent liquid crystal so the polarisation is changed and some light is transmitted through the second polariser (see figure 5.8). This arrangement is convenient because the high contrast makes identifying areas of non-uniform alignment relatively simple.

The first micrograph shows that, since most of the cell and microlenses appear black, there is a general alignment with the rubbing direction. Two others facts are evident from this micrograph:

- Each lens is surrounded by a halo of light, i.e. badly aligned or misaligned liquid crystal.
- In general, there are quite a few particles distorting the liquid crystal.

Of these lenses, the $100\mu m$ lenses had the most spherical photoresist profile as measured by an Alpha step machine [CHI94] (the larger lenses being flat topped) and, therefore, were chosen as the lenses to be studied in more detail.

Examining the liquid crystal structures

If the $100\mu m$ lenses are examined more closely (see figure 6.21 (on page 113)), one further detail becomes apparent - on one side of the lens, the leeward side w.r.t. the rubbing direction, the 'halo' of light mentioned above encroaches onto the lens itself. This cell was taken apart and chromium was deposited on the microlenses in order to inspect the PVA layer in a scanning electron microscope (SEM). The SEM inspection showed 2 characteristics of the PVA layer. The first can be seen from figure 6.22 (on page 114). A distinct flow direction can be seen in the PVA. Near the microlens edge the direction appears to follow the curve of the microlens, but further away from the microlens (the top right hand corner of the picture) the pattern is left to right (the rubbing direction). The left to right pattern predominated except near the microlens edge as shown. Overall, the pattern can perhaps be explained by the alignment layer preparation used. The PVA layer was dip-coated onto the substrate to be rubbed, ensuring that the direction in which the PVA drained away was the same as the rubbing direction. Therefore, the pattern observed could be due to the pre-rubbing drain alignment of the PVA which would flow around the microlens in a similar fashion to the pattern. A 2nd observation from the SEM photographs can be made from figure 6.23 (on page 115). In this photograph, it can clearly be seen that some of the PVA layer has been taken off the top of the microlenses in the rubbing process. It is quite possible that the (rubbed) photoresist, similarly to the PVA, will induce some alignment, however, the generated semi-attached or detached particles of PVA would scatter light (either directly or by deforming the surrounding liquid crystal).

In the results presented so far, alignment has been considered only in its initial state, *i.e.* with no voltage applied. With this first lens cell design, a significant change occurs to the polarisation of the light transmitted as a voltage is applied. This can be seen in figure 6.24 (on page 116). N.B. when a voltage greater than the threshold

voltage is applied, a liquid crystal wall structure forms initially but then disappears (see section 6.4.3), the micrographs are taken after the disappearance of the wall. From the figure, light is clearly being 'lost' into the polarisation orthogonal to the input polarisation. This is verified by looking at the light transmitted through the lens in the input polarisation as in figure 6.25 (on page 117).

The most obvious characteristic of these micrographs is that, as the applied voltage increases, the area of the lens where the light is left in the original input polarisation decreases until it becomes a strip across the centre of the lens. This characteristic is voltage dependent, and does not depend on the previously applied voltages.

These polarisation altering characteristics are almost certainly due to the liquid crystal being twisted (the only alternative being that the whole liquid crystal layer is rotated in one region). As a voltage is applied to the cell, the liquid crystal forms a twisted structure, requiring higher voltages to start twisting where the photoresist is thicker (*i.e.* towards the centre of the lens). The strip across the centre of the lens indicates that there is no twist along the strip (in the rubbing direction).

A possible explanation for this twisting behaviour is that by rotating to point towards the centre of the microlens, the liquid crystal director on the microlens surface minimises the angle away from the electric field (whilst remaining fixed in the plane of the surface). Since in the centre of the cell the director will be much closer to the electric field direction, such a structure reduces the splay (see section 2.3) of the liquid crystal director between the microlens surface and the centre of the cell at the expense of introducing twist and of breaking away from the rubbing direction (see figure 6.9). This assumes that the in-plane anchoring energy is much weaker than the out-of-plane anchoring. Unfortunately, the author is not aware of any directly comparable figures, the nearest being $0.1 \rightarrow 1 \times 10^{-5} J/m^2$ for the in-plane anchoring energy of liquid crystal GR-41 on rubbed PVA [SSU92] as compared to $3 \times 10^{-4} J/m^2$ for the out-of-plane anchoring energy of liquid crystal 5CB on rubbed PVA [SFR+96].

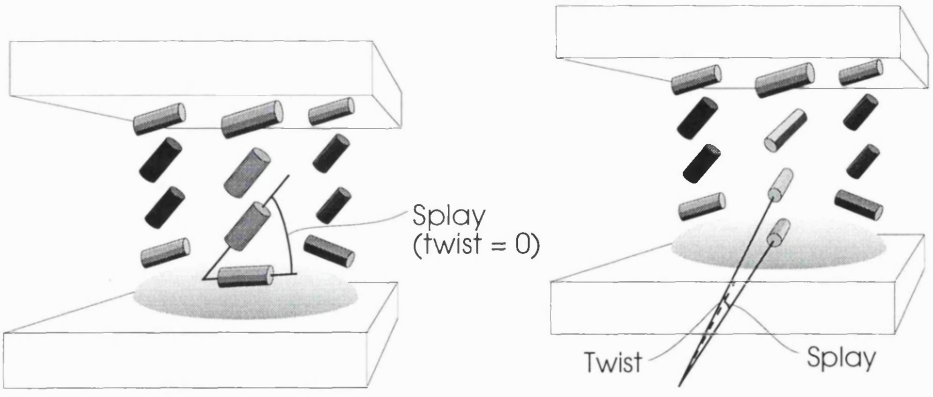

(a) Untwisted structure

(b) Twisted Structure (with less splay)

Figure 6.9: Comparison of a twisted and untwisted liquid crystal structure on the microlens

A second possibility is that the electric field is not completely normal to the cell but has a component in the plane of the cell. The electric field distribution has been calculated using the modelling programs of Fabrizio Di Pasquale (see section 7.5). The electric field distribution for the cases where the director distribution is assumed to be

ideal are shown in figures 7.11 and 7.12. In the case where the director is fully switched, the field distribution is valid for all sections through the microlens (which pass through the centre of the lens). For the off-state, there is a variation for different orientations of the section since there is a variation of the dielectric of the liquid crystal in the cell plane depending on the orientation. It can be seen (figure 7.12) that there is component towards the centre of the lens and, thus, the liquid crystal, following the field, will rotate towards the lens centre (as well as up, out of the cell plane). Therefore, the structure will be something like that shown in figure 6.10. Since this structure assumes the director returns to the alignment direction at the surfaces and the overall twist is zero, then this explanation assumes that the twist is sufficiently tight that the Mauguin limit does not apply (see section 5.4). Also, it can be seen that on the negative pretilt side of the lens a sharp transition of twist might be required; starting at positive pretilt side of the lens (left hand side in figure 6.10), the inclined electric field does not necessitate any twist in the rubbing direction, but then going around the lens the required twist increases until at the other side of the lens 180° is required. However, following the same path but in the opposite direction around the lens (*i.e.* along the far side of lens in the figure), an opposite −180° twist is generated, which meets the previous 180° twist along the line of the rubbing direction on the negative pretilt side of the lens. Thus, a rapid untwist and twist of the liquid crystal is required, given that no disclination is observed.

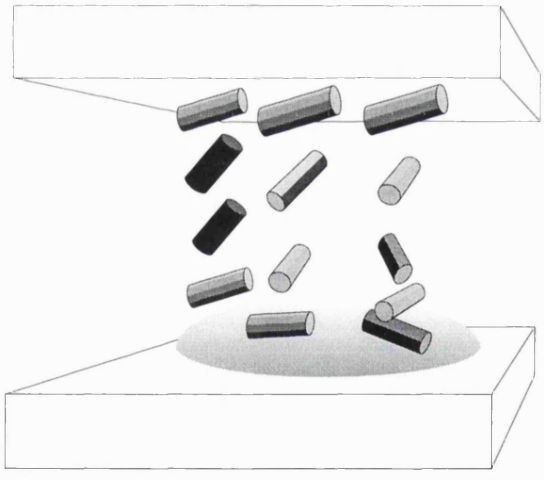

Figure 6.10: Liquid crystal twisting towards the lens centre, immediately above the lens surface to follow the electric field. Notice that that twist increases from the positive to negative pretilt side of the lens (*i.e.* left to right in figure) and that the liquid crystal twists going to towards the centre of the cell and then beyond some point untwists towards the other cell wall.

The 'S' shape at the end of the strip (figure 6.24 (on page 116)) might be thought to be due to bad alignment on the 'leeward' side (w.r.t. to the rubbing direction) of the microlens (see figure 6.21 (on page 113)), however, the basic 'S' shape appeared on all the lenses in the array indicating it to be another characteristic of the original design. The 'S' shape only appears after the wall loop has disappeared (see 6.4.3). When the wall is present with high fields there is the same strip which simply goes through the wall following the rubbing direction.

Effects of the twist on device performance

The change of polarisation of the light transmitted for parts of the aperture could be a serious problem in many systems. The biggest problem the polarisation change creates is that, in effect, it distorts the aperture. If a linearly polarised beam goes into the lens, the light emerging will have a variation of polarisation across the beam. The distribution can be considered as made up of two amplitude functions in orthogonal polarisations which, when focused to a spot, will be two spots in the two polarisations superimposed. Both these spots would be larger than would be the case with a beam of the same width but of a uniform polarisation distribution and both would be distorted away from the circular symmetry of the Airy disc.

A second potential problem arising from the above device characteristics concerns its interaction with the possible other components of an optical system. Since the device only varies its focal length in one polarisation, it might be advantageous to use polarisation sensitive optics elsewhere in the system. However, this approach would probably be jeopardised by the polarisation characteristics of the device described above.

Possible ways to reduce the twisting

There are various approaches that might reduce the twist. If the liquid crystal is breaking away from its alignment layer (rather than twisting sharply above it) then by making a stronger alignment layer the liquid crystal the liquid crystal may be prevented from twisting. Other possible solutions are more speculative. It is possible that the twist is starting because of the misalignment around the edge of the microlens, thus, an alignment technique which was equally effective over all sample might remove the twist. Such an alignment technique would, in fact, be desirable since the misalignment of the liquid crystal around the edge of the lens reduces the useful aperture of the lens. Alternatively, a material could be used with a higher elastic coefficient for twist (relative to the bend and splay coefficients) thus imposing a greater energetic cost for a twist deformation.

If the alignment technique was changed to one which produced a uniform pre-tilt across the sample, the twisting of the liquid crystal maybe reduced, although it is not immediately clear from the above evidence that this should be case. Similarly, a change in the electrode structure could reduce the twist if the lateral electric fields (as suggested above) are causing twist. Both these last suggested changes, however, have more compelling reasons for being tested which will be described in subsequent sections. However, the impact of these design modifications on the polarisation properties of the microlenses is described below.

6.4.2 Polarisation changes with other designs

Cylindrical lens designs

As mentioned earlier, with the original lens design, the liquid crystal does not twist along the line across the microlens centre in the rubbing direction. This implies that a cylindrical lens with the rubbing direction perpendicular to the long axis of the lens should not generate a twisted structure when a voltage is applied. It was partly to test this idea that cylindrical liquid crystal immersed microlenses were fabricated. The first

cylindrical microlenses fabricated were cylindrical versions of the original design (see sections 4.3.2 and 4.4).

When a voltage was applied to the devices, it was initially the case that there was no twist as evidenced by the fact that the polarisation was apparently unchanged. The untwisted structure lasted whilst there was a wall structure seen in the liquid crystal (see section 6.4.3), however, once the wall had receded there was a strip of twisted liquid crystal down one side of the lens. This strip can be seen in figure 6.42 (on page 135).

This observation casts doubt on one of the proposed causes of twist which was that the twisting occurs so that the splay through the cell is minimised whilst remaining parallel to the surface (see previous section). Clearly, with the alignment across the cylindrical microlens the minimum splay condition (whilst remaining parallel to the microlens surface) is already fulfilled. Thus, if the explanation for the induced twist based on reducing the splay by turning to the maximum surface gradient is correct (as a mechanism occurring on the spherical microlenses), it cannot be the complete explanation.

The second explanation for the twist on the microlens, based on the inclined electric field, does not first at sight appear a likely explanation either. On the cylindrical lens, all the inclined fields still lie in the plane defined by the rubbing direction and the cell normal. However, when one remembers that the wall structure has receded and thus one pretilt has predominated over all the cell then it can be seen that on the negative pretilt side of the lens a very large splay is required ($> 90°$). Add in the inclination of the field towards the lens centre and the splay becomes even larger. Since large splays are often replaced by twist where both will meet the boundary conditions (the splay elastic constant, k_{11}, being usually larger than the twist elastic constant, k_{22}), there is a possible mechanism for stabilising the twist with the inclined fields.

In total, three electrode configurations have been tried with the cylindrical microlenses (see chapter 4). The 2 new designs (the designs with a strip electrode and with the electrode on top, *i.e.* ignoring for a moment the cylindrical version of the original design) were not designed with the intention particularly of removing the twist from the liquid crystal structures, however, simply changing the design may have the benefit of reducing the twist. The polarisation properties of the cylindrical lenses were examined by passing a laser beam through them; lasers have the advantage of being more collimated than microscope illumination. The results for the 3 cylindrical lens designs can be seen in figure 6.11. From these pictures, it can be seen that the only design to cause a change in the polarisation of the transmitted light over a significant area of the microlens is the original design, with the continuous electrode under the microlens.

The immediate question is how have the electric field changes avoided the twist of the original design? Unlike the shrinking wall of the original design, the strip electrode design never eliminates the negative pretilt from the structure (see section 7.5) thus not incurring the large splayed structures of the original design. The design with the electrode on top has the field normal to the microlens surface (see figures 7.13 and 7.14) so that the splay is no greater than that in a more usual flat substrate cell. Both these observations support the explanation for the twist originating from large splay.

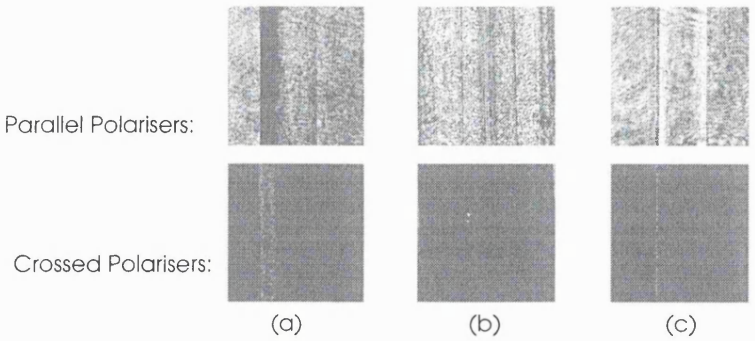

Figure 6.11: Light transmitted by the cylindrical microlenses at 8V (a) the cylindrical version of the original design, (b) the cylindrical lens with a strip electrode opposite and (c) the cylindrical lens with the electrode on top of the lens (cells between crossed and parallel polarisers). The microlens widths are $100\mu m$.

Spherical lens with the electrode on top

Turning back to the spherical microlenses, it was hoped that the absence of polarisation change on the newer design cylindrical microlenses would be mirrored in the spherical microlens with the electrode on top of the lens. Indeed, there was an improvement but the result was not a complete removal of the polarisation change (see figure 6.32 (on page 125)) but the area over which the effect occurs is less than with the original design. Looking between crossed polarisers as the voltage is increased a dark cross appears in the image of the microlens, emerging from the left hand side in the photos (the rubbing direction is from left to right on the microlens surface in these pictures). As with the original design, one possible cause of the cross shape, again as illustrated in figure 6.9, is that the liquid crystal is breaking away from its alignment direction to point towards the centre of the lens to minimise splay. If this behaviour is taken to the extreme then all the directors will be pointing to towards the centre of the microlens resulting in a disclination at that point. This would result in brushes (see chapter 2) which are not in evidence as is shown more clearly if the analyser is rotated by 45° relative to the input polariser and the lenses such that the rubbing direction such that the rubbing direction is at 90° relative to the analyser (see figure 6.33 (on page 126)).

The explanation for the twist on the spherical microlenses again could be the inclined fields (see figures 7.13 and 7.14 for the fields), however, in contrast to the original design the electric fields are normal to the microlens surface not nearly parallel to it. The question is then, why the cross shape? This question does not have a very complete answer. There is one important difference between the inclined fields of the original design and the electrode on top design: in the original design, the inclination causes additional splay (on the negative pretilt side). This difference could mean that higher twists can be supported on the original design, *i.e.* on the original design the twist goes up to 180° whilst on the electrode on top design the twist is not greater than 90°. Thus, with the electrode on top design twist is returning to 0° halfway around the lens causing the cross shape.

The change of polarisation with the electrode on top design starts to become apparent at around 2V. Fortunately, the majority of the change of refractive index should have occured by this point (see figure 4.6) so restricting the voltage to below 2V does not

sacrifice too much of the tunability.

6.4.3 Walls and disclinations

Identification of the defect types

When a voltage is applied to the original microlenses whilst they are being examined in the microscope, lines appear in the liquid crystal structure. The lines form on the leeward side with respect to the rubbing direction making a sort of elliptical shape with kinks at the extremities as defined by the rubbing direction (see figure 6.34 (on page 127)). These shrink down very gradually (in the order of minutes) and finally disappear.

The voltage required to cause the lines depends on the location in the cell. The lowest voltages needed to switch the liquid crystal occur where the liquid crystal is not on the microlens and the highest voltages are required where the liquid crystal is at the centre of the lens.

Occasionally, these thick lines split into two thinner lines (see figure 6.35 (on page 128)) and they are associated with surfaces (evidenced by the fact that the two lines can cross over with no apparent effect on each other and that they can be brought into focus at different depths (see figure 6.36 (on page 129)). This splitting is voltage dependent, *i.e.* for higher voltages the splitting occurs at a faster rate and, in fact, the splitting can be reversed by going to lower voltages. Regions enclosed by *only one* of these thin lines have one further distinction from other areas - when the voltage returns below the voltage required for switching, these regions temporarily form a new structure which takes a few seconds to disappear whereas the other regions return quickly ($<$ 1 sec) to their original off-state (at least, as indicated by their polarisation properties). The new area affects the transmitted light polarisation and is divided into sub-regions since it contains boundaries (identifiable as double lines) separating different parts of the same region (see figure 6.37 (on page 130)).

The first conclusion I have drawn from the micrographs are that there two basic types of liquid crystal non-uniformity in the original structures, thick and thin. The thick lines are *walls* and the thin lines are *disclinations*. This I deduce by comparing my own observations of the line behaviour as described above with work on walls and disclinations in an electric field by Stieb *et al* [SBM75]-see section 2.4.4. The disclinations are associated with one surface only, whereas the walls go from one surface to the other. Walls appear $\sim 10\mu m$ wide whilst the disclinations appear to be $\sim 1\mu m$ wide.

Basic evolution of walls and disclination

There is a straightforward explanation for the generation of walls on the microlenses upon application of an electric field. In two regions separated by the wall, the liquid crystal director is rotating with the opposite sense towards the electric field. In between the two regions, there must be a rapid change in orientation or a discontinuity in the director. Since a change in the orientation translates into a change refractive index, a line is seen.

In a cell with flat substrates, a rubbed PVA alignment layer generates a pre-tilt (orientation offset with no field applied) which is sufficient to prevent such walls. A uniform pre-tilt in a uniform field will induce the liquid crystal director to rotate with

the same sense. However, the pre-tilt is only a few degrees out of the plane of the polymer layer and since, on the sides of the microlens, the polymer layer plane varies by up to 40° with respect to the cell plane (see figure 6.6), the pre-tilt is likely to be swamped by the morphology of the PVA alignment layer. This effect has been seen in the modelling work (see figure 7.9).

The splitting of the thick wall into thin disclinations occurs for voltages higher than one where the wall forms. The structure of the two distortion types can be seen in figure 6.12. The disclinations are of strength (see section 2.4.4), $s = \frac{1}{2}$, since there is only a half rotation of the director around the disclination. The wall, as drawn, is a bend wall, *i.e.* the energy associated with the director distortion entirely corresponds to the k_{33} elastic coefficient, bend. When the orientation of the director in each region is such that it is almost parallel to the electric field then the directors for the 2 regions will be almost anti-parallel. However, since parallel and anti-parallel directors are equivalent, this does not constitute a director distortion at all. Therefore, when the applied voltage is sufficient, the bend wall breaks down into two disclination lines and, between the disclinations, the director is parallel to the applied field. In this configuration, there is nothing holding the disclinations together, thus, they can drift apart. The region in between the two disclinations has opposite pretilts on the two surfaces and when the voltage is turned off the liquid crystal relaxes into a 180° twisted state. This state is degenerate since the twist can be 180° or −180°. This degenerate twisted structure is what is seen in figure 6.37 (on page 130).

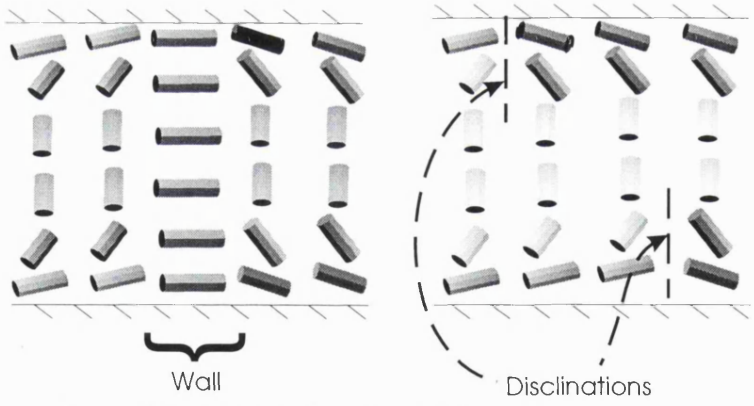

Figure 6.12: The splitting of a wall into two disclinations

Looking at the photo (see figure 6.21 (on page 113)) of the first microlenses there is little evidence of disclinations in the structure once the walls have disappeared despite the sharp change around the edge of the microlenses. The presence or otherwise of disclinations along the microlens edge has important implications for what the structure must be on the microlens. This question is addressed further in the next section on cylindrical lenses.

Cylindrical lenses

It can be seen in figure 6.34 (on page 127) that some of the walls in an array of microlenses (150μm diameter, 165μm pitch) have joined together. The joining together of the walls suggests there is a limit to the proximity of the lenses with this design,

assuming the walls are to be eventually eliminated. If the lenses are brought together (in the direction perpendicular to the rubbing direction) it assured that the walls will join together. In the limit (*i.e.* with no separation), the array will become cylindrical lenses. This provided some extra motivation for the study of cylindrical microlenses (as well that mentioned in section 4.3.2).

The cylindrical microlenses (with electrodes underneath) give rise to structures which are very similar to those on spherical microlenses (see figure 6.38 (on page 131)). On the cylindrical microlenses the walls only start to disappear from the ends suggesting that, if the lenses were infinite in length or terminated outside the liquid crystal at both ends, the walls would be stable. However, there is an alternative to the above sequence of events. The switching threshold voltage is higher in the centre of the microlens and, if the voltage is initially such that the liquid crystal is not switched in the centre of the lens but only at the edge (and outside the lens aperture), then the wall moves towards the lens and when it gets to the lens edge it breaks up into smaller loops (see figure 6.39 (on page 132)) which disappear. Both wall disappearing processes take of the order of 10 minutes for the cylindrical version of the original microlenses. There is no evidence that the final structures are any different from each other.

Identifying the structure that is left behind when the wall has apparently receded was problematic. It is clear that the light polarisation is being changed (see figure 6.40 (on page 133)). What is not clear is whether there is a disclination or wall along the lens edge on the side where the light is changing polarisation since it is hard to tell the difference between a line in the liquid crystal structure and the lens edge. The fact that some part of the wall structure is left behind is suggested by a close look at the disappearing edge of the wall which shows part of the wall adhering to the lens edge instead of disappearing (see figure 6.41 (on page 134)). However, if there is disclination down the side of the lens, it does not form a loop since there is no line down the centre of the lens. A line disclination can only form a loop or terminate at the surface [dP93] therefore, if present, the line would have terminate at the surface somewhere around the end of the lens. Such a structure gives rise to brushes (see section 5.4) which are not seen in the devices, thus indicating that there are no disclinations down the microlens side.

The consequence of the absence of disclinations is that the twisted structure on the side of the microlens has to be continuous with the surrounding untwisted structure. This is possible if the liquid crystal is breaking away from the surface alignment, however, as stated previously, there is no obvious reason for the liquid crystal to do on the cylindrical lenses. Alternatively, it could go through a completely switched state where there is no distinction between twisted and untwisted (see figure 6.13). However, such a structure would most likely be visible since the refractive index profile around the switched transition region would act as a lens. Finally, the liquid crystal could have a double twisted structure allowing a continuous twisting and untwisting across the microlens (see figure 6.14). The figure is drawn to represent the twisted structure and is inaccurate in a couple of points; the bend/splay of the switching is hardly shown in the twisted area and also, as stated previously, the twist would have to be concentrated into a smaller region in order to be under the Mauguin limit.

More clues as to the liquid crystal structure can be gained by switching to a low frequency before the wall has disappeared. When the frequency of the applied signal

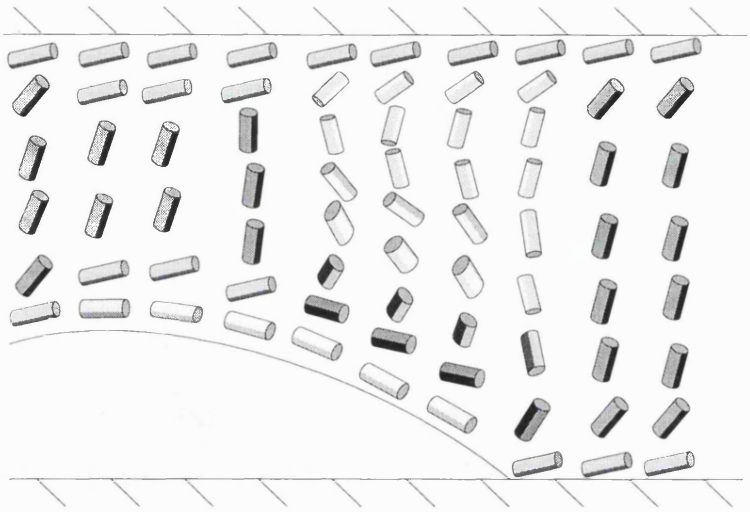

Figure 6.13: A twisted structure going to an untwisted structure through a completely switched state

is taken to the low frequency region, we see structures similar to those seen by Steib at high voltages (see section 2.4.4), namely pinching of the walls and the walls are no longer exactly perpendicular to the substrates. According to Steib, these are caused by hydrodynamic flow in the liquid crystal which is also what occurs when a liquid crystal is driven at a low frequency. The structure of the liquid crystal wall is in essence the same but with the wall tilted sideways so it is easier to see what is happening.

Starting from the unswitched state, the voltage is turned on, taken to a high value (>7V) so that a wall forms in a complete loop. Then the frequency is brought down to the 10-50Hz region. When this is done the wall splits into two thinner lines but, unlike the thin disclination lines mentioned earlier, these lines still have a structure linking them. In between the lines, there is more light transmitted through the crossed polarisers and within this region there are bands similar to those seen in previous photos (see figure 6.37 (on page 130)). These bands occur where previously there was a kink in the wall (see figure 6.43 (on page 137)). The wall on top of the microlens never splits into an associated pair at the lower frequencies, so in general the lines draw back together as they go on to the microlens. Sometimes the region bounded by the two thin lines is transferred onto the microlens and resultant structure is almost indistinguishable from that formed when the wall has shrunk to nothing. Particularly interesting are the bands (former wall kinks) within the region which sometimes remain even though one of the bounding lines of the region (the line which would be at the centre of the microlens) has disappeared (see figure 6.43 (on page 137)). If the frequency is returned to its usual value (1kHz), some, but not all, of these bands disappear and there is no obvious fundamental difference between the structures left on the side of the lens at low and high frequencies.

Similar bands are also seen sometimes at one end of a shrinking wall (see figure 6.44 (on page 138)). The band is always at the same end of the wall, *i.e.* as in figure 6.44 (on page 138) the band always forms at the bottom side (in the picture). This lens design is supposed to be symmetrical about the short central axis of the microlens but the observation that the band always forms on one side shows the symmetry is not perfect.

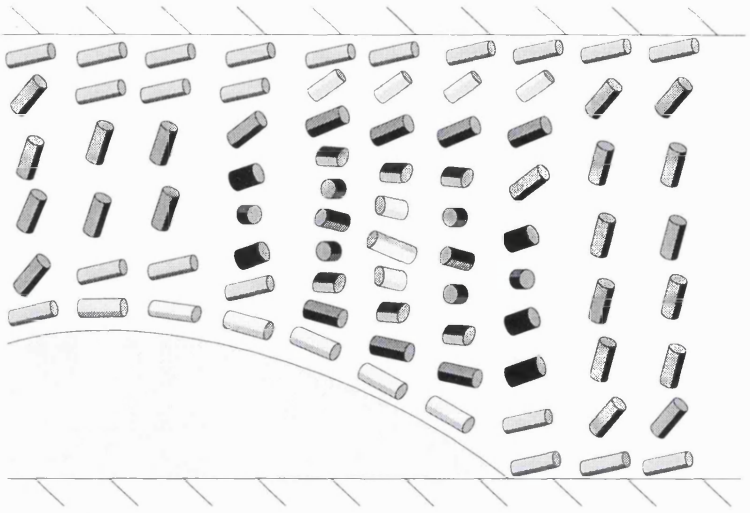

Figure 6.14: A double twisted structure which can untwist continuously

Also, one of these bands are seen near the end of the microlens (the same end as the side of the wall that has the band emanating from it).

If the analyser is rotated (leaving the input polariser and rubbing direction parallel) then the angle is found where the bright regions of the microlens in figure 6.44 (on page 138) become dark (30°). This angle is equal and opposite for the regions either side of bands (see figure 6.45 (on page 139)).

The conclusion from these observations is that the kinks in the wall structures are the same thing as the bands within the transmitting regions at low frequencies which, in turn, are the same as the lines sometimes seen in the transmitting regions on the side of the microlens. Several questions arise from this, one being what are the structures seen at low frequencies and why do the regions between the lines appear to be transmitting the light. These structures are studied further in the next section.

Structure of walls

The structure of these walls has been described by Léger (see section 2.4.4). He calculated how the ellipticity of the wall relates to the ratio of k_{33} and k_{22}. The ellipticity ratio is not usable for these devices since the presence of the surface structure (microlenses) will distort the wall, however, a difference can be seen in the angle of the kink at different voltages (see figure 6.46 (on page 140)). From the work of Steib *et al* (see section 2.4.4), it can be seen that the kinks are actually parts of the wall where the twist sense (*i.e.* right-handed or left-handed) inverts.

The most interesting conclusion of the work using low frequencies is that the kink in the wall (now seen as a band) can be left on the side of the microlens after the 'disappearance' of the wall. Since there is a kink left behind, there must be a wall as well, thus I conclude there is a part of the twist wall on the side of the microlens left by the receding wall. This is also backed up the observation with the polarising microscope that part of the microlens appears to go dark when the analyser is rotated by 30° on one side of the kink band (see figure 6.45 (on page 139)) and the same on the other side of the kink if the analyser is rotated the opposite way.

The twist wall on the microlens must have the twist axis out of the plane of the cell in order to be reorientating the light polarisation, however, at 1 kHz the wall is normal to the cell so the twist axis will be in the plane. Thus, this explanation requires that the wall reorientates. At low frequencies, this is not a problem since the hydrodynamic action does this already. For the higher frequencies this occurs at the receding edge of the wall where birefringence colours can be observed (see figure 6.41 (on page 134)).

There is a more important distinction between the wall structure left on the microlens and the standard wall loop as described by Steib and that is that there is no bounding wall down the centre of the microlens, thus the twist must smear smoothly into the structure on the other side of the microlens.

Strip electrode design

An electrode structure was suggested by Fabrizio Di Pasquale using a strip electrode opposite the microlens [DFDD96]. According to his model, this has the advantage of eliminating the wall at the side of the microlens. The structure suggested by Fabrizio partly eliminates the wall. As he predicted there is no wall at the side of the microlens (see figure 6.47 (on page 141)), however, there is a wall at the centre of the lens. His model could not go to sufficiently high voltages to predict this central wall structure. Where 2 microlenses (and their opposing strip electrodes) are close together the switching propagates sufficiently far that a wall forms in the gap (see figure 6.48 (on page 142)).

Electrode on top design

Another design fabricated was a cylindrical lens with an electrode on top of the microlens. This design was made in order to improve the uniformity of switching since the dielectric of the photoresist was reducing the effective voltage applied to the liquid crystal (since the electrode was underneath the microlens in the original design). The microlenses with the electrode on top do not produce walls. At first sight this is unexpected since the alignment is unchanged, however, the difference is due to the speed of switching. With the electrode on top of the microlens the liquid crystal will always switch fastest at the centre of the lens (see equation 4.1) where it will switch according to the intended pre-tilt. This orientation then propagates down the side of the microlens causing the rest of the structure to switch the same way.

6.4.4 Alternative alignment layers

The first liquid crystal immersed microlenses used a PVA alignment layer. Various other types of alignment layer have been tried to see if an improved performance could be achieved. There were three basic ideas behind these designs: externally definable alignment layers (to give an alignment which is independent of the surface), hybrid alignment layers (no pre-tilt across the microlens surface) and strong anchoring (to eliminate the twist).

Externally definable alignment layers In recent years, a number of photopolymer layers have been discovered to have the property that if they are polymerised with polarised light then they will align a liquid crystal on top of them. This work started

with LPP layers investigated by Schadt *et al* [SSKC92]. Whilst fabricating microlenses, it was a relatively easy task to test if the photopolymers used as photoresist have similar properties. Negative photoresist has to be used since with positive photoresist only the unexposed resist is left after the development process.

With both the negative photoresist and the LPP layer, it was expected that the alignment strength and direction would be the same over all the cell (*i.e.* the microlens profile would not affect it). It was hoped that this uniformity would give an improved performance around the edge of the microlenses and that this might reduce the liquid crystal twist that occurs when a voltage was applied. However, the LPP layer does not generate any pre-tilt unless 2 exposures are used [HSK+95] and then only small pretilts are generated ($\leq 0.30°$). Since this pre-tilt is very small it would quite probably be overwhelmed by the effect of the microlens surface profile which would cause problems when a voltage was applied (see section 6.4.3).

To test the negative photoresist as an alignment layers microscope slides were spin coated with negative photoresist and exposed to varying doses of polarised UV. The resist (HNR120 from OCG Microelectronic Materials Ltd) was spun onto the substrates at 5000rpm for 20 seconds which gives a $0.6\mu m$ layer. The samples were then baked on a hot plate at 90°C for 45 seconds. A mask consisting of a thin slit was prepared using insulting tape on glass and different parts of the slide were exposed through the mask with various exposure times. The exposure times were chosen on the basis of the exposure required for the resist to be completely polymerised taking into account the required UV polariser. The resist would usually require 8 seconds exposure [OCG95] (at $7.6mW/cm^2$) and allowing for the polariser transmittivity [Eal95] this gives a required exposure of 24 seconds. The polarisation of the UV was provided by the insertion of a UV-visible sheet polariser into the optical path of the mask aligner. Strips were exposed for 8, 20, 24, 27, 30 and 40 seconds. The samples were developed in 3 steps: 50 seconds in a bath of WRND (developer), 10 seconds in an equal mixture of WRND and n-butylacetate (rinse) and finally, 10 seconds in n-butylacetate alone.

The negative photoresist proved to be a poor alignment layer as can be seen from the microscope photograph figure 6.26 (on page 118). The strip shown in the micrograph is from the completely exposed strip (40 second exposure). As the micrograph is generally dark across the area of photoresist, it can be seen that there is some alignment which is in the same direction across the photoresist but, since there are many places where light is transmitted, it is clear that the quality of alignment is very poor. It should be remembered that this cell has planar substrates and, thus, it is easier to align the liquid crystal in this cell than on a microlens.

The linearly polymerisable photopolymer(LPP) layer was tried with greater hope of success since it is at least known that it can align liquid crystal. The material used was not exactly the same as that reported by Schadt *et al* (see section 2.4), instead Polyvinyl Cinnamate (PVCi) was used which was easier to obtain and has been reported by other researchers [HSK+95] as a suitable material. Since the LPP layer does not produce pre-tilt (except for a small amount with a double exposure technique) the LPP layer was only used on the microlens cell wall, the non-microlens cell wall being PVA coated so as to provide pre-tilt. Absorption spectra were taken of the LPP layer after various exposure times on a Philips spectrophotometer (PU8625 UV/Vis) to establish exposure times necessary for complete polymerisation of the samples. It was hoped to be able to measure

the dichroism of the layer vs. exposure time as well but the machine proved insufficiently accurate. The LPP layer was illuminated for 16 minutes with polarised light, enough to completely polymerise the alignment layer. The result with the linearly polymerisable photopolymer (LPP) alignment layer was, as with the negative photoresist, also not very encouraging. It was hoped that the LPP alignment would produce a more uniform aligning effect since, compared to rubbing, it should be less affected by the surface profile. However, as can be seen from figure 6.27 (on page 119), although the liquid crystal away from the microlenses was aligned, the alignment on the microlenses was not strong enough to counteract the effect of the surface profile on the liquid crystal. Polyvinylcinnamate is known to be a weak aligning layer with respect to out of plane alignment (see section 2.4.3) and this may well be true for in the in-plane alignment as well.

The effect of the surface profile on the liquid crystal can be estimated using equation 2.34 and treating the edge of the lens as part of a grating profile. The lens edge makes an angle of $\sim 40°$ with the glass substrate which gives an angle of 140° on the outside of the lens. Choosing a ratio of grating period to grating amplitude (18:1) to match this angle, the alignment energy then depends on the grating period chosen, getting stronger for gratings of finer pitch. For a period of $20\mu m$ the energy is $1 \times 10^{-7} J/m^2$ whereas for a $1\mu m$ period the energy is $2 \times 10^{-6} J/m^2$. These energies are weak but not insignificant (cf. table 2.1) and suggest that some of the weaker aligning layers may not be strong enough to counteract the aligning force of the lens profile.

Hybrid alignment layers In a different attempt to get more uniform alignment across the microlenses, a hybrid alignment cell was constructed. This had homeotropic alignment (*i.e.* normal to the surface) across the microlenses (in the hope of avoiding the surface angle dependent problems) and homogeneous alignment across the other substrate. To achieve this, the microlens array was dipped in a solution of Lecithin (see section 2.4) in Isopropyl Alcohol (IPA) and the IPA was baked off. The homogeneous alignment was generated by rubbing a layer of PVA spun onto the other cell wall. The result, as seen in the polarising microscope, is a diamond shape as shown in figure 6.28 (on page 120).

When the cell is rotated in the plane of the cell, the dark diamond shaped areas in the centre of the microlenses do not rotate with the cell or distinctively change shape (see figure 6.28 (on page 120)). Thus, it seems that the liquid crystal is aligning normal to the microlens surface forming a hedgehog director pattern and therefore, there are always regions where the director is between the polarisation directions and thus presenting birefringence to the incident light, changing its polarisation. As mentioned previously, this polarisation changing property (when it varies across the lens) is bad for the quality of the lensing. Since, by using a hybrid alignment, the range of focal length change will be reduced and the alignment of the liquid crystal has not been improved (at least, in terms of the lens performance), this configuration is not worth further investigation for use on the microlenses.

Strong anchoring Polyimide alignment layers generate stronger alignment than a PVA alignment layer [SMI+92]. Potentially therefore, the twisting may be reduced or eliminated by using polyimide in the place of PVA. The first microlenses used to test the

polyimide alignment layer were some microlenses which had been produced for a previous project approximately 2 years before. The polyimide was spun on the microlenses according to a procedure suggested by Philips Research Laboratories (PRL), Redhill. The initial results (see figure 6.29 (on page 121)) did not appear to be any better than those achieved with PVA. When another newer substrate was prepared it was found that the solvent in which the polyimide is dissolved for the purpose of spinning also dissolved the photoresist. Thus, it was decided to leave the investigation of polyimide liquid crystal alignment for a time when quartz microlenses were available.

Optimising the alignment

The rubbing process for the fabrication of the first liquid crystal immersed cells (made by C.H. Chia) was carried out with a single wipe of a lens cleaning tissue. The PVA layer was dip-coated onto the substrate to be rubbed, ensuring that the direction in which the PVA drained away was the same as the rubbing direction. To improve repeatability, the rubbing was carried out on a sliding stage in order that the height of the lens tissue above the substrate should be fixed. The slide was driven mechanically by the operator.

Since the first microlenses have been made, various improvements have been introduced. Firstly, the PVA layer was spun onto the substrates ensuring a more uniform layer thickness. The rubbing tissue was changed for a velvet-like rubbing cloth (supplied by PRL, Redhill). And, finally, the mechanical slide was replaced with the more versatile rubbing machine (as described in chapter 4). The rubbing process was optimised for the height of the cloth above the substrate which was micrometer controlled. The resultant alignment is shown for 3 heights of the rubbing cloth above substrate in figure 6.30 (on page 123).

It can be seen from the figure that the 2nd two micrographs are darker than the first indicating a better quality alignment (the same exposure conditions was used for all 3 micrographs) but that the last micrograph contains a great deal more particles, presumably from the rubbing cloth. The rubbing strengths, RS (see sections 2.4.3 and 4.4.2), are (with increasing fibre deformation) 300mm, 650mm and 1000mm. Assuming the rubbing strengths can be compared to those of Seo *et al* [SKN92] on polyimide then these strengths would be strong above 500mm. Since it is not possible to say which of the 2nd two micrographs are darker, the best result is achieved when rubbing with the rubbing cloth fibres deformed by 1mm due to the fewer particles. A similar exponential increase has been noted by Wako *et al* [WHO$^+$97] in the number of particles with fibre deformation.

Compared to the first microlenses, the cells containing microlenses rubbed with the velvet type cloth (see figure 6.31 (on page 124)) have less contaminants and the liquid crystal is aligned closer to the edge of the microlens without the 'halo' of unaligned liquid crystal (cf. figure 6.24 (on page 116)) although perhaps the strength of the alignment (as measured by the darkness of the extinction) is not as strong as with the original cells.

6.5 Birefringence interferometry

As well looking for alignment deviations, the liquid crystal can be inspected in one other way using the polarising microscope: birefringence fringes. The data obtained from the

birefringence can give information about the structure of the liquid crystal and has the advantage that it relates only to the liquid crystal layer (see section 5.6).

The fringes are symmetrical when no volts are applied (see figure 6.50 (on page 144)). When the voltage is applied and any walls have disappeared, an asymmetry can be seen in the birefringence fringes. The side which is rubbed first (i.e. where the surface angle has the same sign as the pre-tilt) appears to switch earlier (the fringes move first) than the leeward side of the lenses. This is more pronounced where the electrode is on top of the microlenses (see figure 6.51 (on page 145)).

Before the wall disappears, the birefringence can also be observed (this time without the green filter) and it can be seen that, when the microlens is divided by either a disclination or by a wall, the structure is symmetrical (see figure 6.52 (on page 146)).

In order to make a profile of the birefringence over the cylindrical microlenses, the positions of the birefringence fringes were recorded. The method used to do this is described in section 5.6. The results for the strip electrode design and electrode on top design are shown in figure 6.15.

The order of the fringes was assigned thus: The *relative* order of the fringes was determined by adding and subtracting birefringence to the optical path as described in section 5.6. Then a reference point had to be chosen. The simpler case was the electrode-on-top design. It was assumed that when 18V was applied the liquid crystal was completely switched (cf. figure 4.6) and so there was zero birefringence. As can be seen this wasn't completely true, at least not over all the lens width, perhaps because the field was non-uniform (see section 7.5). However, the liquid crystal at the centre of the lens was taken to have zero birefringence at 18V and all fringes emanating from the centre as the voltage decreased were counted as an incremented fringe order. The fringe ordering for the strip electrode design was complicated by the consideration that a wall forms down the centre of the lens and so there is not zero birefringence at the centre of the lens there at high voltages. The reference point chosen for these measurements was instead the theoretical birefringence as determined by the measurement of the cell thickness (see section 4.4).

Finally, what information is gained from the plots? The fringes occur when the quantity $(\bar{n}_x - n_o)d$ is equal to an integral number of wavelengths (n_o is the ordinary refractive index, $\bar{n}_x$ is the averaged extraordinary refractive index and d is the liquid crystal thickness). The plot for the strip electrode design shows that the birefringence at 0V is larger at the edge of the lens than at the centre but that when a voltage is applied the birefringence at the edge reduces but not at the centre. This is because there is a wall down the centre of the lens and, thus, in effect, the central region is not switched. The effect of the wall can be seen directly in the profile at 2V where the profile curvature is greater at the centre than at the edge. This difference is indicative of the fact that the regions around the wall are squeezing it. Above 2V the fringes were too close together to be distinguished reliably. However, it can be seen that because of the wall the lensing profile is deteriorating with increasing voltage.

The electrode-on-top design is more important since it does not produce any wall structures. There are two observations from figure 6.15b worth mention. One is the fact that it can clearly be seen that one side is switching before the other as mentioned near the beginning of this section. The other is that on the sides of the lens the birefringence is not zero. The difference in switching with voltage between the two sides will give rise

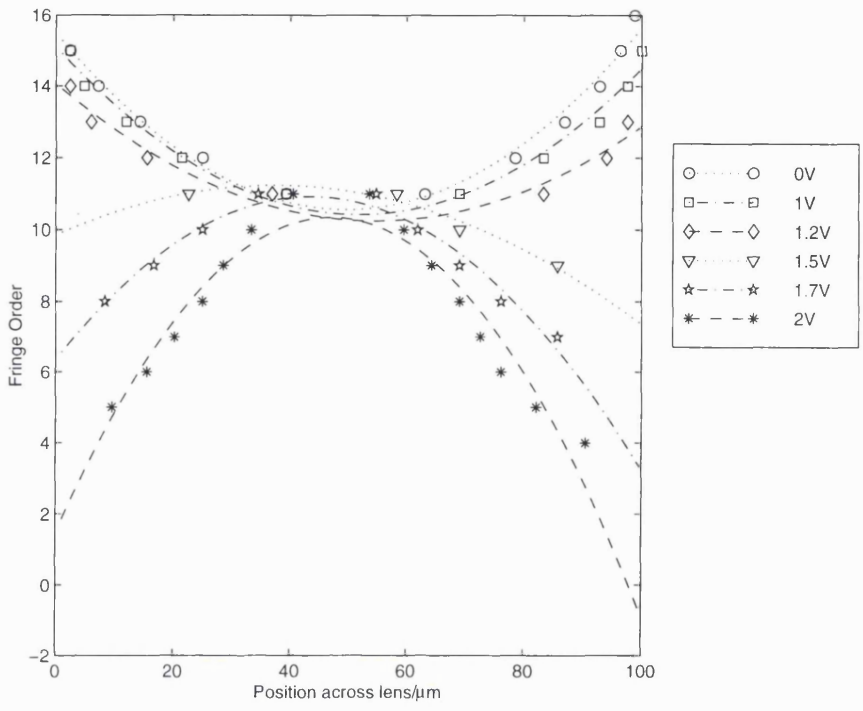

(a) Strip electrode design

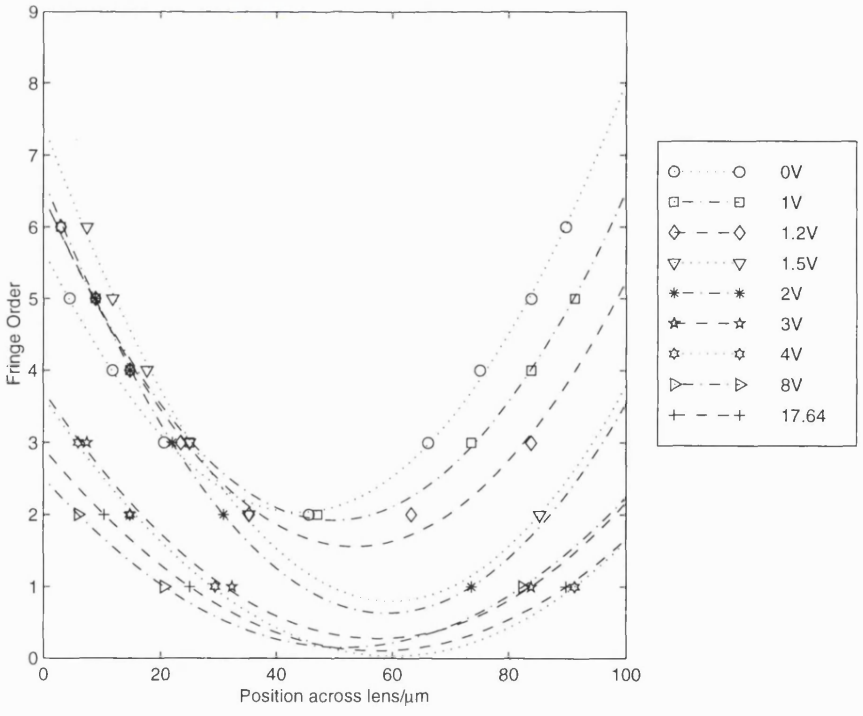

(b) Electrode on top design

Figure 6.15: Birefringence profiles of the strip electrode and electrode on top design. The plot is of fringe order (relative to central fringe for each voltage) vs fringe position (relative to left hand edge).

to a tilt of wavefront passing through the lens. The non-zero birefringence on the sides is a clue to the structure of liquid crystal which might be explained by the non-uniform field.

The tilt of the wavefronts can be calculated by fitting a straight line to the points and multiplying the gradient by the wavelength to give it a physical meaning. The gradient is then equal to the tangent of the deflection angle. The deflection angle vs voltage for the electrode on top design is shown in figure 6.16. The wavelength in air is used (632.8nm) which means the calculated angle is for the beam in air.

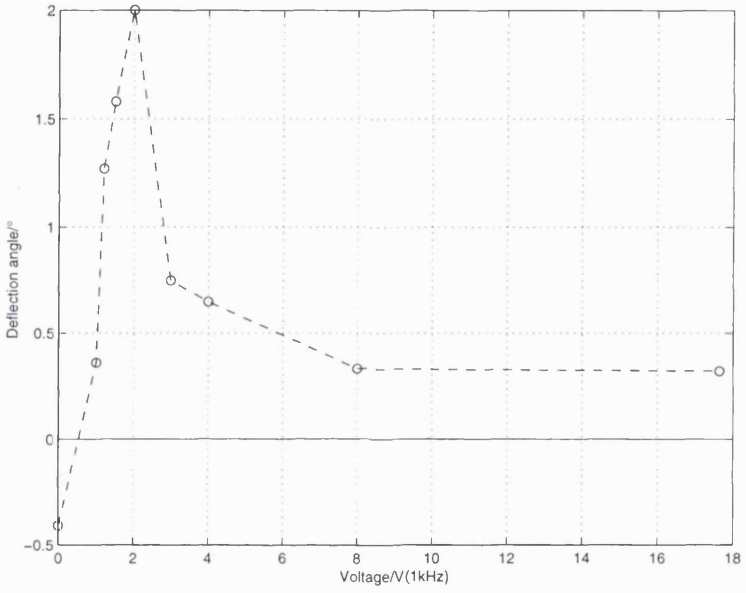

Figure 6.16: The tilt angle (in air) vs voltage for the electrode on top microlenses estimated from the birefringence data

The shift in position in the focal plane depends on the focal length of the microlens or the overall focal length of the components from the microlens onwards. If the focal length of the microlens were 1mm, the biggest shift (at 2V) would be ~0.03mm. Thus, although the electrode on top design a big improvement over the original design in terms of aberrations (see section 6.3), a new potential problem is introduced which would need to be considered in applying the variable focal length microlenses.

6.6 Response times

The response time of the microlenses is one of the parameters which is likely to be important to many systems. Indeed, speed may be the intended advantage in considering a solution without moving parts. The speed of the two spherical microlens designs have been measured using the set-up described in the section 5.7. As was stated there, no optimisation of the response time been attempted.

The results for the original lens design are complicated by the effect of the wall structures (see section 6.4.3). The intensity vs time plot is shown in figure 6.17.

As can be seen from the figure there is a relatively quick response followed by a slower rise to a final intensity almost a minute later. This second rise in intensity occurs

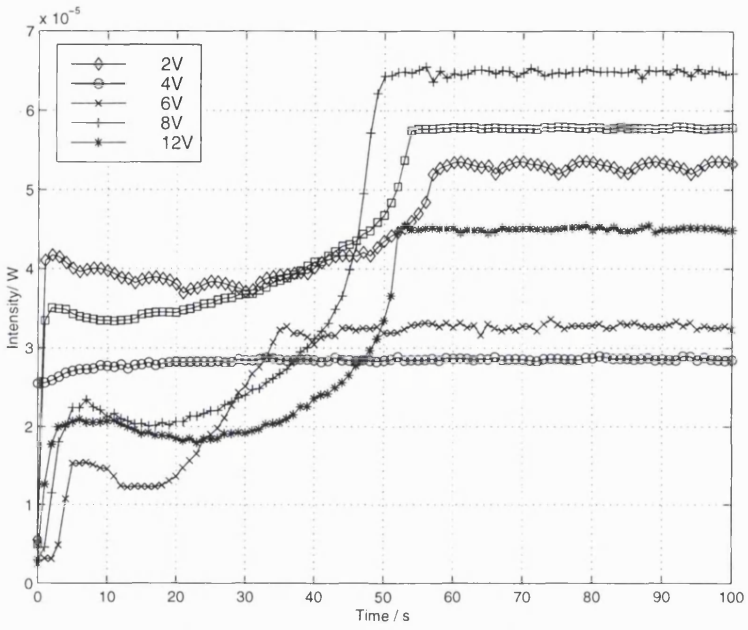

Figure 6.17: The intensity at the focus of the original lens design with time for various applied voltages. The second slow rise is due to the disappearance of the wall structure.

as the wall structure on the side of the lens finally shrinks to nothing and disappears (see section 6.4.3).

Clearly, this response time characteristic is a serious drawback, giving the lenses a response time of 40-50s for most purposes. The faster initial response may be usable depending on the nature of the system.

A more likely way the lenses might be used is after the wall has disappeared (*i.e.* with a constant voltage applied using only parts of the focal length vs voltage graph). For this regime, the useful figure of merit for the response time is the time taken to change between voltages. Thus, the same experiment was carried out except that the voltage was changed by 1V. The results of this experiment are plotted in figure 6.18 for both the original design and the electrode-on-top design.

Two facts are evident from this graph; first, the electrode-on-top design switches faster than the original design and secondly, both lenses are faster at higher voltages. Both observations are not unexpected. That the electrode-on-top design is faster is foreseeable as the electrode separation is less and the faster response at higher voltages is simply due to the director rotation rate being dependent on the field applied (as is suggested by equation 4.1 - although direct comparison is not possible since the intensity at the focus of the lens has been measured).

The electrode -on-top design does not suffer from the wall structures so its response does not have the 2nd rise in intensity when switching from the off-state. Therefore, its responses are, in effect, much faster. The times to turn on and off at various voltages are shown in figure 6.19.

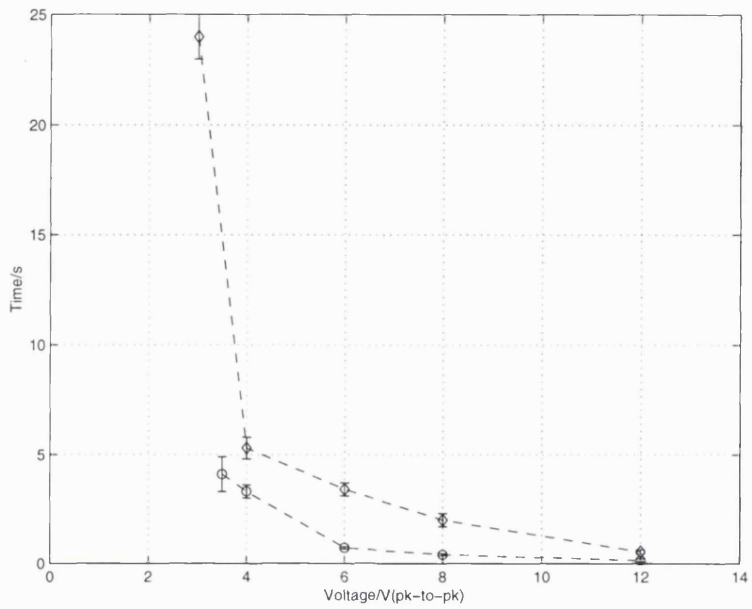

Figure 6.18: The time required to change focus with an increment of 1V for the original lens design (◇) and the electrode-on-top (○).

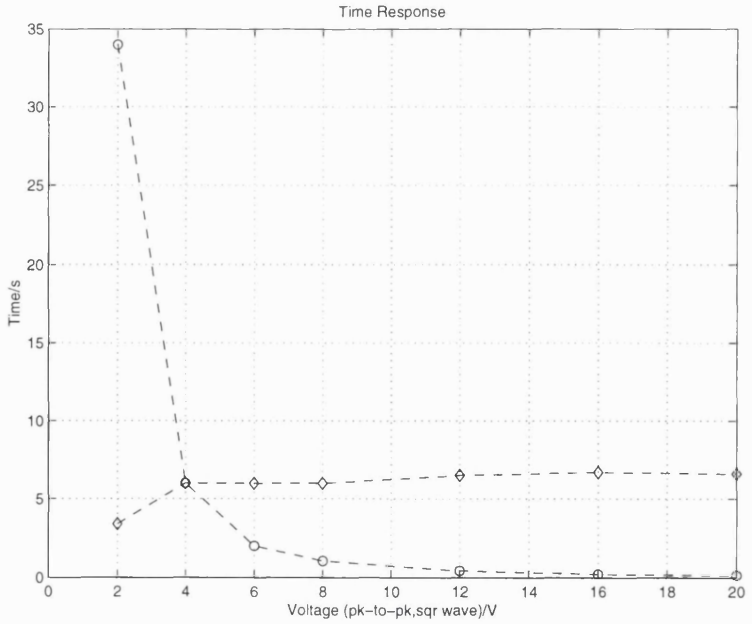

Figure 6.19: The time response time of the electrode-on-top lenses for going to the on-state (○) and the off-state (◇).

6.7 Photographs

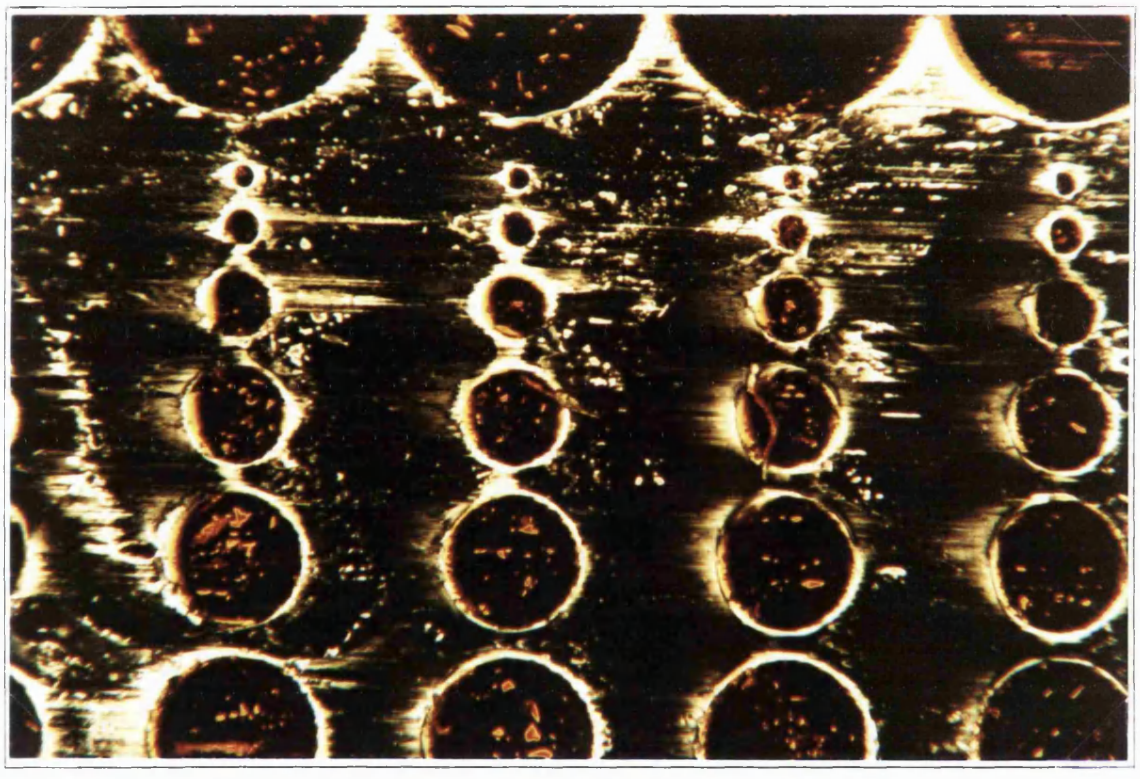

Figure 6.20: Original microlens cell with a polyvinyl alcohol (PVA) alignment layer rubbed (right to left in the photograph) with a lens cleaning tissue (cell between crossed polarisers, orientated for minimum transmission, i.e. the rubbing direction is parallel to the analyser polariser). The microlens diameters are 50, 100, 200, 300, 400, 500, 600, 700 and 800μm (the 600 and 700μm lenses are not in the photograph).

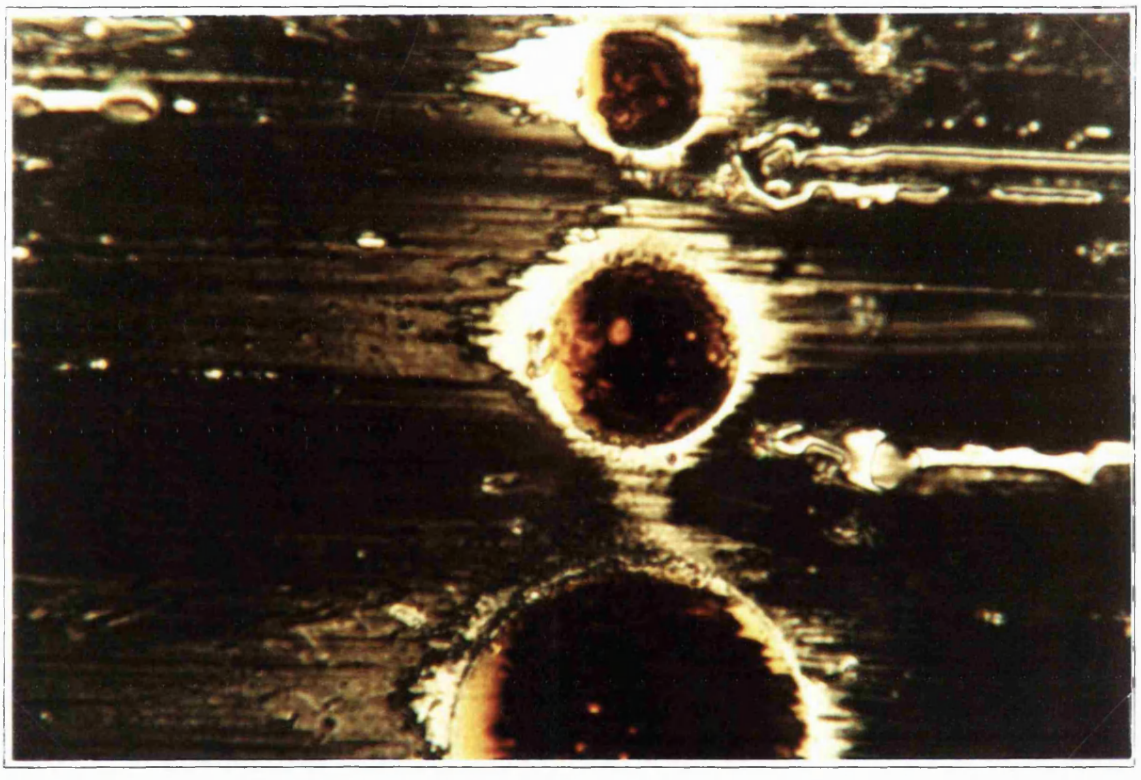

Figure 6.21: Original microlenses, diameters 50, 100 and 200μm with no voltage applied (cell between crossed polarisers, orientated for minimum transmission).

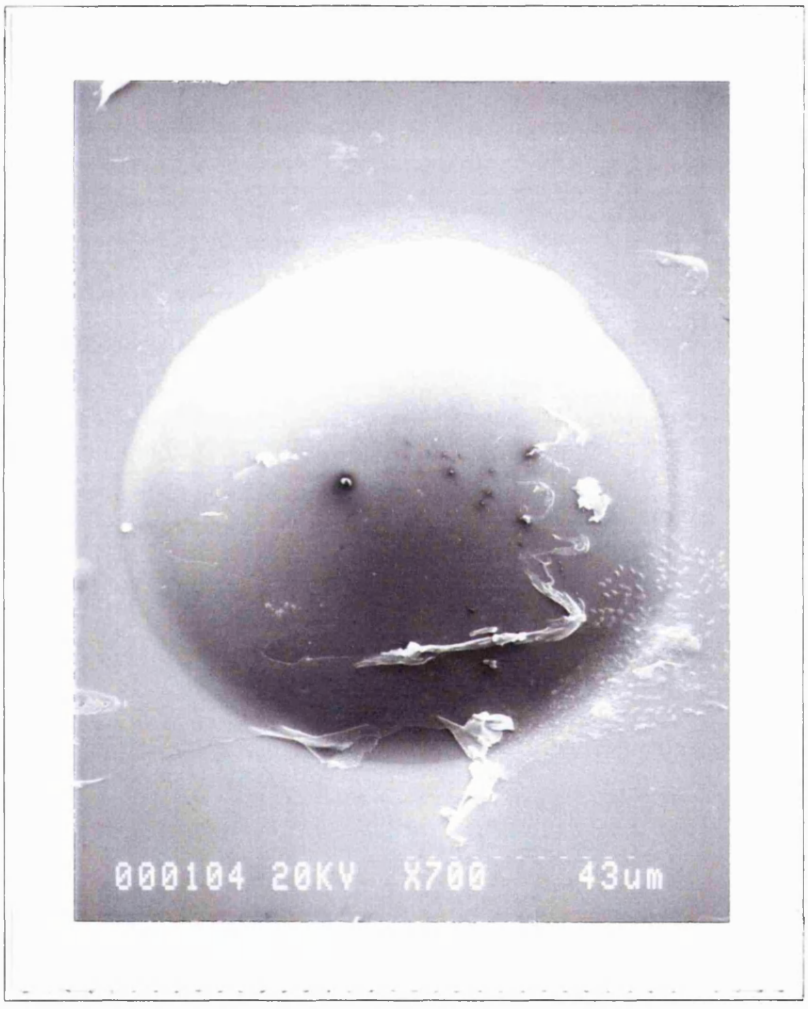

Figure 6.23: Damage to PVA on top of original microlens (diameter $100\mu m$).

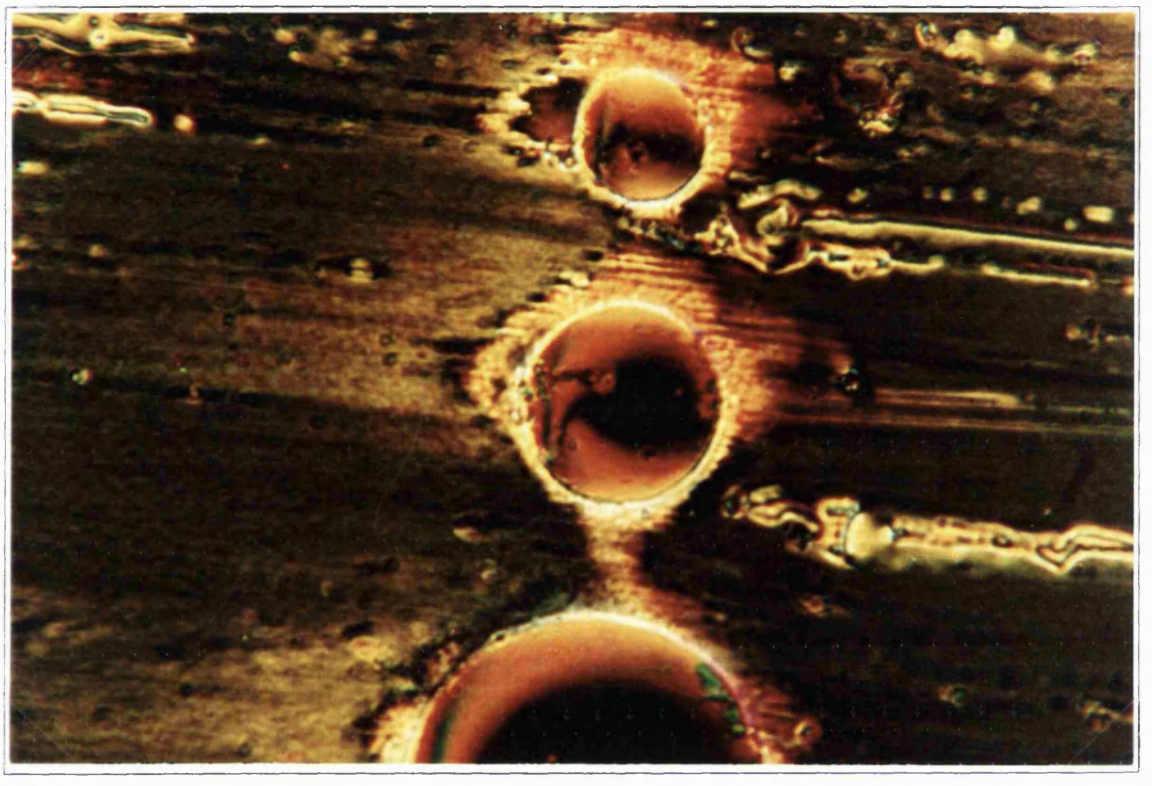

(a) 5.03 V

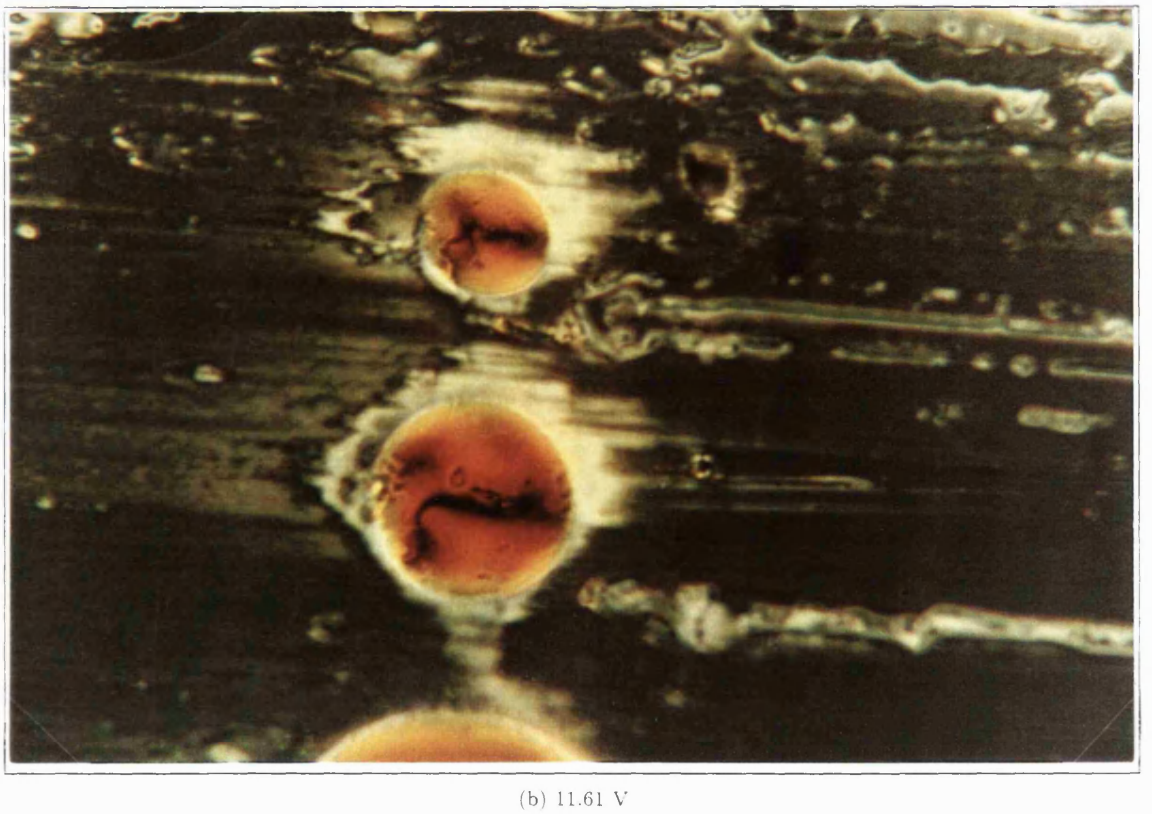

(b) 11.61 V

Figure 6.24: Original microlenses, diameter 50, 100 and 200μm with 5.03 and 11.61 Volts applied (cell between crossed polarisers, orientated for minimum transmission).

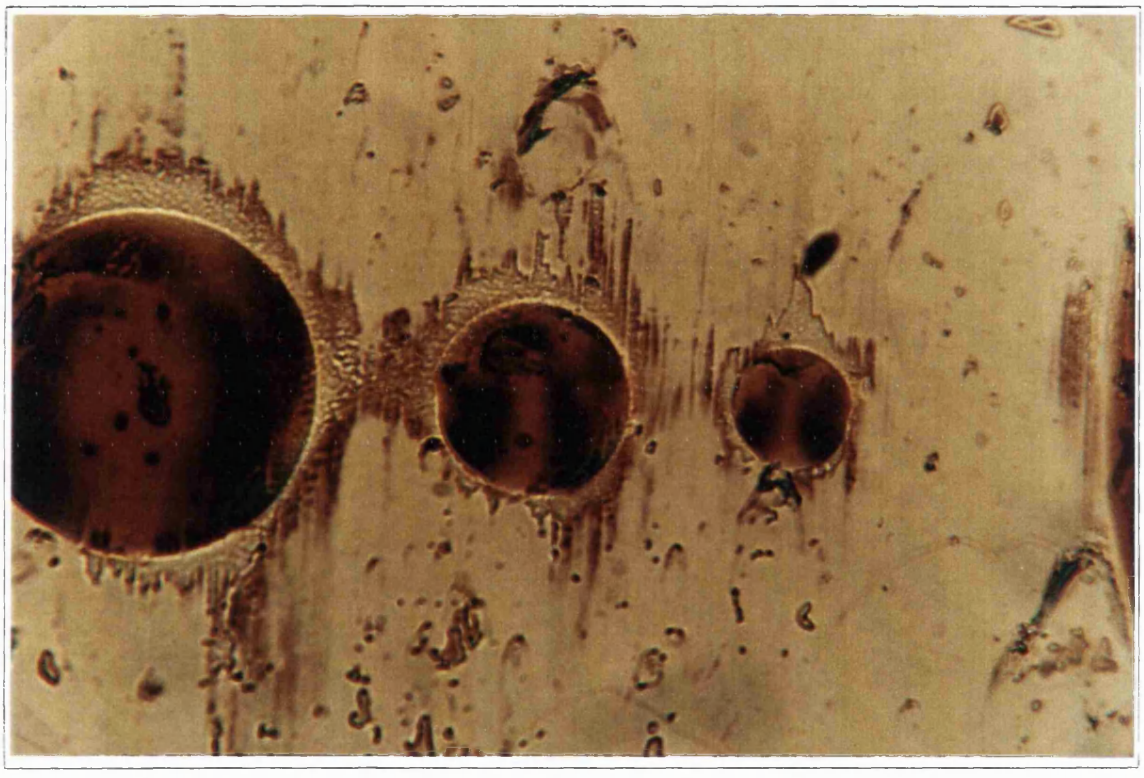

Figure 6.25: Light transmitted by the original microlenses at 11.62 V in the polarisation corresponding to the input polarisation(cell between parallel polarisers, orientated for maximum transmission). The microlens diameters are 50, 100 and 200μm.

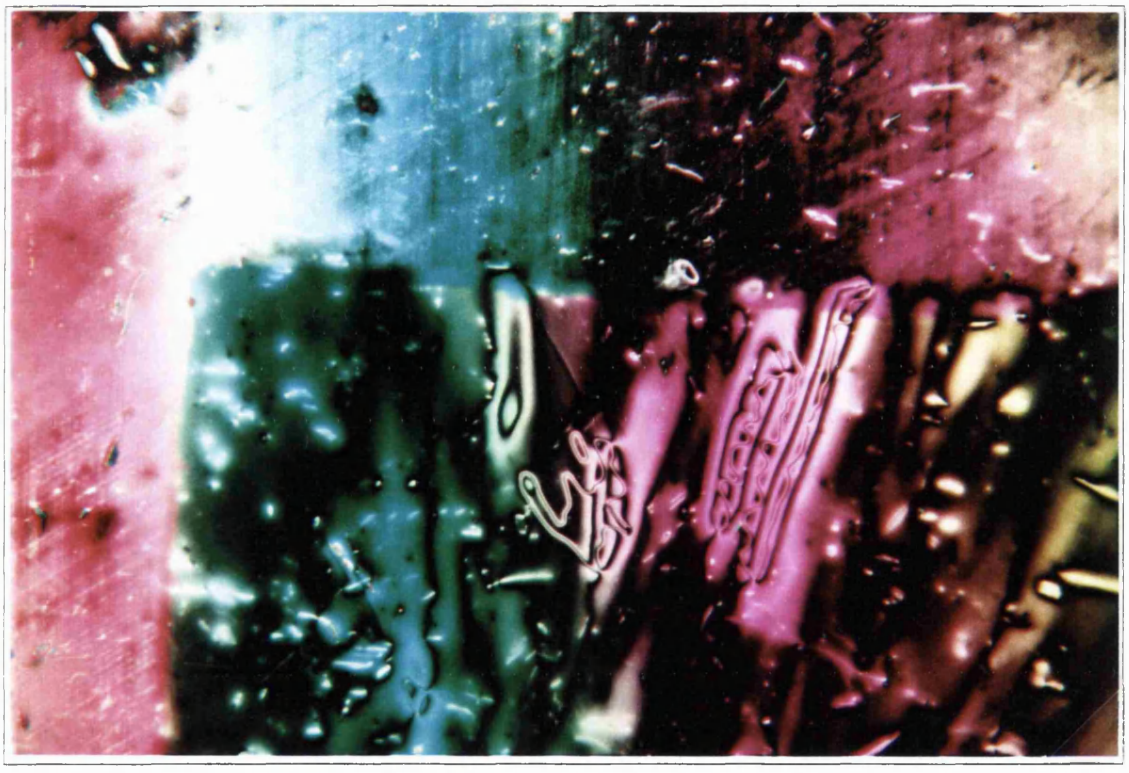

Figure 6.26: Corner (bottom right part of picture) of area of negative photoresist exposed with linearly polarised UV, between crossed polarisers orientated for maximum extinction.

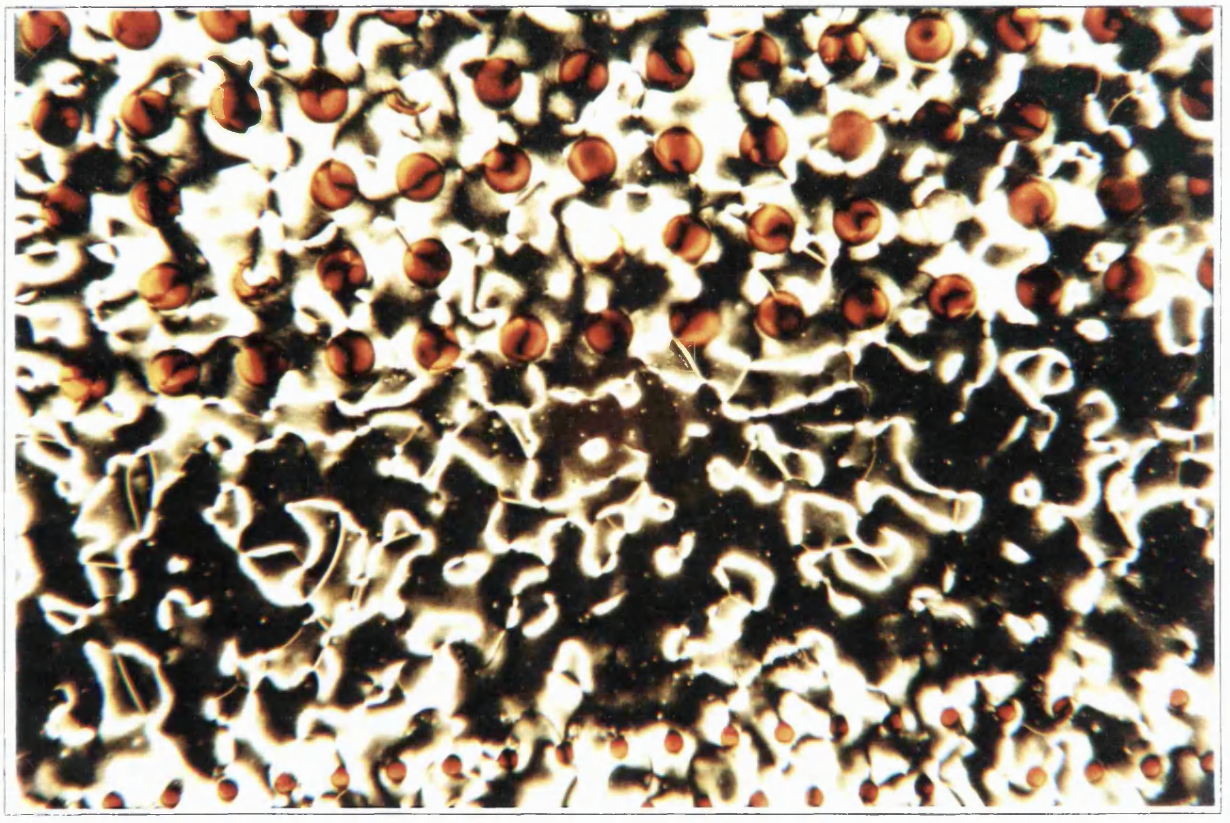

Figure 6.27: Microlens cell with linearly polymerised photopolymer alignment on the microlenses and rubbed PVA alignment on the other surface (cell between crossed polarisers, orientated for minimum transmission)

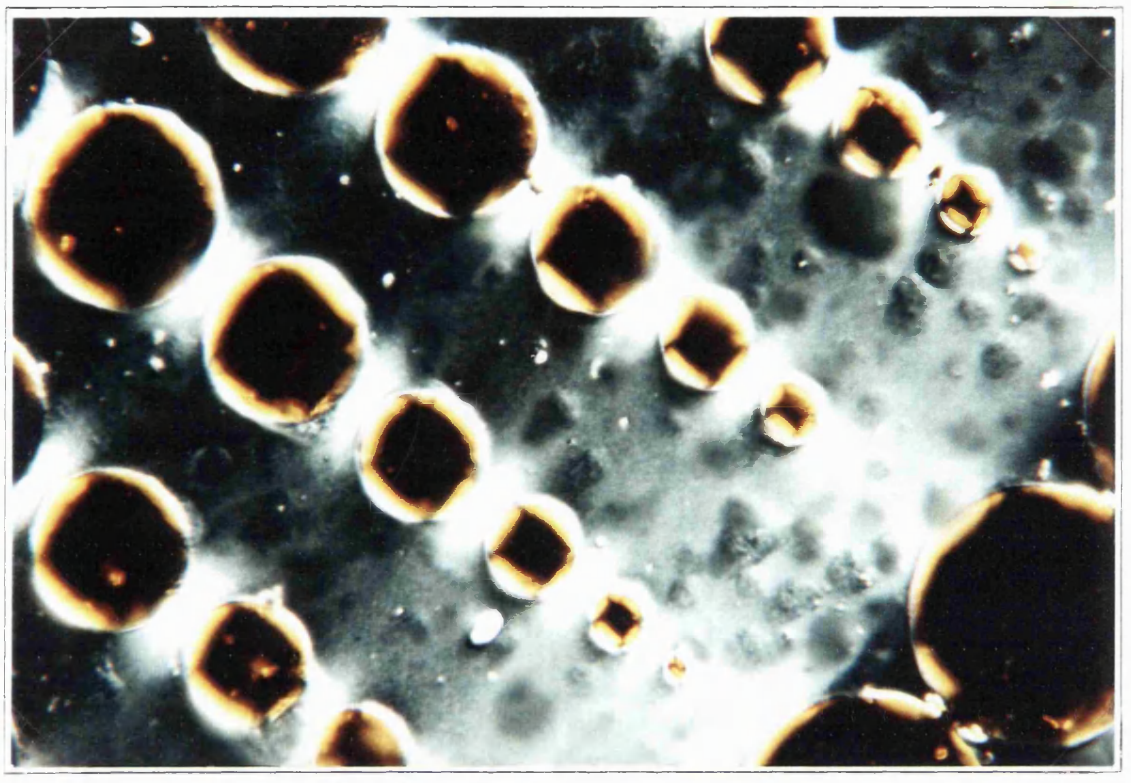

(a) PVA rubbing direction parallel to analyser

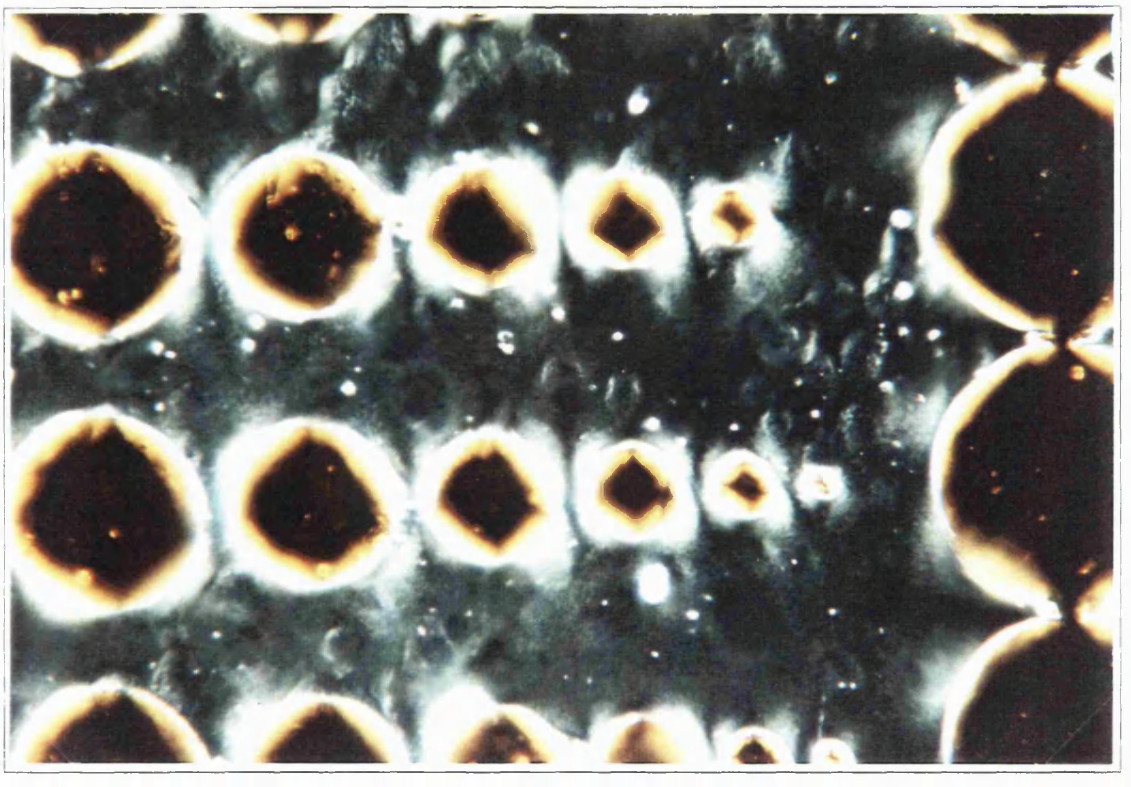

(b) PVA rubbing direction rotated away from analyser

Figure 6.28: Microlens array with liquid crystal aligned by hybrid lecithin and rubbed PVA alignment, two rotational positions of cell (cell between crossed polarisers, orientated for minimum transmission)

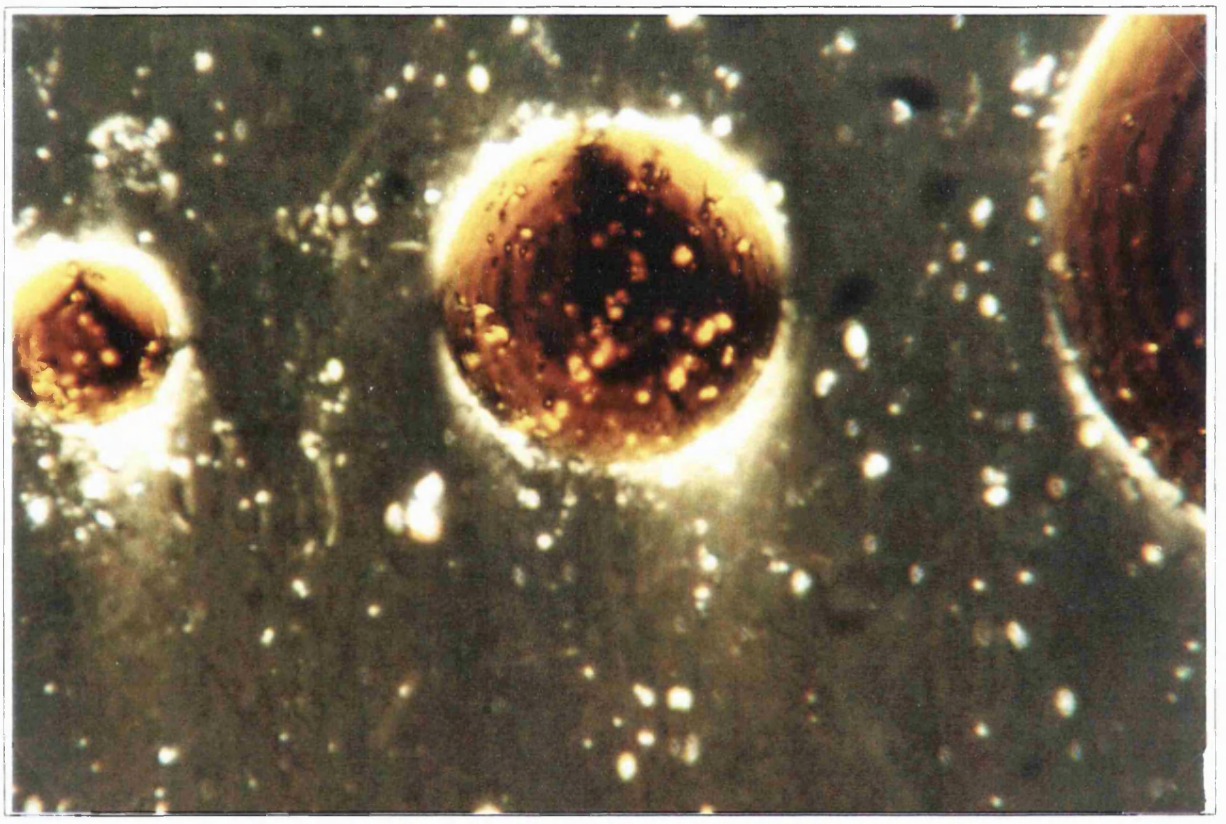

Figure 6.29: Microlens cell with a polyimide alignment layer on the microlenses (cell between crossed polarisers, orientated for minimum transmission)

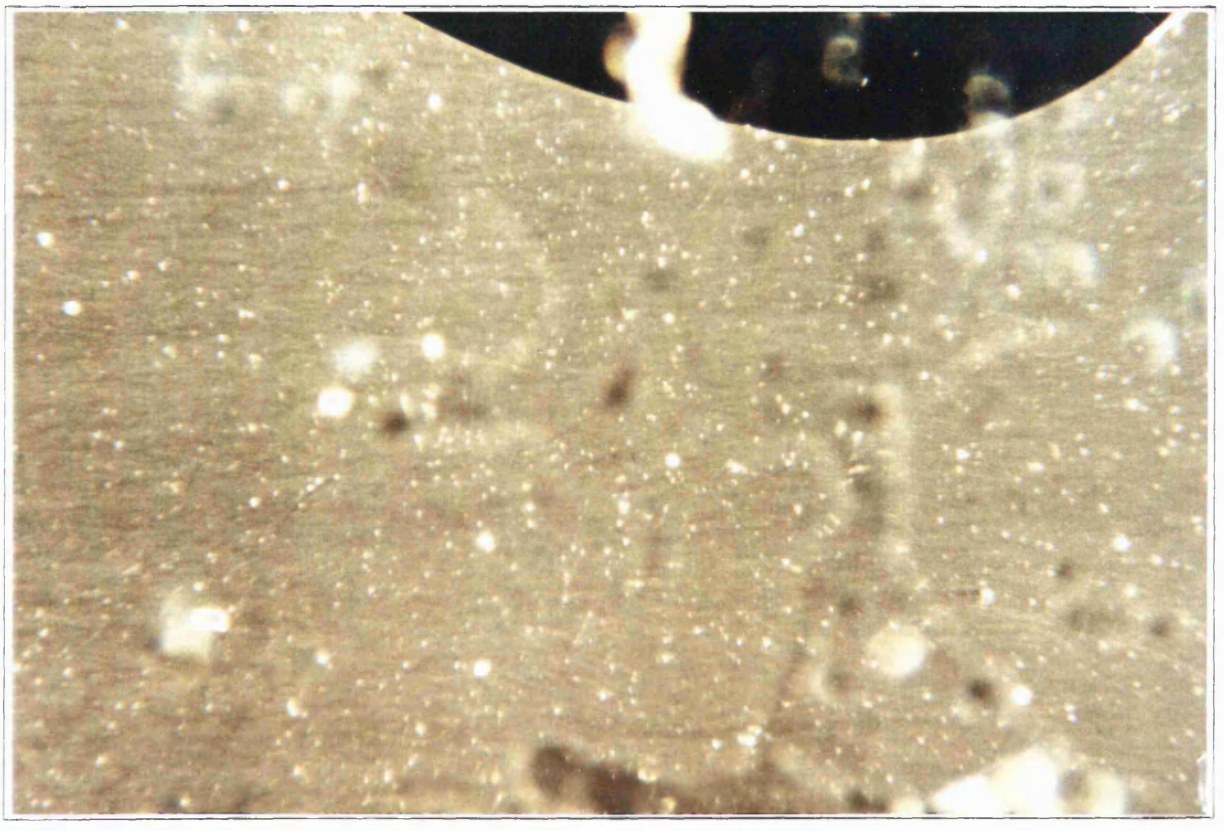

(a) 0.5mm

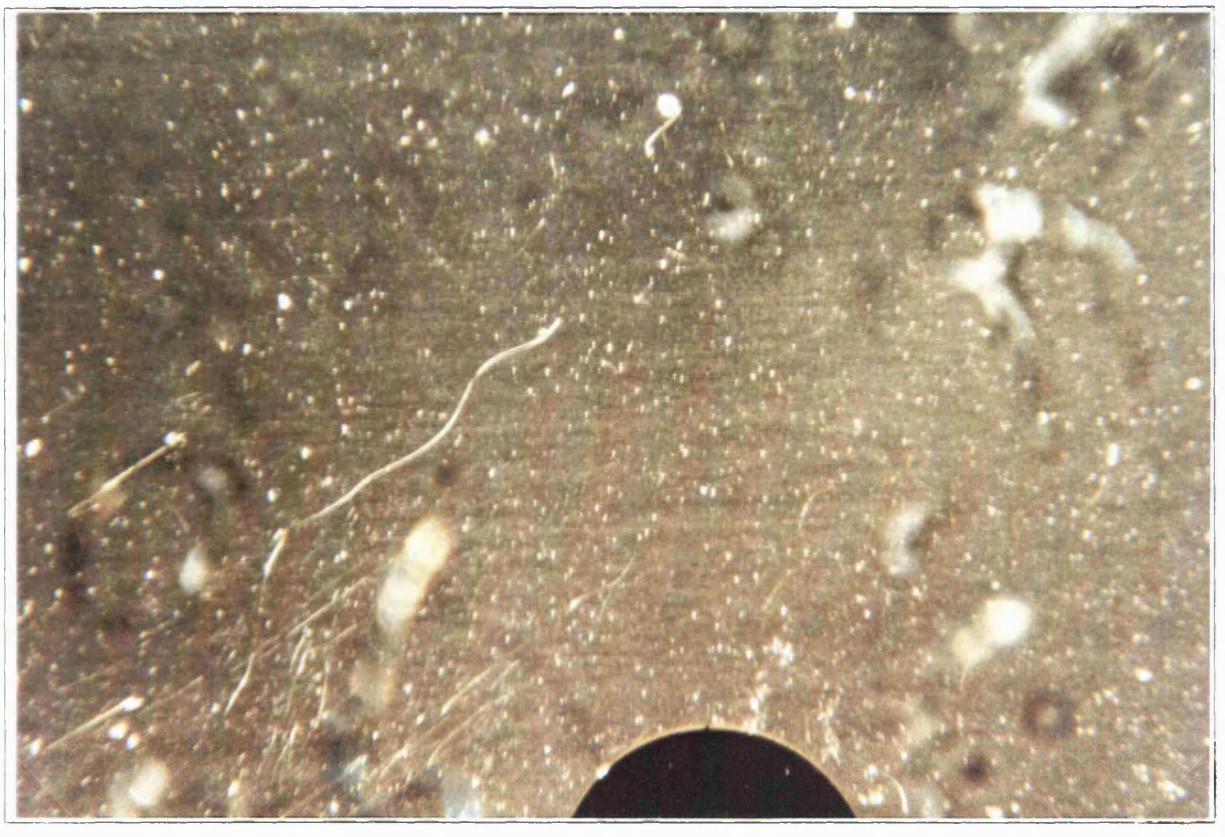

(b) 1mm

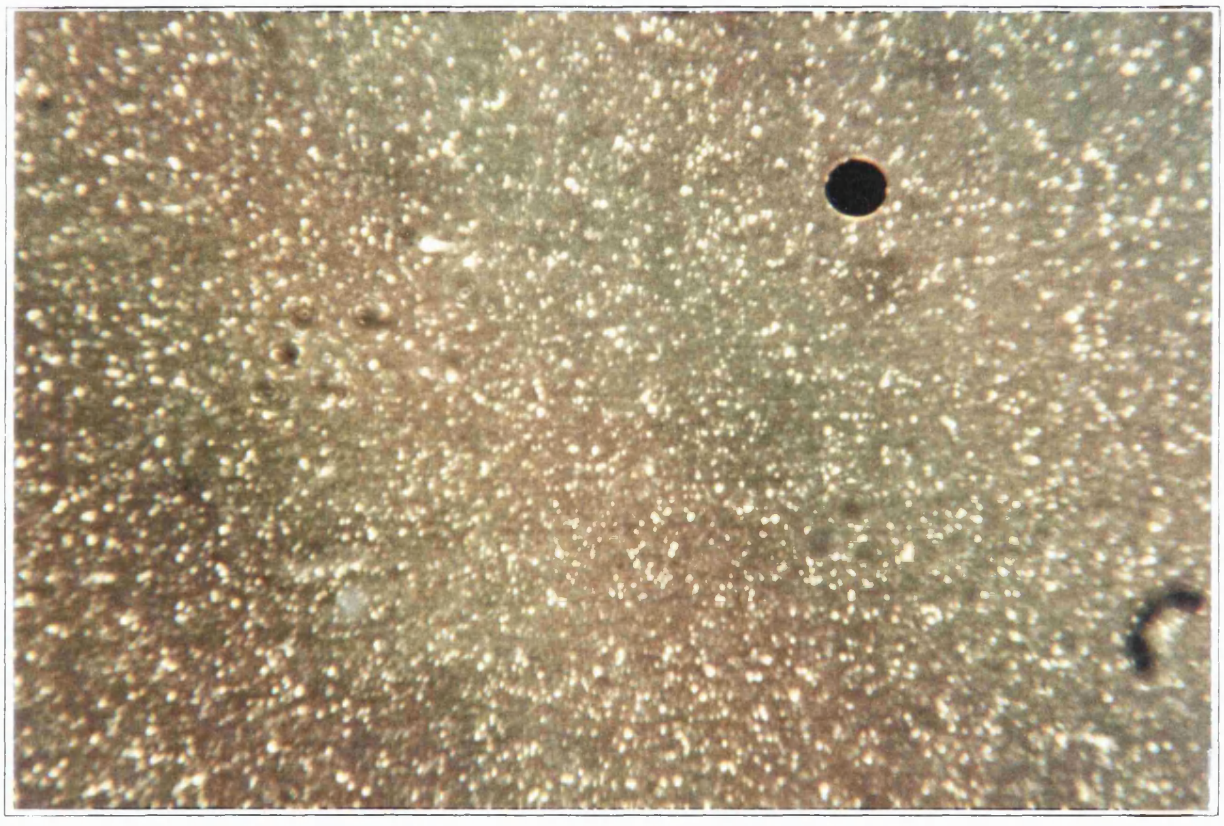

(c) 1.5mm

Figure 6.30: Liquid crystal cell with a polyvinyl alcohol (PVA) alignment layer rubbed using rubbing machine, height of cloth above the substrate, with 0.5mm, 1mm and 1.5mm fibre deformation (cell between crossed polarisers, orientated for minimum transmission). All three photographs taken with the same objective, shutter speed and aperture.

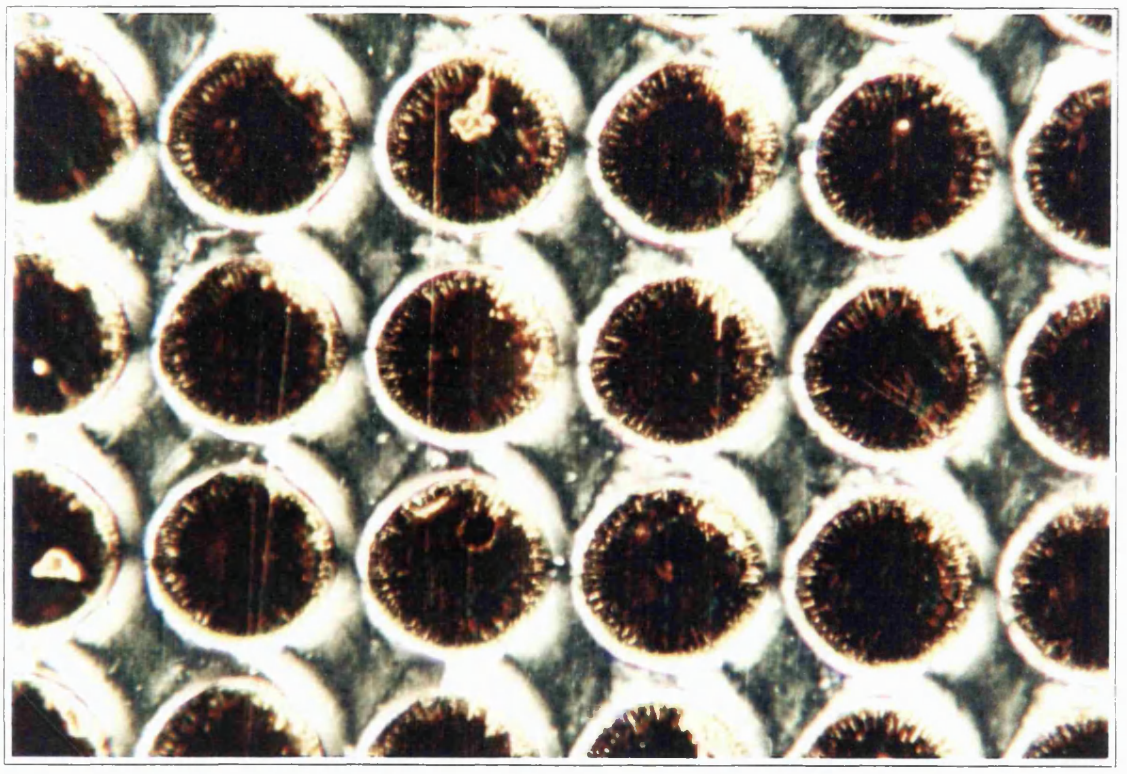

Figure 6.31: 120μm diameter microlenses (pitch 125μm), rubbed with a velvet covered drum (cell between parallel polarisers at maximum extinction, no volts applied).

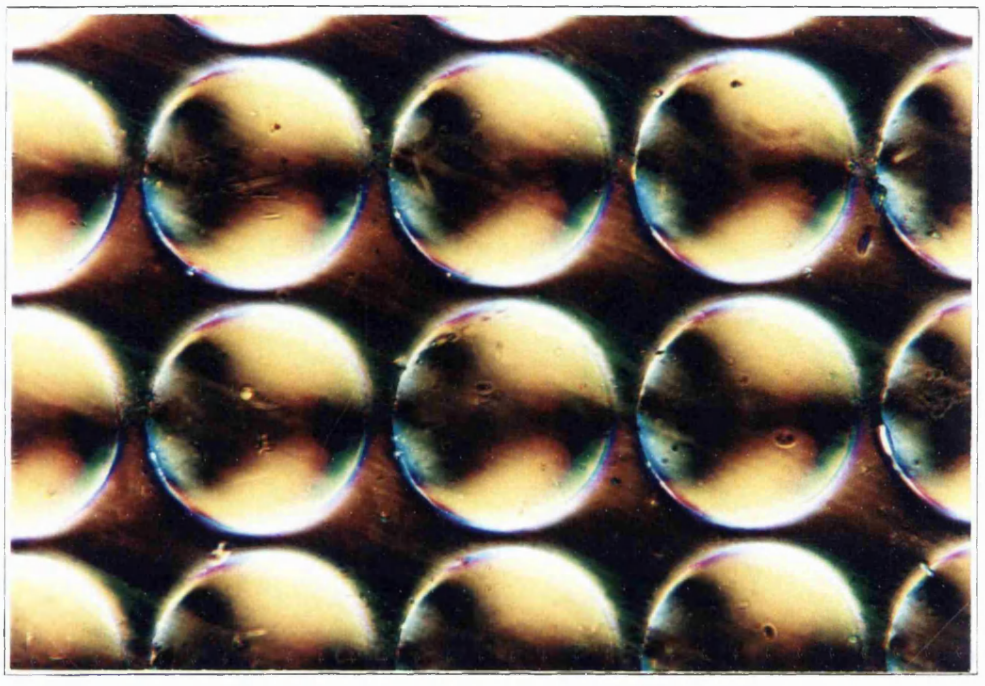

(a) 5.37 V

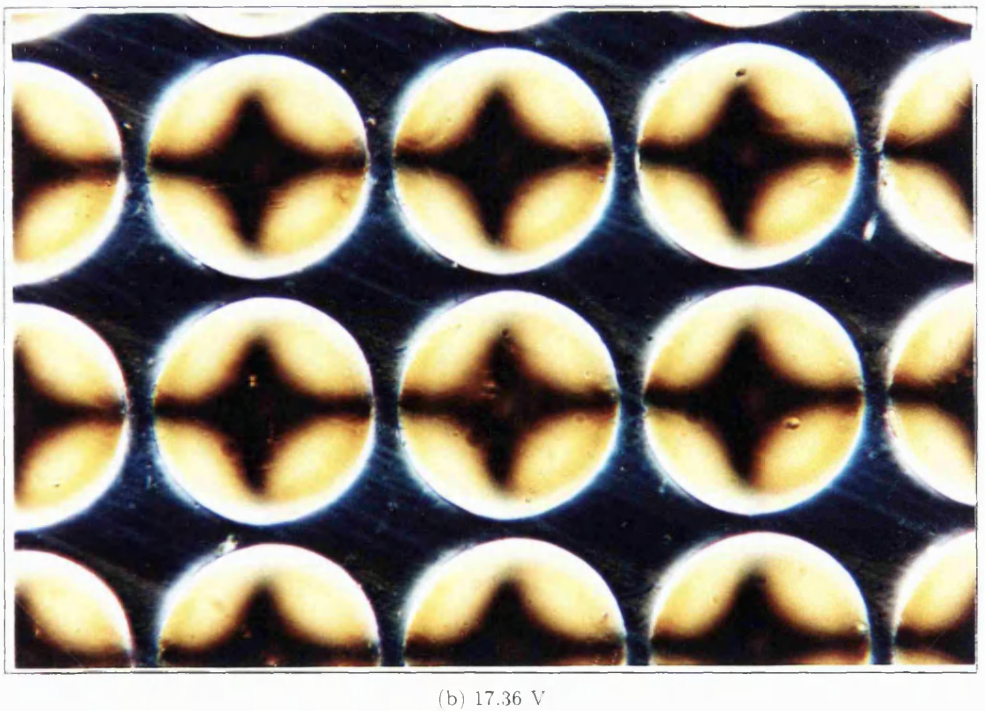

(b) 17.36 V

Figure 6.32: Polarisation change induced by the final design of microlens for 2 voltages. With increasing voltage a dark cross emerging from the left hand side of microlenses. Polarisers crossed, rubbing direction parallel to input polariser. The microlens diameters are $150\mu m$.

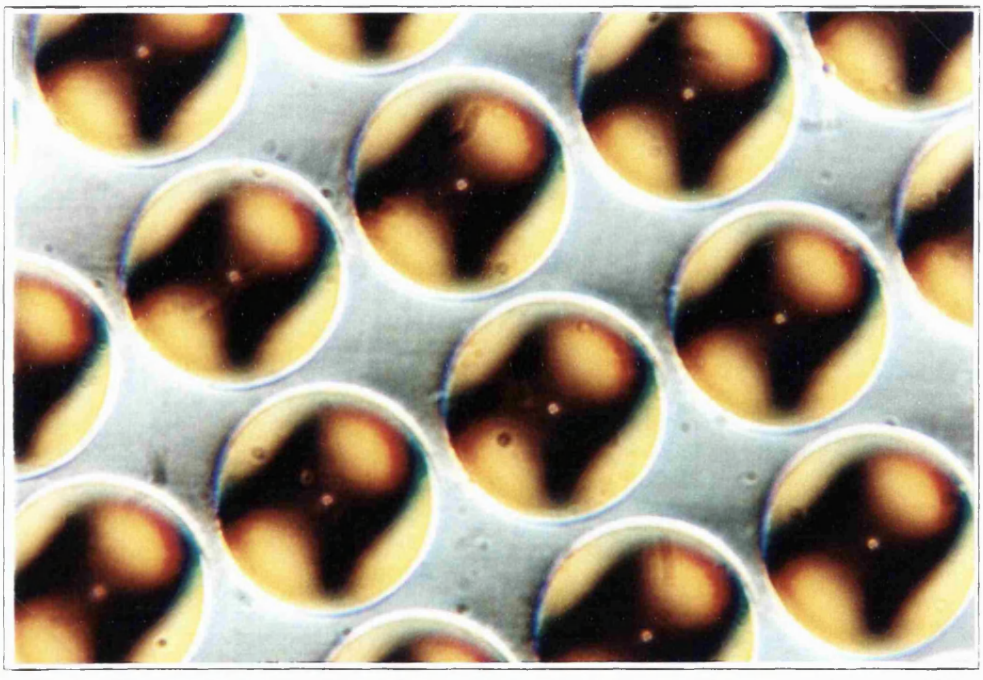

Figure 6.33: 'Figure of 8'. 17.36V applied. Rubbing direction and analyser both at 45° to the input polariser but in opposite directions.

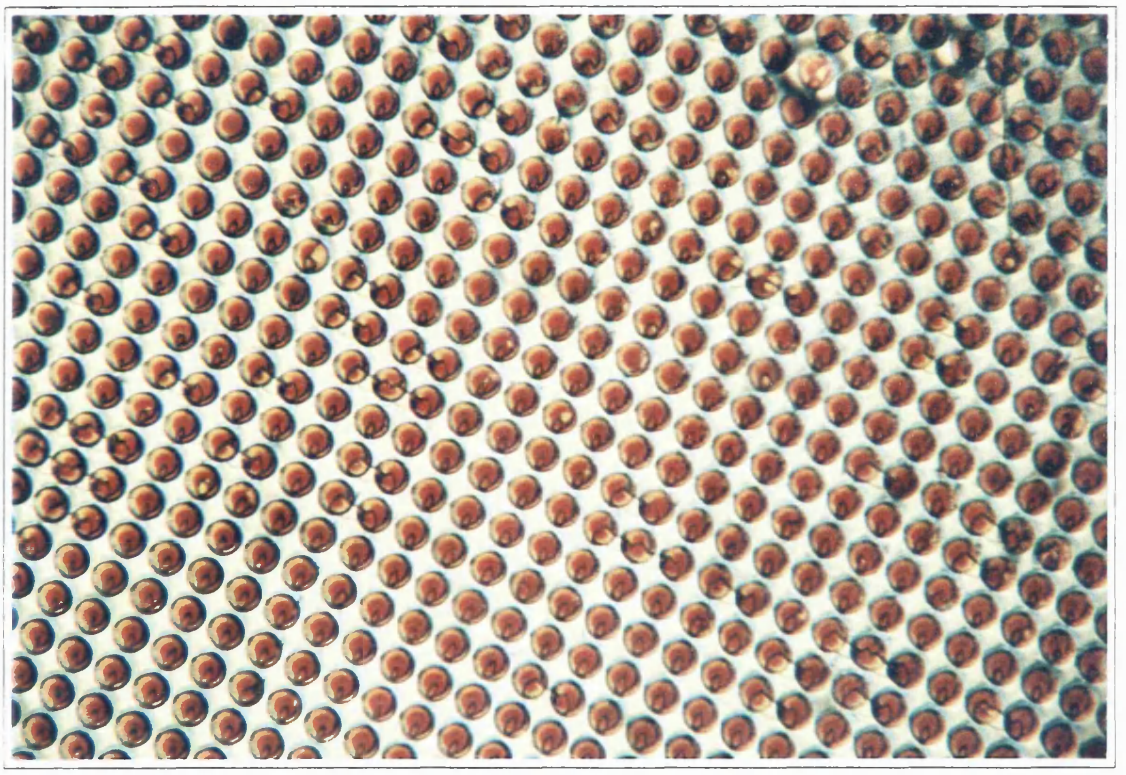

Figure 6.34: Array of $125\mu m$ microlenses, a few seconds after a voltage has been applied. Lines can be seen in the form of a loop on the majority of the microlenses. Crossed polarisers with rubbing direction somewhere in between.

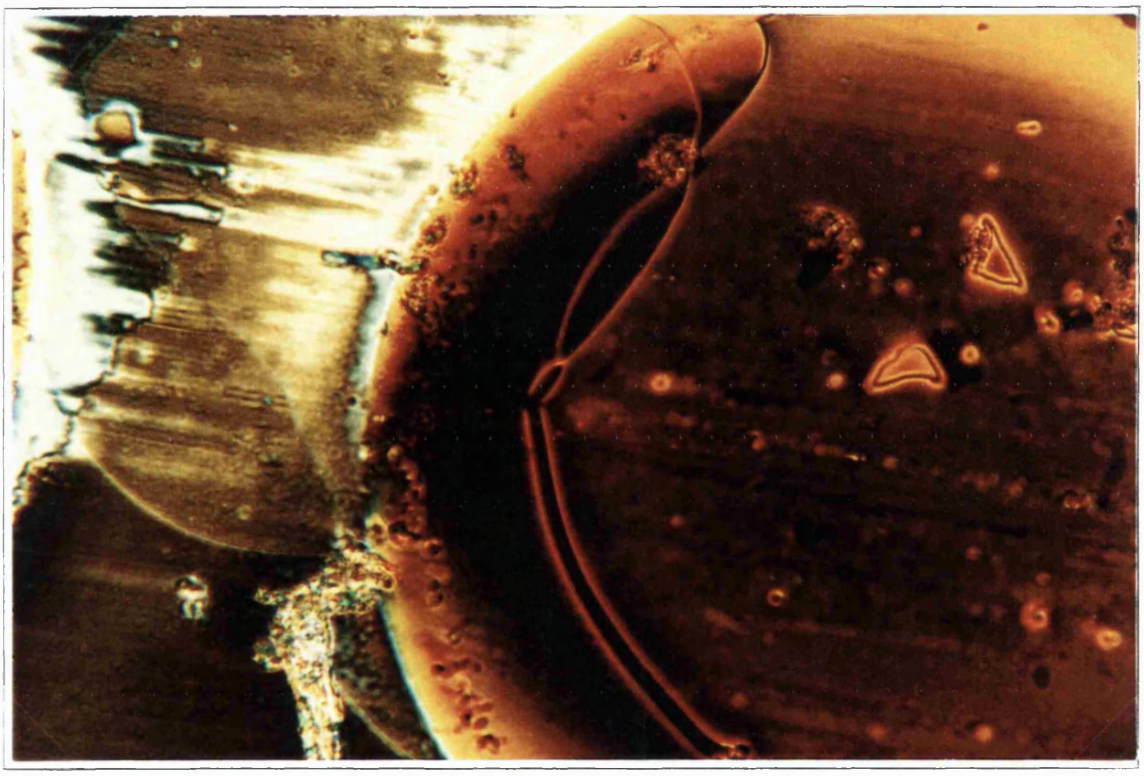

Figure 6.35: C.H. Chia's $600\mu m$ microlens, voltage above Freedericksz threshold $\sim$1 minute after the voltage was applied. The 'thick' line breaks into two 'thin' lines. (Crossed polarisers, rubbing direction parallel to the input polarisation)

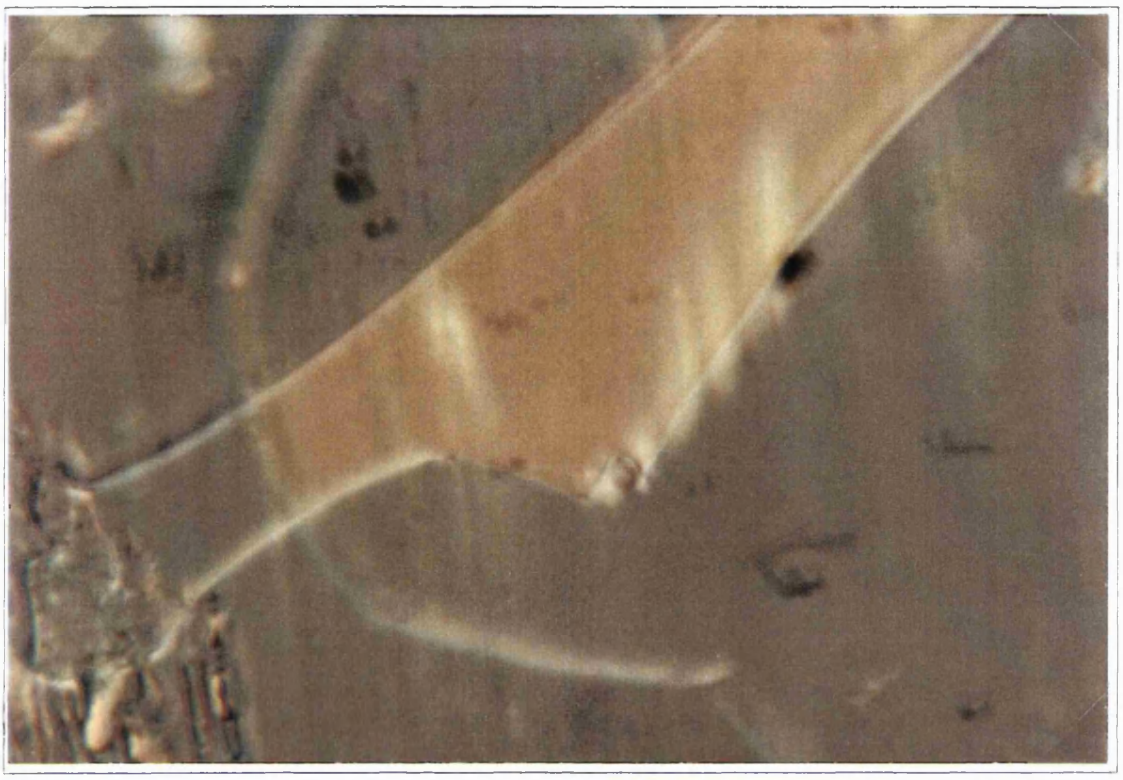

(a) Top substrate in focus

(b) Lower substrate in focus

Figure 6.36: In between microlenses, the lines are associated with the top and bottom surfaces as evidenced by the lines being brought to focus at different heights under the microlens. Crossed polarisers, rubbing direction parallel to the analyser.

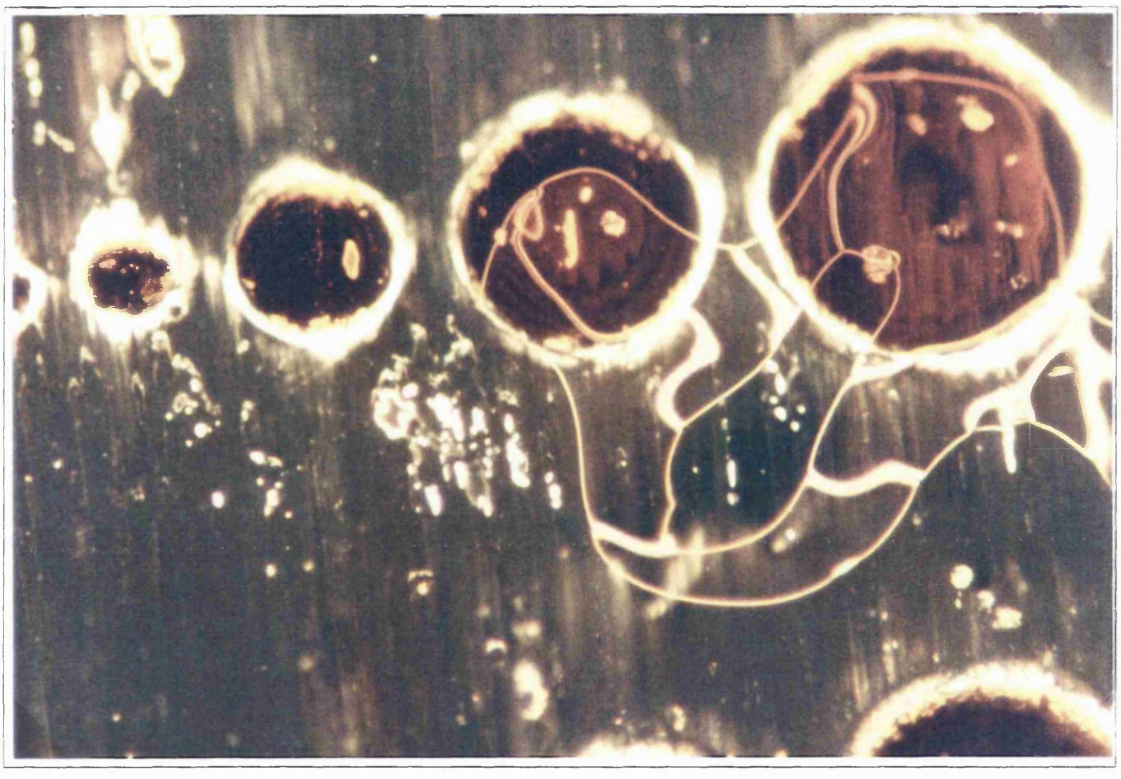

Figure 6.37: C.H. Chia's microlenses after voltage (18V, 1kHz a.c.) turned off. Region within outer loop bounded by only one line. Inner loop contains region bounded by both thin lines. Crossed polarisers, rubbing direction parallel to input polarisation.

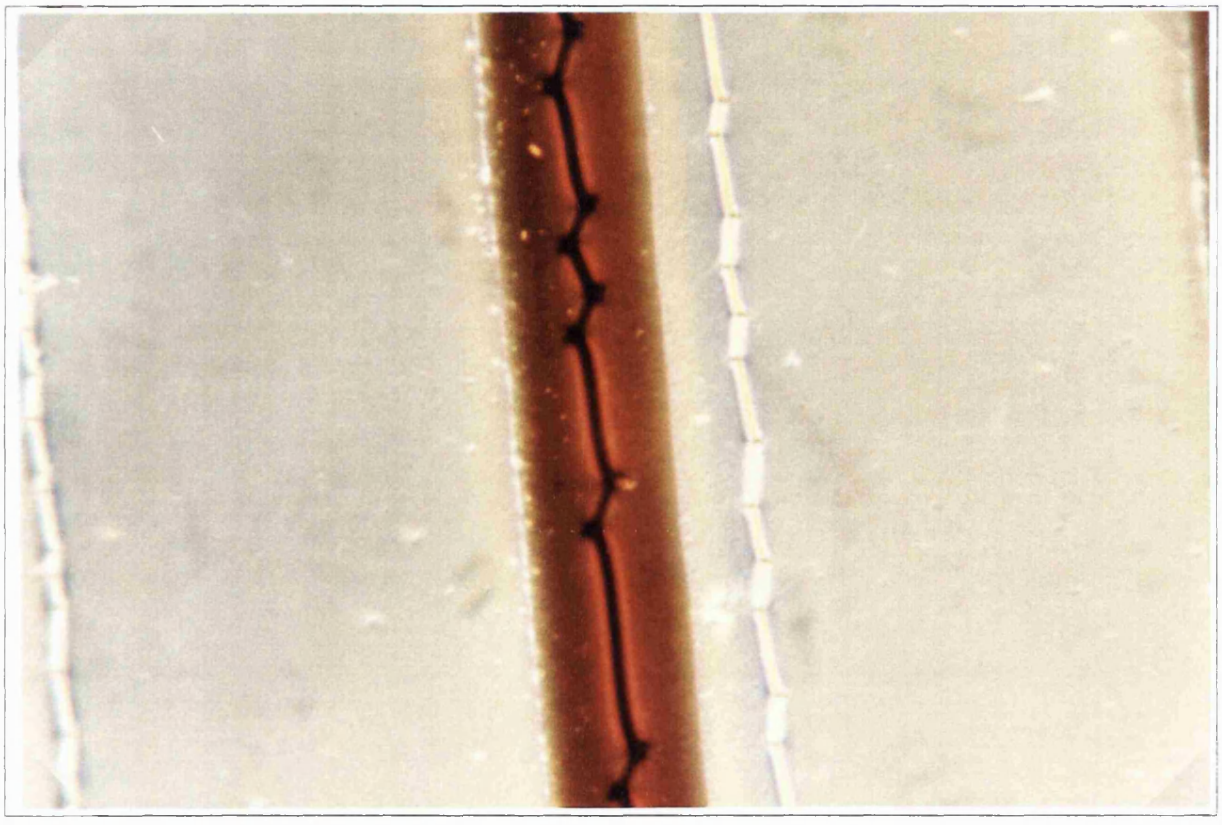

Figure 6.38: Initial wall on the cylindrical lens

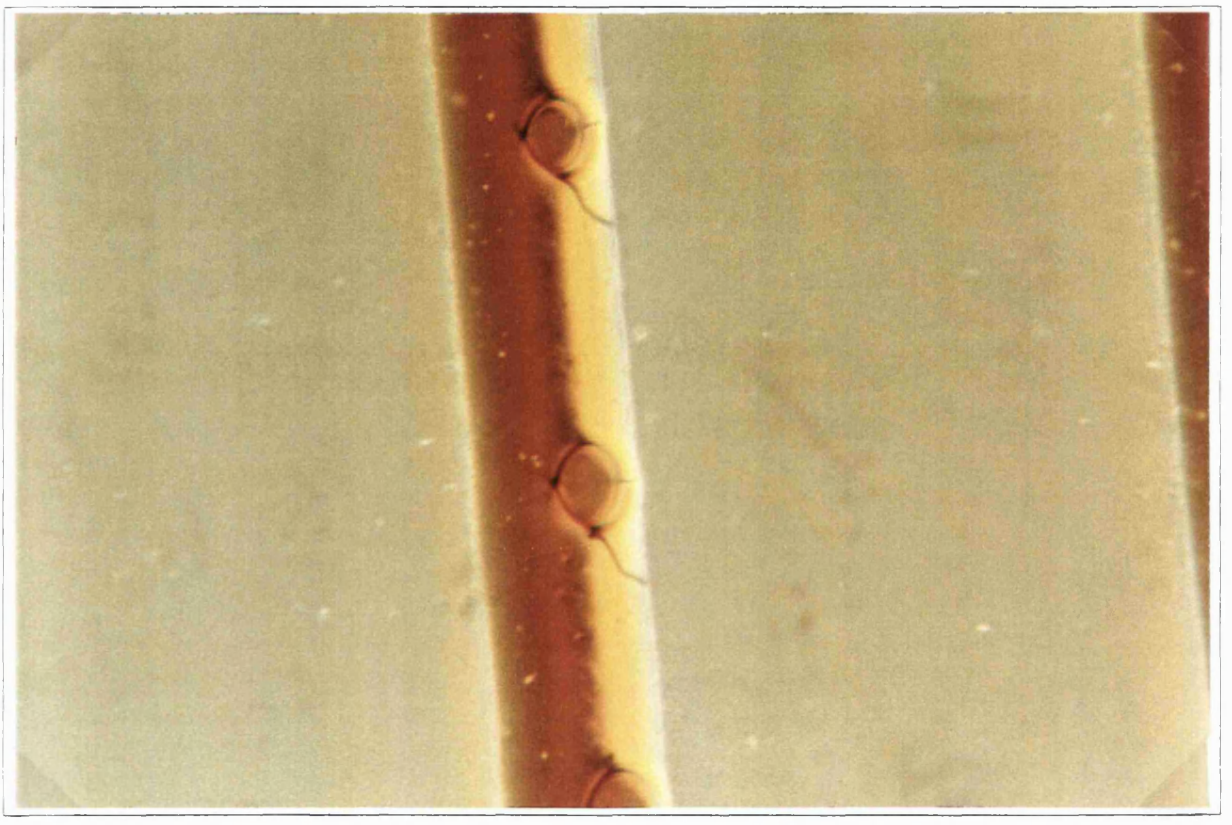

Figure 6.39: Small wall loops left on side of microlens after allowing the wall has broken up at a lower voltage. Polariser, analyser and rubbing directions parallel.

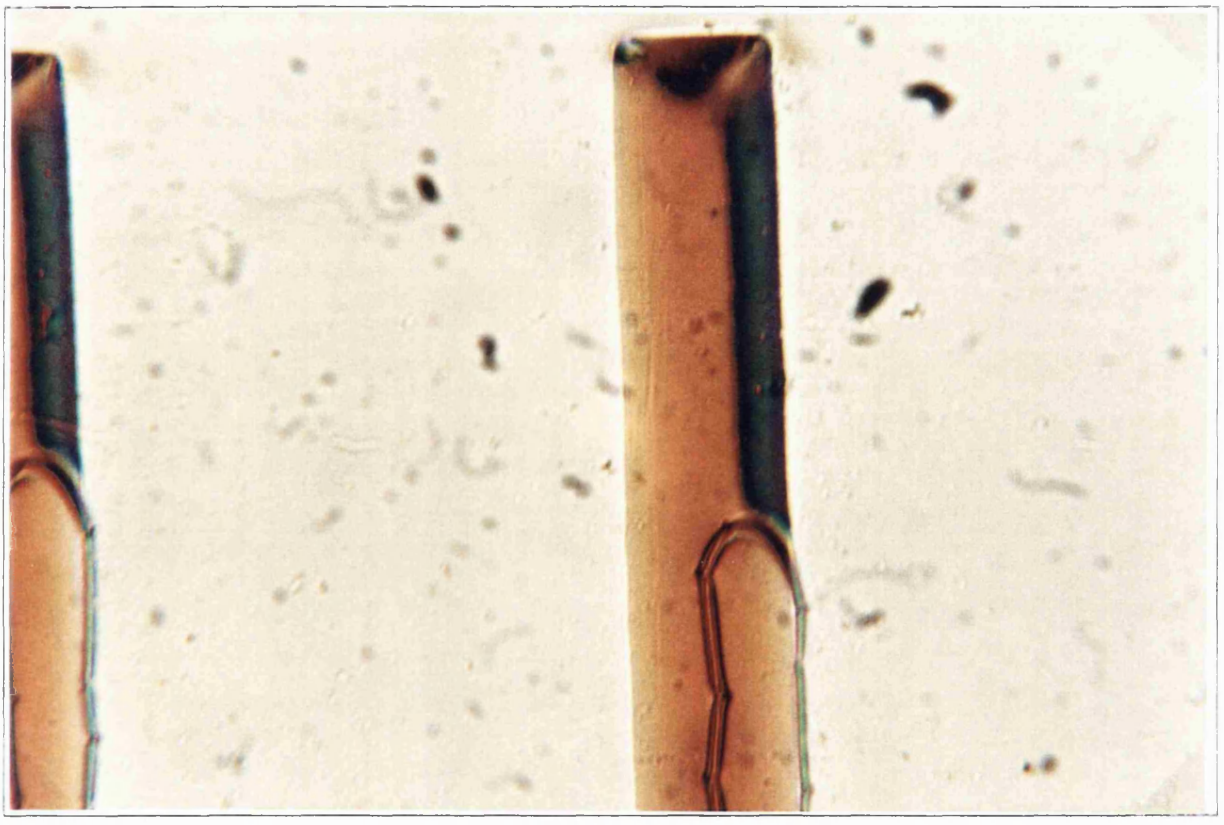

Figure 6.40: Polarisation change on the 'leeward' side (w.r.t. rubbing) of the cylindrical microlens left by the apparently receding wall 14 V applied. Polariser, analyser and rubbing directions parallel.

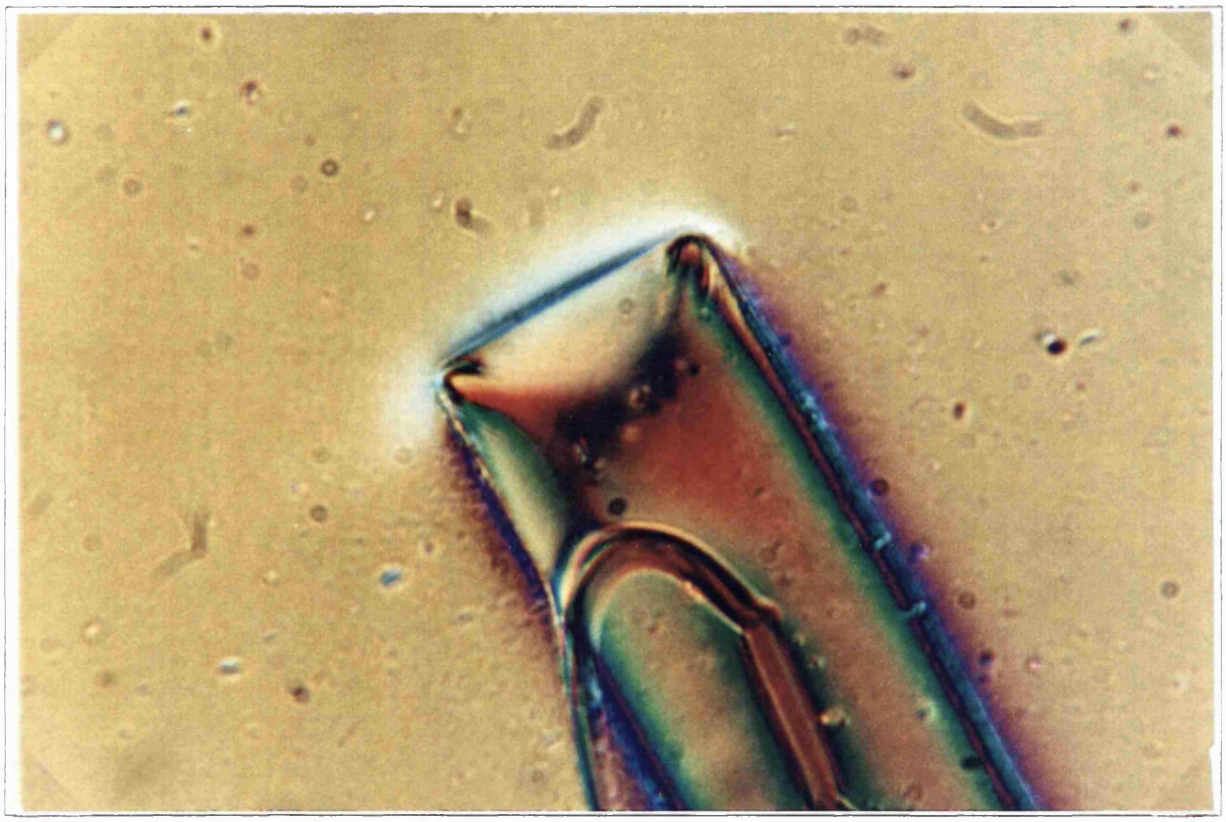

Figure 6.41: Wall receding, note the barely visible line curving away from the wall and along the lens edge. 11.74V applied, polarisers crossed with the rubbing direction at an angle in between.

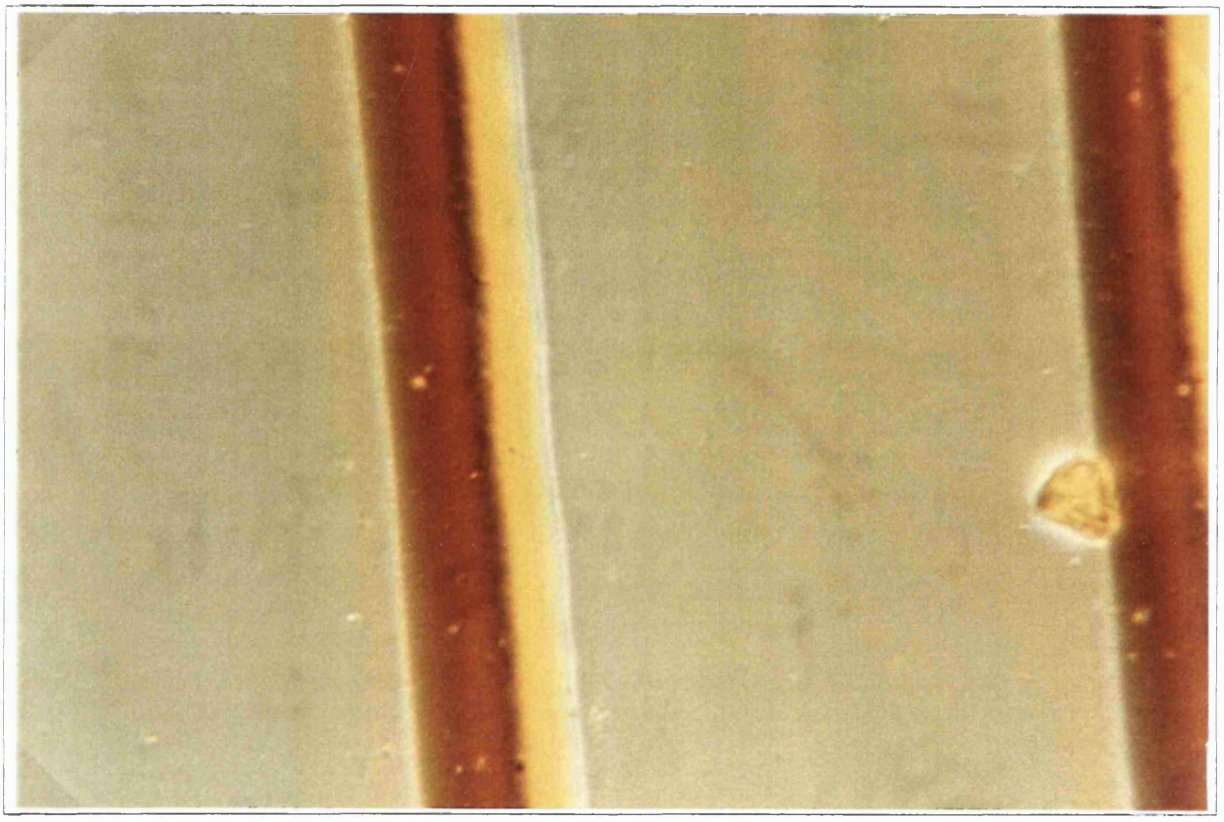

Figure 6.42: Strip of twisted liquid crystal on one side of cylindrical microlens, after wall has receded

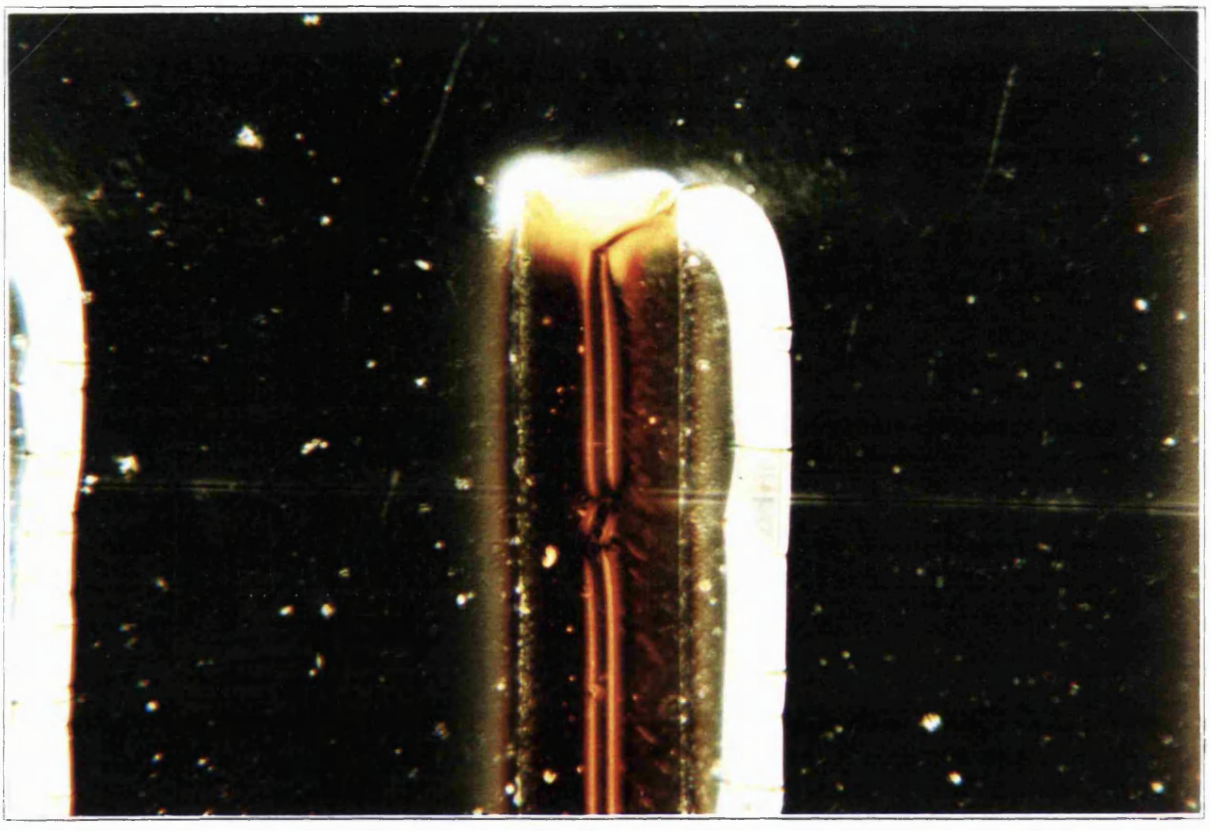

(a)

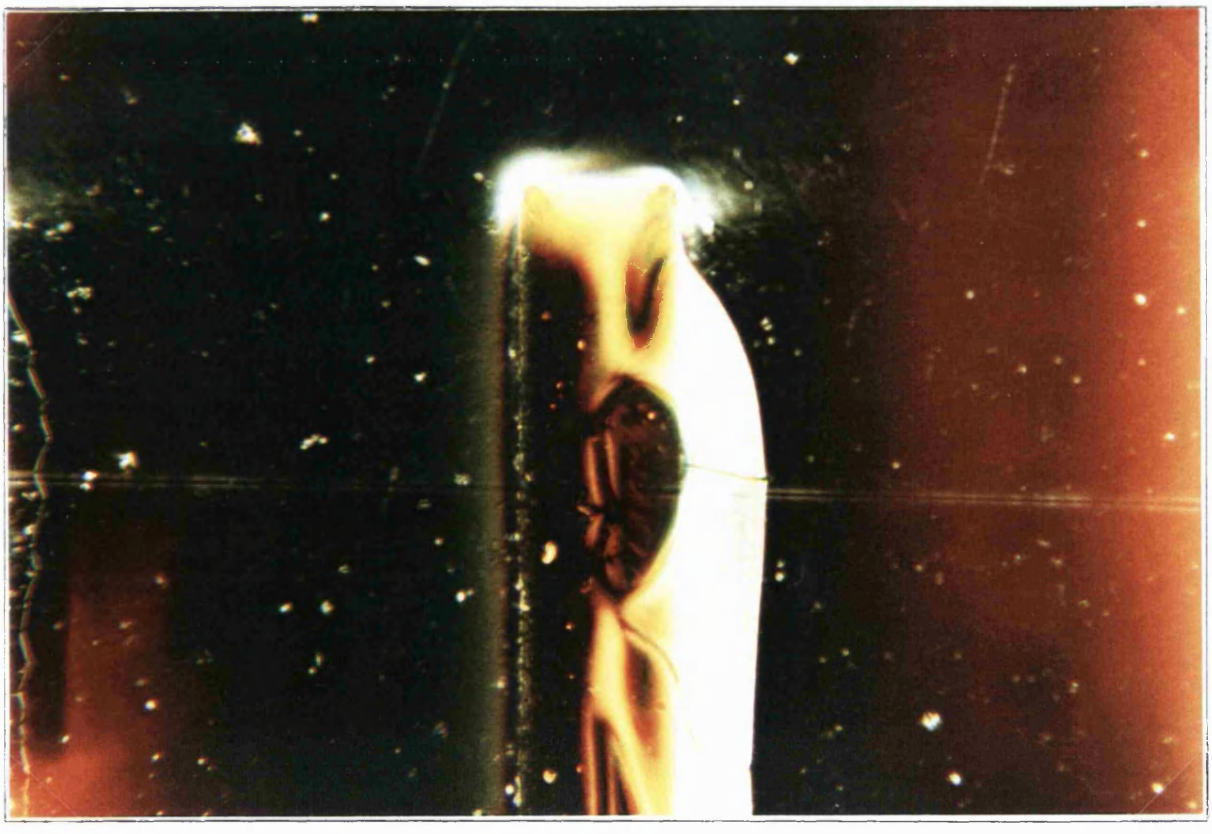

(b)

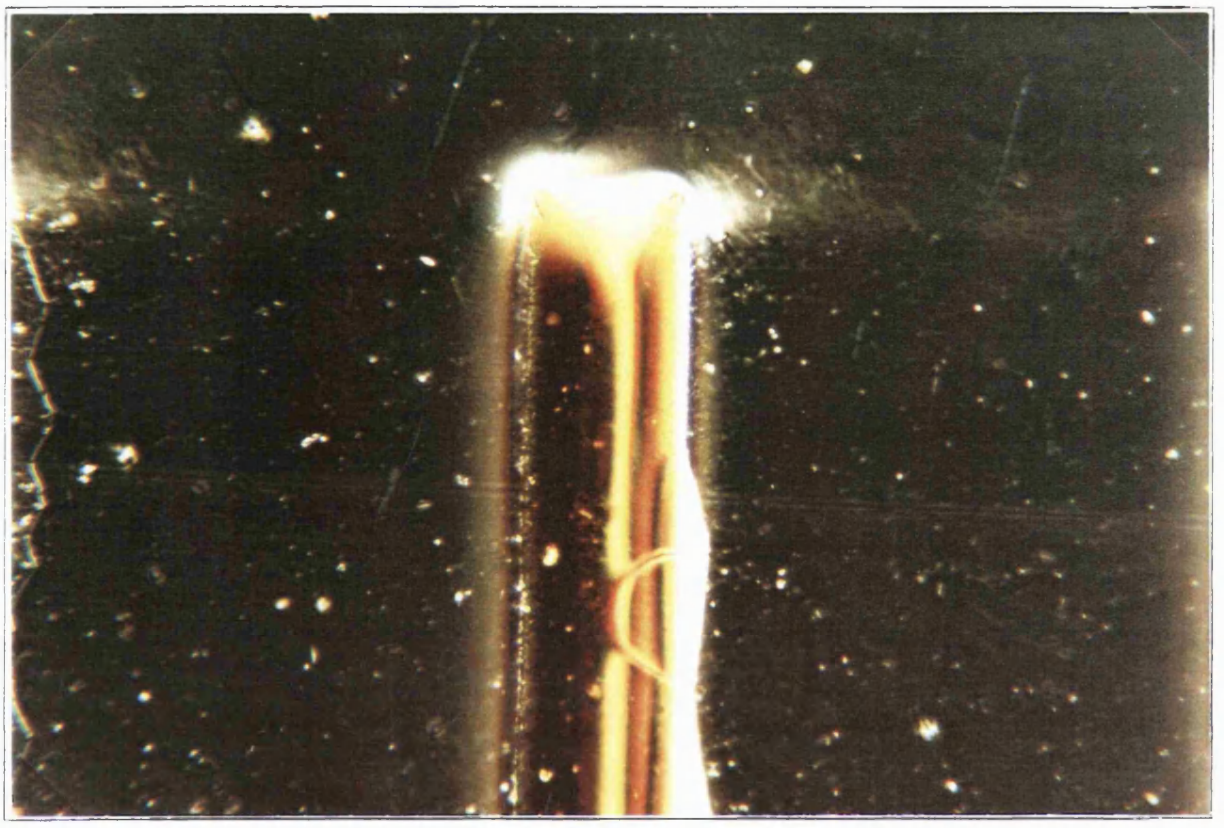

(c)

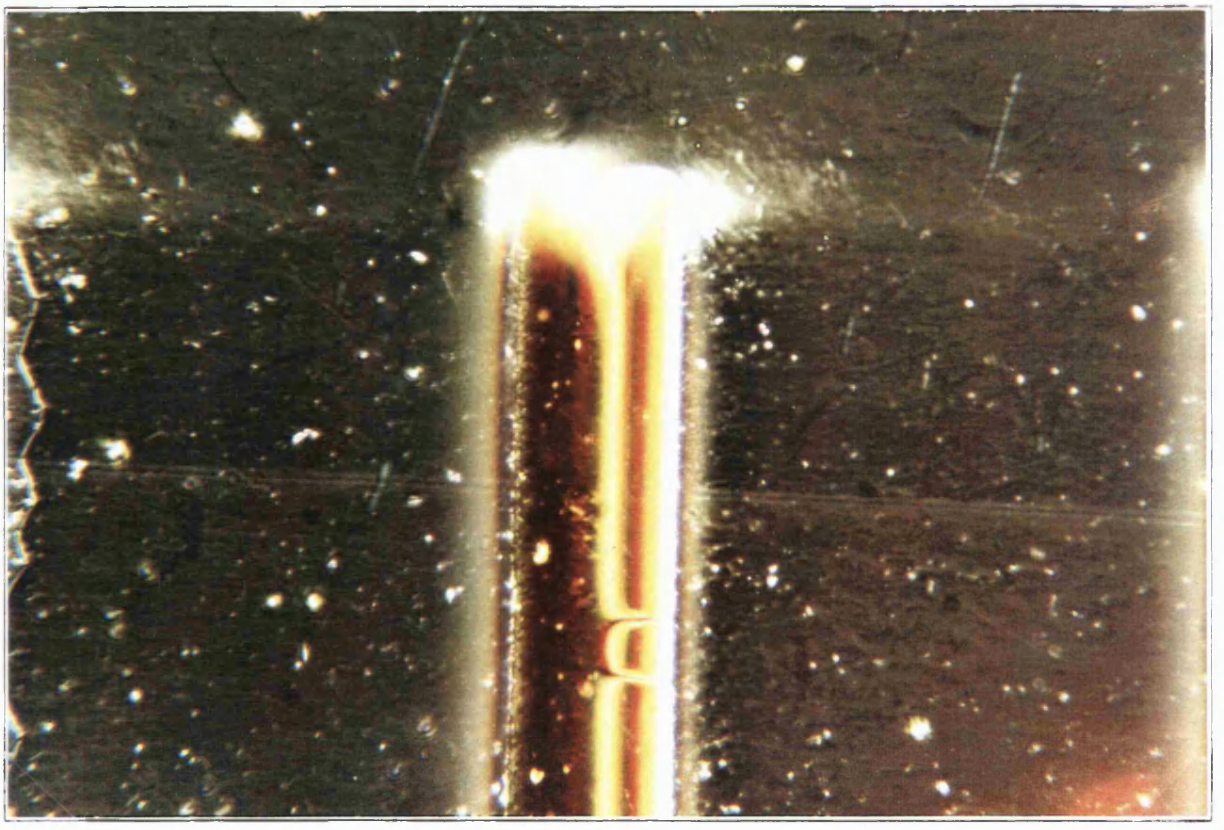

(d)

Figure 6.43: A series of 4 photos of the effect on a wall of switching to a low frequency (18V, 20Hz) where hydrodynamic effects are seen and thus the wall can be seen side-on.

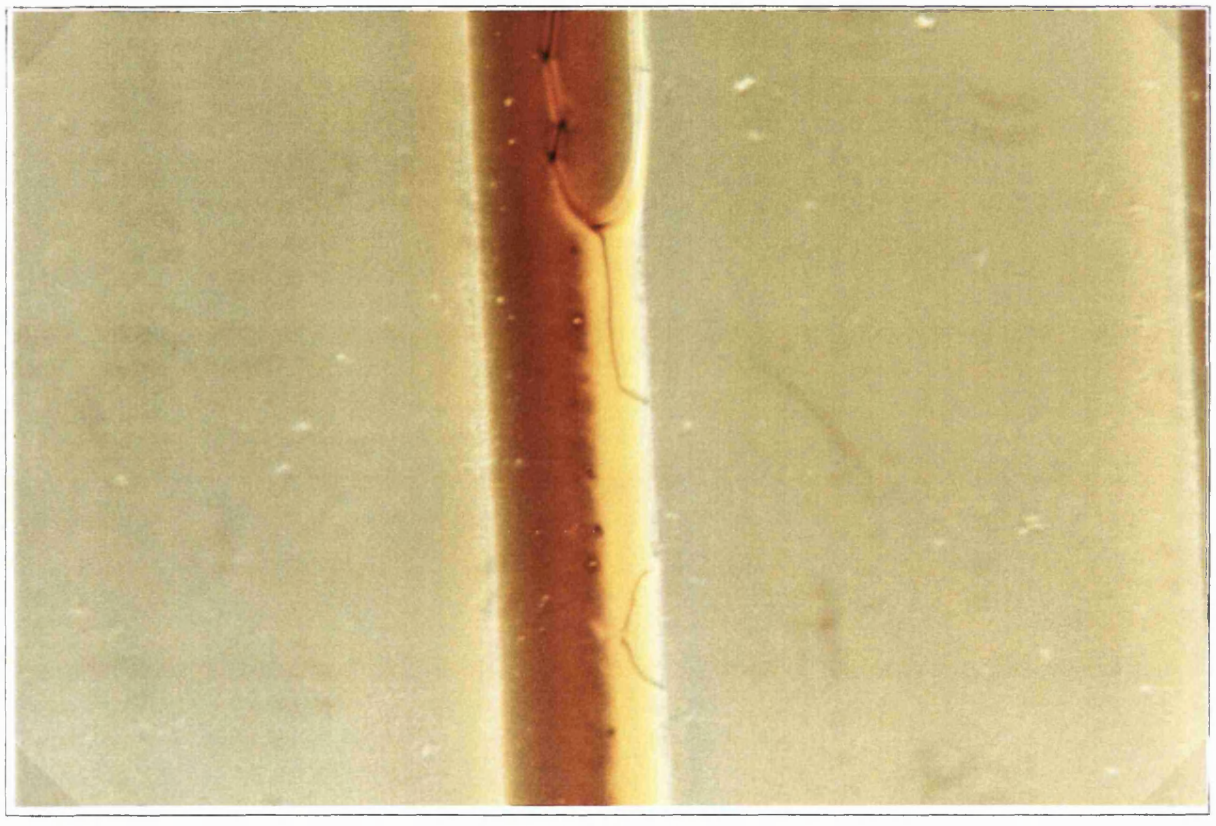

Figure 6.44: Wall kink at end of loop.

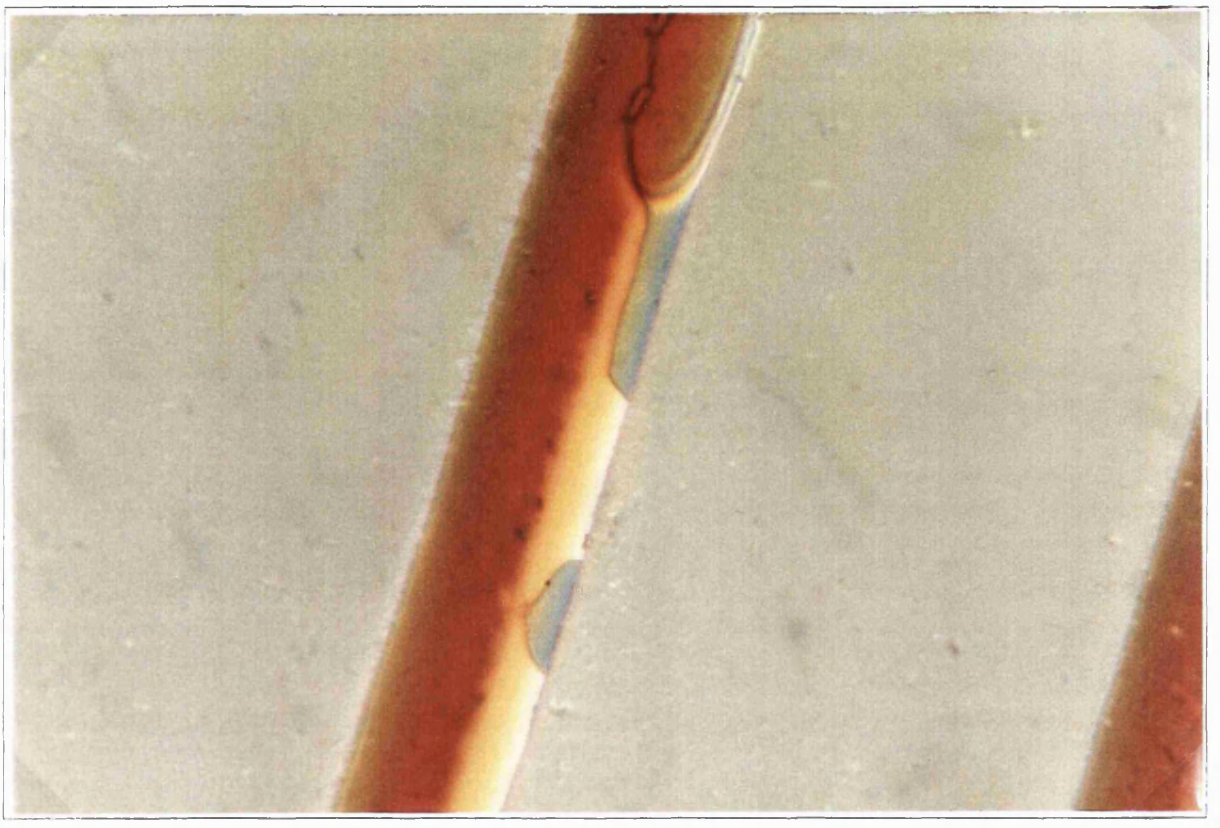

(a)

(b)

Figure 6.45: Photos of extinction either side of wall kink

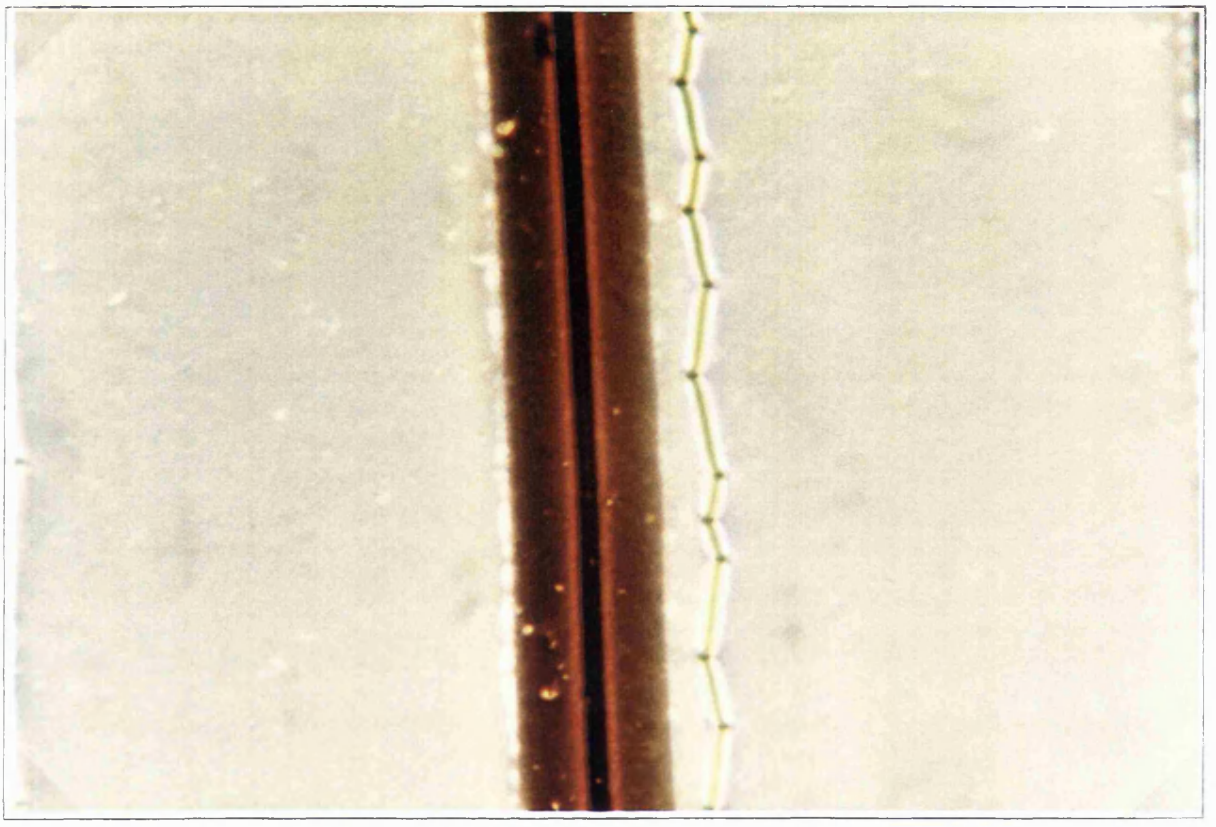

(a) 5.73 V

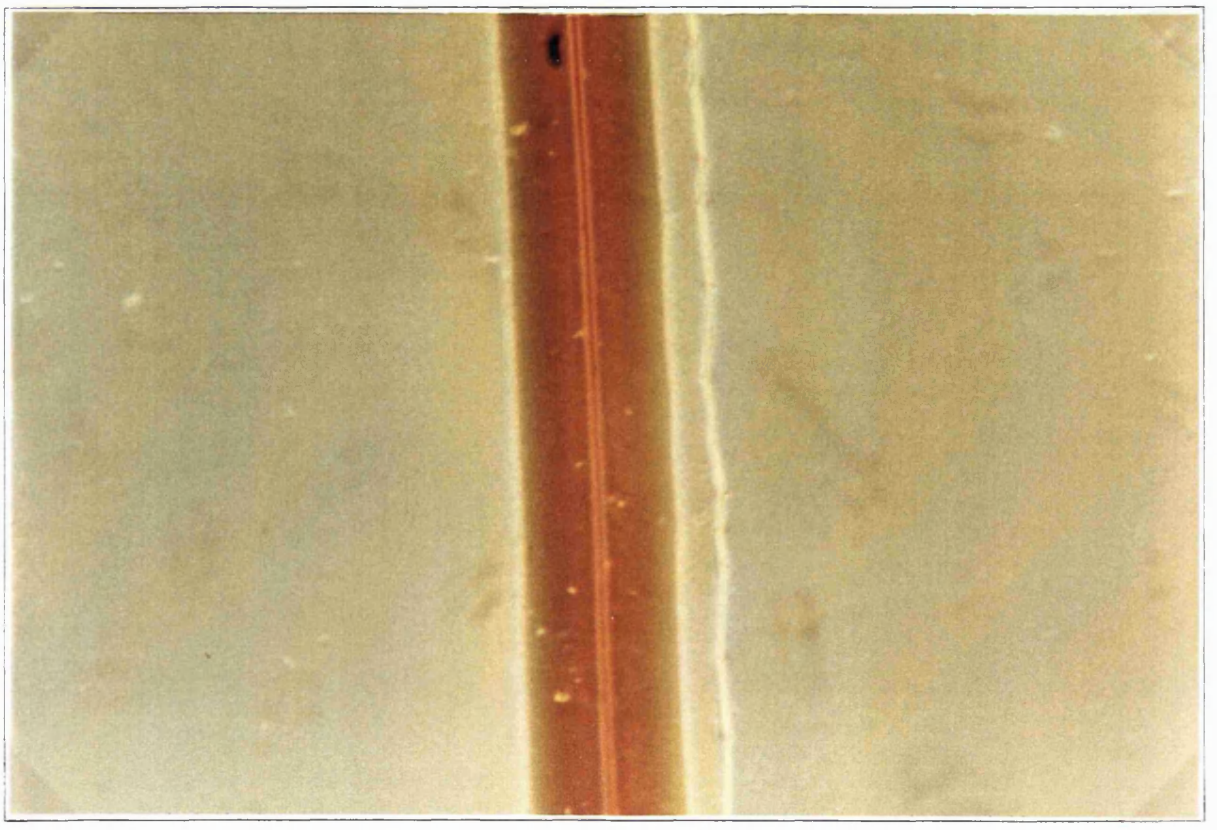

(b) 18.09 V

Figure 6.46: Walls - zig-zag at lower voltages, straight at higher voltages

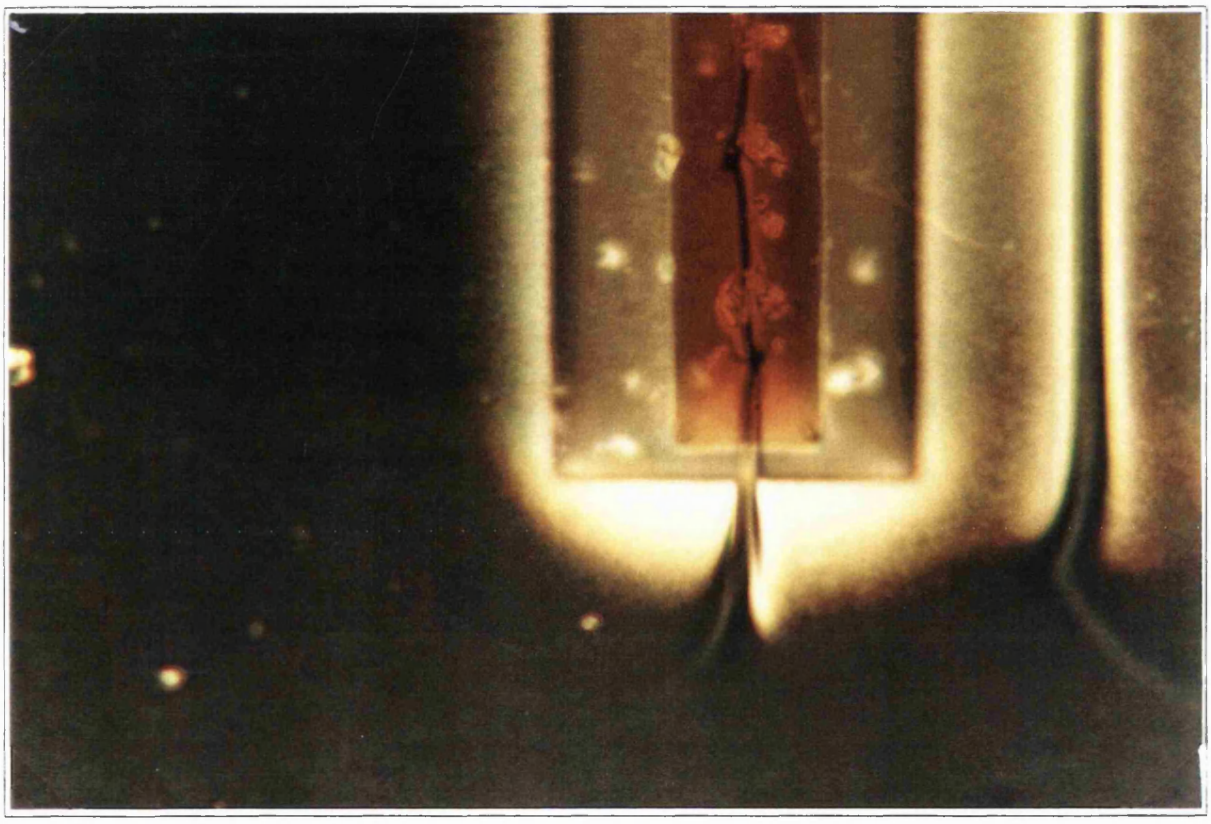

Figure 6.47: Single cylindrical patterned electrode, no wall loop

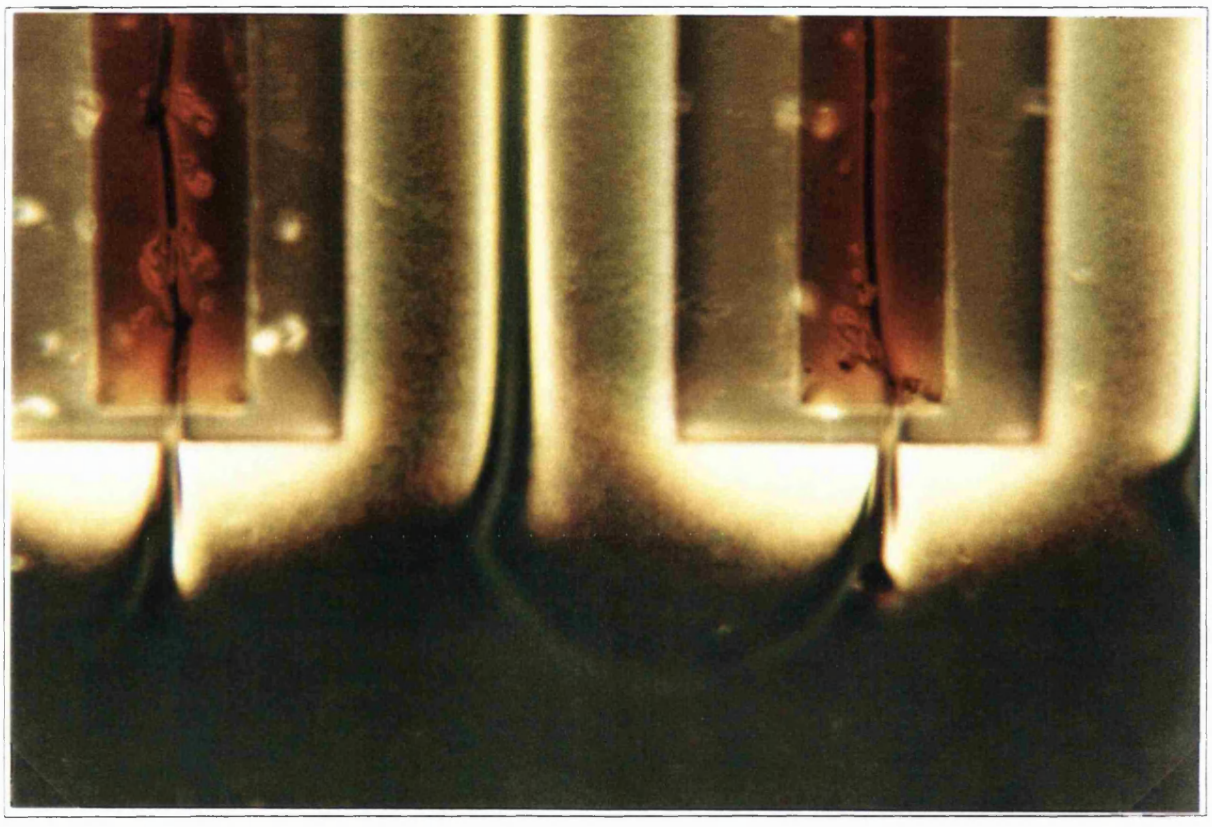

Figure 6.48: Effect of cylindrical patterned electrode pair

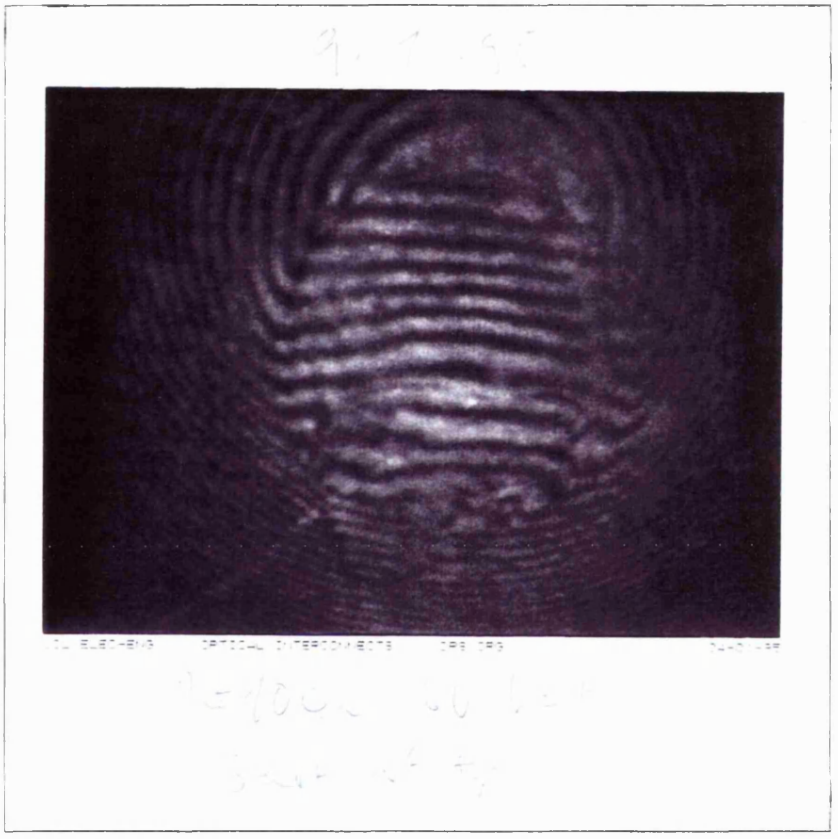

Figure 6.49: Interferogram of original lenses (D=100μm), 6V applied. Note the poor contrast in several places due to the liquid crystal altering the light polarisation in the those areas.

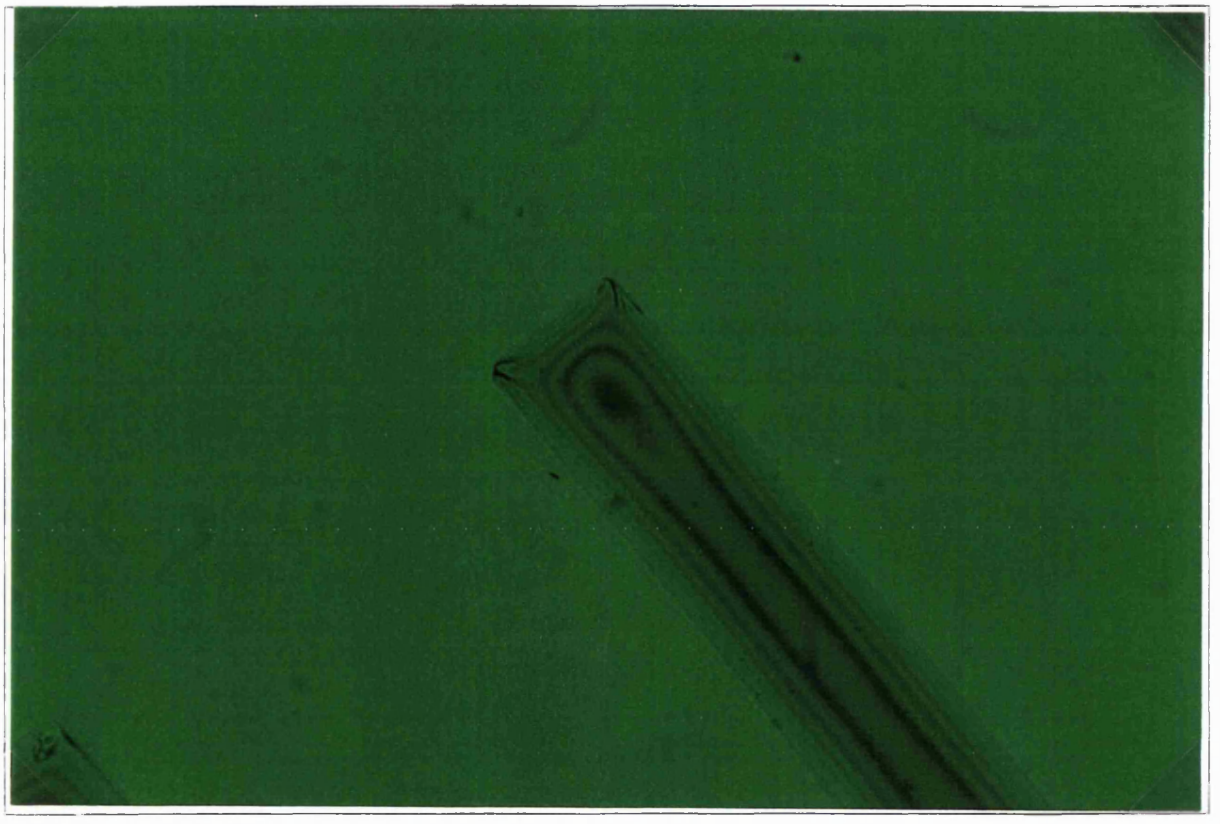

Figure 6.50: Symmetrical birefringence fringes 0V applied (electrode-on-top microlens).

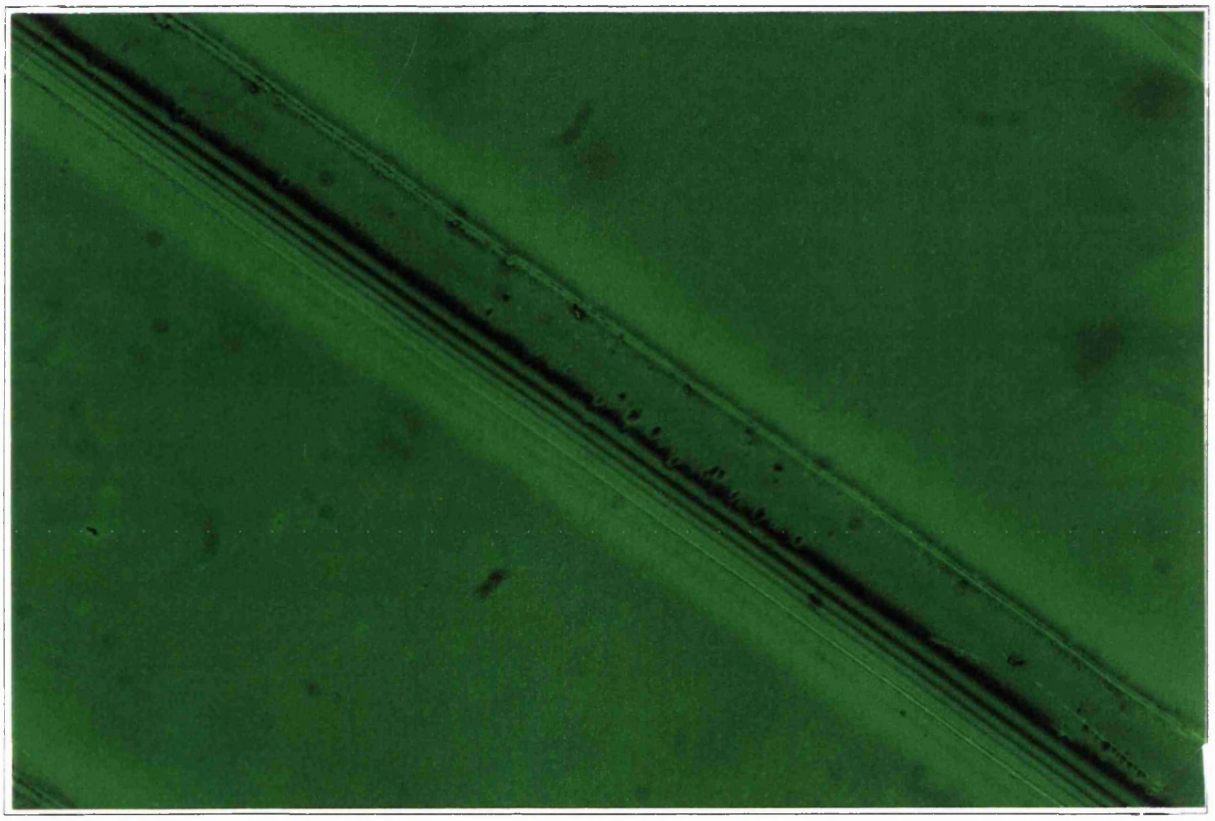

Figure 6.51: Asymmetrical birefringence of electrode-on-top microlens

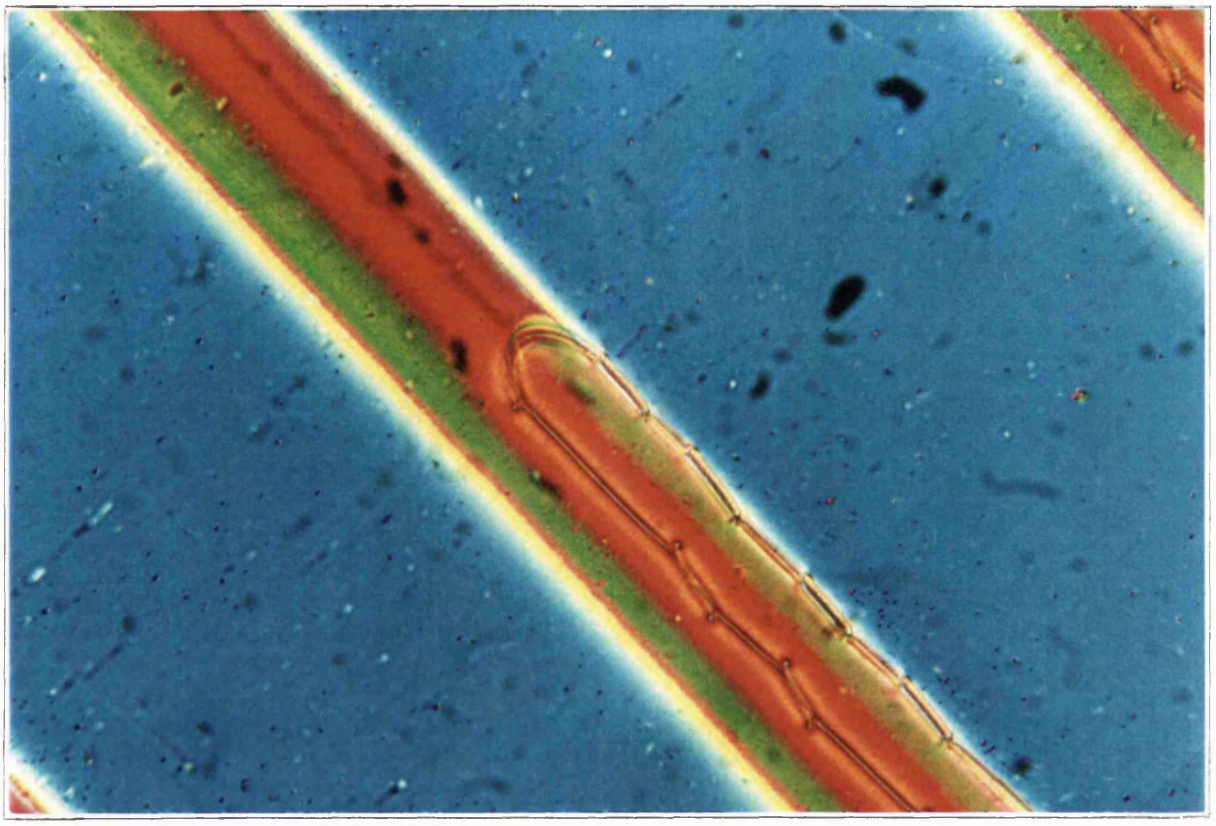

(a) Wall

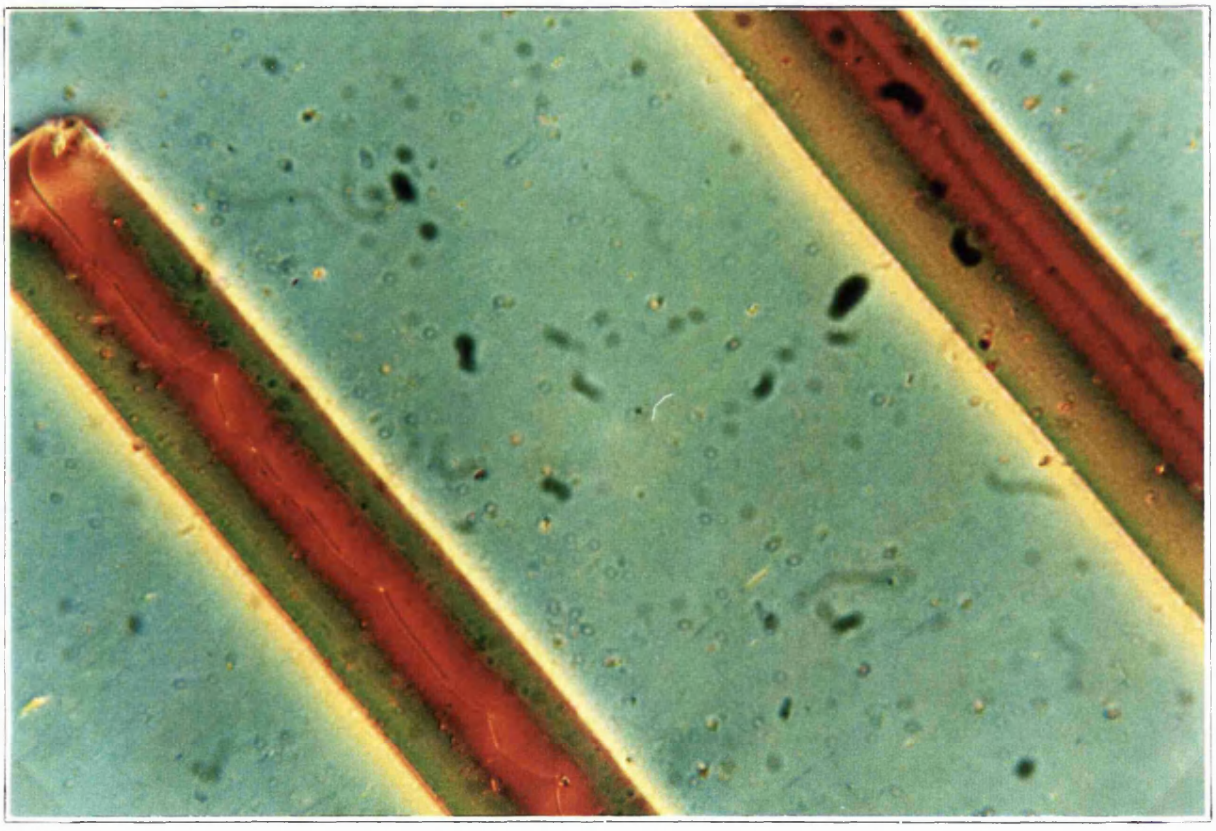

(b) Disclination

Figure 6.52: Birefringence fringes across two types of defect structure. Birefringence symmetrical apart from where the wall has receded.

Chapter 7

Numerical simulation: Modelling liquid crystal and lens aberrations

7.1 Introduction

The liquid crystal structure of the lens cell has been modelled in 2 different ways. The first way is simpler and quicker but less complete. This first method takes the 1 dimensional analysis described by Deuling (see chapter 2) and uses it many times over with different boundary conditions to build up a 3 dimensional model of the lens optical properties (sections 7.2 and 7.3). Since it is only 1-dimensional it cannot predict wall or disclination structures in the liquid crystal. The 2nd approach uses Finite Element and Finite Differences methods to predict the liquid crystal structures (sections 7.4.1 and 7.5). Although a 3 dimensional finite element model has been developed, the liquid crystal structures on the microlens are particularly complex and, to date, only the 2 dimensional model has been applied to them. Both methods require many numerical calculations and thus can only realistically be achieved with a computer.

7.2 1-D model theory

As mentioned above, Deuling's analysis (see section 2.3) is a 1 dimensional analysis which relies on the Euler-Lagrange equation. The analysis calculates an expression for the minima of the free energy equation relating the splay-bend deformation and energy due to the electric field. It is convenient since it is a partially analytic solution, numerical methods only being required for the integration of the resulting equation.

However, the analysis as described by Deuling is insufficient to be able describe the liquid crystal structures on the microlenses even when modelling in 1-dimension. One of the most important deviations from the ideal intended structure is the variation of the pre-tilt across the surface of the microlens, however, Deulings description is only valid for symmetric cells (*i.e.* cells with equal pre-tilts on both cell walls). As well as this, a mechanism is required in order to calculate the effect of the dielectric of the photoresist on the electric field distribution.

Deuling derived (see section 2.3) an equation of the form

$$z(\phi) = k(D_z, \phi_{max}) \int_{\phi_o}^{\phi} f(\phi)\, d\phi \tag{7.1}$$

where z is the normal direction through cell, ϕ is the tilt angle of the director out of the cell plane, ϕ_{max} is the maximum tilt angle, D_z is the displacement current and k and f are functions.

Notice that equation 7.1 gives the desired relation but the wrong way around, *i.e.* for a given tilt, ϕ, its position, z, can be calculated but not the other way around. By dividing equation 7.1 by the same equation for the case where $\phi = \phi_{max}$, the function $k(D_z, \phi_{max})$ is eliminated and the expression is normalised to an expression for $\frac{z(\phi)}{(d/2)}$ (assuming $z(\phi_{max}) = (d/2)$ where d is the liquid crystal layer thickness):

$$\frac{z(\phi)}{z(\phi_{max})} = \frac{z(\phi)}{(d/2)} = \frac{\int_{\phi_{o_1}}^{\phi} f(\phi)\, d\phi}{\int_{\phi_{o_1}}^{\phi_{max}} f(\phi)\, d\phi} \tag{7.2}$$

The assumption that the maximum tilt is in the centre of the cell is valid for the specific case when the pre-tilt on the two surfaces is equal but not necessarily for the more general case.

The extension to the more general case is not difficult, the normalisation can still be done but this time for the whole cell. Taking equation 7.1 and dividing through by $z_1(\phi_{max}) + z_2(\phi_{max})$ (= d), we get

$$\begin{aligned} \frac{z(\phi)}{d} &= \frac{k(D_z, \phi_{max}) \int_{\phi_{o_1}}^{\phi} f(\phi)\, d\phi}{k(D_z, \phi_{max}) \int_{\phi_{o_1}}^{\phi_{max}} f(\phi)\, d\phi + k(D_z, \phi_{max}) \int_{\phi_{o_2}}^{\phi_{max}} f(\phi)\, d\phi} \\ &= \frac{\int_{\phi_{o_1}}^{\phi} f(\phi)\, d\phi}{\int_{\phi_{o_1}}^{\phi_{max}} f(\phi)\, d\phi + \int_{\phi_{o_2}}^{\phi_{max}} f(\phi)\, d\phi} \end{aligned} \tag{7.3}$$

where ϕ_{o_1} and ϕ_{o_2} are the pre-tilts on the two cell walls.

Equation 7.3 can give the position of the maximum $z(\phi_{max})$ which can then be used as the new normalisation factor in equation 7.2 replacing (d/2). With this alteration, the calculation of the tilt profile is the same as for the symmetric case with the addition that it has to be done twice for the two pre-tilts, ϕ_{o_1} and ϕ_{o_2}.

In a similar fashion, the equation for the voltage needs to be adapted for non-symmetric cells. The original expression (see section 2.3) for the voltage was of the form:

$$V = 2 \int_{\phi_0}^{\phi_{max}} g(\phi)\, d\phi \tag{7.4}$$

where g is a function of ϕ and the factor of 2 is due to the symmetry of the cell. The formulation for the non-symmetric cell is the only different in that the simplification due to symmetry cannot be made:

$$V = \int_{\phi_{0_1}}^{\phi_{max}} g(\phi)\, d\phi + \int_{\phi_{0_2}}^{\phi_{max}} g(\phi)\, d\phi \tag{7.5}$$

The next change which is required in order to deal with the microlens structure is the addition of a layer of dielectric (photoresist). This can be done in a similar way to the calculation of the voltage across the liquid crystal. It does not affect the calculation for ϕ, accept that d, the liquid crystal layer thickness, varies across the microlens.

Calculating the maximum tilt angle (required for the tilt profile equation above) directly for a particular voltage (*i.e.* $\phi_{max}(V)$) is not possible using Deuling's analysis. However, as with the position vs tilt relation (see equation 7.1) an expression has been calculated for the reverse, i.e. $V(\phi_{max})$-what voltage is necessary to give a particular maximum tilt (see section 2.3) and hence it is simple to calculate an approximation for the maximum tilt at a particular voltage by changing ϕ_{max} until the voltage is given to a desired accuracy. The calculation for the voltage necessary for a particular maximum tilt can be extended to include a dielectric layer, effectively calculating the additional voltage dropped across the dielectric. From Maxwell's equations we know that the displacement current, D_z, is constant through a volume containing no current flows, and thus, it is the same in the dielectric and the liquid crystal. The expression for $z(\phi)$ (the form of which is shown in equation 7.1) can be rearranged as an expression for D_z:

$$D_z = \frac{1}{z}\sqrt{\frac{\epsilon_o \epsilon_\perp k_{11}}{\gamma}}\sqrt{(1+\gamma\sin^2\phi_{max})}\int_{\phi_o}^{\phi}\sqrt{\frac{(1+\kappa\sin^2\phi)(1+\gamma\sin^2\phi)}{\sin^2\phi_{max}-\sin^2\phi}}\,d\phi \tag{7.6}$$

and using the fact that $z_{centre} = z(\phi_{max})$

$$D_z = \frac{1}{z_{centre}}\sqrt{\frac{\epsilon_o \epsilon_\perp k_{11}}{\gamma}}\sqrt{(1+\gamma\sin^2\phi_{max})}\int_{\phi_o}^{\phi_{max}}\sqrt{\frac{(1+\kappa\sin^2\phi)(1+\gamma\sin^2\phi)}{\sin^2\phi_{max}-\sin^2\phi}}\,d\phi \tag{7.7}$$

The centre position, z_{centre}, can be calculated from equation 7.3. Then the electric field, E_z, in the dielectric is given by

$$E_z = \epsilon_{photoresist}\epsilon_o D_z \tag{7.8}$$

where $\epsilon_{photoresist}$ is the relative dielectric permittivity of the photoresist and ϵ_o is the permittivity of free space. Finally, to get the voltage dropped across the photoresist, $V_{photoresist}$, we need only multiply the electric field by the photoresist thickness:

$$V_{photoresist} = E_z \times d_{photoresist} \tag{7.9}$$

where $d_{photoresist}$ is the thickness of photoresist at that point.

It is then just a case of adding the voltage across the photoresist to the voltage across the liquid crystal and putting this extra step into the iterative process of finding the maximum tilt angle, ϕ_{max}, at a particular voltage.

There is one further adjustment to the formulae which is not to account for any extra physical phenomenon but simply to make the numerical computation easier.

The function $g(\phi)$ in equation 7.4 is given by

$$g(\phi) = \sqrt{\frac{k_{11}}{\epsilon_o \epsilon_\perp \gamma}} \sqrt{(1 + \gamma \sin^2 \phi_{max})} \sqrt{\frac{(1 + \kappa \sin^2 \phi)}{(1 + \gamma \sin^2 \phi)(sin^2 \phi_{max} - \sin^2 \phi)}} \, d\phi \tag{7.10}$$

This expression is integrated numerically in a computer which creates a problem because there is asymptote generated by the $1/(\sin^2 \phi_{max} - sin^2 \phi)$ term as ϕ approaches the ϕ_{max} limit.

To remove this asymptote, a substitution is made:

$$p = \sin^{-1}\left(\frac{\sin \phi}{\sin \phi_{max}}\right) \tag{7.11}$$

To complete the substitution an expression for $d\phi$ is needed:

$$dp = \frac{1}{\sqrt{\sin^2 \phi_{max} - \sin^2 \phi}} \cdot \frac{\cos \phi}{\sin \phi_{max}} \, d\phi \tag{7.12}$$

Also, an expression for $\sin \phi$ is required:

$$\sin p = \frac{\sin \phi}{\sin \phi_{max}} \tag{7.13}$$

Rearranging,

$$\sin \phi = \sin p \sin \phi_{max} \tag{7.14}$$

Therefore,

$$\begin{aligned} \cos \phi &= \sqrt{1 - \sin^2 \phi} \\ &= \sqrt{1 - \sin^2 p \sin^2 \phi_{max}} \end{aligned} \tag{7.15}$$

Combining all these equations together we can say:

$$\frac{1}{\sqrt{\sin^2 \phi_{max} - \sin^2 \phi}} \, d\phi = \frac{\sin \phi_{max}}{\sqrt{1 - \sin^2 p \sin^2 \phi_{max}}} \, dp \tag{7.16}$$

Substituting this into the integral of $g(\phi)$:

$$\begin{aligned} V = &\sqrt{\frac{k_{11}}{\epsilon_o \epsilon_\perp \gamma}} \sqrt{(1 + \gamma \sin^2 \phi_{max})} \times \\ &\int_{p(\phi_0)}^{p(\phi_{max})} \sqrt{\frac{(1 + \kappa \sin^2 \phi_{max} \sin^2 p)}{(1 + \gamma \sin^2 \phi_{max} \sin^2 p)}} \cdot \frac{\sin \phi_{max}}{\sqrt{1 - \sin^2 \phi_{max}}} \, dp \end{aligned} \tag{7.17}$$

The new limits are simply calculated:

$$p(\phi_o) = \sin^{-1}\left(\frac{\sin\phi_o}{\sin\phi_{max}}\right) \tag{7.18}$$

and

$$\begin{aligned} p(\phi_{max}) &= \sin^{-1}\left(\frac{\sin\phi_{max}}{\sin\phi_{max}}\right) \\ &= \frac{\pi}{2} \end{aligned} \tag{7.19}$$

As mentioned above, equation 7.17 is only half of the equation for V since there are two pre-tilts so the real voltage is sum of the two as expressed in equation 7.5.

Equation 7.17 will only contain an asymptote when $\sin\phi_{max} = 1$, *i.e.* when $\phi_{max} = 90°$ which is a significant improvement on the original equation where there was an asymptote for $\phi = \phi_{max}$ irrespective of the value of ϕ_{max}.

The integrals for $z(\phi)$ (equation 7.3 also contain asymptotes due to a $1/(\sin^2\phi_{max} - \sin^2\phi)$ term which can be similarly improved upon with the same substitution as was employed with the voltage expression.

Considering one of the integrals of $z(\phi)$ (which are all of the same form):

$$I = \int_{\phi_0}^{\phi} f(\phi)\,d\phi = \int_{\phi_0}^{\phi} \sqrt{\frac{(1+\kappa\sin^2\phi)(1+\gamma\sin^2\phi)}{\sin^2\phi_{max} - \sin^2\phi}}\,d\phi \tag{7.20}$$

The substitution yields

$$\begin{aligned} I = &\int_{p(\phi_0)}^{p(\phi)} \sqrt{(1+\kappa\sin^2\phi_{max}\sin^2 p)(1+\gamma\sin^2\phi_{max}\sin^2 p)} \\ &\qquad \times \frac{\sin\phi_{max}}{\sqrt{1-\sin^2\phi_{max}\sin^2 p}}\,dp \\ = \sin\phi_{max} &\int_{\sin^{-1}(\frac{\sin\phi_o}{\sin\phi_{max}})}^{\sin^{-1}(\frac{\sin\phi}{\sin\phi_{max}})} \sqrt{\frac{(1+\kappa\sin^2\phi_{max}\sin^2 p)(1+\gamma\sin^2\phi_{max}\sin^2 p)}{1-\sin^2\phi_{max}\sin^2 p}}\,dp \end{aligned} \tag{7.21}$$

The improvements can be seen from the following set of figures. In figure 7.1 are the integrands of the original and new equations of the voltages for 3 different maximum tilt angles. In figure 7.2 is the same plots but for the original and new tilt integrands.

The numerical integrations are done using a simple step approximation to the integrands but with an adaptive step size. Here advantage is taken of the known shape of the integrands. As can be seen from figures 7.1 and 7.2 the functions are fairly linear except as they approach the maximum tilt angles where they become large and vary faster (more so for larger maximum tilts). Since the most significant errors will be introduced where the function varies fastest, the step size needs to be made smaller. This can be achieved by setting a limit on how much any step can contribute to the overall

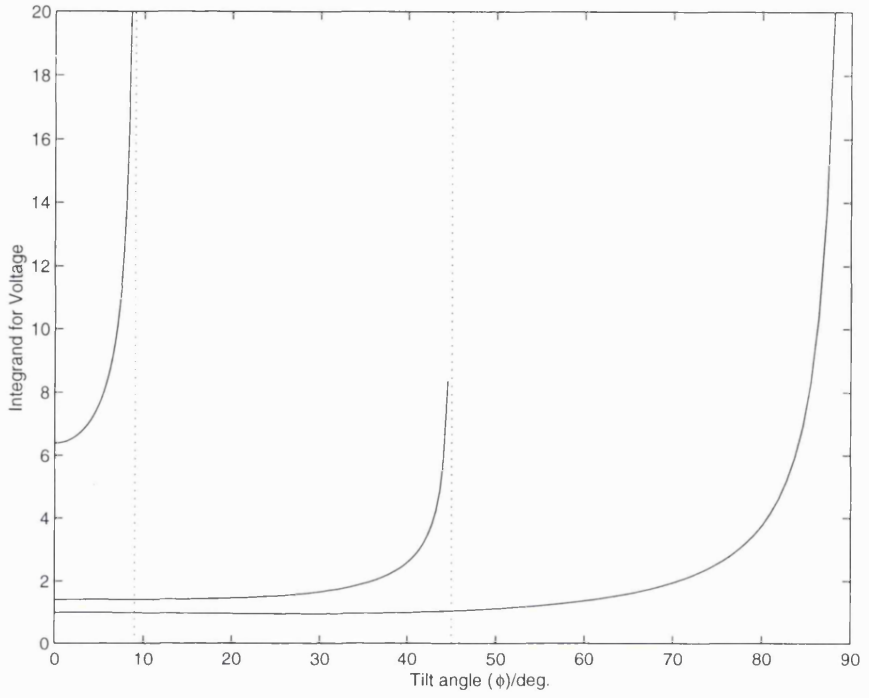

(a) The integrand of the voltage equation as given by Deuling

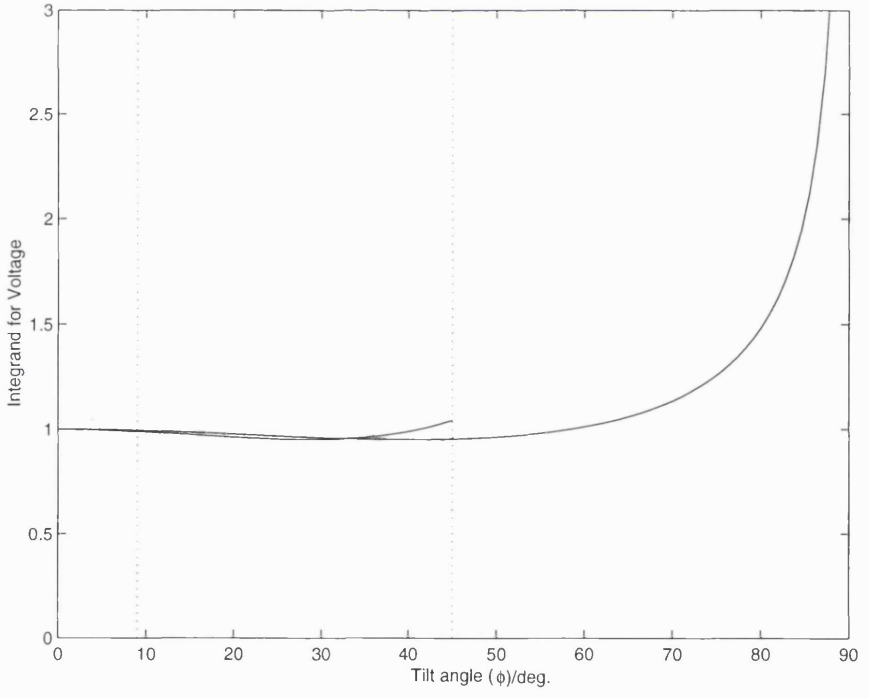

(b) The integrand of the new voltage equation (after substitution)

Figure 7.1: Plots of integrands for $\phi_{max} = 9°, 45°$ and $90°$. In (a), all the lines go to asymptotes at their maximum tilt angles. In (b), only the plots with $\phi_{max} = 90°$ has an asymptote.

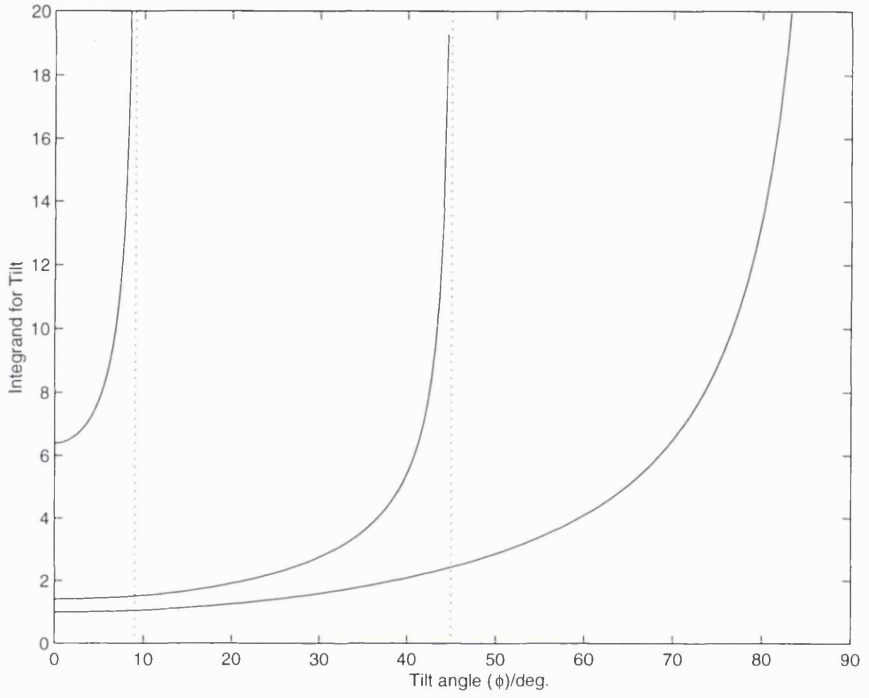

(a) The integrand of the tilt equation as given by Deuling

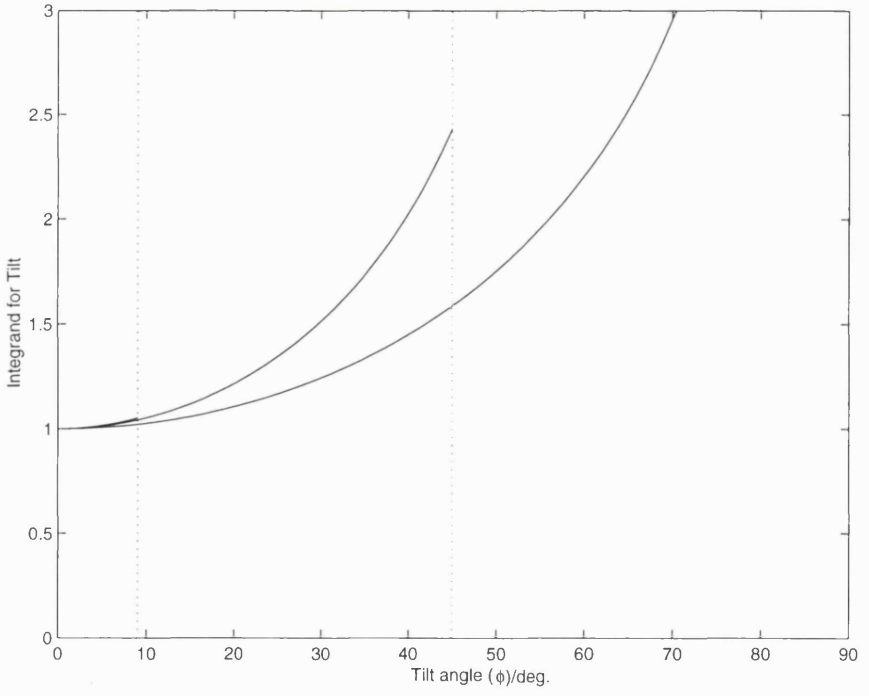

(b) The integrand of the new tilt equation (after substitution)

Figure 7.2: Plots of integrands for $\phi_{max} = 9°, 45°$ and $90°$. In (a), all the lines go to asymptotes at their maximum tilt angles. In (b), only the plots with $\phi_{max} = 90°$ has an asymptote.

integration result. Since the size of the final integration is not known beforehand, this limit is set as a fraction of the total.

By integrating these functions many times a cell tilt angle profile can be built up. Two examples are shown in figure 7.3, one for differing voltages, the other for differing pre-tilts and constant voltage.

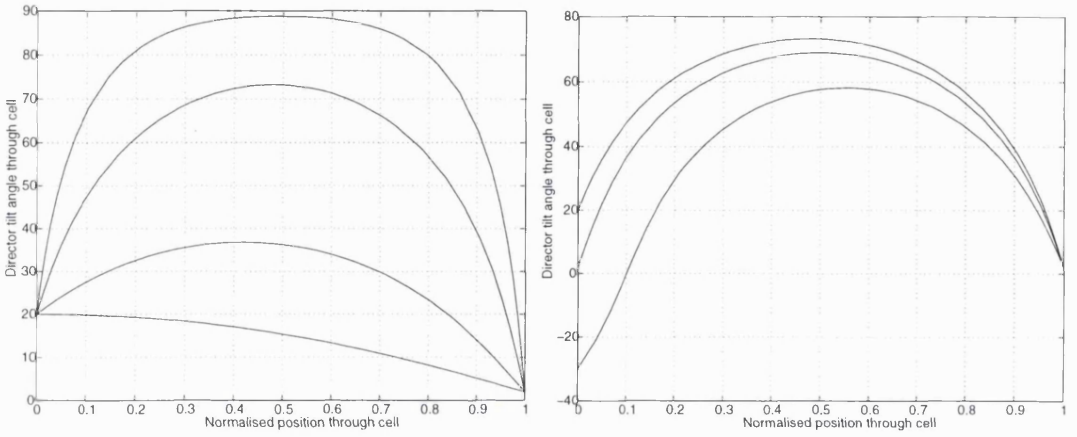

(a) With different applied voltages (0V, 1V, 2V and 4V). The pretilts are 20° on the left hand cell wall and 2° on the right.

(b) With three different pretilts on the left hand wall (−30°, 2° and 20°) with 2V applied

Figure 7.3: Tilt angle (ϕ) profile through the cell calculated for 2 different conditions

The maximum tilt angle is found by iteration of voltage vs tilt relation. A few examples of the profile of maximum tilt vs voltage are shown in figure 7.4. For the negative pretilt, it can be seen that the voltage required for the profile to change is higher than for the positive pre-tilts, a fact that leads to a tilt of the phase wavefronts (see figure 7.7 and section 6.5). It can also be seen from figure 7.4 that for the negative pretilt case, the voltage initially decreases as the maximum tilt increases, *i.e.* the maximum tilt for low voltages will not start at the negative of the pretilt, but slightly less. This possibility was allowed for in calculating the microlens structure profiles.

To compare with the optical measurements, a phase profile of the lenses needs to be constructed. This is done by calculating director profiles through the cell for various positions across the lens with the pre-tilt appropriate to the lens surface angle and a dielectric layer equal to the lens thickness. For each profile, an average refractive index is calculated which is then multiplied by the layer thickness to give an optical path thickness profile for the cell (when combined with the photoresist lens). The optical phase profile is simply the negative of the optical path and thus this generates the theoretical phase profile exiting the lens. To get the aberration from the phase profile, the best fit sphere must be subtracted. This sphere was generated by a least squares fit. The radius of curvature of the sphere is the modelled focal length, giving a second way to compare the 1-D theory and the experiment.

The model is likely to predict aberrations which are higher than those measured, since neighbouring strips of liquid crystal are effectively considered to be independent of each other which clearly is not true. The likely effect of two neighbouring strips will be, in general, to reduce the distortion between them and, since this 1-D model does not

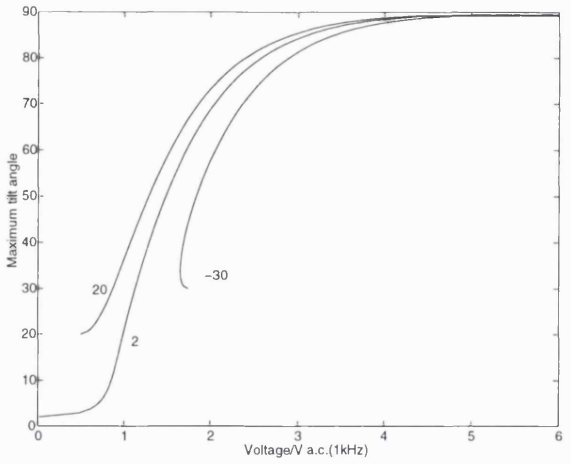

Figure 7.4: Maximum tilt angle (ϕ_{max}) vs voltage for pre-tilts of $-30°, 2°$ and $20°$ on one cell wall with $2°$ on the other.

include this possibility, the predicted differences are likely to be higher than in reality will be the case.

7.3 Results of 1-D model

The focal lengths of the $150\mu m$ original design predicted from the modelling are shown in figure 7.5. What can just be seen from this figure is that the modelled focal length starts to rise above 6V but only by a small amount. The rise in the *measured* focal lengths for higher voltages (above 4V) was the clearest departure from the ideal behaviour of the design (see section 4.3.1), thus it was one of the goals of the modelling to reproduce it.

Clearly, the modelled rise and the measured rise are not identical, the measured rise starts at a lower voltage and rises faster although the increase is similar (measured rise: $490 \rightarrow 1100\mu m$, modelled rise: $790 \rightarrow 1080\mu m$).

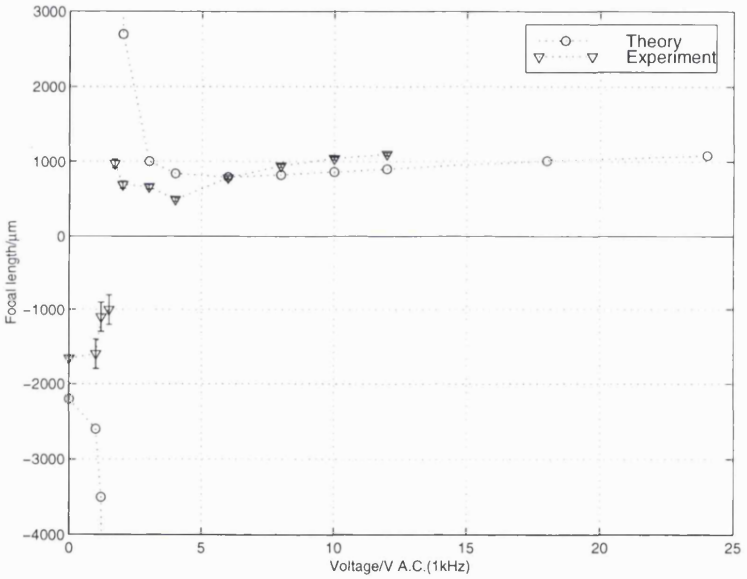

Figure 7.5: The focal lengths as predicted from the model.

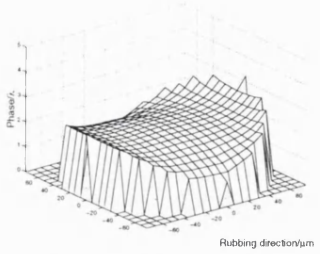

(a) 0.001V (f = -0.0022m, RMS: 0.329λ)

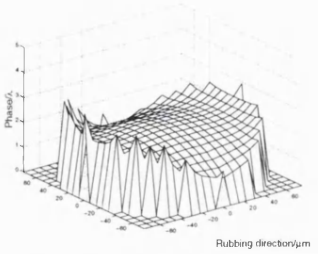

(b) 1V (f = -0.0026m, RMS: 0.359λ)

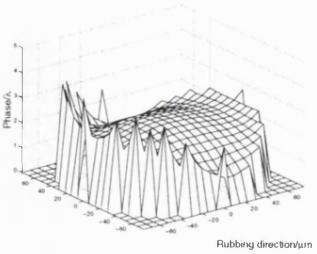

(c) 1.2V (f = -0.0035m, RMS: 0.446λ)

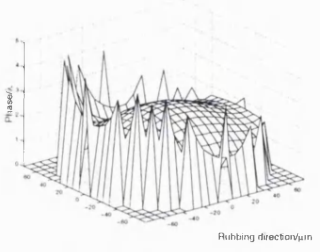

(d) 1.5V (f = -0.012m, RMS: 0.608λ)

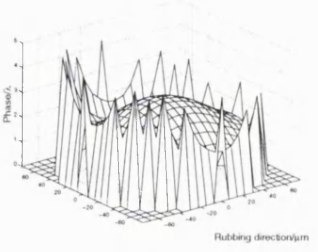

(e) 1.7V (f = 0.0097m, RMS: 0.718λ)

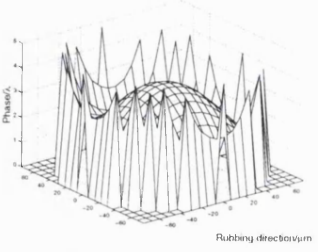

(f) 2V (f = 0.0027m, RMS: 0.835λ)

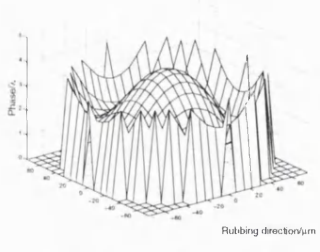

(g) 3V (f = 0.001m, RMS: 0.766λ)

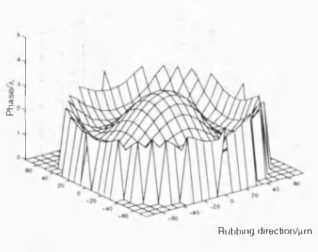

(h) 4V (f = 0.00084m, RMS: 0.543λ)

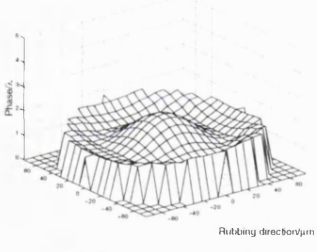

(i) 6V (f = 0.00079m, RMS: 0.265λ)

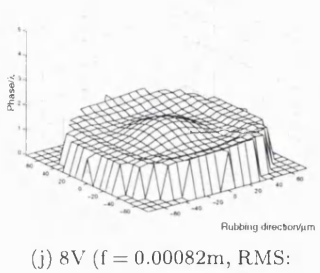

(j) 8V (f = 0.00082m, RMS: 0.148λ)

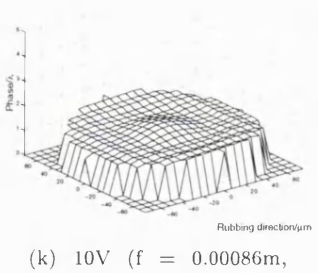

(k) 10V (f = 0.00086m, RMS: 0.107λ)

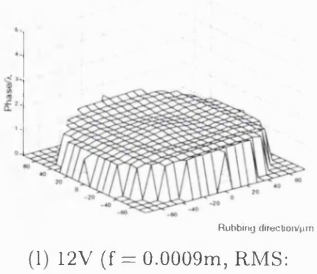

(l) 12V (f = 0.0009m, RMS: 0.097λ)

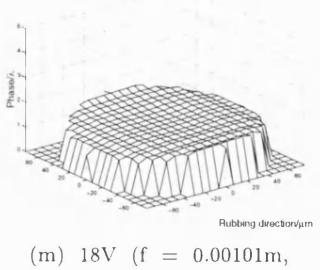

(m) 18V (f = 0.00101m, RMS: 0.096λ)

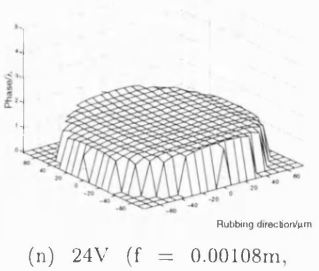

(n) 24V (f = 0.00108m, RMS: 0.097λ)

Figure 7.6: Modelled wavefront aberration plots of the original microlenses (D=150μm). Compare with experimental results in figure 6.4.

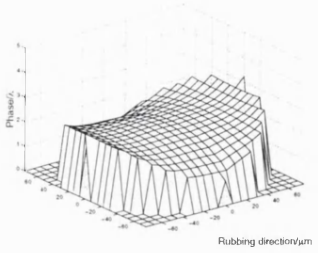

(a) 0.001V (f = -0.0023m, RMS: 0.350λ)

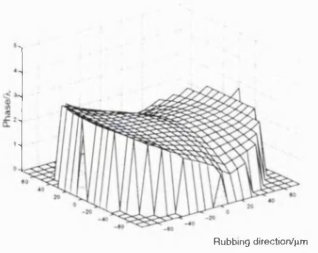

(b) 1V (f = -0.0028m, RMS: 0.412λ)

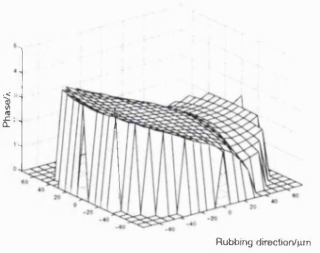

(c) 1.2V (f = -0.0034m, RMS: 0.558λ)

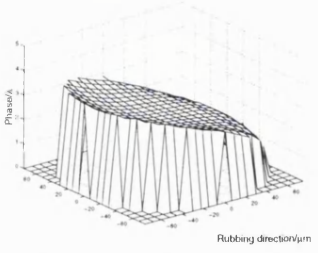

(d) 1.5V (f = -0.0072m, RMS: 0.563λ)

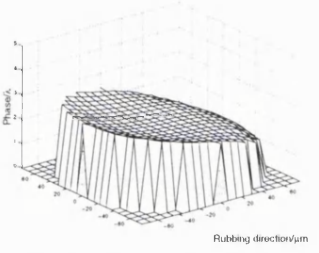

(e) 1.7V (f = 0.019m, RMS: 0.353λ)

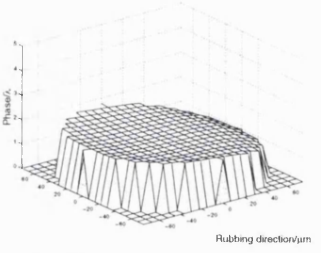

(f) 2V (f = 0.0041m, RMS: 0.170λ)

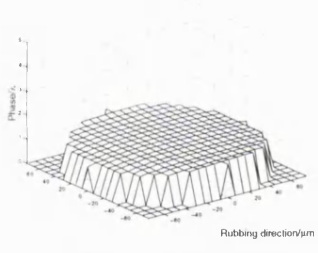

(g) 3V (f = 0.0019m, RMS: 0.0635λ)

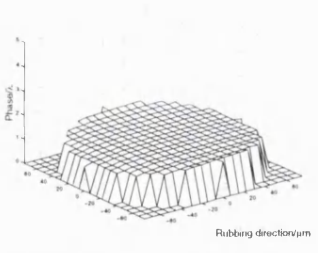

(h) 4V (f = 0.00165m, RMS: 0.0806λ)

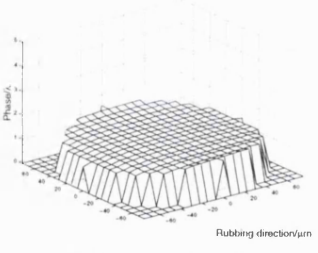

(i) 6V (f = 0.00147m, RMS: 0.0875λ)

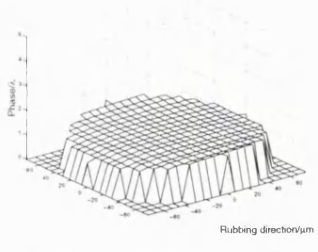

(j) 8V (f = 0.00141m, RMS: 0.0870λ)

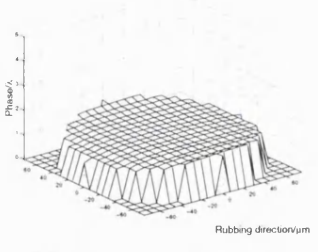

(k) 10V (f = 0.00137m, RMS: 0.0864λ)

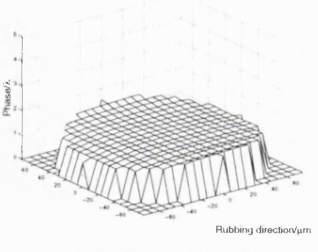

(l) 12V (f = 0.00135m, RMS: 0.0862λ)

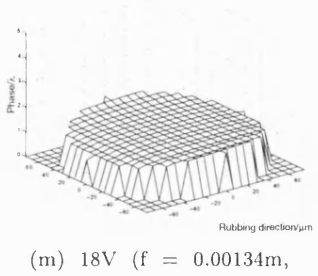

(m) 18V (f = 0.00134m, RMS: 0.0875λ)

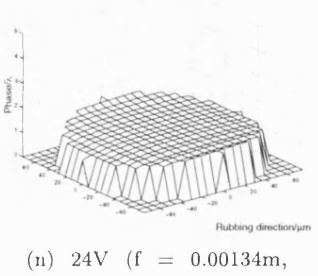

(n) 24V (f = 0.00134m, RMS: 0.0875λ)

Figure 7.7: Modelled wavefront aberration plots of the microlenses (D=150μm) the electrode on top. Compare with experimental results in figure 6.8.

The theoretical aberrational plots for the original design are shown in in figure 7.6. As mentioned in the previous section, one of the likely effects of the model being 1-D is that greater variations will occur across the lens than in reality. This can be seen in a comparison of the modelled results and the interferometrically measured results in section 6.3, figure 6.4. In the measured result for 0V, for example, a saddle shape is shown as in the modelled results, however, the measured saddle-shape is rounded off at the edges whereas in the model the slope is cut off as it is still rising. Comparing the rest of the results, the modelled aberrations for 0 to 2 volts are similar in character to those measured.

The modelled aberrations of the system with the electrode on top of the lens are shown in figure 7.7. The first obvious difference is that there is a large tilt component across the wavefront which was not seen in the modelled aberrations of the original design. In the measured aberrations (see figure 6.8 the tilt was automatically removed by the inteferogram analysis software. In the birefringence measurements (see section 6.5), the tilt component could be seen and there was a clear increase in the tilt for the electrode-on-top design.

The next feature which is very apparent is a line (for $1 \rightarrow 1.5V$) where there is a sharp change in the wavefront. This line is due to the liquid crystal on one side of the lens switching at lower voltages than the side with negative pre-tilt (see figure 7.4). The abrupt change is again something which would be smoothed out by the effect of the liquid crystal surrounding it and, thus, the model predicts a sharper change than is seen in practice.

The focal lengths predicted from the model when the electrode is on top of the microlenses is shown in figure 7.8. It can be seen from this figure, the focal length predicted does not have the rise in focal lengths of the original design. The focal lengths predicted from the model, both original and electrode on top designs, agree very well qualitatively with those measured (see section 6.2).

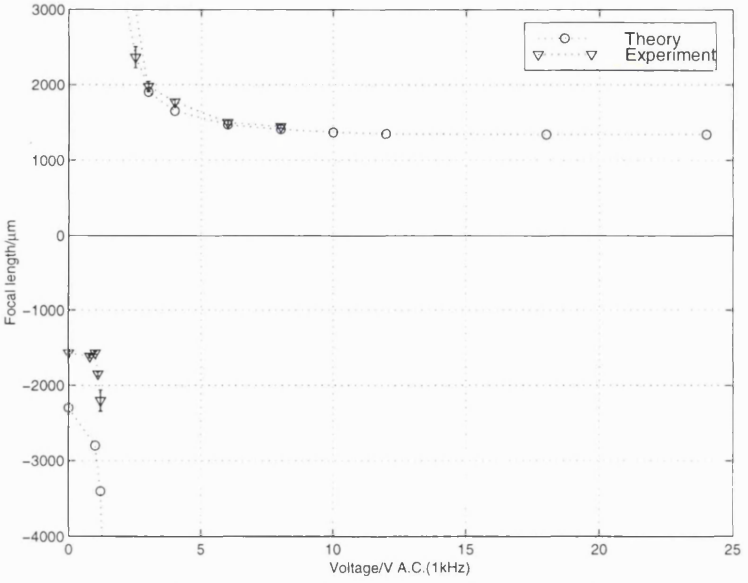

Figure 7.8: The focal lengths of a design with the electrode on top of the microlenses as predicted from the model.

7.4 Finite element modelling

7.4.1 Steady state model

Finite Element modelling is a numerical method for calculating the value of a function over a region. It can be used where an analytical solution is very difficult or impossible. The region under investigation is broken into sub-regions or *elements* and an approximate function is assumed for each element. Finite element methods have been applied to many systems. Typically it might be used by mechanical engineers for the calculation of the distribution of stress in a structure or by electronics engineers to calculate the electric potential distribution in a waveguide.

Fabrizio Di Pasquale, a researcher at UCL, has been developing a model of the structure in liquid crystal devices using finite element methods (also, he has constructed a model using finite differences - see section 7.4.2). Some of the microlens structures have been studied using his modelling program.

In the case of the liquid crystal devices, it is the director orientation and electric potential across the sample which is being modelled. The program uses a first order model with triangular elements, that is, the director orientation is assumed to vary linearly within each element and, thus, the director orientation within each element is completely described by the orientations at each vertex. The solution can be found considering only the values at the triangle vertices or *nodes* (since each vertex is the vertex for several triangles). The function must be continuous which for the linear element system is automatically achieved by having the nodes of each element in common with their neighbours. An energy term can then be calculated for each element and then the director distribution be varied iteratively in a computer such that the total energy is minimised.

F. Di Pasquale's model is based on the Oseen-Frank free energy equation [dP93]:

$$\begin{aligned} F = \frac{1}{2}\int_V \Big\{ & k_{11}(\nabla \cdot \hat{n})^2 + k_{22}\left(\hat{n} \cdot \nabla \times \hat{n} + \frac{2\pi}{\xi}\right)^2 \\ & + k_{33}(\hat{n} \times \nabla \times \hat{n})^2 \\ & - \epsilon_o[\Delta\epsilon(\hat{n} \cdot \bar{E})^2 + \epsilon_\perp \bar{E} \cdot \bar{E}] \Big\} dV \end{aligned} \tag{7.22}$$

where k_{11}, k_{22} and k_{33} are the splay, twist and bend elastic coefficients, $\hat{n}$ is the director orientation, $\bar{E}$ is the electric field, ξ is the pitch induced by a possible chiral dopant, ϵ_o is the vacuum permittivity, $\epsilon_\perp$ is the liquid crystal dielectric constant perpendicular to the director and $\Delta\epsilon$ is its dielectric anisotropy.

A program has been developed to model 3-D structures[DFDD97], however, the microlens structures are too complex to be modelled in a reasonable time scale thus only the 2-D model has been applied to the microlenses. Since the model is a 2-D model, the structure is assumed to be invariant in one of the cell axes (z). Also, the liquid crystal is assumed to have no dopant ($\xi \to \infty$). These two assumptions simplify equation 7.22 such that, in Cartesian coordinates in can now be written as:

$$F = \frac{1}{2}\int_S \Bigg\{ k_{11}\left(\frac{\delta n_x}{\delta x} + \frac{\delta n_y}{\delta y}\right)^2 + k_{22}\left(n_x\frac{\delta n_z}{\delta y} - n_y\frac{\delta n_z}{\delta x} + n_z\frac{\delta n_y}{\delta x} - n_z\frac{\delta n_x}{\delta y}\right)^2 + k_{33}\Bigg(\left[n_y\frac{\delta n_y}{\delta x} - n_y\frac{\delta n_x}{\delta y} + n_z\frac{\delta n_z}{\delta x}\right]^2 + \left[n_z\frac{\delta n_z}{\delta y} - n_x\frac{\delta n_y}{\delta x} + n_x\frac{\delta n_x}{\delta y}\right]^2 + \left[n_x\frac{\delta n_z}{\delta x} + n_y\frac{\delta n_z}{\delta y}\right]^2\Bigg) - \epsilon_o[\Delta\epsilon(n_xE_x + n_yE_y)^2 + \epsilon_\perp \bar{E}\cdot\bar{E}]\Bigg\} dS \tag{7.23}$$

The director of the nematic liquid crystal is non-polar which means that $\hat{n}$ and $-\hat{n}$ are equivalent. The equation above shows this as all the terms containing the director are squared. Since the director cannot change length (it is a unit vector), F. Di Pasquale used the above equation in spherical polar coordinates (r, θ, ϕ) which makes the director $(\cos\phi\cos\theta, \cos\phi\sin\theta, \sin\phi)$ which eliminates the necessity of checking after each alteration that ${n_x}^2 + {n_y}^2 + {n_z}^2 = 1$.

The program breaks the problem into two parts, the director distribution and the potential distribution. The director distribution is calculated by minimising the free energy (assuming an initial potential distribution) and then a new potential distribution is calculated due to the now modified dielectric distribution of the liquid crystal. This process is then iterated until a stable solution is reached. The program must also calculate the electric field in the dielectric since the boundary conditions for the potential are defined by the electrode under the photoresist. The program works well if a suitable starting condition is chosen, ie a solution is best found by finding solutions for lower voltages and using those solutions as the initial conditions for the next voltage.

The numerical calculations use a matrix formulation and take advantage of the NAG library of Fortran routines. These routines are able to perform many calculations quickly by taking advantage of the sparsity of the matrices.

7.4.2 Time evolution model

F. Di Pasquale has also developed a model which models the evolution over time of a liquid crystal structure [DFDD97], based on finite differences. This program is based on a tensor formulation:

$$n_\nu[\gamma\frac{\partial}{\partial t}(n_\nu n_\mu) - k\nabla^2(n_\nu n_\mu) - \epsilon_0\Delta\epsilon E_\nu E_\mu] = 0 \tag{7.24}$$

where γ is the viscosity coefficient, n_ν, n_μ the Cartesian coordinates of the director, $\hat{n}$ and k is the elastic constant. Note that, unlike the steady state model, only one elastic constant is used.

In fact, the program is hybrid of finite differences and finite elements, different techniques being applied to the various aspects of the problem. Because the system is highly non-linear, it is advantageous to split the calculation up in this way. The potential is calculated in the same way as the steady state model, using finite elements. For each iteration, the potential is calculated first treating the current director distribution as a

constant. Then the new potential is used to generate a new director distribution with finite differences, now treating the potential distribution as constant. For each increment in time, the iterations are performed until are the director and potential are consistent.

7.5 Results of finite element modelling

7.5.1 Steady state results

Using the steady state model, F. Di Pasquale produced the structure shown in figure 7.9 for the original design of microlens [DFDD96]. As stated previously, the intention was to describe the original, spherical microlenses but since the model is only 2-D, the lens actually being modelled is a cylindrical lens (subsequently, cylindrical lenses were produced, see below). It can be seen that there is a sharp change in director orientation at the side of the microlens (figure 7.9). This is a wall structure in the liquid crystal. No twist is predicted in these plots (identifiable by the dashes indicating the director being shortened). It should also be pointed out that although the location of walls can be predicted, the structure of the liquid crystal in the walls cannot be modelled well with this program since the variation of the director due to the wall occurs over a small region.

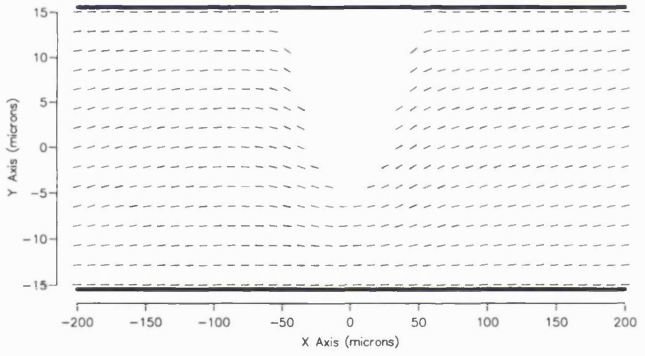

(a) 1V

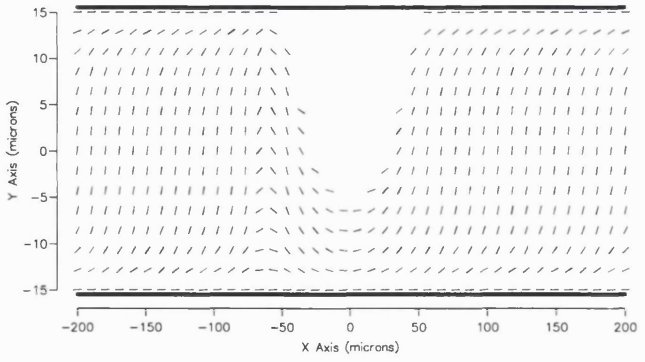

(b) 3V

Figure 7.9: The original design of microlens as modelled using a 2-D finite element method. The dashes are the director orientations, the gap (top, centre) is where there is the photoresist and the thick black lines (top and bottom) are the electrodes. Note that the plot axes are stretched vertically.

F. Di Pasquale then predicted [DFDD96] a new structure using a strip electrode op-

posite to the photoresist microlens (see section 4.3.2) which eliminated the wall structure above. This strip electrode, when modelled, produced the structure shown in figure 7.10.

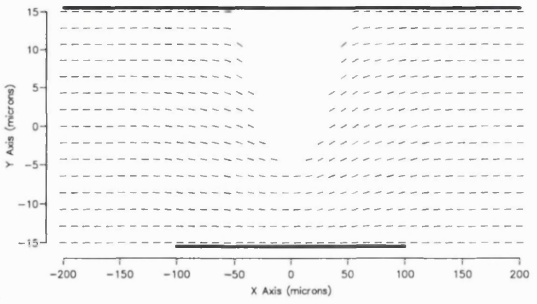

(a) 1V

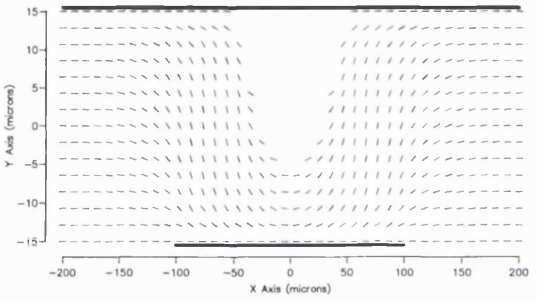

(b) 3V

Figure 7.10: The strip electrode design of microlens as modelled using a 2-D finite element method.The dashes are the director orientations, the gap is where there is the photoresist.

Unfortunately, the program became unstable at higher voltages so it was not possible to model the full range of voltages that could be applied experimentally. If figure 7.10b is examined carefully, it will be realised that, at the centre of the lens, a wall is present which is relatively spread out (cf. section 6.5).

7.5.2 Time evolution results

One major advantage of the time evolution model is that it is more physically realistic than the steady state model (except that it uses a one constant approximation for the elastic constants). Sometimes, it is possible to get more than one solution with the steady state method depending on what starting conditions are chosen. With the time evolution model, it is possible to get the 'correct' solution straightaway, at least when starting from 0V where the initial conditions can be described with reasonable certainty. The first results from the time evolution model could have been obtained with either program (steady state or time evolution) since they depend only on the potential calculation routine which both programs have in common.

Although the finite element models described above are primarily intended to provide a realistic description of the director, it is possible to get useful results from the program from the first iteration of the program when the potential is calculated. At the first iteration, the director distribution is not likely to be physically realistic, however, it is interesting to view the potential distribution for this step assuming the 'ideal' director distribution. In this case, ideal means completely homogeneous. The resulting data is useful when trying to understand the factors at work in producing the actual director

distribution.

The first results from the program are simply the calculated potential field when the director is completely switched and unswitched (completely switched meaning the directors are all vertical and unswitched means the directors are all horizontal). Figures 7.11 and 7.12 show the result for the original design of the microlens. Figure 7.11 is for the case where the liquid crystal is unswitched, *i.e.* the directors lie in the plane of the cell. The potential is calculated perpendicular to and in the plane of the rubbing direction (and normal to the cell). Figure 7.12 is for the case where the liquid crystal is switched, *i.e.* the directors lie in the normal to the cell. Since this is same for both parallel and perpendicular directions to the rubbing direction only one potential field is calculated. The significant variation between the switched and unswitched plots is due to the change in the difference between the dielectric of the liquid crystal and the photoresist. The dielectric constant of the photoresist, $\epsilon_{photoresist}$, was 3.38 not too different from the dielectric constant perpendicular to the liquid crystal, $\epsilon_{\perp}$, which is 5.2. The value parallel to the liquid crystal, $\epsilon_{||}$, was markedly different at 19.

When we consider that the director will try to align perpendicular to the equipotentials shown, then it is straightaway clear that, even when the liquid crystal is completely switched, the directors will lie at an angle to the normal. There are two conclusions which derive from this observation. The first is that the averaged switched refractive index for these regions will be greater than n_o, the theoretical minimum. The second, more important conclusion, is seen when we consider a similar section through the microlens but at an angle to the rubbing direction. The 2 potential distributions will be the same or very similar for all orientations of the section. The only difference will be that, in the off-state, the component of electric field in the plane of the cell (i.e. away from the normal) will see a variation of dielectric constant depending on whether it is parallel or perpendicular to the rubbing direction. Since, for which ever section is considered, there will be a component towards the centre of the microlens, this means there will be a component in the cell plane which is not, in general, in the rubbing direction. This causes a twist in the liquid crystal and a possible reason for the light to change polarisation (see section 6.4.1).

Similar calculations have been performed on the design with the electrode on top of the microlens (see figures 7.13 and 7.14). The results are similar in form to the results for the fully switched case with the original design and so by the same logic they suggest a mechanism which might give rise to twist in the liquid crystal.

A calculation has been performed using the time stepping program to demonstrate that the inclined fields can give rise to optical polarisation changes. A $100\mu m$ diameter lens has been modelled, analysing a 2-D section through the lens at 45° to the rubbing direction. The resultant structure is shown in figure 7.15. The calculation was carried out in 2 stages; firstly, the structure was allowed to find a natural off-state by applying 0V for 2 seconds, then 3V was applied. The structure is shown after 4 seconds at which point there are no significant changes between iterations so equilibrium is assumed.

Note that the modelling results here are not intended as a prediction of the actual structure, merely a demonstration that the inclined fields can give rise to the polarisation changes observed. The spherical microlens modelled is a 3-D structure and only a slice through it has been analysed. Also, since the time evolution model uses only one elastic constant (see section 7.4.2), it is not expected that all the proposed twist structures will

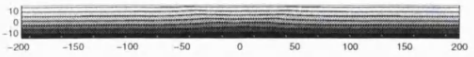

(a) Correct aspect ratio (in rubbing direction)

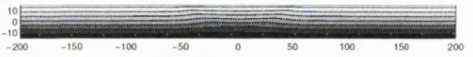

(b) Correct aspect ratio (across rubbing direction)

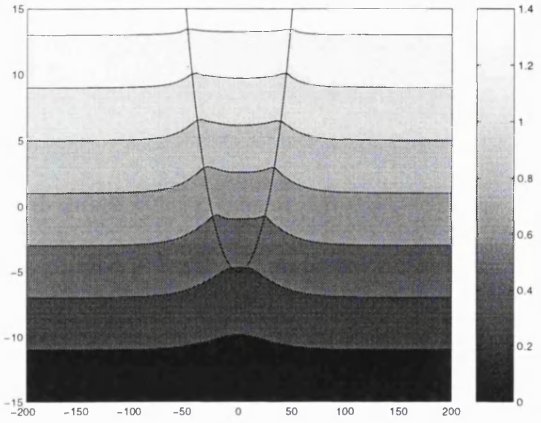

(c) Vertical scale expanded (in rubbing direction)

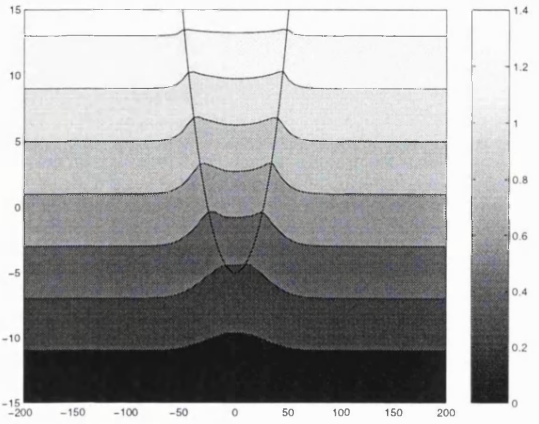

(d) Vertical scale expanded (across rubbing direction)

Figure 7.11: The electric field in the off-state across the original design of microlens as modelled using a 2-D finite element method. The director distribution is idealised, *i.e.* all horizontal

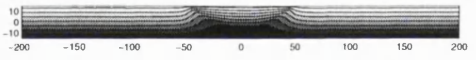

(a) Correct aspect ratio

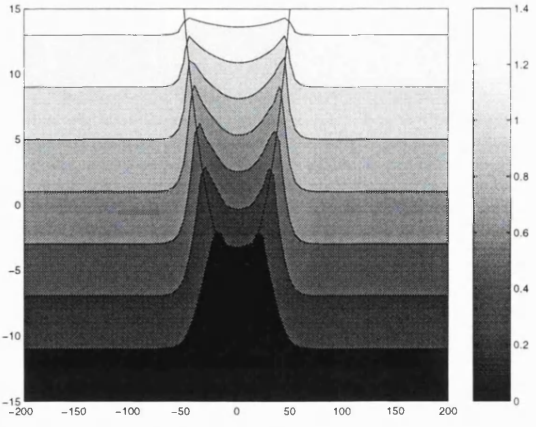

(b) Vertical scale expanded

Figure 7.12: The electric field in the on-state across the original design of microlens as modelled using a 2-D finite element method. The director distribution is idealised, *i.e.* all vertical

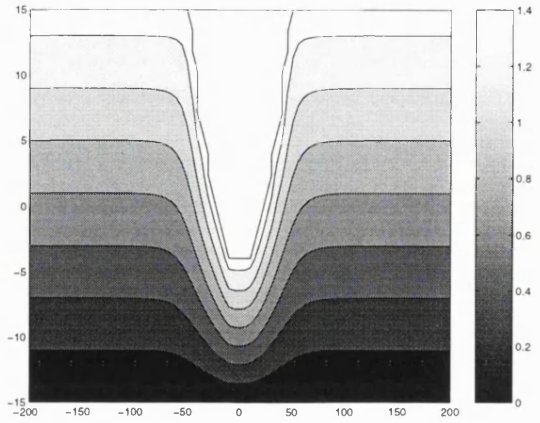

(a) Field calculated in the plane of the director

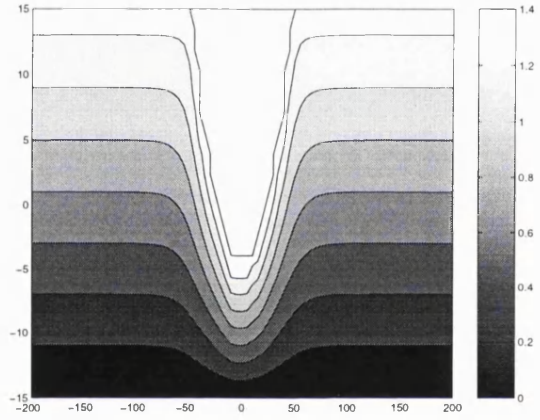

(b) Field calculated perpendicular to the director

Figure 7.13: The electric field in the off-state across the design of microlens with the electrode on top as modelled using a 2-D finite element method. The director distribution is idealised, *i.e.* all horizontal

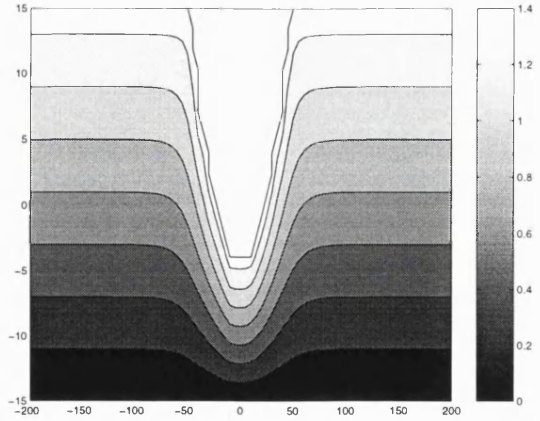

Figure 7.14: The electric field in the on-state across the design of microlens with the electrode on top as modelled using a 2-D finite element method. The director distribution is idealised, *i.e.* all vertical

be seen since they rely on the twist elastic constant, k_{22}, being less than the splay, k_{11}.

The effect on a light beam has been calculated using Jones' 2×2 matrix method [Hec87], using routines written by R. Kilpatrick [KGDS98] modified appropriately for the cell structure. The intensity has been calculated for the liquid crystal surrounded by two ideal polarisers, *i.e.* no reflection losses were taken into account. The polarisers were orientated parallel to the rubbing direction. The resultant intensity profile is shown in figure 7.16.

The intensity profile shows clearly a double drop in the intensity across the lens. This observation agrees with the cross shape observed when the spherical lens with the electrode on top was viewed between crossed polarisers (see section 6.4.2). The sharp peaks in the plot structure are due to the finite element discretization. Since the finite element mesh is generated from a rectangular array, each divided into two triangles, the microlens surface profile is represented by the elements of the mesh. The effect of this discretization can clearly seen in the potential field distribution. The director distribution is also affected since it must be continuous along the surface even where this means there are two 'surface' directors in one column of elements. Both these effects distort the calculated structure exaggerating the polarisation changes.

The results from the finite differences give a reasonable demonstration that the inclined fields could give rise the polarisation changes observed in the micrographs (see section 6.4.1) much as the 1D model has shown qualitative agreement that the pretilt variation and electrode positions could give rise to the type of lens aberrations observed. In both cases, the structures could be more completely described with better modelling of twist and a 3D structure, however, such a model is liable to be very complex and require long computation times.

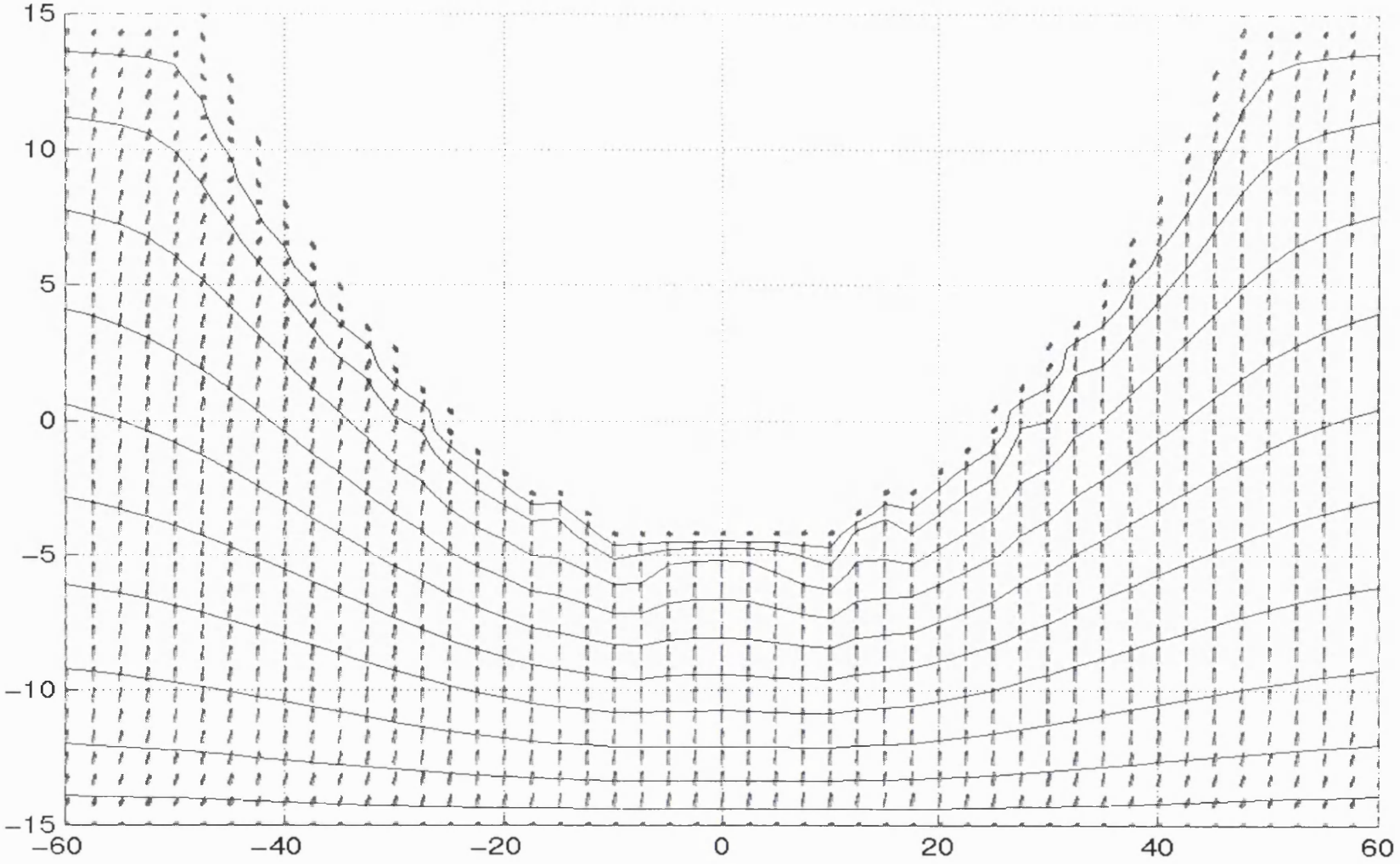

Figure 7.15: Electrode on top microlens, modelled at 45° to the rubbing direction. The equipotentials are overlaid on the directors.

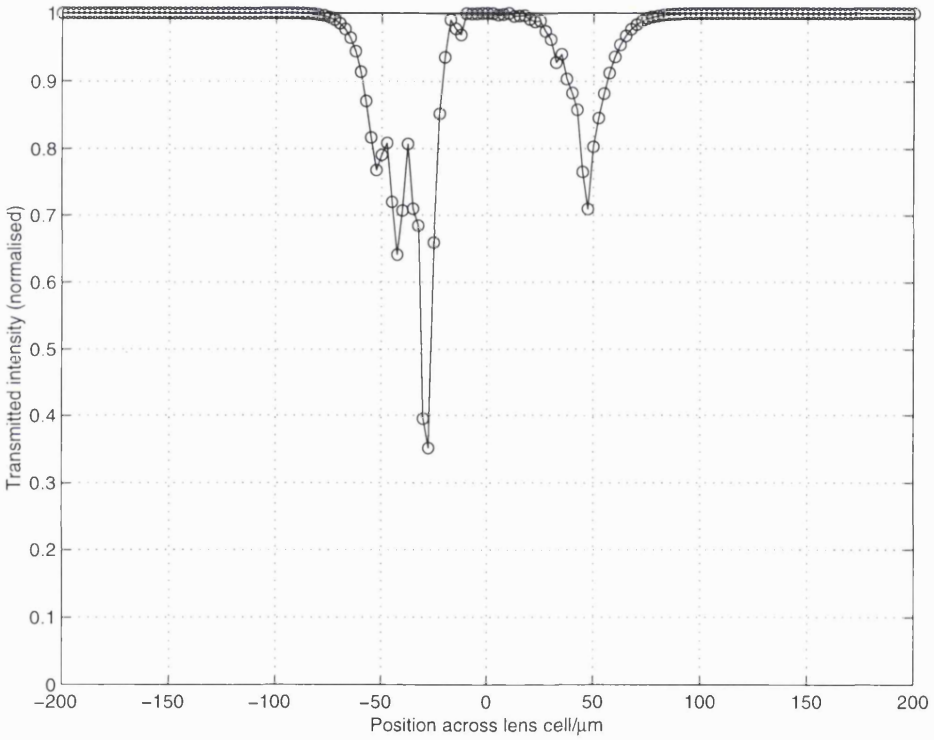

Figure 7.16: Intensity transmitted through structure in figure 7.15 calculating the effect of the liquid crystal between parallel polarisers.

Chapter 8

Discussion and conclusions

8.1 Introduction

The goal of the work described here is to fabricate lenses whose focal length can be varied electrically. This tunability has been demonstrated from the first design. In order to find applications, however, the quality of the focus needs to fulfil the appropriate system requirements. Some applications, eg. a diffuser, are relatively undemanding, but many are much more so and, needless to say, the ideal is a diffraction limited performance for all voltages. Therefore, the majority of the work presented in this thesis has been concerned with the lens aberrations and the liquid crystal structure that produces them.

8.2 Discussion

8.2.1 Focal length variation

The first liquid crystal immersed microlenses were built to demonstrate the idea that a liquid crystal immersed lens would be tunable. It has been shown, as intended, that the focal length can be controlled by an applied voltage. The characteristics are similar to those expected, the $100\mu m$ diameter lens acts as a diverging ($f = -910\mu m$) lens without a voltage, the focal length increasing to $-\infty$ at around 1.5V and above 1.5V the focal length is positive (usable focal length range $360\mu m$ to $560\mu m$).

There is one intriguing distinction between the expected characteristic and what was actually observed. A monotonic decrease of the refractive index with voltage was expected uniformly across the lens and, hence, a monotonic increase in the optical power of the lens was predicted. However, the optical power increased until the voltage reached 3V where it started to reduce (cf. figure 4.7 on page 62 and figure 6.1 on page 84). From this initial evidence, it is clear that the liquid crystal structure was not as had been intended in this first design. It was subsequently found (see next section) that this unexpected behaviour was due to the electrode configuration which, in effect, superimposed a converging electric field lens (*i.e.* a converging lens produced by the field configuration) on top of the photoresist/liquid crystal microlens. This is also evidenced by the fact that the focal length is shorter (where the focal length is positive) than the simple theory predicts. A subsequent design, using an electrode on top of the photoresist microlens, had a focal length vs voltage characteristic which was similar to the original theoretical pattern. Comparing these results with those given in Table 3.2 on page 51,

it can be seen that the NA (0.05) is one of the highest of any reported, plus the lens can be varied from a negative to a positive focal length.

The focal length vs voltage characteristic of the lenses presented here, with the focal length going to infinity at around 1.5V, is the result of the two materials used to form the lens, photoresist (refractive index 1.64) and liquid crystal E7 (refractive index 1.52-1.74). If the photoresist microlens profile were transferred into a substrate, a common substrate to use for visible wavelengths is quartz (see section 3.2.3) which has a refractive index around 1.5. Using quartz would result in a negative lens with 0V ($f = -625\mu m$ for the $150\mu m$ diameter lens) which would become less and less powerful with increasing voltage, finally having an almost infinite focal length at around 8V. The commercially available (Merck) liquid crystals have refractive indices spanning the ranges 1.47-1.54 (ordinary index) and 1.53-1.80 (extraordinary index) [Mer92b], thus, if a lens is desired which is always positive, a substrate of refractive index higher than the liquid crystal extraordinary refractive index will be required (or the lens shape could be changed, perhaps using a cast of the lenses [GRS93]).

8.2.2 Wavefront phase profiles

Independently of the structure of the liquid crystal layer, the resolution and focal spot size of the lens depend on the optical phase profile induced in the transmitted light beam. Measuring the phase profile thus gives a much more complete picture of the optical properties of the lens and provides clues as to what must be happening within the liquid crystal structure.

The optical phase profile of the liquid crystal immersed microlenses has been measured using a Mach-Zehnder interferometer. The lenses produced according to the original design had aberrations which varied with the applied voltage from 0.18λ to a peak of 0.55λ. At the higher aberration values, the focus was very poor, limiting the usable focal length range to $0V$ and $\gtrsim 4V$.

Considering the phase profiles of the original lens design (see figure 6.4 on page 87), it was clear that there was a focal length difference between the central and outer regions of the microlenses. The difference in the focal length between the outer and inner region of the original lens design is due to the inner region having a higher threshold voltage. In the centre of the lens, some of the voltage is dropped across the dielectric of the photoresist, thus, reducing the effective voltage applied to the liquid crystal, producing an effect much like that of Nose, Masuda and Sato [NMS91], *i.e.* an electric field lens.

Most liquid crystal cells are built with no varying thickness of dielectric. For these cells, the response of the liquid crystal is dependent on the voltage not the applied field, *i.e.* the response with voltage is independent of the cell thickness (see equation 2.33 on page 31). For this reason, it was assumed in designing the original lens that the fact that the liquid crystal layer thickness varies across the microlens would not be important. However, the independence of the voltage from the layer thickness is only true if the layer thickness and electrode separation are proportional by a constant factor. Since, in the original design, the electrode separation is constant whilst the liquid crystal layer thickness varies, the threshold voltage is not constant across the cell.

From the conclusions of the aberration results of the original microlens design, it was decided to build microlenses with the electrode on top of the photoresist. The electrode on top lenses had a much better aberration performance, varying from 0.071λ to 0.19λ

which is much closer to the diffraction limit of 0.07λ. This is doubly beneficial since the improvement occurs where the variation of refractive index is varying fastest (1-3V, see figure 4.6) with voltage.

A second, non-ideal feature of the original design is that the alignment layer is only an approximation of what is required for the desired liquid crystal structure. The structure was envisaged to have the liquid crystal directors parallel, with no field applied, *i.e.* the pre-tilt on the two cell walls was intended to be uniform across the area of the microlens. This would ensure that the liquid crystal refractive index would be uniform for all positions across the lens with no voltage applied. However, to achieve this homogeneous structure it is necessary, as stated above, to have a uniform pre-tilt on both cell walls. A uniform pre-tilt is not difficult to achieve on the non-microlens cell wall, a flat surface, but is less easy across the microlens surface. In part, the problem arises from the fact that the topology of a surface can, even without any alignment layer, induce alignment in a liquid crystal (Schulze and von Reden [Sv95], when fabricating liquid crystal immersed gratings, restricted the alignment to be parallel to the grating for this reason). Thus, the alignment layer has to overcome the topological aligning effect as well inducing a uniform pre-tilt. However, what is probably worse is that the alignment layer is not completely appropriate for the job, it was only the best readily available. It causes the liquid crystal to align almost parallel to the layer (in the rubbing direction) but with the liquid crystal deviating a few degrees up from the layer (in the rubbing direction). On a flat surface this deviation would be the desired pretilt but since the polymer alignment layer follows the topology of the surface and the angle of the lens surface is greater than the pre-tilt, inevitably on one side of the lens the pre-tilt is negated by the surface topology.

The two deviations from the intended structure have been included in a simple 1-D model of the microlenses. Clearly, a 1-D model can only be an approximation to the liquid crystal structure, but it does allow the above analysis to be tested.

Considering the focal lengths calculated using the 1-D model (see section 7.3 on page 155) for the cases of the electrode underneath the photoresist (original design) and the electrode on top of the microlens, it can be seen that the rise in focal lengths above 3 volts (see section 8.2.1) can be attributed to the electrode being under the microlens.

The second general observation which corroborates the experimental analysis of the microlenses, is the tilt induced in the wavefronts transmitted by the electrode on top design (cf. the birefringence measurements-section 6.5 on page 106). This tilt is due to the increased threshold voltage where the pre-tilt is negative (see figure 7.4 on page 155) which results in lower maximum director tilts, ϕ_{max}, for the lower pre-tilts at the same voltage and, hence, higher refractive indices. Since the pre-tilt, following the photoresist microlens surface profile changes monotonically across the lens, the result is approximately a phase wedge or a tilt of the transmitted wavefronts.

One factor missing from all of the above analysis is polarisation changes due to twist in the liquid crystal which also will affect the lensing characteristics of the devices. The polarisation changes are discussed in the next section.

8.2.3 Wavefront polarisation characteristics

When the lens cells are examined in a polarising microscope, it is soon clear that there is a change in the polarisation of the light transmitted by the lens. This change is

dependent on the applied voltage and the position within the light beam across the microlens. The polarisation change is almost certainly caused by a twist of the liquid crystal (see section 6.4.1).

There are two ways in which the polarisation change is important. Firstly, it is important as it alters the lensing properties of the devices. Consider a light beam incident on the microlenses in the case where the director orientation in the plane of the cell varies across the lens. If the light transmitted by the microlenses is divided non-uniformly between two orthogonal polarisation components then, each component being treated separately, there will, in effect, be two focal spots superimposed. Both spots, having been transmitted by effectively non-circular aperture, will be distorted from the Airy disc by the partial aperture obscuration. The second consequence of the observation of the polarisation change is simply that it indicates a twist in the liquid crystal. The twist is neither intended in the design, nor is it allowed for in the modelling. It demonstrates that the liquid crystal structure is more complex than has been suggested so far (*i.e.* after allowing for the 2 factors mentioned in the previous section) and that more detailed analysis is required to get to a possibly accurate liquid crystal structure. The significance of the polarisation changes for the understanding of the liquid crystal are discussed in the next section.

8.2.4 Liquid crystal structure

The liquid crystal structure envisaged in the first design concept was relatively simple. In essence, the intention was to combine the optical properties of a parallel sided liquid crystal cell with those of a microlens. Evidently, the microlens cell is not parallel sided, but the properties of parallel sided cells are well understood and so they provide a good starting point. The desired liquid crystal optical properties were that the extraordinary refractive index should be voltage controlled and that, at any voltage, there should be one refractive index for all incident parallel rays. In fact, this is a simplification since, in general, the director orientation varies through the depth of the cell. However, to keep things simple an averaged refractive index (normal to the cell plane) for each position across the lens is considered when trying to understand how the lens affects the phase of the light passing through it. However, for the purposes of studying the device defects, a more detailed understanding is required.

When viewing the microlenses (original design) through a polarising microscope, there are two structural effects which are particularly striking. Both occur upon the application of a voltage. The first is a loop which forms on one side of the microlenses - a liquid crystal wall structure (see section 6.4.3). The second is the change in transmitted intensity of light through the microlens - the effect of twist (see section 6.4.1).

Walls

Liquid crystal wall structures were seen on the original design of microlens, both spherical and cylindrical, and the design with the strip electrode opposite to the microlens when a voltage sufficient to switch the liquid crystal was applied. Liquid crystal walls are distortion of the liquid crystal director and, as such, scatter light reducing the performance of the lens. Walls occur between regions of liquid crystal which have rotated towards an applied field but with opposite rotations. Walls are usually initiated by

variations of the surface pretilt and when an electric field causes the liquid crystal to rotate further, they continue in opposite directions creating a wall in between. Since the pretilt of rubbed PVA is presumed to follow the microlens surface profile, it is not surprising that walls are formed on the microlenses.

The effect of the walls on the original design device performance can be limited by how the lenses are used. The walls on the original design form in a loop on one side of the lens and this loop gradually shrinks and eventually disappears. The walls do not reappear unless the liquid crystal is allowed to relax back its initial state and then a voltage is reapplied. Thus, by limiting the voltage range applied, always staying above the threshold voltage, the walls can be avoided for practical purposes. On the strip electrode design, the walls did not form in a loop so they did not disappear and, for this reason, the walls cannot be eliminated before using the device.

The structure of the walls themselves is relatively well understood since they are the same type of walls as described by Steib et al [SBM75]. The director deformation associated with the walls is a combination of bend and twist, with twist tending to dominate due the lower elastic constant of the twist, k_{22}. The evolution of the wall structure does not always finish with the shrinking to nothing. Occasionally, the walls will split into 2 disclination lines (strength $\frac{1}{2}$) associated with the two cell surfaces. The disclination on the microlens surface usually remains stable whilst the disclination on the flat surface disappears. The structure left behind is the same structure as found in the "pi-cell", a structure sometimes used in LCDs [WL94].

The aspect of the liquid crystal wall structure which is least well understood is the structure left behind by the wall receding from the side of the microlens (when the wall has not split into disclinations). It is apparent from the microscope observations that some part of the wall is left behind on the microlens side but it is not clear exactly what is occurring. One factor which is important in interpreting the resulting structure is whether it includes disclinations hidden down the side of the lens. It has been decided that none are present (see section 6.4.3 on page 98) which has important implications for what the liquid crystal structure left by the wall could be (see below).

The wall defects were eliminated in the design with the electrode on top of the microlens, both spherical and cylindrical. At first, this might seem strange since the pretilt in this design is unchanged from the original design. The difference lies in the switching times across the lens. With the electrode on top design, there is a uniform voltage difference across the cell and in these conditions the liquid crystal switches fastest where the cell is thinnest. In this case, the liquid crystal switches first at the centre of the microlens where the pretilt has the desired orientation. The central region of the liquid crystal then pulls the surrounding directors in the same direction regardless of its original pretilt thus avoiding the formation of walls.

Twist

The twist observed in the microlens cells (once any walls have disappeared) is less easily explained than the walls. First of all, a reason for a twisted structure needs to be given in what is supposed to be a parallel aligned structure. Then the structure needs to be consistent with the walls and disclinations observed. Finally, any explanation has to be consistent with the the experimental observation that the twist increases with voltage.

One possible cause for a twisted structure to form between parallel aligned substrates

is given by the pretilt structure. If the pre-tilts are such that the liquid crystal directors would have to splay to remain parallel to the alignment direction then twist can be favoured. For example, if the pre-tilts are equal and opposite then the directors in between can satisfy the boundary conditions by a splay deformation or a twist deformation. Since, in general, $k_{22} < k_{11}$ the twist is preferred given sufficient pre-tilt. On one side of the microlens we have a negative pre-tilt (as discussed above) which could give rise to such a twisted structure. Assuming rigid, parallel boundary conditions (but with different pre-tilts) the twist is inherently a multiple of 180° (including 0°).

It might be imagined that the twisted structure on one side of the microlens is a 180° structure created by opposite pre-tilts. However, a wall or disclination is required if the liquid crystal on the microlens is assumed to be a 180° twisted region surrounded by untwisted liquid crystal. Since, in general, there are no walls or disclinations between the twisted and untwisted regions (see above), this cannot be the explanation. Indeed, when the wall breaks into disclination lines instead of receding from the side of the lens, this 180° twisted structure surrounded by an untwisted structure is what is formed (see section 6.4.3 on page 98).

Another possibility is that the liquid crystal across the microlens is breaking away from the rubbing direction. This again has the benefit of reducing splay at the cost of introducing twist, however, the splay is only introduced as the liquid crystal switches. When switched, the liquid crystal in the centre of the cell is close to the normal to the cell, so, if the liquid crystal on the microlens surface points towards the centre of the microlens, the liquid crystal on the microlens surface reduces its angle to the normal whilst remaining parallel to the surface and hence reduces the splay between the microlens surface and the centre of the cell (see figure 6.9 on page 93). Thus, if this explanation is true, the liquid crystal director on the microlens surface remains parallel to the alignment layer but not the rubbing direction. This second possibility, twisting towards the centre of the lens, seems more promising as it can change from twisted to untwisted continuously. The difficulty with this argument is that it cannot explain the twist on the cylindrical microlens since, on the cylindrical microlens, the rubbing direction already points in the direction which would minimise splay.

A third possibility is comes from the electric field distribution. The original design concept assumed the electric field was normal to the cell, however, the presence of the microlens means that the electric field will have components in other directions, towards or away from the microlens centre depending on the electrode configuration. Since the directors rotate towards the applied field, they will then be inclined to the normal even when fully switched. The inclination for the original design necessitates a splay of almost 180° which might easily be replaced by a twisted structure even though the liquid crystal must untwist again before the other cell wall.

The final explanation seems the most likely, the only problem with it being that it must be accepted that the liquid crystal is operating outside the Mauguin regime (*i.e.* the light is not 'guided', the light polarisation does not follow the twist of the liquid crystal-see section 2.2.1 on page 16) even though the cell is relatively thick. This is acceptable if the twist does not occur linearly through the cell thickness but, instead, is concentrated into a smaller region [KW93]. The change of polarisation caused by inclined field induced twist has been modelled and a polarisation change has been demonstrated (see section 7.5.2 on page 163).

8.2.5 Design improvements

The goal of studying the structures and effects in the liquid crystal on the lenses is to understand what improvements can be made that would most improve the device performance. Hopefully, as a result, better designs can then be suggested. Indeed, as understanding of the device properties deepened, it became clearer which areas needed improvement and some improvements have been implemented.

Alignment

The alignment is one area where changes have been made. One of the fundamental requirements for all of the designs of the microlenses studied here is that the liquid crystal lies in the plane containing the alignment/rubbing direction and the normal to the cell. For the off-state, the crucial factor is the alignment layer. In the first lenses, the alignment was not effective right up to the edge of the lenses, instead they were surrounded by a 'halo' of poorly aligned or misaligned liquid crystal. To improve the uniformity, the alignment layer rubbing has been changed from a manually driven swipe with a lens tissue, to a motor driven drum with a velvet type cloth surrounding it. The velvet type cloth ensures the alignment layer is rubbed up to the edges of the lens and the 'halo' has almost disappeared (cf. figures 6.21 (on page 113) and 6.31 (on page 124). Additionally, the motor driven drum should give more reproducible alignment. A change from dip-coating to spin coating of the alignment polymer gives a more uniform PVA layer thickness and, thus, improves reproducibility. The rubbed alignment layer has one other important effect which is that it causes a variation of pre-tilt across the lens. An alignment technique which can avoid this variation is to use a photoalignment layer instead. Such a photoaligning layer would have to have a definable pre-tilt such that achieved by Schadt *et al* with the LPP alignment [SSSK95a]. Unfortunately, such materials have been unobtainable whilst I have been working on this project.

Alternative designs

One major variation of the design has been to fabricate cylindrical as well as spherical lenses. This is a simplification of the structure to aid in understanding the liquid crystal properties. The cylindrical lenses have proved valuable for the study of the wall and disclination structures. Motivation for the change was also provided by results from a 2-D Finite Element model (by Fabrizio Di Pasquale). This model was able to predict wall structures seen in some of the designs. From his model, F. Di Pasquale was able to suggest a new structure which did not have a wall at the side of the microlens. The structure, consisting of the original cylindrical lens, but replacing the planar electrode opposite with a strip electrode, was fabricated and shown to have the behaviour predicted by the model. However, for voltages higher than the model could operate, there was a wall structure at the centre of the microlens. These walls have been eliminated with the next design change.

The next modification of the design was derived from the observation in the aberration measurements of a focal length difference between the centre and the edge of the lens. It was decided this was due to an effective lower voltage being applied across the liquid crystal at the centre of the lens. Therefore, the new design had an electrode on top of the microlens but returned to planar electrode for the non-microlens substrate.

For the cylindrical microlenses, this electrode change eliminated the wall structure and the twist of the liquid crystal. Spherical lenses were also fabricated with electrode on top of the lenses and they also avoided the formation of wall structures although they did cause twisting of the liquid crystal with an applied field. The elimination of the walls is caused by the dependency of the time response upon the layer thickness. The response time of a liquid crystal layer is dependent on the square of its thickness (assuming the liquid crystal layer thickness and electrode separation are proportional by a constant factor). Thus, since the liquid crystal layer is thinner in the middle of the microlens, the response time will be quicker at the centre of the lens. This area will rotate according to the pretilt which, in the centre of the lens, is in the desired direction. Then, however, the central area rotates its neighbours as well causing them to have the same tilt orientation and thus the central pretilt propagates and prevails over all the lens. However, this does not alter the fact that near the microlens surface the director will be very splayed on the negative pre-tilt side which thus requires a greater voltage for it to reorientate.

Twist

The twist of the liquid crystal is then perhaps the most important effect still needing improvement. On the cylindrical lenses, it has been removed but it is still significant on the spherical lenses. The simplest way to tackle this is to increase the resistance to twist of the liquid crystal by choosing a material with a higher k_{22} value (relative to k_{11} and k_{33}). The material used in the lenses described in this thesis, E7, has a splay/twist ratio of $\frac{k_{11}}{k_{22}} = 1.26$ and a bend/twist ratio of $\frac{k_{33}}{k_{22}} = 1.94$ (see table 4.2). An example alternative material is E170 which has $\frac{k_{11}}{k_{22}} = 0.99$ and $\frac{k_{33}}{k_{22}} = 1.0$ [Mer92b]. Other alternatives depend on the explanation for the twist in the first place. If it is breaking away from the alignment layer, a stronger alignment layer (eg. polyimide) would help.

The explanation I consider most likely for the twist is that it is due to the electric field being angled away from the normal to the cell (see section 8.2.4). Therefore, the obvious solution is to reduce the lateral components of the electric field. However, the ideal field is impossible to achieve because of two contradictory requirements: Consider the potential along two lines through the liquid crystal layer, one at the lens edge and one at the centre. For simplicity, we will treat the field as linear. Since the liquid crystal responds to the applied voltage we desire to have the same potential difference along the two lines. However, as stated above, we desire no variation of potential across the lens. Thus, the potential at the top of the lens should be the same as the potential at the same height on the line at the edge and, similarly, the potential on the non-microlens ends of the lines should be the same. However, since the two lines are of different lengths but with the same potential difference they have different gradients of potential along their length, contradicting the previous statement.

Note that the above argument assumes nothing about the electrode configuration, or dielectric layers and thus is true for any variants of electrode position. It is also true not just for microlenses, but for any other optical device incorporating a surface relief structure modulated by immersion in a liquid crystal structure (eg Fresnel lens or hologram).

The one possibility which is consistent with the above, is that the location through

the cell where the field has the largest lateral components can be varied. In the current design, the lateral field is strongest near the surface of the microlens, around the microlens rim. Since the surfaces are the regions where the liquid crystal is least switched, a lateral field component here may have a disproportionate effect.

8.3 Conclusions

The lenses have been much improved from the original design which had very significant aberrations for an important part of its tuning range. The final design with the electrode on top of the microlens has phase aberrations much closer to diffraction limited in the most significant part of the tuning range. Also with the design changes, walls have been eliminated from the devices removing the need for a restriction on the applied voltages. The final design performance could still be improved, in particular, twisting of the liquid crystal with its accompanying polarisation problems and tilting of the transmitted beam could be eliminated and the speed of the switching could be improved.

Here is a breakdown of the main results described in this thesis:

- Lenses have been fabricated with a variable focal length for one polarisation of light. This variability has been achieved by immersing a microlens in nematic liquid crystal. The lenses built have a focal length which capable of being varied from negative to positive. The lenses studied had focal length ranges of $-910\mu m$ and $360\mu m$ to $580\mu m$ (original design, diameter $100\mu m$), $-1660\mu m$ and $490\mu m$ to $1100\mu m$ (original design, diameter $150\mu m$) and $-1570\mu m$ and $1450\mu m$ to $3350\mu m$ (electrode-on-top design, diameter $150\mu m$).

- The phase aberrations of the lenses have been measured in an interferometer. The first lens design had an rms aberration of 0.18λ to 0.55λ (diameter $150\mu m$) whereas the electrode-on-top design had an aberration of 0.071λ to 0.19λ.

- The amplitude aberrations (or variation of transmitted polarisation) of the lenses has been measured (qualitatively). The areas where the polarisation is altered is indicative of a twist in the liquid crystal structure. The liquid crystal is clearly twisting around the sides of the lens and the area where it twists increases with voltage.

- Cylindrical immersed lenses have also been fabricated. These lenses have been studied primarily in order to compare their behaviour with modelling work and to study the liquid crystal properties with a simpler structure.

- The structure of the liquid crystal has been studied and structures have been suggested to match the observed optical properties. In particular, wall structures which form in the liquid crystal have been matched to structure described by Stieb *et al.* Similarly, possible causes of the twisted structure have been proposed which could match the observed polarisation characteristics.

- A 1-D computer model of the liquid crystal has been developed incorporating the effects of the varying pre-tilt and the dielectric on the response of the liquid crystal. Using the program, the focal length vs voltage characteristic of the lenses has been modelled and so have the optical phase aberrations.

- A 2-D model finite element model for the liquid crystal structure has been used to test a proposed cause of the twist in the liquid crystal. A program has been written calculate the optical properties of the modelled structure and the polarisation effect has been reproduced.
- New designs have been produced from the modelling work. One of these new designs, the electrode-on-top design eliminated wall structures, eliminated twisted structures from cylindrical microlenses and showed a significantly improved aberration performance (see above).
- The time response of the lenses has been measured. The effect of eliminating the wall structures has been shown to have a dramatic benefit on the time response.

Chapter 9

Further Work

9.1 Introduction

In this chapter, the studies of what is needed to improve further the performance of the microlenses are considered. Also, suggestions are made which relate to devices other than microlenses.

9.2 Microlenses

It is clear that the microlenses do not yet perform in the way originally envisaged. There is a variation of focal length but the quality of the focus is poor for a lot of the available tuning range. The original design suffers from large aberrations in the 1-3V range limiting its usable range to above 4V. The electrode on top design is a lot better in terms of phase aberrations but induces a tilt in the 1-3V which may be problematic in a system and the liquid crystal on the lens twists, changing the polarisation of the transmitted light in parts of the lens aperture.

Removing the twist is a major goal in the improvement of the microlenses. The 2nd major aim is to remove the tilt introduced by the microlenses. Finally, it would be useful to be able to choose different focal length ranges over which the lenses can vary. This depends on the application but from the research point of view it would be useful to have the lens always producing a focal spot (*i.e.* without infinite focal length for any voltage) simply because the focal length could always be measured and the nature of the focal spot gives an immediate indication of the combined phase/amplitude aberrations.

There is more than one way that the liquid crystal twist can be lessened. Either the electric field pattern could be altered, or the surface structure or the liquid crystal could be changed. Two approaches would be either to reduce the cause of the twist or to increase the liquid crystal resistance to it. However, since the cause of the liquid crystal twist is not completely understood, it seems wiser to try to increase the liquid crystal's 'resistance' to twist.

Liquid crystal materials

The simplest way to reduce the twist in the liquid crystal is to change the material used, choosing one with a higher twist elastic constant, k_{22}. In fact, it is the ratio of elastic constants that is important as this determines the energy of associated with each

type of deformation and thus can cause one to be favoured over the others. k_{22} is often the smallest of the elastic constants [KW93], for example, the liquid crystal used in the microlenses, E7, has elastic constant ratios of $k_{33}/k_{22} = 1.94$ and $k_{33}/k_{11} = 1.54$ (see table 4.2). A material with a better k_{33}/k_{22} ratio is E170 [Mer92b] for which the ratios are $k_{33}/k_{22} = 1.0$ and $k_{33}/k_{11} = 1.01$.

One other aspect of device performance which can be improved by a change of material is the response time. The response time of the microlenses has been measured but no attempt has been made to optimise their performance. The response can be improved by choosing materials with a lower rotational viscosity or a higher splay elastic constant (see equation 4.2). The rotational viscosity of E7 is 0.20 Pa s [KW93] whilst there are materials commercially available with viscosities down to 0.105 Pa s [Mer92b].

Liquid crystal alignment

A different approach is to carry on the work presented in section 6.4.1, *i.e.* to try different alignment techniques. One such technique which has not been tried on the microlenses is alignment of the bulk of the liquid crystal.

Bulk liquid crystal alignment has been demonstrated by Jain and Kitzerow [JK94] who demonstrated homogeneous alignment by UV curing a mixture of PVCi with liquid crystal using polarised UV light. However, whilst it is clear that this type of alignment will change the liquid crystal elastic response, it is not clear what the new response will be. Alignment of the bulk is likely to increase resistance to twist but not necessarily any more than the resistance to any other deformation, thus the final result may simply be an increase in the voltage required for switching much like PDLC. Also, since Jain and Kitzerow report no pre-tilt, wall structures are likely to arise. Therefore, although the approach may be worth exploring due to its ease of implementation, a more promising idea is to try PDLC (see below).

An alternative change of alignment technique would be to try the LPP alignment layers described by Schadt *et al* [SSSK95a] where pre-tilt has been achieved. This technique is particularly promising as alignment should be achieved over the whole substrate and with (hopefully) uniform pre-tilt. However, the problem here is obtaining any of the polymer. I have talked to Martin Schadt and he has promised a 'research material' when one is available but so far none has been forthcoming due to commercial licensing restrictions.

Tilt

There are other aspects of the microlenses which could be improved significantly. One is the tilt observed with the "electrode on top" design. What is required is a way of balancing the difference in switching across the microlens due to the pre-tilt difference (see section 6.5). Of course, the ideal is to eliminate the pre-tilt variation in the first place using a different alignment technique (see LPP above) but if this is not possible, an alternative solution may be to vary the electric field strength. This may be achieved by measuring the refractive index vs voltage response across the lens (treating each part of the lens as independent) and then calculating the required voltage profile and applying this profile across the lens. A voltage profile may be achieved with patterned electrodes, a resistive pattern or by inserting a dielectric distribution between the electrode and

the liquid crystal (c.f. the photoresist microlenses). All these solutions add a significant degree of complexity and, most likely, would need to be recalculated for a new microlens design. Also, care must be taken not to jeopardise the benefit of the "electrode on top" design, *i.e.* the switching starting from the top of the lens. Therefore, this option is not attractive except as a last resort.

Focal length range

The last change is not so much an improvement but a modification. Currently, the focal length goes from negative to positive via infinity. It would be instructive, however, to be able to see the focus for all voltages. Currently, the aberrations are smallest for the voltage giving infinite focal length. Thus, it would be useful to change the refractive indices. Unfortunately, the substrate material can easily be etched if it is quartz but not if it is glass. This limits the lens refractive index to ~ 1.46 (or 1.64 for photoresist). Also, the liquid crystal refractive indices all seem to have ordinary refractive indices around 1.5 ($1.47 \rightarrow 1.54$ [Mer92b]). Thus, most combinations will result in a range of focal lengths from infinity to a negative lens. An alternative solution is to emboss the microlenses into plastic by hot embossing or injection moulding [GRS93]. However, whichever material is used would have to be compatible with the later processing steps (alignment layer in a solvent and deposition of an electrode).

Design changes

Other changes to the design are more radical in the sense that they change the way the design works. These are ideas outlined in the design chapter; namely, a PDLC lens or a Fresnel lens. The PDLC lens is certainly worth investigating with its potential advantages of polarisation insensitivity and increased speed. The likely disadvantages are the difficulty of reducing the scattering or the residual scattering and the reduced refractive index modulation available.

The Fresnel lens has the attraction of increased speed and being able to keep a constant thickness of liquid crystal layer with different lens apertures. However, creating structures using either halftone masks or multilevel structures requires more control for exposures/alignment than the melt and reflow technique and the mask design is more difficult.

9.3 Alternative devices

There are one or two general observations from the work presented here which could form the basis of further study. In terms of liquid crystal devices, the novel characteristics of these devices is that the liquid crystal has a surface relief structure for one of its substrates. Many of the observations which have been recorded in the course of the microlens work are likely to be reproduced with other relief structures, especially non-binary ones. Holograms and diffractive optics could be made switchable in the same way that the microlens have been but care would need to be taken in designing the structures if the effects described in this thesis are to be avoided. In particular, one of the advantages of liquid crystal immersed surface relief structures is higher possible spatial frequencies that are possible over a pure liquid crystal device (eg. an SLM [Sv95]).

However, 2 potential dangers of the higher spatial frequencies have been highlighted, one is competitive alignment generated between the alignment layers and surface structure and the other is the extra distortion in the electric fields introduced by the higher gradient of the surface. Both effects can lead to twist of the liquid crystal and hence a change of polarisation of the transmitted light. Schulze and von Reden [Sv95] have fabricated gratings liquid crystal on top and, due to the aligning behaviour of a grating, they restricted themselves to liquid crystal alignments parallel to the grating. Stadler and Ehbets [SE94] produced a computer generated hologram immersed in liquid crystal and, even with only a steepest slope of $\sim 3°$ on the surface, they reported disclinations in the liquid crystal.

An alternative response to the effects is to try to turn them on their head, *i.e.* to turn a problem into an opportunity. There are 2 possibilities:

1. The twist of the liquid crystal is not desired in the optical phase modulation device however twist is desired in a display. In particular, recently a new configuration, In-Plane Switching (IPS) has been commercialised by Hitachi[OK95]. In the IPS configuration, the liquid crystal is untwisted in the off-state and twist induced by the application of a field. IPS has an advantage in viewing angle but requires higher voltages and the switching time is longer [JSvdPO97]. The twist mechanism presented in this thesis may provide an alternative way of achieving a similar effect with possibly better performance (although recent studies have shown [OYOK97] that the IPS viewing characteristics are adversely affected by larger pretilts).

2. The 2nd observation is the effect of response times on eventual structures. In the lens structures the pre-tilt of the area with the shortest response times propagates to other parts of the device thus deciding the final structure, thus care has to be taken in designing the structure.

However, again this could be investigated for display devices. There are several alignment techniques which provide alignment but no pre-tilt. It may be possible to induce the desired pre-tilt. It may be possible to induce the desired pre-tilt with a side electrode of thickness variation.

Bibliography

[AKR+98] D. Andrienko, Y. Kurioz, Y. Reznikov, C. Rosenblatt, R. Petschek, O. Lavrentovich, and D. Subacius. Tilted photoalignment of a nematic liquid crystal induced by a magnetic field. *J. App. Phys.*, 83(1):50–55, January 1998.

[AMIY95] Haruhisa Akiyama, Masayuki Momose, Kunihiro Ichimura, and Shigeo Yamamura. Surface selective modification of poly(vinyl alcohol) films with azobenzenes for in-plane alignment photocontrol of nematic liquid crystals. *Macromolecules*, 28:288–293, 1995.

[BBS96] G.P. Bryan-Brown and I.C. Sage. Photoinduced ordeing and alignment properties of polyvinylcinnamates. *Liquid Crystals*, 20(6):825–829, 1996.

[Ber73] Dwight W. Berreman. Alignment of liquid crystals by grooved surfaces. *Molecular Crystals and Liquid Crystals*, 23:215–231, 1973.

[Ber80] Dwight W. Berreman. Variable focus liquid crystal lens system. US Patent No. 4,190,330, 1980. (Filed in 1977).

[Ber83] D.W. Berreman. Numerical modelling of twisted nematic devices. *Phil. Trans. R. Soc. Lond. A*, 309:203–216, 1983.

[BH91] K. Bird and T.J. Hall. The computer controlled generation of microlens arrays. *IOP Short Meetings*, 30:35–40, 1991.

[BL93] Chris W. Barnard and John W.Y. Lit. Mode transforming properties of tapered single-mode fiber microlenses. *Applied Optics*, 32(12):2090–2094, 1993.

[Bli83] Lev Mikhaylovich Blinov. *Electro-optical and magneto-optical properties of liquid crystals.* John Wiley & Sons, Chicester, England, first edition, 1983.

[BMBM85] Nicholas F. Borrelli, David L. Morse, Robert H. Bellman, and Walter L. Morgan. Photolytic technique for producing microlenses in photosensitive glass. *Applied Optics*, 24(16):2520–2525, 1985.

[BNPY92] S.E. Broomfield, M.A.A. Neil, E.G.S. Paige, and G.G. Yang. Programmable binary phase-only optical device based on ferroelectric liquid crystal SLM. *Electronics Letters*, 28(1):26–28, 1992.

[Bra96] Dr. J.J.M. Braat. Personal communication, 1996. Philips Optical Design, Eindhoven.

[BW80] Max Born and Emil Wolf. *Principles of Optics.* Pergamon Press, Oxford, England, sixth edition, 1980.

[CB79] J. Cheng and G.D. Boyd. The liquid crystal alignment properties of photolithographic gratings. *App. Phys. Lett.*, 35(6):444–446, 1979.

[CB93] Alan G. Chen and David J. Brady. Two-wavelength reversible holograms in azo-dye doped nematic liquid crystals. *App. Phys. Lett.*, 62(23):2920–2922, 1993.

[CDC96] W.K. Choi, A.B. Davey, and W.A. Crossland. Use of deformed helix ferroelectric liquid crystals in Fabry-Perot etalons. *Ferroelectrics*, 181:11–19, 1996.

[Cha92] S. Chandrasekhar. *Liquid Crystals.* Cambridge University Press, Cambridge, England, second edition, 1992.

[CHI94] Choon Hoong CHIA. Assessment of liquid crystal microlenses. Technical report, 3rd year report, Department of Electronic and Electrical Engineering, University College London, Torrington Place, London WC1E 7JE, June 1994.

[CJB+96] J. Chen, D.L. Johnson, P.J. Bos, S. Sprunt, J. Lando, and J.A. Mann. Radially and azimuthally oriented liquid crystal alignemnt patterns fabricated by linearly polarised ultraviolet exposure process. *App. Phys. Lett.*, 68(7):885–887, February 1996.

[Cle97] Cleveland Crystals Inc. Online store. World Wide Web site, http://www.clevelandcrystals.com/store.html, 1997.

[Cog82] Jacques Cognard. Alignment of nematic liquid crystals and their mixtures. *Mol. Crys. Liq. Crys., Suppl. 1*, 78:1–77, 1982.

[Col90] Peter J. Collings. *Liquid Crystals.* Adam Hilger, Bristol, England, first edition, 1990.

[CP96] Yvonne Carts-Powell. Microlenses improve display efficiency. *Laser Focus World*, pages 24–28, September 1996.

[DCG+96] Lawrence H. Domash, Yong-Ming Chen, Badri Gomamtam, Conrad Gozewski, Richard L. Sutherland, Lalgudi V. Natarajan, Vincent P. Tondiglia, and Timothy J. Bunning. Switchable-focus lenses in holographic polymer dispersed liquid crystal. *Proc. SPIE*, 2689:188–194, 1996.

[De Jeu80] W.H. De Jeu. *Physical properties of liquid crystalline materials.* Gordon and Breach Science Publishers, New York, first edition, 1980.

[Deu72] Heinz J. Deuling. Deformation of nematic liquid crystals in an electric field. *Molecular Crystals and Liquid Crystals*, 19:123–131, 1972.

[DFDD96] Fabrizio Di Pasquale, F. Aníbal Fernández, Sally E. Day, and J. Brian Davies. Two-dimensional finite-element modeling of nematic liquid crystal devices for optical communications and displays. *IEEE J. Selected topics in Quantum Electronics*, 2(1):128–134, 1996.

[DFDD97] Fabrizio Di Pasquale, F. Aníbal Fernández, Sally E. Day, and J. Brian Davies. Time domain modelling of liquid crystal display cells in two- and three- dimensions. *Proc. of the 11th Conf. on the Computation of Electromagnetic Fields*, 1:47–48, 1997.

[DGW+88] J.W. Doanne, A. Golemme, J.L. West, J.B. Whitehead Jr., and B.-G. Wu. Polymer Dispersed Liquid Crystals for Display Application. *Molecular Crystals and Liquid Crystals*, 165:511–532, 1988.

[dP93] P.G. de Gennes and J. Prost. *The Physics of Liquid Crystals.* Oxford Science Publications, Oxford, England, second edition, 1993.

[DSHD91] D. Daly, R.F. Stevens, M.C. Hutley, and N. Davies. The manufacture of microlenses by melting photoresist. *IOP Short Meetings*, 30:23–34, 1991.

[Eal95] Ealing electro-optics. *Ealing catalogue*, 1995.

[EC96] Bob Evans and Moses Chan. To wet or not to wet. *Physics World*, pages 48–52, April 1996.

[EDMM96] Johannes Eschler, Stefan Dickmann, Dieter A. Mlynski, and Henning Molsen. Fast adaptive lens based on deformed helical ferroelectric liquid crystal. *Ferroelectrics*, 181:21–28, 1996.

[EHSS93] M. Eisner, S. Haselbeck, H. Schreiber, and J. Schwider. Reactive ino etching of microlens arrays into fused silica. *EOS Topical Meetings Microlens Arrays*, 2:17–19, 1993.

[FF96] M. Ferstl and A.M. Frisch. Static and dynamic Fresnel zone lenses for optical interconnections. *J. Modern Opt.*, 43(7):1451–1462, 1996.

[FS89] J. Fünfschilling and M. Schadt. Fast responding and highly multiplexable distorted helix ferroelectric liquid crystal displays. *J. Appl. Phys.*, 66(8):3877–3882, 1989.

[GBW95] Christopher B. Gorman, Hans A. Biebuyck, and George M. Whitesides. Control of the shape of liquid lenses on a modified gold surface using an applied eletrical potential across a self-assembled monolayer. *Langmuir*, 11:2242–2246, 1995.

[GFM95] J. Göttert, M. Fischer, and A. Müller. High-aperture surface relief microlenses fabricated by x-ray lithography and melting. *EOS Topical Meetings Microlens Arrays*, 5:21–25, 1995.

[GHA+93] G. Gal, B. Herman, W. Anderson, D. Shough, D. Purdy, and A. Berwick. Development of the dispersive microlens. *EOS Topical Meetings Microlens Arrays*, 2:38–41, 1993.

[GRS93] M.T. Gale, M. Rossi, and H. Schütz. Fabrication and replication of continuous relief DOEs. *IEE Conf. Proc.*, 379:66–70, 1993.

[GS94] Wayne M. Gibbons and Shao-Tang Sun. Optically generated liquid crystal gratings. *Appl. Phys. Lett.*, 65(20):2542–2544, 1994.

[GSSS94] Wayne M. Gibbons, Paul J. Shannon, Shao-Tang Sun, and Brian J. Swetlin. Surface mediated alignment of nematic liquid crystals with polarized laser light. *Nature*, 351:49–50, 1994.

[HDH97] H.G. Hänsel, F. Drosch, and S. Heinemann. Method of characterizing the state of alignment of a microlens in respect to a diode laser array. *EOS Topical Meetings Microlens Arrays*, 13:70–72, 1997.

[HDS91a] M.C. Hutley, D.Daly, and R.F. Stevens. Microlens Arrays. *Physics World*, pages 27–32, July 1991.

[HDS91b] M.C. Hutley, D.Daly, and R.F. Stevens. The testing of microlens arrays. *IOP Short Meetings*, 30:67–81, 1991.

[Hec87] Eugene Hecht. *OPTICS*. Addison-Wesley, Reading, Massachusetts, second edition, 1987.

[HGRK95] Th. Hessler, M.T. Gale, M. Rossi, and R.E. Kunz. Fabrication of Fresnel microlens arrays by direct writing in photresist. *EOS Topical Meetings Microlens Arrays*, 5:37–43, 1995.

[HRP+97] Th. Hessler, M. Rossi, J. Pedersen, M.T. Gale, M. Wegner, and T.J. Tiziani. Microlens arrays with spatial variation of the optical functions. *EOS Topical Meetings Microlens Arrays*, 13:42–47, 1997.

[HSD90] M.C. Hutley, R.F. Stevens, and D. Daly. The manufacture of microlens arrays and fan-out gratings in photoresist. *IEE colloquim "Optical connection and switching networks for communication and computing"*, pages 11/1–11/3, 1990.

[HSK+95] T. Hashimoto, T. Sugiyama, K. Katoh, T. Saitoh, H. Suzuki, Y. Iimura, and S. Kobayishi. TN-LCD with quartered subpixels using polarised UV-light-irradiated polymer orientation films. *SID'95 Digest*, 41:877–880, 1995.

[HSSS93] S. Haselbeck, H. Schreiber, J. Schwider, and H. Sickinger. Fabrication and measurement of microlenses. *Proc. of SPIE*, 1983:917–918, 1993.

[Hut90a] M.C. Hutley. Optical techniques for the generation of microlens arrays. *J. Modern Optics*, 37(2):253–265, 1990.

[Hut90b] M.C. Hutley. The manufacture and testing of microlens arrays. *Proc. of SPIE*, 1319:491–492, 1990.

[Hut95] M.C. Hutley. Simple "Photosculpture" techniques for making arrays of lenses with controlled aberration. *EOS Topical Meetings Microlens Arrays*, 5:44–47, 1995.

[IAA+95] A. Ishizaki, H. Abe, N. Ando, Y. Iimura, and S. Kobayahsi. Measurements of the azimuthal anchoring energy of a nematic liquid crystal (5CB) aligned as-stacked polyimide Langmuir-Blodgett films. *Mol. Crys. Liq. Crys.*, 258:277–283, 1995.

[IiKK+93] Yasufumi Iimura, Jun ichi Kusano, Shunsuke Kobayashi, Yoshinobu Aoyagi, and Takuo Sugano. Alignment control of a liquid crystal on a photosensitive polyvinylalcohol film. *Jap. J. Appl. Phys.*, 32:L93–L96, 1993.

[IKK95] Yasufumi Iimura, Norihiko Kobayashi, and Shunsuke Kobayashi. Measurement of temperature behaviour of azimuthal anchoring energy at liquid crystal/Si0 interface using new method. *Jap. J. Appl. Phys.*, 34:1935–1936, 1995.

[Jan72] John L. Janning. Thin film surface orientation for liquid crystals. *Appl. Phys. Lett.*, 21:173–174, 1972.

[JK94] Sukhmal C. Jain and Heinz-S. Kitzerow. Bulk-induced alignment of nematic liquid crystals by photopolymerisation. *Appl. Phys. Lett.*, 64(22):2946–2948, 1994.

[JSvdPO97] M.T. Johnson, S. Stallinga, A.A. van der Put, and U. Opik. An analytic approach to LC dynamics in ECB and IPS displays. *SID conference record of the IDRC*, pages 17–20, 1997.

[Kah82] Frederic J. Kahn. The molecular physics of liquid crystal devices. *Physics Today*, pages 66–74, May 1982.

[KCK84] Stephen T. Kowel, Dennis S. Cleverly, and Philipp G. Kornreich. Focusing by electrical modulation of refraction in a liquid crystal cell. *Applied Optics*, 23(2):278–289, 1984.

[KCMM97] B.P. Keyworth, D.J. Corazza, J.N. McMullin, and L. Mabbott. Single-step fabrication of refractive microlens arrays. *Applied Optics*, 36(10):2198–2202, 1997.

[KFM+88] Seiyu Kuniyasu, Hiroyoshi Fukuro, Shigeo Maeda, Kenji Nakaya, Michio Nitta, Norihiko Ozaki, and Shunsuke Kobayashi. The strength of rubbing worked on polyimide films for aligning nemaic and chiral smectic liquid crystals: controlling pretilt angles and some electrooptic performances of LCDs. *Jap. J. App. Phys.*, 27(5):827–829, 1988.

[KGDS98] R.E. Kilpatrick, J.H. Gilby, S.E. Day, and D.R. Selviah. Liquid crystal televisions for use as spatial light modulators in a complex optical correlator. *Proc. SPIE*, 3386:70–77, 1998.

[KKTS97] K.Tanaka, K. Kato, S. Tsuru, and S. Sakai. A liquid crystal/polymer optical device formed by holography for reflective colour display applications. *Proc. SID*, pages 109–111, 1997.

[KLY95] H. Kikuchi, J.A. Logan, and D.Y. Yoon. Mechanisms of liquid crystal alignment on buffed polyimide surfaces. *ANTEC conf. proc.*, 2:2621–2622, 1995.

[KM97] Yasushi Kawata and Yasushi Mori. Control of nematic liquid crystal alignment using stripped film method. *Jap. J. App. Phys.*, pages L1695–L1698, December 1997.

[KW73] M. Kléman and C. Williams. Anchoring energies and the nucleation of surface disclination lines in nematics. *Phil. Mag.*, 28:725–731, 1973.

[KW93] Iam-Choon Khoo and Shin-Tson Wu. *Optics and non-linear optics of liquid crystals.* World Scientific Publishing, Singapore, first edition, 1993.

[Lan97a] M.F. Land. Personal communication, 1997. University of Sussex.

[Lan97b] M.F. Land. Microlens Arrays in the Animal Kingdom. *EOS Topical Meetings Microlens Arrays*, 13:1–4, 1997.

[LDWM89] Z.L. Liau, V. Diadiuk, J.N. Walpole, and D.E. Mull. Gallium phosphide microlenses by mass transport. *Appl. Phys. Lett.*, 55(2):97–99, 1989.

[Lég73] L. Léger. Walls in nematics. *Mol. Cry. and Liq. Crys.*, 24:33–44, 1973.

[Lip08] G. Lippman. Epreuves réversibles donnant la sensation du relief. *J. Phys. Theor. Appl.*, 7:821–824, 1908.

[LSU93] E.S. Lee, Y. Saito, and T. Uchida. Detailed morphology of rubbed alignment layers and surface anchoring of liquid crystals. *Jpn. J. Appl. Phys.*, 32(12):L1822–L1825, 1993.

[LVMU93] Eung Sang Lee, Peter Vetter, Tetsuya Miyashita, and Tatsuo Uchida. Orientation of Polymer molecules in rubbed alignment layer and surface anchoring of liquid crystals. *Jpn. J. Appl. Phys.*, 32(9):L1339–L1341, September 1993.

[Man96] David Manners. Fujitsu MicroLens makes flat panels. *Electronics Weekly*, October 1996. Online version: http://www.electronicsweekly.co.uk/ew/-archive/archiveview.cgi?961030/story3.htm.

[Mau91] Ch. Mauguin. Sur les cristaux liquides de Lehmann. *Bull. Soc. Franc. Mineral.*, 34:71–85, 1991.

[Mer92a] Merck Industrial Chemicals. *'Licrite', liquid crystals catalogue*, 1992.

[Mer92b] Merck Industrial Chemicals. *'Liquid crystal mixtures for electro-optic displays', liquid crystals catalogue*, 1992.

[Mer97] Merck Industrial Chemicals, Poole, UK. Purchase of 5g liquid crystal E7, 1997.

[MGH93] P.W. McOwan, M.S. Gordan, and W.J. Hossack. A switchable liquid crystal binary Gabor lens. *Optics Communications*, 103:189–193, 1993.

[MHHK96] S. Matsumoto, M. Houlbert, T. Hayashi, and K. Kubodera. Fine droplets of liquid crystal in a transport polymer and their response to an electric field. *App. Phys. Lett.*, 69(8), August 1996.

[MLES91] J.D. Margerum, A.M. Lackner, J.H. Erdmann, and E. Sherman. Addressing factors for polymer dispersed liquid crystal displays. *Proc. SPIE*, 1455:27–38, 1991.

[MNFT92] Keith Mersereau, Casimir R. Nijander, Avi Y. Feldblum, and Wesley P. Townsend. Fabrication and measurement of fused silica microlens arrays. *Proc. of SPIE*, 1751:229–233, 1992.

[Nis86] Kimihiko Nishioka. Automatic focusing device using liquid crystal lens. Jap. Patent No. 61-156228, 1986.

[NLGV98] A.F. Naumov, M.Y. Loktev, I.R. Guralnik, and G. Vdovin. Liquid crystal adaptive lenses with modal control. *Opt. Lett.*, 23(13):992–994, July 1998.

[NMS91] Toshiaki Nose, Shin Masuda, and Susumu Sato. Optical properties of a liquid crystal microlens with a symmetric electrode structure. *Jap. J. Appl. Phys.*, 30(12b):L2110–L2112, 1991.

[OCG95] OCG Ltd. Waycoat HNR120/80 series. Product literature, 1995.

[OGI+97] C. Oßmann, J. Göttert, M. Ilie, J. Mohr, and P. Ruther. Fabrication of PMMA based microlenses using the LIGA-process. *EOS Topical Meetings Microlens Arrays*, 13:54–58, 1997.

[OK95] Masahito Ohe and Katsumi Kondo. Electro-optical characteristics and switching behviour of the in-plane switching mode. *Applied Physics Letters*, 67(26):3895–3897, 1995.

[Oka86] Takao Okada. Liquid crystal spectacle device. Jap. Patent No. 61-156226, 1986.

[OYOK97] M. Ohe, M. Yoneya, M. Ohta, and K. Kondo. Dependance of viewing angle characteristics on pretilt angle in the in-plane switching mode. *Liquid Crystals*, 22(4):391–400, 1997.

[Pan80] J.I. Pankove, editor. *Display Devices.* Topics in Applied Physics. Springer-Verlag, Berlin, first edition, 1980.

[PBJ66] Roger S. Porter, Edward M. Barrall II, and Julian F. Johnson. Some flow characteristics of mesophase types. *J. Chem. Phys.*, 45(5):1452–1456, 1966.

[POO95] Chun Ho Peter POON. *Free space optical interconnections for an incoherent correlator.* PhD thesis, University College London, Torrington Place, London WC1E 7JE, March 1995.

[PR91] J.S. Patel and K. Rastani. Electrically controlled polarization independent liquid crystal Fresnel lens arrays. *Optics Letters*, 16(7):532–534, 1991.

[PRS+93] P.C.H. Poon, M.G. Robinson, D.R. Selviah, D. Daly, and J.E. Midwinter. Long focal length microlenses. *EOS Topical Meetings Microlens Arrays*, 2:13–16, 1993.

[PSC88] Zoran D. Popovic, Robert A. Sprague, and G.A. Neville Connell. Technique for monolithic fabrication of microlens arrays. *Applied Optics*, 27(7):1281–1284, 1988.

[Pur93] D.R. Purdy. Fabrication of complex micro-optic components using halftone transmission masks to photosculpt positive resist. *EOS Topical Meetings Microlens Arrays*, 2:20–25, 1993.

[RD93] Nabeel A. Riza and Michael C. DeJule. Three-terminal adaptive nematic liquid-crystal lens device. *Optics Letters*, 19(14):1013–1015, 1993.

[RTD79] E.P. Raynes, R.J.A. Tough, and K.A. Davies. Voltage dependence of the capacitance of a twisted nematic liquid crystal layer. *Mol. Crys. Liq. Crys.*, 56:63–68, 1979.

[RXM+95] Sun Ruipeng, Huang Ximim, Jiang Min, Ma Kai, Wang Zongkai, Jing Hai, Yuan Jianfeng, and Jin Changfeng. Investigation of surface torsional anchoring energy for pure nematic liquid crystals. *Mol. Crys. Liq Crys.*, 265:335–340, 1995.

[Sat79] Sumusu Sato. Liquid crystal lens-cells with variable focal length. *Jap. J. Appl. Phys.*, 18(9):1679–1684, 1979.

[Sav94] Pekka Savander. Microlens arrays etched into glass and silicon. *Optics and Lasers in Engineering*, 20:97–107, 1994.

[SBM74] A. Stieb, G. Baur, and G. Meier. Inversionswände in dielektrisch deformierten Flüssigkristallschichten. *Berichte der Bunsen-Gesellschaft*, 78(9):899–902, 1974.

[SBM75] A. Stieb, G. Baur, and G. Meier. Alignment inversion walls in nematic liquid crystal layers deformed by an electric field. *J. de Physique*, 36(3):C185–C188, 1975.

[Sch93] M. Schadt. Plenary Lecture: Linear and non-linear liquid crystal materials, electro-optical effects and surface interactions. *Liquid Crystals*, 14(1):73–104, 1993.

[Sch98] Schott. Glass catalogue. World Wide Web site, http://www.schottglasstech.com/ (download), 1998.

[SD95] Jürgen Schweizer and Eugen Dumitrescu. Microlens array overcomes interferometer's limitations. *EuroPhotonics*, pages 32–33, August 1995.

[SE94] M. Stalder and P. Ehbets. Electrically switchable diffractive optical element for image processing. *Opt. Lett.*, 19(1):1–3, 1994.

[SFR+96] D.N. Stoenescu, S. Frunza, Y. Roques, J. Farenc, and J.P. Traverse. Anchoring energy of some nematic liquid crystals at alignment layers of different topography. *Crystal Research and Technology*, 31(8):1095–1099, 1996.

[SGS94] P. J. Shannon, W. M. Gibbons, and S. T. Sun. Patterned optical properties in photopolymerized surface aligned liquid crystal films. *Nature*, 368:532–533, 1994.

[SK92] D.S. Seo and S. Kobayishi. Effects of high polymer concentration for alignment of liquid crystal on rubbed polyimide surfaces containing trifluoromehtyl moities. *Jpn. J. Appl. Phys.*, 34(6B):L786–L788, 1992.

[SKN92] Dae-Shik Seo, Shunsuke Kobayishi, and Michinori Nishikawa. Study of the pretilt angle for 5CB on rubbed polyimide films containing trifluoromethyl moiety and analysis of the surface atomic concentration of F/C(%) with an electron spectroscope for chemical analysis. *Appl. Phys. Lett.*, 61(20):2392–2394, 1992.

[SKS+90] Takashi Sugiyama, Seiyu Kuniyasu, Daeshik Seo, Hiroyoshi Fukuro, and Shunsuke Kobayashi. A simple model for pretilted nematic liquid crystal medium and its torsional surface coupling strength. *Jap. J. Appl. Phys.*, 29(10):2045–2051, 1990.

[SMI+92] D.S. Seo, K. Muroi, T. Isogami, H.Matsuda, and S. Kobayishi. Polar anchoring strength and temperature dependence of nematic liquid crystal (5CB) aligned on rubbed polystyrene films. *Jpn. J. Appl. Phys.*, 31:2165–2169, 1992.

[SNTB93] R.L. Sutherland, L.V. Natarajan, V.P. Tondiglia, and T.J. Bunning. Bragg gratings in an acrylate polymer consisting of periodic polymer-dispersed liquid crystal planes. *Chem. Mater.*, 5(10):1533–1538, 1993.

[SSK+93] Takahiro Seki, Masako Sakuragi, Yuji Kawanishi, Yasuzo Suzuki, Takashi Tamaki, Ryo ichi Fukuda, and Kunihiro Ichimura. 'Command surfaces' of Langmuir-Blodgett films. Photoregulations of liquid crystal alignment by molecularly tailored surface azobenzene layers. *Langmuir*, 9:211–218, 1993.

[SSKC92] M. Schadt, K. Schmitt, V. Kozinkov, and V. Chigrinov. Surface-Induced Parallel Alignment of Liquid Crystals by Linearly Polymerised Photopolymers. *Jpn. J. Appl. Phys.*, 31:2155–2164, 1992.

[SSS85] Sumusu Sato, Akira Sugiyama, and Rumiko Sato. Variable-focus liquid crystal Fresnel lens. *Jap. J. Appl. Phys.*, 24(8):L626–L628, 1985.

[SSSK95a] Martin Schadt, Hubert Seiberle, Andreas Schuster, and Stephen M. Kelly. Photo-induced alignment and patterning of hybrid liquid crystalline polymer films on single substrates. *Jap. J. App. Phys.*, 34(6B):L764–L767, 1995.

[SSSK95b] Martin Schadt, Hubert Seiberle, Andreas Schuster, and Stephen M. Kelly. Photo-generation of linearly polymerized liquid crystal aligning layers comprising novel, integrated optically patterned retarders and color filters. *Jap. J. App. Phys.*, 34(6A):3240–3249, 1995.

[SSU92] Yumiko Sato, Katzutoshi Sato, and Tatsuo Uchida. Relationship between rubbing strength and surface anchoring of nematic liquid crystal. *Jap. J. Appl. Phys.*, 31(5):L579–L581, 1992.

[Sv95] Emil Schulze and Wolf von Reden. Diffractive liquid crystal spatial light modulators with optically integrated fine-pitch phase gratings. *Proc. of SPIE*, 2408:113–120, April 1995.

[Tam92] Eddy C. Tam. Smart electro-optical zoom lens. *Optics Letters*, 17(5), 1992.

[TNS+95] V.P. Tondiglia, L.V. Natarajan, R.L. Sutherland, T.J. Bunning, and W.W. Adams. Volume holographic storage and electro-optical readout in a polymer dispersed liquid crystal film. *Optics Letters*, 20(11):1325–1327, 1995.

[TRL+95] Michael F. Toney, Thomas P. Russell, J. Anthony Logan, Hirotsugu Kikuchi, James M. Sands, and Sanat K. Kumar. Near-surface alignment of polymers in rubbed films. *Nature*, 374:709–711, 1995.

[TRM+95] V. Tarazona, M. Rabaarot, E. Molva, V. Marty, and J.M. Combes. Long focal length microlenses in laser materials for the stabilization of microchip lasers. *EOS Topical Meetings Microlens Arrays*, 5, 1995. Post-deadline paper.

[vMC93] C. van Berkel, B.P. McGarvey, and J.A. Clarke. Microlens arrays for 2D large area image sensors. *EOS Topical Meeting Microlens Arrays*, 5:81–85, 1993.

[WGK73] U. Wolff, W. Greubel, and H. Krüger. The homogeneous alignment of liquid crystal layers. *Mol. Crys. Liq. Crys.*, 23:187–196, 1973.

[WHO+97] K. Wako, K.Y. Han, T. Oshima, T. Miyashita, and T. Uchida. Evaluation of the achoring strength of liquid crystal based on the rubbed area density. *SID conference record of the IDRC*, pages L73–L76, 1997.

[WL94] S.T. Wu and A.M. Lackner. Mylar-film-compensated-pi and parallel-aligned liquid crystal cells for direct-view and projection displays. *App. Phys. Lett.*, 64(16):2047–2049, 1994.

[WPPC89] G. Williams, N.J. Powell, A. Puris, and M.G. Clark. Electrically controllable liquid crystal Fresnel lens. *Proc. of SPIE*, 1168:352–357, 1989.

[WVO+92] Michael D. Wand, Rohini Vohra, Mike O'Callaghan, Beth Roberts, and Claus Escher. An easily aligned deformable helix ferroelectric liquid crystal mixture and its use in devices. *Proc. SPIE*, 1665:176–183, 1992.

[WWLK95] J.L. West, X. Wang, Y. Li, and J.R. Kelly. Polarised UV exposed polyimide films for liquid crystal alignment. *SID'95 Digest*, 41:703–705, 1995.

[WYA+81] O. Wada, S. Yamakoshi, M. Abe, Y. Nishitani, and T. Sakurai. High radiance InGaAsP/InP lensed LED's for optical communication systems at 1.2-1.3μm. *IEEE Journal of Quantum Electronics*, 17(2):174–178, 1981.

[YPP+97] O. Yaroshchuk, G. Pelzl, G. Pirwitz, Y. Reznikov, H. Zaschke, J.H. Kim, and S.B. Kwon. Photosensitve materials on a base of polysiloxane for the alignment of nematic liquid crystals. *Jap. J. Appl. Phys.*, 36(9):5693–5695, 1997.

[YS89] Rumiko Yamaguchi and Susumu Sato. Dispersion properties of refractive indices of nematic liquid crystals. *Electronics and Communications in Japan*, 72(6):108–115, 1989.

[YY84] Amnon Yariv and Pochi Yeh. *Optical waves in crystals.* John Wiley & Sons, New York, first edition, 1984.